TD15 Complementary simulation cases in support of SR-PSU

Contents

DokumentID
1578373, (1.0)

Sekretess
Öppen

Sida
2(165)

TD15 Complementary simulation cases in support of SR-PSU

SVENSK KÄRNBRÄNSLEHANTERING AB

1   Introduction

Sweden's final repository for low and intermediate level short-lived radioactive waste (SFR) was constructed in its first stage and taken into operation in 1987. As of today, the facility must be extended to manage the forecasted amounts of radioactive waste and the Swedish Nuclear Fuel and Waste Management Company (SKB) has therefore recently applied for the license to extend SFR (PSU). As part of the license application, a Site-Descriptive Model, SDM-PSU (SKB 2013), was developed to describe the hydrogeological setting at SFR.

A number of hydrogeological issues in SDM-PSU have been raised in SSM's consultant reviews[1,2,3]. In response to these, SKB has undertaken an inventory of remaining significant hydrogeological uncertainties (compiled in Appendix A). This pro memoria addresses some of the issues that were identified as important in this inventory. The following approaches are employed:

1) Complementary field investigations to *resolve* hydrogeological modelling uncertainties (summarised in Appendix B and C),
2) Numerical sensitivity analysis to *quantify the significance* of hydrogeological modelling uncertainties in SR-PSU (described in this PM), and
3) Complementary flow modelling, to *demonstrate* an alternative localisation of SFR3 (the Forsmark lens), as well as, an alternative conceptual interpretation to the ongoing decline in tunnel inflow to SFR1.

The execution of the field investigations and the detailed results are reported separately (Hedström et al. 2017). However, these investigations provide further insight to some of the hydrogeological issues raised, and therefore the main findings and conclusions thereof are compiled in Appendix B and C. The purpose of this PM is to present the exectution and results of the modelling exercises undertaken to address hydrogeological modelling uncertainties for SR-PSU.

1.1   Background

As part of the license application for the planned extension of SFR, a Site-Descriptive hydrogeological model has been formulated based on the available data (SDM-PSU). The hydrogeological model is used to predict the long-term repository performance of SFR1 and SFR3 for selected stages of future land uplift (referred to as time slices), by means of flow simulations (SR-PSU). A number of issues concerning the parameterisation of hydraulic domains were raised during the hydrogeological modelling of SDM-PSU (Öhman et al. 2012, 2013); e.g., related to conceptual uncertainties or effects of heterogeneity). The significance of such issues has been evaluated in preceding SR-PSU Tasks (Task Descriptions, TD08, TD10, TD11, and TD14); the significance is quantified in terms of impact on performance measures (see Öhman et al. 2014). A part of this task (TD15) has been to:

1) identify remaining issues, based on a literature review of Öhman et al. (2012) and Öhman et al. (2013),
2) judge their expected significance for long-term safety, and
3) based on this judgement, select those which are expected to be most relevant for SR-PSU (the hydrogeological issues selected for analysis in TD15 are listed below; see also Section 1.3).

---

[1] [SFR-U SSM2015-1016-6 SDM-PSU hydrogeologi Joel Geier Clearwater Hardrock Consulting.pdf]

[2] [SFR-U SSM2015-1017-4 SDM-PSU hydrogeologi Alan Herbert & Alastair Black SRK Consulting AB.pdf]

[3] [SFR-U SSM2015-1018-5 SR-PSU hydrologi Joel Geier Clearwater Hardrock Consulting.pdf]

DokumentID
1578373, (1.0)

Sekretess
Öppen

Sida
4(165)

TD15 Complementary simulation cases in support of SR-PSU

This study employs the currently most recent version of DarcyTools, v. 4.0.11. Analogous to previous modelling exercises, the significance of hydrogeological issues are evaluated in terms of a sensitivity study, in which the results of alternative model set ups are compared to those of a reference case, (here: the base-case used in the radionuclide transport calculations for periods with temperate conditions in the main scenario of the safety assessment (SKB 2014).

The scope of this study (Section 1.3) is introduced by a brief presentation of the studied hydrogeological issues and their role in SDM-PSU (Section 1.2).

1.2 Hydrogeological modelling issues assessed by flow simulation

1.2.1 HSD parameterisation

One of the remaining issue concerns the uncertainty in HSD parameterisation (i.e., hydraulic conductivity of the Quaternary deposits). The HSD parameterisation in SR-PSU flow simulations is taken as the effective values calibrated for SDM-Site/SR-Site Forsmark. Effective calibration values do not only reflect intrinsic material properties (such as hydraulic conductivity), but are also specific to: 1) the setup and underlying principles of the calibrating model (i.e., numerical shortcomings) and 2) the specific prevailing hydrological conditions at the Forsmark site (i.e., topography, river discharge, groundwater levels, lake levels, net precipitation, bedrock recharge; which may not necessarily be representative for the area which is currently below sea). Furthermore, the Quaternary deposits below sea have not yet been exposed to terrestrial dynamics (e.g., tree roots, frost heaving, and worm holes).

This motivates quantification of the model sensitivity to HSD parameterisation, particularly in the area which is currently below sea.

1.2.2 HCD parameterisation (role of historic packer data)

SDM-PSU is based on two data sets: 1) "the historic data set" from the early site investigations before and during the construction of the existing SFR facility (1980-1985), and 2) "the recent data set" from the site investigation for the ongoing PSU (project extension of SFR; 2008-2009). The historic data set primarily consists of short-term double-packer tests, while the recent data set consists of PFL data, which reflect borehole inflow after several days of pumping. The two data sets exhibit a systematic difference in transmissivity, with higher values among the historic data (Figure 1-2). At least to some extent this difference reflects the short duration in the packer tests that implies inclusion of compartmentalised fracture transmissivity (see Appendix C). However, the extent to which this only reflects a discrepancy in hydraulic test condition versus a *true difference* in host-rock properties between the existing facility and its planned extension is not fully clear.

A drawback of packer data is that, at SKB's standard test scale (3 m in the historic data and 5 m in recent investigations), it does not resolve the details of fracture flow, and hence it is less applicable for stochastic DFN-modelling (i.e., the approach to model HRD in SDM-PSU). It may also be argued that the PFL data are more representative for the parameterisation of deformation zones, as it reflects effective properties of a large-scale pump test, and thus are more representative for the flow modelling in SR-PSU. However, some of the key deformation zones around SFR are only supported by the historic data set (e.g., ZFM871, ZFMNNE0869, and ZFMNNW1209).

Ten out of 40 deformation zones were given an initial hydraulic parameterisation in SDM-PSU, based on historic data, but were then re-assessed for SR-PSU, based on a suspicion of overestimated effective deformation-zone properties (Table 1-1). HCD parameterisation based on historic data is therefore identified

SVENSK KÄRNBRÄNSLEHANTERING AB

TD15 Complementary simulation cases in support of SR-PSU

as a conceptual uncertainty in SR-PSU. The significance of this uncertainty is evaluated by comparing the flow-simulation output (performance measures) between the two model setups in Table 1-1.

Table 1-1. Studied variants of HCD parameterisation[1]; base case (SR-PSU) compared to conservative parameterisation based on historic data (SDM-PSU)

Zone	SR-PSU[2] Log $T_{eff}(0)$	$\sigma_{LogTeff(0)}$	SDM-PSU Log $T_{eff}(0)$	Basis for conservative parameterisation (SDM-PSU)
ZFM871	-5.2	0.81	-4.8	Table 6-1 in Öhman et al. (2012)
ZFMA1	-4.8	0.55		
ZFMB10	-4.8	0.55		
ZFMENE3115	-6.5	0.91		
ZFMENE3135	-6.7	0.55		
ZFMENE3151	-6.7	0.55		
ZFMENE8031	-6.7	0.55		
ZFMENE8034	-6.7	0.55		
ZFMNE0870	-6.3	0.46	-6.2	Table 6-1 in Öhman et al. (2012)
ZFMNE3112	-6.6	0.62		
ZFMNE3118	-6.6	0.29	-6.2	Table 6-1 in Öhman et al. (2012)
ZFMNE3134	-6.7	0.55		
ZFMNE3137	-7.3	0.3		
ZFMNNE0725	-4.0	0.55		
ZFMNNE0869	-4.6	0.28		
ZFMNNE2308	-6.1	0.55		
ZFMNNE3130	-6.7	0.55		
ZFMNNE3264	-6.7	0.55		
ZFMNNE3265	-6.7	0.55		
ZFMNNE3266	-6.7	0.55		
ZFMNNW0999	-7.8	0.55		
ZFMNNW1034	-4.4	0.27		
ZFMNNW1209	-5.9	0.55		
ZFMNNW3113	-7.8	0.55		
ZFMNS3154	-4.4	0.55		
ZFMNW0002	-4.6	0.55	-3.6	Table 6-1 in Öhman et al. (2012)
ZFMNW0805a	-4.7	0.55	-4.3	Table 6-1 in Öhman et al. (2012)
ZFMNW0805b	-5.5	0.48	-4.7	Table 6-1 in Öhman et al. (2012)
ZFMWNW0001	-3.9	0.56	-2.9	Table A-1 in Öhman et al. (2013) (Data revision)
ZFMWNW0813	-5.9	0.55	-5.7	Table 6-1 in Öhman et al. (2012)
ZFMWNW0835	-5.2	0.71		
ZFMWNW0836	-7.1	0.55		
ZFMWNW1035	-5.0	0.64	-4.0	Table 6-1 in Öhman et al. (2012)
ZFMWNW1056	-7.1	0.55		
ZFMWNW3259	-5.3	0.55	-4.2	Table 6-1 in Öhman et al. (2012)
ZFMWNW3262	-4.6	0.55		
ZFMWNW3267	-6.7	0.55		

SVENSK KÄRNBRÄNSLEHANTERING AB

TD15 Complementary simulation cases in support of SR-PSU

ZFMWNW3268	-5.8	0.55
ZFMWNW8042	-6.0	0.55
ZFMWNW8043	-6.5	0.55

1) $T_{eff(0)}$ is the effective transmissivity parameterisation at ground surface (z = 0 m). The base case parameterisation assumes a depth trend, $T_{eff(z)} = T_{eff(0)} * 10^{(z/k)}$, where k is the depth interval over which transmissivity declines an order of magnitude. Internal variability in the hydraulic properties of HCDs is addressed by heterogeneous parameterisation variants, where the normal distributed random component N(0, σ) is superimposed onto $T_{eff(z)}$ in log space; here σ is the standard deviation of logarithmic transmissivity data at HCD intercepts (details in Öhman et al. 2012). The same variability is assumed in both the SR-PSU and SDM-PSU variants.
2) Table A6-1 in SKB 2013.

1.2.3   HRD parameterisation

The hydrogeological modelling divides the underlying bedrock into two conceptual components. The model components are defined based on confidence in geometrical inference: 1) the deterministic Hydraulic Conductor Domains (HCDs, which contain geological deformation zones and SBA structures) and 2) the less-fractured bedrock outside, the Hydraulic Rock-mass domain (HRD, consisting of spatially conditioned Unresolved PDZs, and the remnant flowing fracture network which is represented by means of a stochastic DFN model). This modelling task addresses two aspects of HRD parameterisation.

Parameterisation inside SFR Regional domain (alternative transmissivity-size model)

The DFN parameterisation was calibrated by means of a connectivity analysis (see Appendix G in Öhman et al. 2012), in which size-transmissivity relationships were established for each set and depth domain (Figure 1-1). This calibration is executed on a trial-and-error basis with the objective to match geometrical scan-line sampling of stochastic DFN realisations to the borehole-data set (i.e., the purpose of scan-line sampling is to achieve consistency between simulations and data in terms of geometrical bias and variability related to sample size). In principle, the size distribution of fractures is inferred by assuming that the discrepancy in borehole frequency between open fractures and PFL-f anomalies reflects the connectivity of the flowing fracture network. Three key assumptions in this approach are:
1) that the smallest fracture in the borehole data set is assumed to be equal to the borehole radius, $r_{bh} = 0.038$ m domain (purple line in Figure 1-1).
2) The PFL-f data set is truncated by a detection limit, taken as $T_{lim} = 2.5 \cdot 10^{-9}$ m^2/s (dark red line in Figure 1-1). In reality, the detection limit varies depending on local conditions in the logged boreholes. Also, the detection limit is controlled by two factors: the physical limitations in the measuring device and the practical limitations, related to the inference of discrete flow anomalies (e.g., Hurmerinta and Väisäsvaara 2009).
3) Fracture transmissivity is directly correlated to size (i.e., set-specific slopes in Figure 1-1)

Moreover, only fractures exceeding a side length of 4 m are included in the regional-scale numerical flow simulations (i.e., more precisely, a 2 m cut off is used for the horizontal set in the repository domain, while a 16 m cut off is used for all sets in the deep domain; illustrated by the purple-shaded area in Figure 1-1). Finally, the upper tail of transmissivity is trimmed by maximum values observed in data for each depth domain (red ovals in Figure 1-1) to avoid constraining the parameterisation to the maximum values observed in data. Note that this trimming is made based on elevation of the lowest corner of the simulated fractures, z (m), as opposed to categorisation by the three depth intervals.
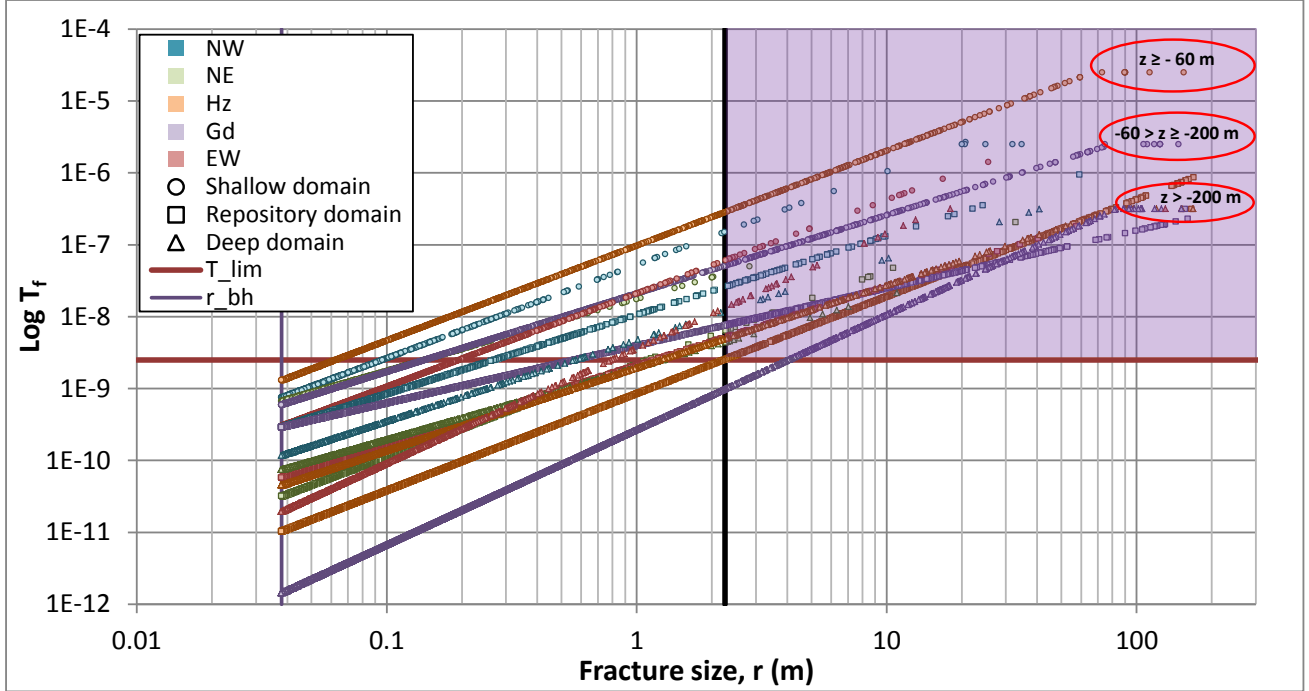
DokumentID
1578373, (1.0)

Sekretess
Öppen

Sida
7(165)

TD15 Complementary simulation cases in support of SR-PSU

Figure 1-1. Size-transmissivity correlation in the original DFN parameterisation (i.e., 5 fracture sets in three depth domains; see Appendix G in Öhman et al. 2012) with applied cut-off limits (indicated by lines, purple area, and red ovals).

The fracture transmissivity parameterisation, T_f, can be coupled to fracture size by the parameters *a* and *b*

$$T_f = \left(a\, r^b\right) 10^{\sigma_{stoch}\, N(0,1)}. \tag{1-1}$$

if *r* (m) is the fracture radius and, σ_{stoch}, is the standard deviation in log-space of the stochastic component in fracture transmissivity. The DFN parameterisation in SDM-PSU (Öhman et al. 2012) is assumed to be directly size-correlated, i.e., the stochastic component σ_{stoch} in Eq. (1-1) is set to null, which is regarded to be a pessimistic assumption (i.e., rendering higher flows through the rock vaults).

As an alternative in SR-Site, the stochastic component was set to $\sigma_{stoch} = 1.0$ (or less, for sets with small variability in transmissivity) in a parameterisation variant referred to as the semi-correlated relationship. In this variant, the size parameters *a* and *b*, Eq. (1-1), had to be adjusted to preserve the total variability in fracture transmissivity as seen by a simulated borehole (see Follin 2008).

Hence, one of the objectives in this modelling task is to examine if the semi-correlated transmissivity parameterisation will render a more pessimistic performance measures in PSU. The numerical implementation is described in section 2.4 and Appendix D.

Heterogeneity outside SFR Regional domain (stochastic DFN realisations)

The sensitivity analysis of uncertainty in performance measures arising from the combined effects of heterogeneity and conceptual uncertainty in bedrock parameterisation was limited to address the bedrock inside the SFR Regional domain (Öhman et al. 2014). The HRD outside the SFR Regional domain was parameterised based on a single DFN realisation. Thus, the hydraulic heterogeneity outside the SFR Regional domain was represented as a "static" component in the sensitivity analysis. The reasons for doing so were:

SVENSK KÄRNBRÄNSLEHANTERING AB

DokumentID
1578373, (1.0)

Sekretess
Öppen

Sida
8(165)

TD15 Complementary simulation cases in support of SR-PSU

1) Priorities: uncertainties in the SFR nearfield (where data are abundant) were prioritised over the more peripheral regions (where little or no data are available)
2) Relevance: preliminary simulations demonstrated that the vast majority of flow paths (99.9% for SFR1 and 95% for SFR3) discharge inside the SFR Regional domain, which was taken as support for prioritising the SFR nearfield.

On the other hand, the particle discharge locations are controlled by structural channelling (HCD or HRD), and hence, there may exist other DFN realisations that redirect the flow paths across the SFR Regional domain boundary, which in turn implies that the downstream HRD parameterisation indeed may affect the performance measures. One of the objectives in this modelling task is therefore to examine the sensitivity to stochastic DFN variability in the bedrock outside the SFR Regional domain.

1.2.4 Deterministic SBA structures

The hydrogeological model SDM-PSU is based on the established model components HRD and HCD, but also involves the additional components unresolved PDZ and SBA structures (SBA1 to SBA8). These new model components are modelled separately in order to make the most out of deterministic information (Appendices A and B in Öhman et al. 2012). It is preferable to make the most out of deterministical information on hydrogeological anomalies in the vicinity of the planned SFR extension in order to resolve features that may be of particular relevance for the location of SFR3 and its safety assessment, as it allows honouring the location of both intercepts and hydraulic connections. However, deterministic modelling has two drawbacks:
1) Risk of over-determinism, as the uncertainty of interpolated geometry/parameterisation between conditional data (borehole intercepts) tends to be overlooked (i.e., this uncertainty could be handled by studying variants)
2) Risk of underrepresentation the potential existence of similar features in unchartered parts of the domain (i.e., as structural modelling is intimately associated to supporting data, and data support is only provided in investigated areas). As a comparison, the deterministic modelling of deformation zones (Curtis et al. 2011) relies on extrapolation of lineament data, which is ubiquitous and thus less affected by gaps in borehole coverage. The deterministical modelling of SBA structures lacks the support from aerial data coverage (i.e., geometrical conditioning) and is therefore comparatively more uncertain.

The most straightforward approach to tackle the uncertainty regarding coverage in unchartered areas is stochastic modelling (e.g., a tentative approach for SBA structures is suggested in Appendix B in Öhman et al. 2013). However, the deterministic modelling of SBA structures is based on a range of underlying data types, and therefore their role in stochastic model representation – in an alternative approach without deterministic SBA inference – will vary depending on type (i.e., as indicated by "Yes" or "No" in Table 1-2). In most cases, the deterministic SBA structures *do not replace* stochastic modelling, but are based on data that are not stochastically modelled. Four data types are identified:
1) Three borehole intercepts are included in deformation-zone parameterisation. These do *not* require an alternative stochastic modelling approach.
2) The hydrogeological modelling only includes PFL-f data (i.e., discrete flow anomalies associated to core-logged fractures) in the hydraulic parameterisation of rock mass outside deformation zones the historic data set (see Öhman et al. 2012); therefore, six SBA intercepts supported by: a) historic data and b) recent boreholes that lack PFL-f data do *not* require alternative modelling,
3) Four borehole intercepts are identified as Unresolved PDZs. The alternative stochastic representation is by means of the structural inference of Unresolved PDZs suggested in Appendix A of Öhman et al. (2012), which would increase the intensity of Unresolved PDZs by $4/7 = 57\%$.

4) Two borehole intercepts are covered by PFL-f data and lack alternative structural inference (i.e., 193 m in KFR27 and 187-207 m in KFR102A; Table 1-2). The alternative model representation is inclusion in the stochastic (poissonian) DFN model.

Table 1-2. Alternative interpretation of modelled SBA intercepts (Based on Table B-1, Öhman et al. 2012)

SBA	Borehole	Intercept (BHL, m)	Data support	Alternative stochastic interpretation
SBA1	KFR27	55	5m PFL, radar, geophysics	**No**. Flow anomalies not resolved in 5m PFL; hence not included in DFN-model support[1].
SBA1	HFR102	eoh[2]	Hydraulic response, drilling responses, injection test	**No**. The injection test does not resolve flow anomalies; hence not included in the DFN-model support.
SBA2	KFR27	98	5 m PFL, geophysics	**No**. Flow anomalies not resolved in 5m PFL; hence not included in DFN-model support[1].
SBA2	KFR102A	72	PFL-f (hidden by installation)	**No**. The flow anomaly cannot be coupled to boremap; hence not included in the DFN-model support.
SBA2/ SBA3	KFR103	86	PFL-f, drilling responses	**Yes,** in the model for Unresolved PDZ
SBA3	HFR106	39	HTHB, radar reflector, drilling responses	**Yes,** in the model for Unresolved PDZ
SBA4	KFR106	71	PFL-f, drilling responses	**No**. Data used in parameterisation of ZFMWNW3262
SBA4/ SBA5	KFR103	182	PFL-f, drilling responses	**No**. Data used in parameterisation of ZFMWNW3262
SBA5	KFR106	155	PFL-f, drilling responses	**Yes,** in the model for Unresolved PDZ
SBA6	KFR27	193	PFL-f, drilling responses	**Yes,** in DFN model[3] (Single fracture; $T \approx 7 \cdot 10^{-6}$ m^2/s)
SBA6	KFR101	181	PFL-f, drilling responses	**Yes,** in the model for Unresolved PDZ
SBA6	KFR102A	187-207	PFL-f, drilling responses	**Yes,** in DFN model[3] (Fracture cluster; $T \approx 2 \cdot 10^{-6}$ m^2/s)
SBA6	KFR102B	172	PFL-f, drilling responses	**No**. Data used in parameterisation of ZFMENE3112
SBA7	Table D-2, Öhman et al. (2012)		Based on earlier interpretation of (Carlsson et al. 1985)	**No**. Historic data are not included in the support of the DFN-model.
SBA8	KFR69, tunnel mapping			**No**. Historic data are not included in the DFN-model support.

1) It has been demonstrated that the hydraulic 5m PFL data are covered by the heterogeneity of the DFN model (Figure G-19, Appendix G of Öhman et al. 2012)
2) eoh = end of borehole
3) The alternative interpretation of these data is inclusion in the stochastic DFN model.

The two intercepts – which alternatively could have been stochastically represented by DFN modelling – belong to the upper tail of transmissivity data. The DFN model relies on an assumed correlation between power-law scaled fracture size and transmissivity, where high-transmissive fractures are few compared to the abundance of fractures close to detection limit. The skewed size distribution implies a relatively large uncertainty in the upper-tail of the calibrated DFN transmissivity (i.e., the power law is best fit to the

SVENSK KÄRNBRÄNSLEHANTERING AB

DokumentID
1578373, (1.0)

Sekretess
Öppen

Sida
10(165)

TD15 Complementary simulation cases in support of SR-PSU

transmissivity-size interval where fractures are numerous; the sample size is small in the upper-tail, but has high leverage on simulated flow). Moreover, the DFN representation of highly transmissive fractures, as large homogeneous squared planes, is not very realistic (discussed in Öhman et al. 2012).

The role of these two SBA intercepts is therefore analysed in context of stochastic variability by means of simulated borehole exploration of connected DFN realisations for the SFR Regional domain, R01 to R99 (SR-PSU TD05, Öhman and Bockgård 2013). Non-connected fracture clusters (compartmentalisations) are removed, and the fracture generation employs relevant size cut-offs[4] for flow modelling in SR-PSU, which partly censors the fracture populations at low transmissivity, below $T \approx 10^{-7}$ m^2/s. The sampled fracture transmissivity is binned per 5 m borehole length and compared against 5 m sequential PFL data, using the true geometries of the underlying "DFN boreholes" (i.e., which is important for weighting fracture orientations and depth domains; Figure 1-2b). Note that this comparison differs from the DFN calibration, which was conducted in terms of PFL-f frequency, per set and depth domain. The simulated exploration demonstrates that the PFL data set – including HRD, PDZ, and Unresolved PDZs – are well-covered by the stochastic, poissonian HRD model parameterisation (i.e., sampled DFN transmissivity; Figure 1-2b). Again, this reinforces the notion that the deterministic SBA structures *do not replace* stochastic modelling, but should be envisaged as an *additional* deterministic representation.

The historic short-term packer data are compared correspondingly at the 3 m scale (Figure 1-2a). The sampled DFN fractures in simulated exploration are clearly less transmissive than the historic data (red line; Figure 1-2a). This could be interpreted as evidence of different hydrogeological conditions between the existing facility and its planned extension (i.e., since the DFN is parameterised based on data from the planned location for SFR3). However, for two reasons, the comparison is not fully valid:

1) the short test duration of double-packer tests in the historic data implies inclusion of compartmentalised fracture transmissivity. These data are therefore not fully comparable with simulations, as non-connecting fractures have been removed from the DFN realisations.
2) The historic data set is of poorer quality, and therefore the differentiation between HRD, Unresolved PDZs, and SBA cannot be made with the same level of confidence as in the new data set.

---
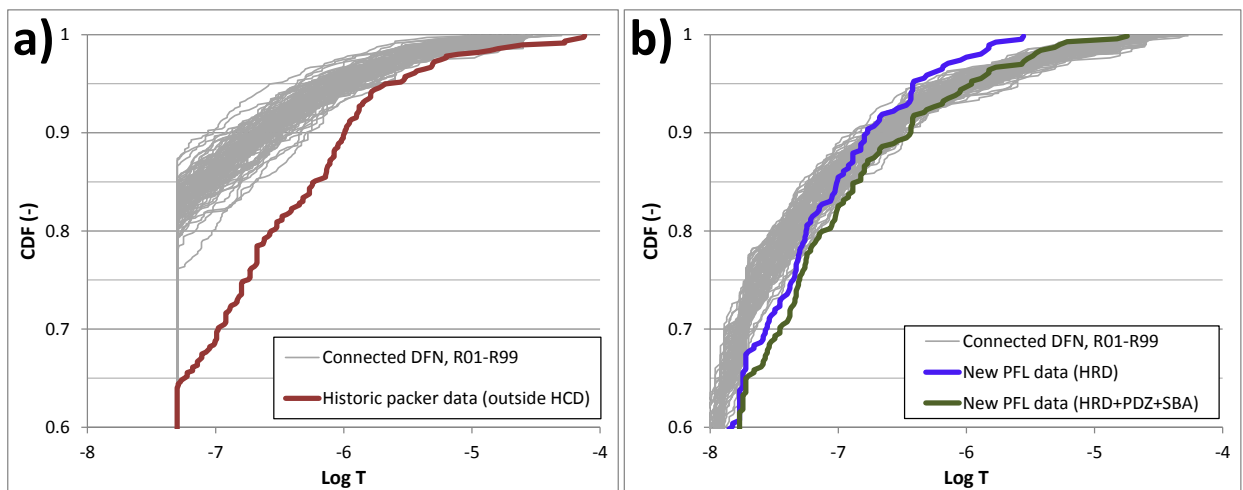
[4] More precisely, only fractures within a specified size interval are included; minimum fracture side length ranges from 2 to 16 m, depending on fracture set and depth domain. Furthermore, only the hydraulically connected subset of the fracture network is modelled, details provided in Öhman and Bockgård (2013).

Figure 1-2. Transmissivity data compared against simulated exploration of DFN realisations at the SFR Regional-domain scale (grey lines). Note truncation of y-axis to resolve the upper tail of distributions and that the simulations are censored below $T \approx 10^{-7}$ m^2/s by the applied size cut-off and – for the comparison against historic data – the removal of non-connected fractures.

The simulated fracture transmissivity covers the upper tail of the new data set comparatively well, provided that the two SBA intercepts and all Unresolved PDZ are included (green line; Figure 1-2b). This demonstrates that all the underlying data of the SBA structures are, either covered within the variability of the DFN model (Figure 1-2b), included as Unresolved PDZs or HCDs (Table 1-2), or simply lack alternative interpretation (Table 1-2). In conclusion, the alternative case to deterministic SBA structures is a parameterisation variant *without SBA structures*.

The geometrical extrapolation of SBA structures is also recognised as highly uncertain. Alternative spatial extensions of the SBA structures (i.e., terminations against steeply dipping deformation zones) could be explored to evaluate the significance of this uncertainty in terms of performance measures. However, an analogy can be made to a previous analysis of an extended structural ZFM871 (SR-PSU TD08; Öhman 2014), where the effects on simulated performance measures was found to be surprisingly small. The reason for this insensitivity to horizontal extent of ZFM871 is that, irrespectively if it extends across NW0805 and NNE0869 (or not), these structures tend to re-direct the particle trajectories from ZFM871, upwards, to exit at biosphere object 157_2 (Figure 1-8). Thus, the following can be concluded:

1) The SBA structures are not more likely to extend across deformation zones NW0805 and NNE0869 than is ZFM871
2) Even if the structures do extend beyond deformation zones NW0805 and NNE0869, the experiences from similar modelling of ZFM871 (Öhman 2014) indicates that, at the intersection with steeply dipping zones, the flow paths are re-directed towards ground surface (biosphere object 157_2; Figure 1-8), and hence the effects of geometrical extension are expected to be small.
3) The hydrogeological premises are favourable for particle exit at biosphere object 157_2, more or less irrespectively of structural geometry (as analysed in detail in Appendix E, along with a probabilistic analysis of re-direction to downstream biosphere objects via stochastic SBA features, as well as the homogeneous model setup, without deformation zones, in SR-PSU TD10, Öhman (2013)).

In this study, the role of SBA structures is evaluated in terms of performance measures by a separate model setup where the deterministic SBA structures are not included (base case, 5000 AD; Section 1.3).

1.2.5   ECPM-scaling effects in model output (grid discretisation)

DarcyTools is a porous-medium code, and as such employs continuum-approximation approach in which fractured rock is represented by the properties of a so-called Equivalent Continuum Porous Medium (ECPM). ECPM properties are calculated based on the deterministic and stochastic components of the hydrogeological model (HCD and HRD), and as such bears the traits of the underlying structural model as well as fracture-network realisations. The calculation of ECPM properties is referred to as upscaling, as unlike the underlying HCD and HRD model components, ECPM properties refer to a specific modelling scale (i.e. cell size). Thus, ECPM properties are valid only for a given grid discretisation (i.e., spatial resolution), and therefore must be re-calculated if the grid is refined. Furthermore, DarcyTools employs a geometrical upscaling method, which is referred to as the GEHYCO algorithm (Svensson et al. 2010). The key concept of the GEHYCO algorithm is to lump the properties of all fractures that are geometrically associated to each cell by means of a control-volume concept. However, this implicitly assumes that all fractures within each control volume are hydraulically connected, which is not necessarily true. Therefore, the hydraulic connectivity is to some extent controlled by the size of cell control volumes (i.e., grid resolution). As the result, geometrical upscaling is not

DokumentID
1578373, (1.0)

Sekretess
Öppen

Sida
12(165)

TD15 Complementary simulation cases in support of SR-PSU

necessarily hydraulically consistent over a wide range of geometrical scales (i.e., grid resolutions). Furthermore, geometrically upscaled ECPM modelling is not necessarily conservative, as for instance, the ECPM porosity in travel-time calculations risk being exaggerated by including undue nearby fractures that fall inside the property-averaging control volume, without being connected to the flow path.

On the other hand, the large-scale flow paths which are typically assessed by particle-tracking performance measures tend to be controlled by the most dominant hydraulic structures (i.e., the most transmissive deformation zones or fractures), which typically exceed grid cells in size, and hence their hydraulic connectivity is less sensitive to grid-scaling effects. As the rule of thumb, it is recommended that the grid resolution is on par with the minimum fracture size (as the fracture connectivity is reasonably well resolved if the fractures and the gaps between fractures are resolved by cells of smaller size).

Moreover, DarcyTools employs an unstructured grid which allows local grid refinement in locations of particular interest, where detailed geometry must be resolved, and vice-versa; the computational demand can be significantly reduced by a rudimentary resolution in peripheral parts of the domain. The drawback of this utility is that large-scale model setups typically employ complex nesting of grid refinement levels, in which scaling effects are difficult to assess.

Consequently, potential scaling effects of the ECPM conversion are analysed here.

1.2.6   Transient tunnel inflow

Since its construction in 1985, both the monitored tunnel inflow to SFR (Figure 1-3a) and the pressure in surrounding boreholes (see Öhman et al. 2012, 2013) exhibit a long-term decline, at a more or less constant rate. Tunnel inflow and borehole pressure data are key to conceptualising the large-scale hydrogeological system, and provide potential means to calibrate, constrain, or confirm a model parameterisation that is based on local-scale borehole data (i.e., borehole data typically reflects point or line measurements of the hydrogeological system, which does not provide a holistic characterisation of the large-scale system). Moreover, the borehole data used in model parametrisation reflect hydraulic tests where the time scale is very short compared to the 30 year time series of tunnel inflow (i.e., the construction and operation of SFR can be envisaged as a long-duration, large-scale constant-head test). The duration of hydraulic tests typically range from c. 5 minutes (i.e., double-packer tests) to days (i.e., PFL logging), and where a duration of several days is typically envisaged as "large-scale" and "pseudo stationary" (see discussion on PFL data in Öhman et al. 2012).

The integration of borehole data and tunnel inflow data was identified as a key challenge in the site-descriptive modelling of SFR. Owing to conceptual uncertainty, two end points were identified for the interpretation of the transient state of tunnel inflow and surrounding drawdown:

1) **non-permanent artefacts**: it is caused by flow-resistances that develop successively under open-tunnel conditions, but are assumed to be *reversible* over the time scales addressed in SR-PSU. Several possible phenomena are offered in Öhman et al. (2013), including hydro-mechanical fracture closure, chemical precipitation, bacterial or clay-particle clogging, developing unsaturated fracture flow, etc. This flow resistance is unrepresentative of the rock-mass properties under saturated conditions that are relevant for long-term safety analysis. Thus, borehole data, and perhaps also the early inflow data, are more representative of the hydrogeological system at SFR, as they reflect the virgin rock (i.e., less affected by skin artefacts).

2) **natural scaling effects**: the long-term trend signifies the scale-dependency in the connectivity of the flowing fracture network. Thus, the gradually declining tunnel inflow represents the hydrogeological system at wider scales (i.e., both temporal and spatial) than is resolved in hydraulic borehole data.

Thus, data reflecting large scale and long test periods (i.e., tunnel inflow and monitored head in boreholes, with emphasis to the later phase) are more representative for the long-term safety analysis of SFR.

Thus, the main difference between the two end points is a conceptual uncertainty concerning the integration of scale dependency in data, or more precisely, how to place the long-term data in context of the hydrogeological model parameterisation. In practise, this dilemma implies a parameterisation uncertainty; place confidence in borehole data and early inflow data (i.e., end point 1) leads to a higher conductivity parameterisation than its alternative, to place more confidence in the late-phase of inflow data (i.e., end point 2). The site-descriptive modelling decided to rely more on borehole data, as: 1) it was considered to be more conservative for long-term safety analysis, 2) the inference from long-term data (pressure and inflow) are severely subject to the uncertainty of equifinality, 3) documented grouting is a confirmed flow resistance which reduces the representativity of inflow data, and 4) more applicable for parameterising the bedrock around the planned extension, as compared to an inflow-based parameterisation (see discussion in Öhman et al. 2013).

This study explores end point 2 (i.e., in contrast to the inference in Öhman et al. 2013), namely that the transient pattern in tunnel-inflow data is *not* attributed to the development of artificial skin effects, but instead to scaling effects of a poorly connected fracture-network system (see Section 1.3). The transient state of inflow and pressure data, after more than 30 years of operation under open-tunnel conditions, indicates that the hydrogeological system is extremely slow-responding. Moreover, diagnostic analysis of the derivative of reciprocal inflow (Figure 1-3b) suggests the possibility of a system of limited areal extent, with little or negligible net inflow from outside of the hydrogeological system (Jan-Erik Ludvigson, personal communication).
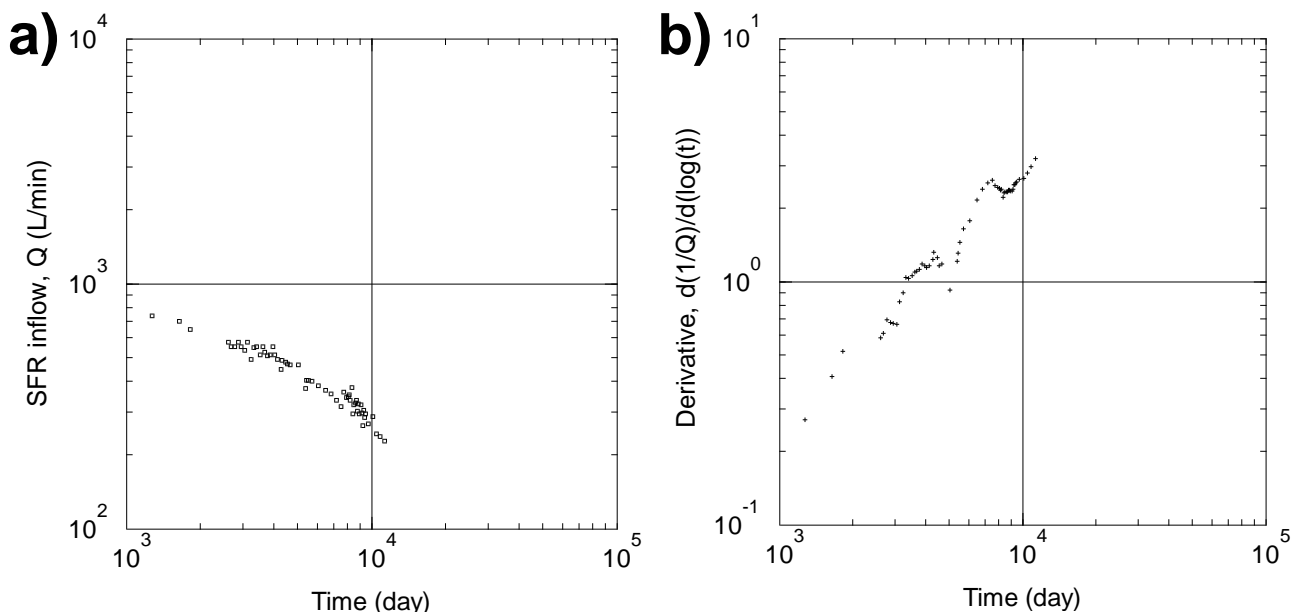
Figure 1-3. Declining inflow to SFR since 1988; a) total inflow to the lower pumping pit at SFR (Nedre DränageBassäng; NDB) and b) corresponding diagnostic derivative of reciprocal inflow versus time.

On the one hand, it is questionable if this extremely slowly responding flow regime can be attributed to *true* scaling effects of hydrogeological properties alone (i.e., assuming that no flow resistances arise from open-tunnel conditions). Note that although the documented grouting is a known source to tunnel-wall resistance that makes tunnel inflow less representative of the true hydrogeological system, no grouting was performed

SVENSK KÄRNBRÄNSLEHANTERING AB

DokumentID
1578373, (1.0)

Sekretess
Öppen

Sida
14(165)

TD15 Complementary simulation cases in support of SR-PSU

after the completion of SFR, and hence its should not affect the long-term trend in data. On the other, this alternative hypothesis has data support from several indications of fracture-network compartmentalisation and presence of extremely isolated groundwater types (Öhman et al. 2012).

1.2.7   Alternative localisation of SFR3 (Forsmark lens)

An alternative localisation of SFR3 in the low-conductive Forsmark lens (Figure 1-4) is studied in order to provide a reference case for the performance at its planned localisation (i.e., referring to its location in SFR Regional domain). The evaluation of repository performance is based on flow modelling, which requires underpinning by an underlying Site-Descriptive Model.

A notable shortcoming of the evaluation is that the alternative emplacement of SFR3 (i.e., the shallow bedrock in the Forsmark lens) has not been characterised at the same high level of detail as in the SFR Regional model domain. This causes a disparity in the model setups of the two localisation studies, which must be kept in mind in the evaluation of performance and its uncertainty. More precisely:

1) The resolution level for deterministical modelling of geological structures is 1,000 m in the Forsmark lens, as compared to 300 m employed in SFR Regional domain. In other words, structures in the size interval 300 to 1,000 m are deterministically modelled for the host rock of the *planned* localisation, while it is stochastically modelled in the *alternative* localisation. This model discrepancy affects the uncertainty in model predictions, which introduces a bias in the comparison between the two locations. For example, if the structural model of the alternative location was resolved to the same level of detail, it might demonstrate that the SFR3 repository cannot be entirely located outside deformation zones, as is the case for its applied location in the SFR Regional domain.

2) The layout of the planned localisation, including its waste content of specific disposal rooms, has – to some extent – been adapted to local structural setting in the SFR Regional domain. The corresponding detailed adaptation is not possible for the alternative localisation of SFR3, as its structural model does not hold the same level of resolution outside the SFR Regional domain. To compensate for this discrepancy, all 6 disposal rooms of SFR3 are treated as interchangeable in the alternative localisation (i.e., as it may be expected that, once the local hydrogeology is known in better detail, the layout may be adapted so as to avoid the most waterbearing structures in the disposal room that is most critical in the safety analysis).

The comparatively larger stochastic model component in the Forsmark SDM has a (i.e., a larger subpopulation of structures without deterministic inference), implies a larger focus on uncertainty analysis in the alternative localisation study. An exploratory statistical analysis of the stochastic DFN model variability is therefore provided in Section 2.8.

The deep repository for spent nuclear fuel is not included in the flow simulations. Moreover, this study does not address the advantages or disadvantages of the joint construction, operation, and post-closure safety of the two co-existing repositories.

DokumentID
1578373, (1.0)

Sekretess
Öppen

Sida
15(165)

TD15 Complementary simulation cases in support of SR-PSU

Fracture domains at repository depth (-470 m)

▨ (FFM01 blue)	FFM01
▨ (FFM06 teal)	FFM06
––––	Deformation zones at repository depth (-470 m)
▨ (grey)	Respect distance to deformation zones
▭	Local model domain, 2.1
▦	Repository
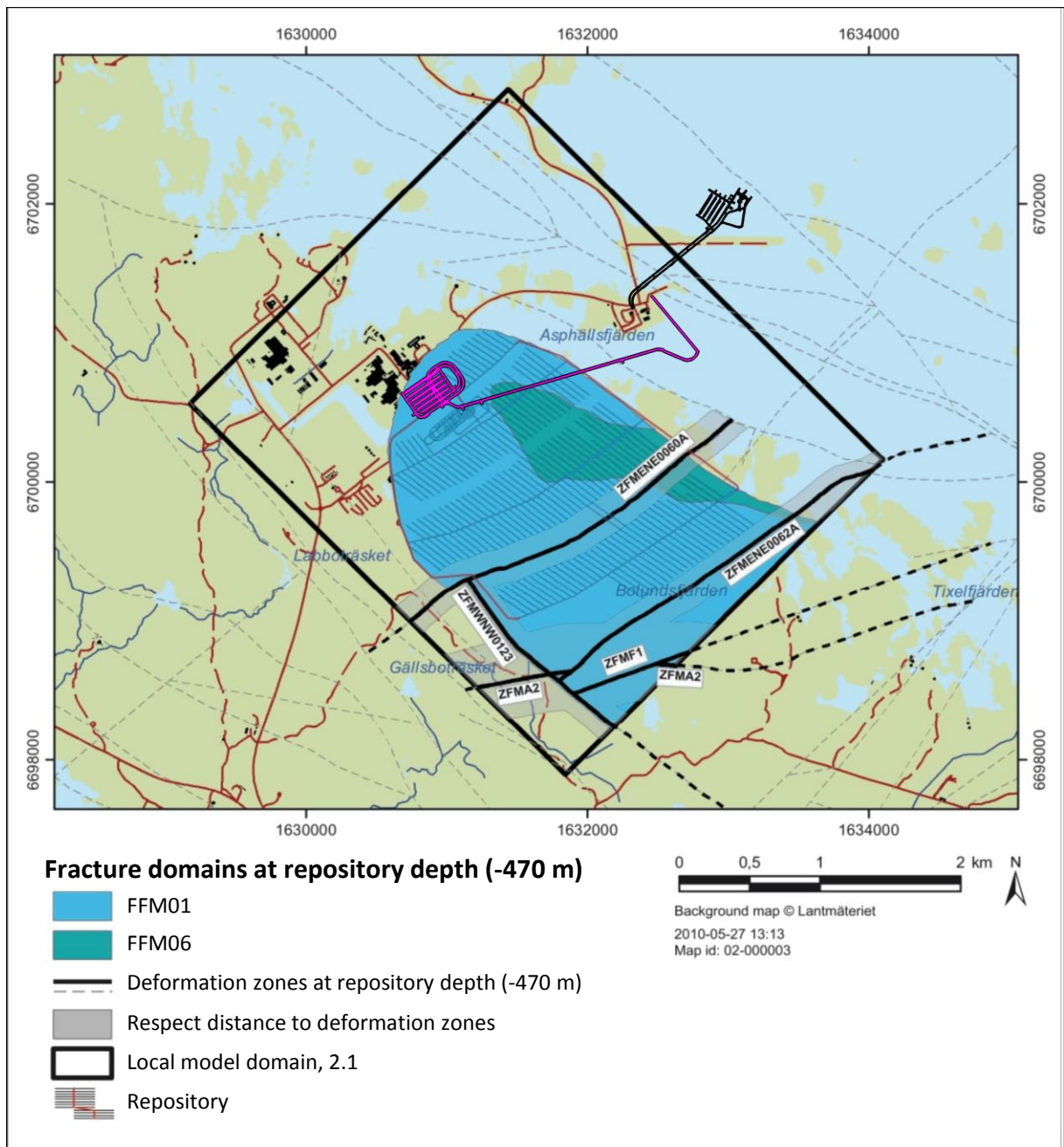
Figure 1-4. Alternative location of SFR3 near the planned ramp for the deep geological repository in the tectonic Forsmark lens (pink tunnel geometry; see close-up in Figure 1-5).

1.3 Objectives

The two objectives of this modelling task are to address selected issues in the hydrogeological model:
1) Numerical sensitivity analysis to quantify the significance of hydrogeological modelling uncertainties in SR-PSU (Section 1.3.1), and

DokumentID
1578373, (1.0)

Sekretess
Öppen

Sida
16(165)

TD15 Complementary simulation cases in support of SR-PSU

2) Complementary flow modelling, to demonstrate an alternative localisation of SFR3 (the Forsmark lens), as well as, an alternative conceptual interpretation to the ongoing decline in tunnel inflow to SFR1 (Section 1.3.2).

1.3.1 Sensitivity analysis of aspects in flow modelling

An inventory of uncertainties raised in SDM-PSU (Öhman et al. 2012, 2013) and in SR-PSU has identified a number of issues in the hydrogeological modelling (Appendix A). It has been decided to evaluate the significance of the following issues in the current modelling task:

- HSD parameterisation
- HCD (role of historic packer data)
- HRD: Size-transmissivity correlation in DFN parameterisation
- HRD: Heterogeneity outside SFR Regional domain
- ECPM scaling effects

The sensitivity to selected modelling issues is studied by exploring the effect of perturbations in the model setup. In a first step, parameterisation variants are defined, which are intended to cover the range of uncertainty. In the second step, groundwater flow is solved by numerical simulation (DarcyTools) to determine performance measures for each parameterisation variant. Finally, the performance measures are compared against those from a reference case, to evaluate the significance of uncertainty in the model setup. The reference case is defined as the base-case parameter setting for the shore-line displacement at 5000 AD, which has been considered to be the most relevant case in earlier sensitivity studies (see Öhman et al. 2014 and Odén et al. 2014). As stated above, the variants include HSD parameterisation, size-transmissivity correlation in DFN parameterisation, stochastic variability in the DFN outside the SFR Regional domain, and scaling effects in the ECPM approach. The parameterisation variants are listed in Table 1-3. The details of their numerical implementation are provided in Chapter 2, and the results are presented in Chapter 3.

Table 1-3. Parameterisation variants

HSD parameterisation variants

	HSD case	Hydraulic conductivity, K_{HSD} (m/s)
1	Reference cases (DFN R85 and R18)	Base case K_{HSD} (i.e., Table 4-5 in Öhman et al. 2014)
2	Homogeneous	$K_{HSD} = 10^{-8}$ (all regolith layers)
3	Low-conductive	Base case K_{HSD}/ 10
4	High-conductive	Base case K_{HSD} × 10
5	Bedrock surface choking	Reduce HSD/HRD interface, $K_z = 10^{-7}$
6	Sea-floor choking[1]	Reduce uppermost layer below sea, 1/10

HCD parameterisation (role of historic data)

1	Data-support variants (Table 1-1)	Reference: Base case, DFN R85

HRD: Semi-correlated transmissivity parameterisation (DFN)

	Geometrical reference case[2]	Parameterisation realisation
1	Base case, DFN R85	SC [R01 … R05]
2	Base case, DFN R18	SC [R01 … R05]

HRD: Heterogeneity outside SFR Regional domain

	Inside the SFR Regional domain	Outside the SFR Regional domain
1	Reference case	Original realisation (i.e., static DFN in Öhman et al. 2014)
2	Stochastic DFN realisations	DFN [R01 … R05]

Role of SBA structures

1	Case without SBA structures	Reference: Base case, DFN R85

ECPM scaling effects

Grid refinement case	Target cell size (m)

1	Reference case	8
2	Refinement in particle-tracking domain	4
3	Refinement along particle trajectories	2

1) Only applies to the uppermost HSD layer (1 m), applied at the time slice 2500AD.
2) The original DFN realisation defines the geometry of fractures, while the random seed 1 to 5 defines the random component in the semi-correlated transmissivity parameterisation.
3) The parameterisation inside the SFR Regional domain is kept constant [Base case, DFN R85], while the HRD outside the SFR Regional domain (in a defined domain downstream from SFR; see Figure 2-7) is addressed by means of stochastic realisations.

1.3.2 Complementary flow modelling

Alternative localisation of SFR3 (Forsmark lens)

The alternative localisation of SFR3 is emplaced in the Forsmark lens, near the planned ramp to the deep geological repository for spent nuclear fuel (Figure 1-5). The shallow bedrock of the Forsmark lens is referred to as a Shallow Bedrock Aquifer and deterministically modelled by means of sheet-joint structures down to a depth of c. 150 m (Follin 2008). To avoid highly transmissive fractures associated to shallow bedrock, the alternative localisation employs a depth interval z = -200 to -220 m. Moreover, it is accommodated to avoid contact with closeby deterministic deformation zones, which requires a minor rotation of SFR3 relative to its planned localisation.

The deterministically modelled deformation zones can be avoided (i.e., at least those with side lengths exceeding 1,000 m), which implies that the repository performance is primarily subject to stochastic model components. The stochastic model components include smaller deformation zones (those with side lengths in the range 300 to 1,000 m) and the less fractured bedrock outside zones (HRD). These model components are modelled by means of a stochastic Discrete Fracture Network (DFN) model to reflect heterogeneity in both geometry and hydraulic parameterisation. Thus, the repository performance must be evaluated for a minor ensemble of DFN realisations that covers a reasonable range of the heterogeneity in bedrock properties. As the stochastic model component is larger in SDM-Site Forsmark, as compared to SDM-PSU (i.e., no deterministic inference for structures with side lengths in the range 300 to 1,000 m), the alternative localisation study is more subject to uncertainty, compared to the host rock for the planned localisation.

The following approach is taken to provide a reasonable estimate of the variability range of local bedrock properties in the alternative localisation of SFR3:
1) nine DFN realisations[5] are explored geometrically, to identify three representative realisations that are expected to cover the range of crossflow through disposal rooms (Section 2.8).
2) the three realisations are implemented into DarcyTools, and flow is solved under three time slices (2000AD, 2500AD, and 5000AD).

---

[5] Realisations R01 to R08 and R12 in delivery from AMEC [SRS-FFM01-06_v4_alterFinal_r1-12_asc]

SVENSK KÄRNBRÄNSLEHANTERING AB

DokumentID
1578373, (1.0)

Sekretess
Öppen

Sida
18(165)

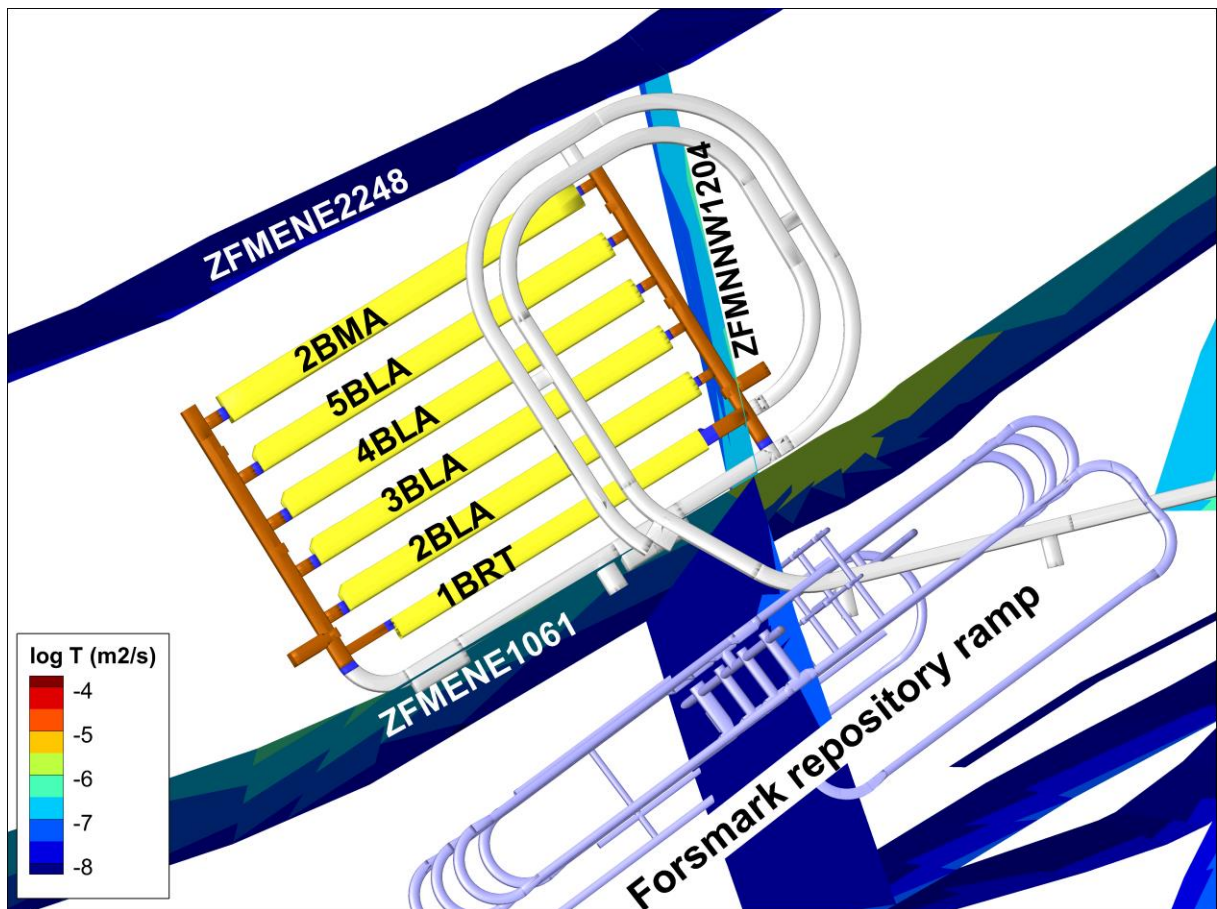TD15 Complementary simulation cases in support of SR-PSU

Figure 1-5. Alternative location of SFR3 in the tectonic Forsmark lens in context of deterministic deformation zones and the ramp to the deep repository for spent nuclear fuel (overview in Figure 1-4).

Simulating the declining inflow to SFR1 as a transient effect

Earlier simulations have assumed that the declining tunnel inflow to SFR is caused by a gradually developing resistance in the surrounding bedrock. In addition to grouting efforts (i.e., a known, but static flow resistance), this flow resistance can arise from several phenomena, or more likely a combination of several phenomena (i.e., including hydro-mechanical closure, microbial growth, chemical precipitation, re-distribution of clay infill, development of unsaturated flow, or gas-bubble formation from depressurisation of dissolved gas; see discussion in Öhman et al. 2012). Collectively, these phenomena may be referred to as skin effects. Note however, that all processes are not necessarily limited to the proximity of the tunnel wall.

This study examines (apparent) transient storage effects of a compartmentalised fracture network as an alternative explanation to the declining inflow. That is: under what premises it is possible to simulate the declining inflow as a pure transient effect, i.e., under the assumption that *no* flow-resistance effects develop (i.e., apart from documented grouting, Öhman et al. 2012). The continuing decline after more than 30 years of operation under open-tunnel conditions implies that the hydraulic system must be extremely slow. The response rate of a hydraulic system (or rate of hydraulic communication) is controlled by diffusivity, defined by the ratio $\alpha = T/S$ (for a structure). For radial flow in a formation of thickness b (m), T can be substituted by $K \cdot b$ and S by $S_s \cdot b$, rendering $\alpha = K/S_s$ (in terms of volumetric ECPM properties). Thus, modelling the gradually declining inflow to SFR as a transient storage effect implies that the hydraulic diffusivity must be

low, or in other words that the specific storage, S_s, is unusually high compared to the hydraulic conductivity, K.

DarcyTools employs upscaled volume-averaged bedrock properties of an underlying fracture network, referred to as Equivalent Continuum Porous Medium (ECPM) properties (Section 2.1; Svensson et al. 2010). Thus, its specific-storativity parameterisation, $S_{S,ECPM}$ (1/m), is upscaled from the storativity of fractures. However, storativity is an uncertain model parameter, as it assessment from field data relies on idealised conditions that are not necessarily valid for fractured bedrock (see discussion on *apparent* storativity, below). The default assumption in DFN upscaling is to assume that all fractures have a specific storativity of $S_{S,Frac}$ $=10^{-6}$ m^{-1}. Rhén et al. (1997) has suggested an empirical correlation between fracture storativity and transmissivity

$$S = 0.0007\,\sqrt{T}\ . \tag{1-2}$$

This empirical relation suggests renders low storativity values (e.g., $S \approx 10^{-7}$ for $T = 10^{-7}$ m^2/s).

Storativity, as evaluated from hydraulic tests in porous media, is a physical property of the aquifer that reflects its capacity to release groundwater under depressurisation, and is related to the strength of the aquifer skeleton (i.e., hydromechanical coupling to loading). Apparent storativity, S_0 (-), as evaluated from crosshole tests in bedrock, is well known to be an indicator of fracture connectivity and/or transmissivity heterogeneity (e.g., Meier et al. 1998). The term apparent is used to emphasise that the evaluated property should *not* be mistaken for the local material properties of the rock, analogous to tests in porous media, but instead, an effective property reflecting fracture connectivity along a flow path (i.e., between two boreholes in an interference test; Meier et al. 1998, Sánchez-Villla et al. 1999, Ludvigson and Hjerne 2014).

The PSU investigation programme included two controlled interference tests (HFR101 and KFR105), as well as interpretation of responses to various drilling activities (Walger et al. 2010). The responses to the interference tests are recognised as notably slow, and taken as evidence of poor connectivity in the fracture system. In the transient evaluation (i.e., type-curve fitting under assumptions of idealised conditions), the slow hydraulic responses translate into high apparent storativity (Figure 1-6). These apparent storativity values exceed the empirical relationship of fractures, Eq. (1-2), by at least two orders of magnitude, which is taken as a quantification of limited fracture connectivity.
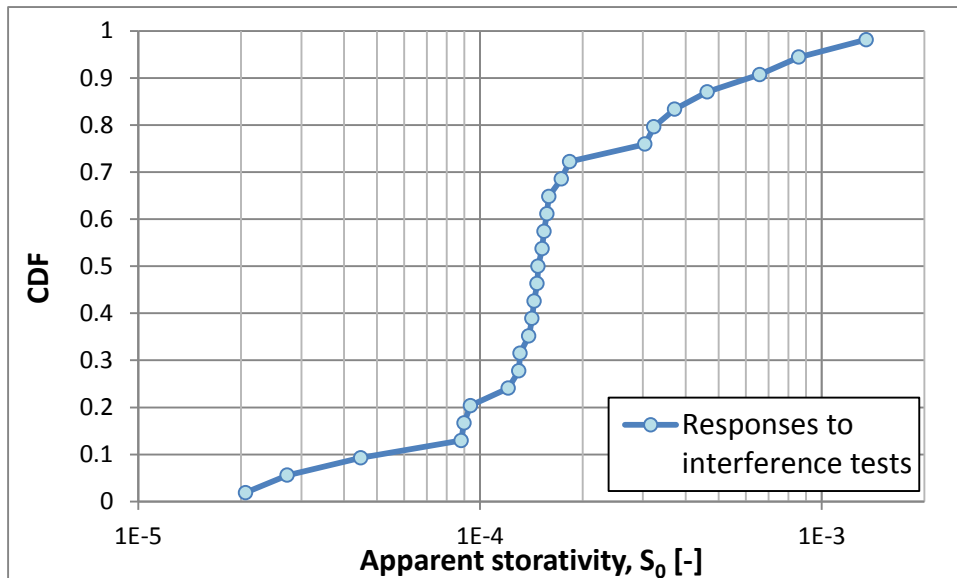
TD15 Complementary simulation cases in support of SR-PSU

Figure 1-6. *Apparent storativity evaluated from observed responses to the interference tests at SFR (HFR101 and KFR105; from Walger et al. 2010).*

The connected fracture network can be divided into two components: fractures which are continuously flowing and detectable in PFL logging (even if potentially choked by hydraulic bottlenecks; Appendix C), and compartmentalised fracture clusters and hydraulic bottlenecks, which contribute to apparent storativity in transient hydraulic tests (Figure 1-7). The main objective of SR-PSU flow simulations is modelling long-term safety by means of steady-state scenarios. As such the hydraulic parameterisation (i.e., the DFN model) is based on continuous flow anomalies in PFL logging, which are representative for the sustainable fracture flow at steady state. Modelling short-term events, on the other hand, where the system is still in transient state (i.e., the declining SFR inflow), requires attention to the parameterisation of aquifer storage. Thus, the contribution from compartmentalised fracture networks and hydraulic bottlenecks are modelled by elaborating the hydraulic diffusivity.

Here, the apparent specific storage is envisaged as a parameter to represent poorly connected fractures (i.e., the unresolved fracture component in the PFL data, which underpin the hydraulic parameterisation in the modelling of long-term safety). Two simplified models are setup to analyse if hydraulic diffusivity can be used as a macroscopic fitting parameter to reproduce the 30 year period of inflow to SFR and monitored drawdown (Table 1-4).

1. The first case addresses the role of hydraulic diffusivity for inflow to SFR in a homogeneous model setting: both hydraulic conductivity and apparent specific storage are modelled as spatially uniform. A wide range of hydraulic diffusivity is examined by keeping the hydraulic conductivity static, while gradually increasing the apparent specific storage, S_S, from 10^{-8} m^{-1} to 1 m^{-1}.

2. The second case employs a heterogeneous parameterisation, as upscaled from a stochastic DFN realisation. Here, analysis of hydraulic diffusivity employs the upscaled ECPM properties as a reference point, from which the local hydraulic diffusivity is varied by means of a scaling factor, F. As hydraulic diffusivity is the ratio between K and S_s, both parameters are rescaled by the square-root of F (i.e., $S_s = S_{s,ECPM} \times \sqrt{F}$, and $K = K_{ECPM} / \sqrt{F}$). This scaling factor is intended to represent limitation in fracture connectivity.

Note that the imposed apparent storativity is intended to control the hydraulic diffusivity, which is envisaged as a characteristic of the fracture-network connectivity, and should therefore not be mistaken for its porous-medium analogy (i.e., a physical formation property).

SVENSK KÄRNBRÄNSLEHANTERING AB

DokumentID
1578373, (1.0)

Sekretess
Öppen

Sida
21(165)

TD15 Complementary simulation cases in support of SR-PSU

Table 1-4. Parameterisation variants for transient inflow simulations

Case		Apparent specific storage, S_s [1/m]	Hydraulic conductivity, K (m/s)
1	Homogeneous	Homogeneous, $S_s = 10^{-8}$ to 1	Homogeneous, $K = 10^{-10}$ m/s
2	ECPM[1]	Heterogeneous, $S_s = S_{s,ECPM} \times \sqrt{F}$	Heterogeneous, $K = K_{ECPM} / \sqrt{F}$

1) ECPM properties from the base case (DFN R85) are scaled by a factor F to impose different diffusivity levels. In order to scale the hydraulic diffucivity by the factor F, both specific storage and hydraulic conductivity are scaled by $\sqrt{F}$ and $1/\sqrt{F}$, respectively. The factor F is varied from 1 to 10^7.
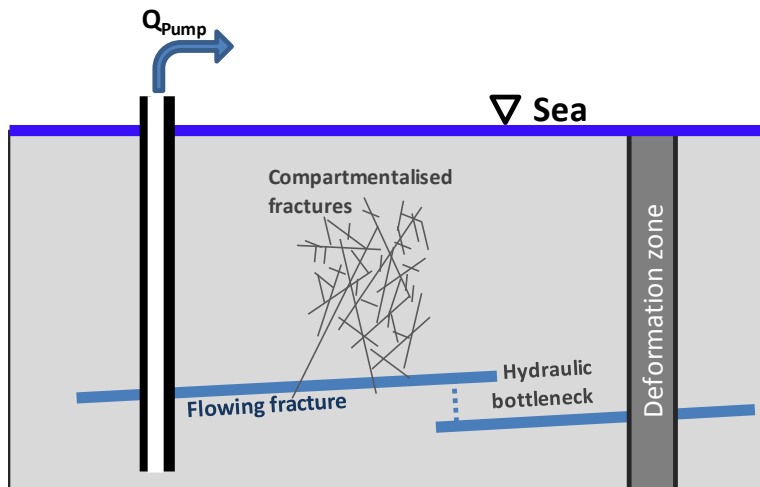

Figure 1-7. Conceptualisation of two fracture types: 1) flowing fracture, detectable in PFL logging, and 2) compartmentalised fracturing and hydraulic bottlenecks, contributing to apparent storativity in transient hydraulic tests.

1.4 Considered performance measures

The significance of the hydrogeological issues (i.e., identified aspects of uncertainty and heterogeneity; Sections 1.2 and 1.3) are quantified in terms of performance measures. The evaluated performance measures (output) from the groundwater flow modelling are:

- Disposal-room cross flow, Q (m³/s);
- Particle exit location at the bedrock/regolith interface;
- Flow-related transport resistance along bedrock flow paths, F_r (y/m);
- Advective travel times along bedrock flow paths, $t_{w,r}$ (y).

A performance measure of supporting character is:
- Path length of bedrock flow paths, L_r (m).

The cross flow through disposal rooms, *Q*, is directly assessed from the flow solutions, whereas the other performance measures refer to flow paths, and therefore involve a preceding step of particle tracking. The measures F_r (y/m), $t_{w,r}$ (y), and L_r (m) are integrated bedrock properties along particle trajectories (i.e., flow paths), which is defined from the point of bedrock entry to the point of bedrock exit. The particle tracking is initiated by releasing particles randomly within disposal-room volumes. The released particles will redistribute and follow different flow paths to reach a point of entry into the surrounding bedrock. The starting point of a particle trajectory is initiated at its tunnel-wall passage (i.e., bedrock entry), and its termination point is defined as its bedrock/regolith interface passage (i.e., bedrock exit). The performance measures are

DokumentID
1578373, (1.0)

Sekretess
Öppen

Sida
22(165)

TD15 Complementary simulation cases in support of SR-PSU

described briefly below, whereas a more detailed description of the calculations are provided in Öhman et al. (2014).

Disposal-room cross flow (Q)

Cross flow refers to the total flow, Q (m^3/s), over a predefined cross-sectional area in the computational grid. This area is the interface between a subunit of interest and the surrounding, arbitrary grid cells. Cross flow through disposal rooms occurs over an enclosed surface, and therefore inward-directed and outward-directed flow components must be summed separately. Cross flow is an important output (performance measure) in the groundwater flow modelling as it affects the strength of the source term in radionuclide transport modelling.

Flow-related transport resistance (F$_r$)

The flow-related transport resistance in rock, F_r (y/m), is an entity, integrated along flow paths, that quantifies the flow-related (hydrodynamic) aspects of the possible retention of solutes transported in a fractured medium. It is an important output (performance measure) in groundwater flow modelling. In SR-PSU, information about the flow-related transport resistance governs the calculation of nuclide migration, hydrogeochemical calculations of salt diffusion into and out from the matrix, as well as oxygen ingress. In its most intuitive form, although not necessarily most generalised, the flow-related transport resistance is proportional to the ratio of flow-wetted fracture surface area (FWS) and flow rate (Joyce et al. 2010). An alternative definition is the ratio of FWS per unit volume of flowing water multiplied by the advective travel time.

Advective travel time (t$_{w,r}$)

The cumulative advective residence time for a particle along a trajectory in the rock, $t_{w,r}$ (y).

Particle exit location

Exit locations are determined by means of forward particle tracking, and defined as the point where the particle passes the bedrock/regolith surface (expressed in RT90 coordinates). Model performance is also evaluated by associating particle-exit locations to so-called biosphere objects, which have been defined for the principal exit locations from SFR (Figure 1-8).
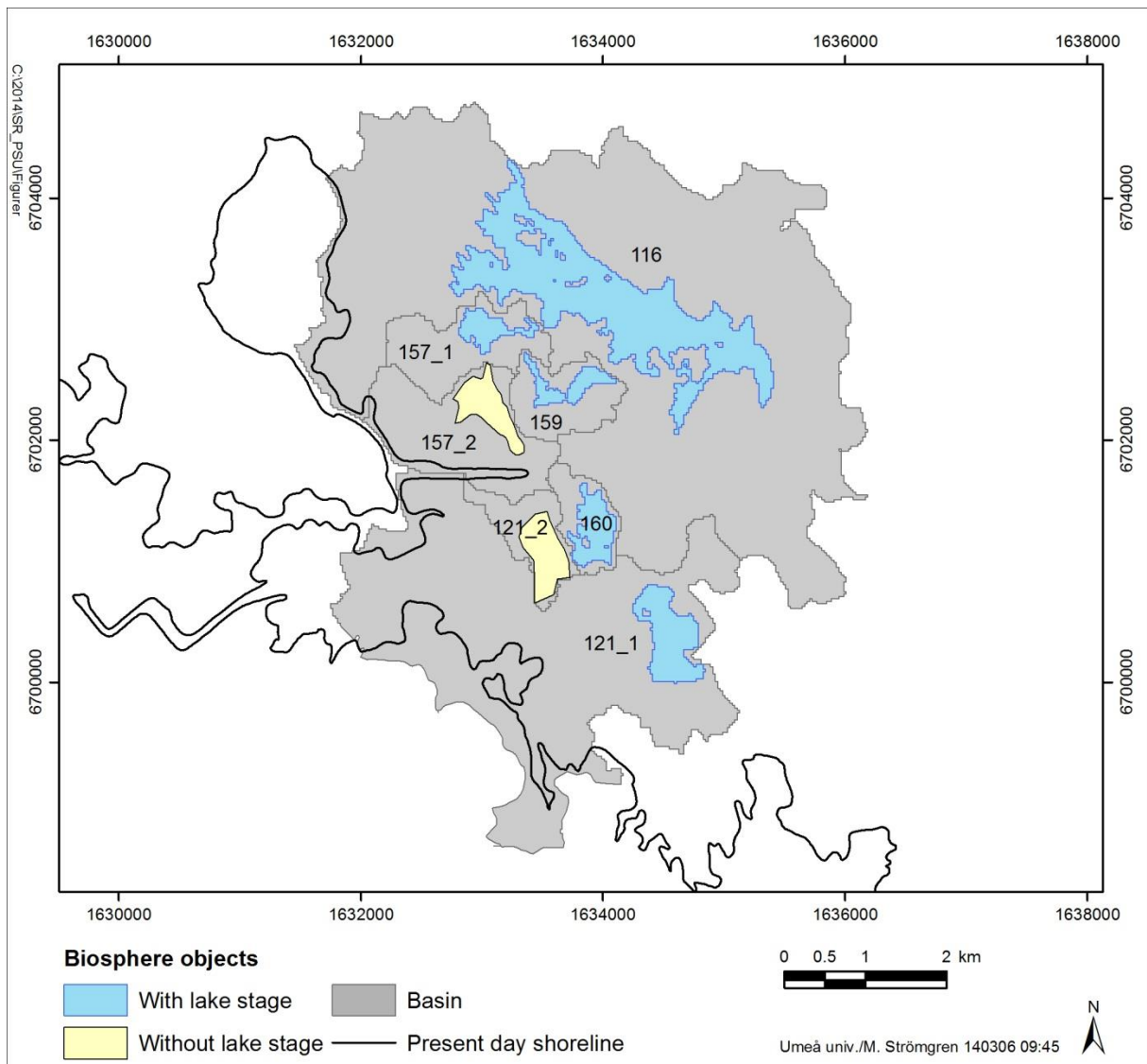
Figure 1-8. Modelled future biosphere objects identified as key recipients of particles from SFR (existing facility and its planned extension).

2 Implementation

2.1 Modelling tool

The flow simulations in this study employ the computer code DarcyTools (v. 4.0.11), which has been specifically developed for the analysis of a repository for spent nuclear fuel (Svensson et al. 2010). DarcyTools is based on the Continuum Porous-Medium (CPM) approach (Svensson et al. 2010), in which the hydraulic properties of a flowing fracture network are approximated by those of a porous medium. DarcyTools allows transferring fracture-network characteristics, as observed in borehole data, onto its computational grid by means of geometrical upscaling over grid cells. These upscaled properties are referred to as Equivalent Continuum Porous Medium (ECPM) properties. As the ECPM approach is based on an

DokumentID
1578373, (1.0)

Sekretess
Öppen

Sida
24(165)

TD15 Complementary simulation cases in support of SR-PSU

underlying stochastic DFN model, the resulting ECPM properties are also stochastic. The uncertainty related to hydraulic heterogeneity can therefore be handled by addressing multiple DFN realisations.

The appeal of the ECPM approach is its computational parsimony and an upscaled hydraulic conductivity field that bears the hydraulic traits of an underlying fracture network, for example anisotropic correlation structures. Unfortunately, geometrical up-scaling does not always ensure hydraulic consistency between the complex heterogeneity of the underlying flowing fracture network and the approximated ECPM. It must therefore be emphasised that the term "equivalent" requires a fine resolution of the computational grid in order to be valid.

Another key feature in DarcyTools is its unstructured Cartesian grid system, which allows great flexibility in local grid refinement to represent detailed geometry of objects (e.g. tunnel layout). All grid geometry is handled via so-called DarcyTools objects (i.e. code-specific file format), which have been constructed from original CAD data geometry. The fundamentals of the model set up (i.e., the base case, which is used as the reference case in evaluation) are described in detail in Öhman et al. (2014), and is hence not repeated here.

Boundary conditions

The bottom of the model ($z = -1,100$ m elevation) is prescribed a no-flow condition based on consideration to declining hydraulic conductivity and flow at depth. The outer perimeter of the model area is defined based on topographical water divides and the seafloor trench Gräsörännan (Figure F-1 in Appendix F), which motivates assuming no-flow boundary conditions at the vertical sides of the model. The top-boundary of the model is prescribed a so-called mixed-boundary condition, i.e., either prescribed flux or prescribed head, which is determined locally depending on the local hydrological conditions. This is accomplished by the codes [fif-RECHARGE_TD11_NEW_Pier.f] and [fif_TD11_Steady_state_NEW_Pier.f] (Appendix G), which steer the DarcyTools simulation. In principle, the simulations start of from a prescribed flux condition at the uppermost active cell layer. The flux is thereafter adjusted iteratively depending on the simulated groundwater level (or more precisely, the simulated head in the uppermost cell layer). Flooded cells (i.e., head rising above ground elevation) imply excessive net-precipitation, relative to infiltration, which is re-directed as runoff. Runoff is not explicitly resolved in the model, and instead the local recharge is reduced in order to allow the local head to align with ground surface. If the flooding prevails, even for small local recharge, the recharge algorithm switches over to prescribed-head boundary conditions, $H = z$ m (see recharge algorithm in Öhman et al. 2014).

2.2   Reference case

The work here is a continuation of the earlier sensitivity analyses (i.e., referred to as TD11 (Öhman et al. (2014) and TD14 (Öhman and Odén 2017)), and as such the model setup and execution follow the principles described in Öhman et al. (2014) (hence, the details in model setup and execution is not repeated here). The significance of, or model sensitivity to, the hydrogeological issues addressed in this report (Section 1.2) is quantified in terms of comparing the performance measures (Section 1.4) of a selection of model-parameterisation variants (Section 1.3) against a reference case. The reference case here is the base-case scenario used in the radionuclide transport calculations for periods with temperate conditions in the main scenario of the safety assessment (SKB 2014), at time slice 5000 AD (also referred to as bedrock case 1 in Öhman et al. 2014). The same reference case was also employed in the analysis of future drinking-water wells (TD12). Note that the analysis of semi-correlated transmissivity parameterisation requires a second reference case, the DFN realisation R18 (which is referred to as bedrock case 2 in Öhman et al. 2014).

At the more detailed level, the following two updates have been made since the reporting of the SR-PSU sensitivity analysis (Odén et al. 2014, Öhman et al. 2014):

- The layout for the planned SFR extension has been finalised as version L2 (the significance of the geometrical update since its predecessor L1BC was evaluated in TD14)

DokumentID
1578373, (1.0)

Sekretess
Öppen

Sida
25(165)

TD15 Complementary simulation cases in support of SR-PSU

- The computational software for flow simulations DarcyTools has been updated to version 4.0.11 (compared to v.3.4.18 used in TD11 and v. 3.5 used in TD14)

To serve as reference cases in the sensitivity analysis, both scenarios (bedrock case 1 and 2 for time slice 5000 AD) were re-run using both the updated layout and DarcyTools versions, in order to eliminate contribution from altered circumstances in evaluated sensitivity in performance measures. The purpose is to eliminate unwanted uncertatiny components from the later sensitivity analysis (i.e., by ensuring that observed effects on performance measures do not stem from layout or DarcyTools versions). Nevertheless, it should be pointed out that the effect of these updates has a minor impact on the simulation output (e.g., Figure 2-1).
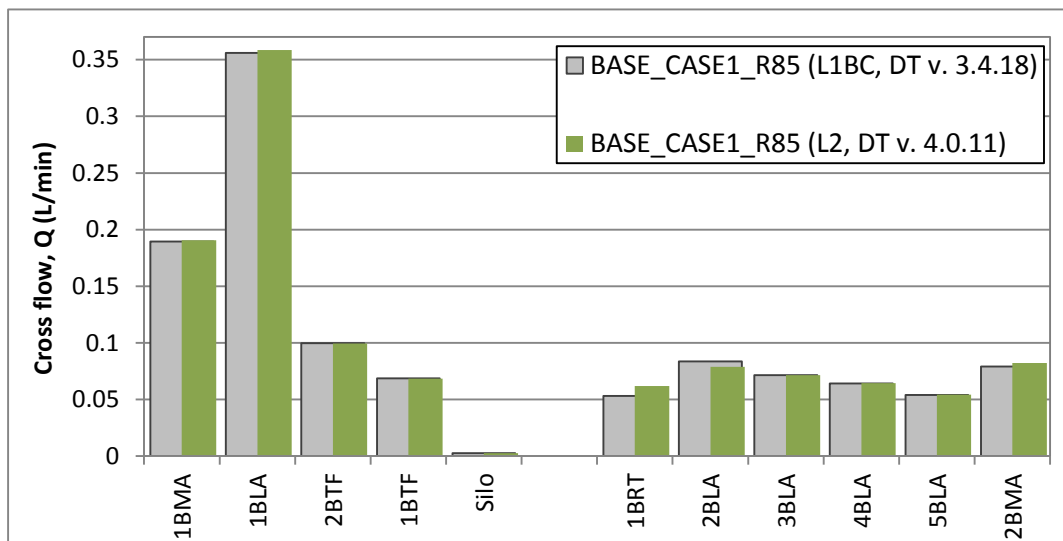

Figure 2-1. Re-calculated tunnel cross flows using the updated tunnel layout, L2, and the updated DarcyTools version 4.0.11, for the base-case scenario, 5000 AD (green bars) compared to the corresponding simulation results in Öhman et al. (2012) (grey bars).

2.3 HSD parameterisation

The implementation of HSD parameterisation variants (Table 1-3) does neither involve ECPM translation, nor grid re-discretisation, and can therefore be hard-coded in the DarcyTools module PropGen, which is used to finalise the ECPM property fields prior to simulation. The PropGen code used in this study is named [prpgen_TD15_ALTER_HSD.f] (Appendix G). The hydraulic conductivity parameterisation of the 6 HSD cases is verified by visual inspection of the nearfield around the SFR pier (e.g., Figure 2-2, Figure 2-3, Figure 2-4). Note that the wave shelter from the SFR pier causes an asymmetry in the occurrence of low-conductive clay (Figure 2-5), which must be accounted for in the analysis of HSD parameterisation cases.

The following should also be pointed out:
1) HSD case 5: the hydraulic conductivity reduction is applied vertically only (as K_z at the HSD/bedrock interface), which is very different from the isotropic hydraulic conductivity reduction in HSD case 2
2) HSD case 6: tests a hypothesised contrast between terrestrial and marine properties (applied as hydraulic conductivity reduction in the uppermost seafloor sediment) and hence, is implemented at an early stage of land uplift where this contrast is considered to be relevant (2500 AD).

SVENSK KÄRNBRÄNSLEHANTERING AB

TD15 Complementary simulation cases in support of SR-PSU
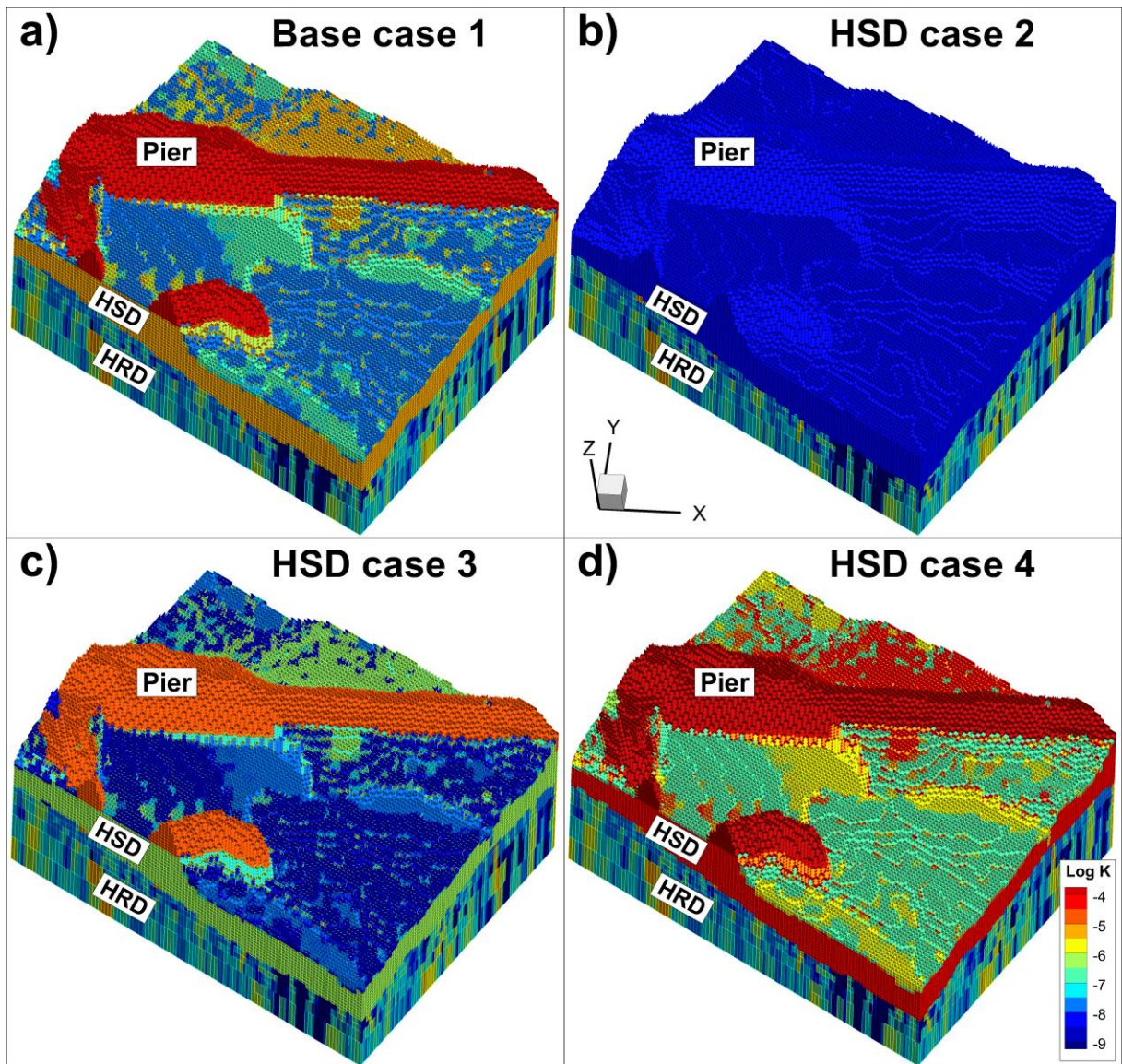
Figure 2-2. *HSD conductivity cases compared against base case; b) all $K_{HSD} = 10^{-8}$ m/s, c) reducing K_{HSD} an order of magnitude, and d) increasing K_{HSD} an order of magnitude.*

DokumentID
1578373, (1.0)

Sekretess
Öppen

Sida
27(165)

TD15 Complementary simulation cases in support of SR-PSU
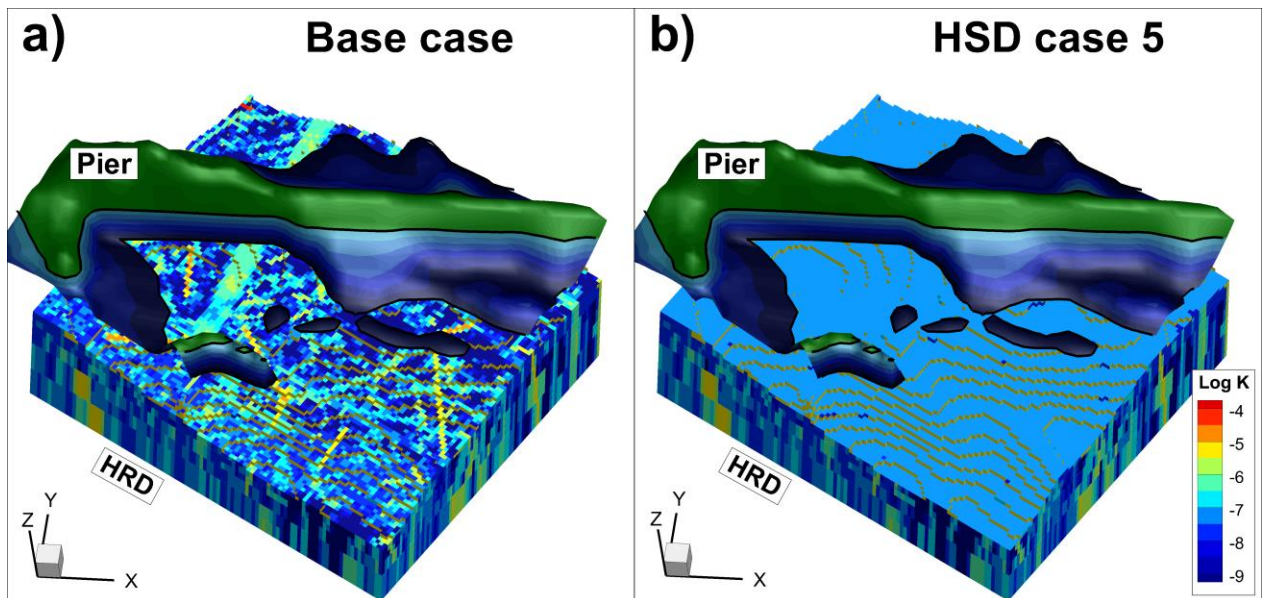
Figure 2-3. Bedrock surface in HSD case 5 compared to base case; vertical hydraulic conductivity set to $K_z = 10^{-7}$ m/s at bedrock surface (for reference, overlying pier shown down to 3 m below current sea level). Note that the contour-like lines arise from the undulation of rock surface as discretised by grid layers.

Figure 2-4. Hydraulic conductivity parameterisation in HSD case 6 compared against base case; seafloor sediments reduced by one order of magnitude in the uppermost 1 m, below sea level.

DokumentID
1578373, (1.0)

Sekretess
Öppen

Sida
28(165)

TD15 Complementary simulation cases in support of SR-PSU

Figure 2-5. *Regolith thickness, b (m), in the nearfield of the SFR pier; a) underlying highly conductive till layer, and b) overlying low-conductive clay layers.*

2.4 HRD: Size-transmissivity correlation in DFN model

In SR-Site Forsmark, three levels of stochastic components were considered in the transmissivity parameterisation of the DFN model (Tab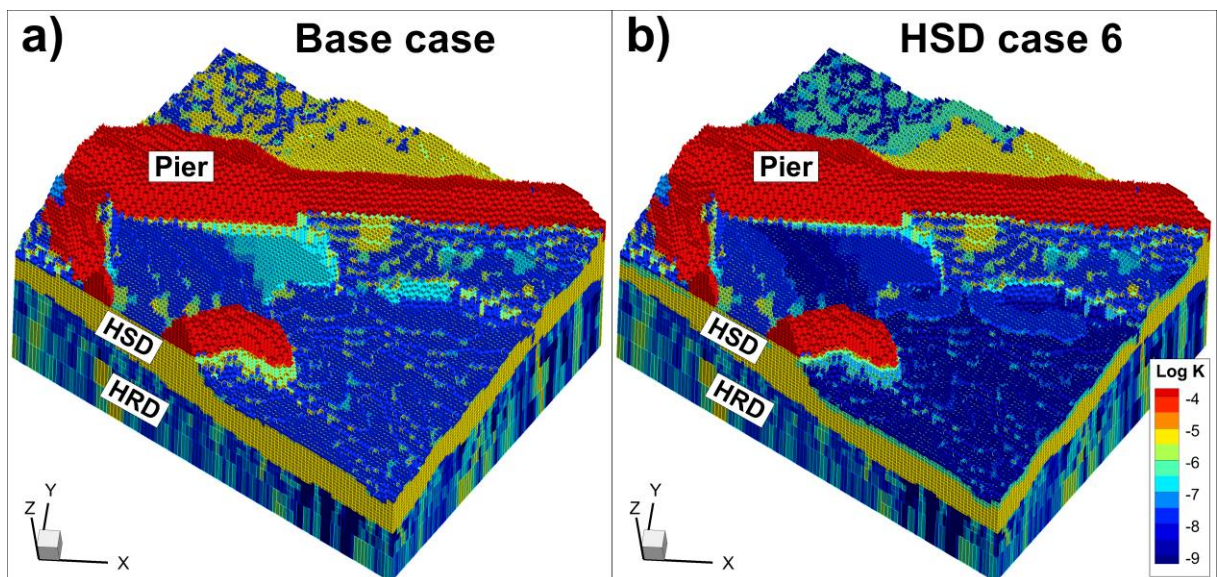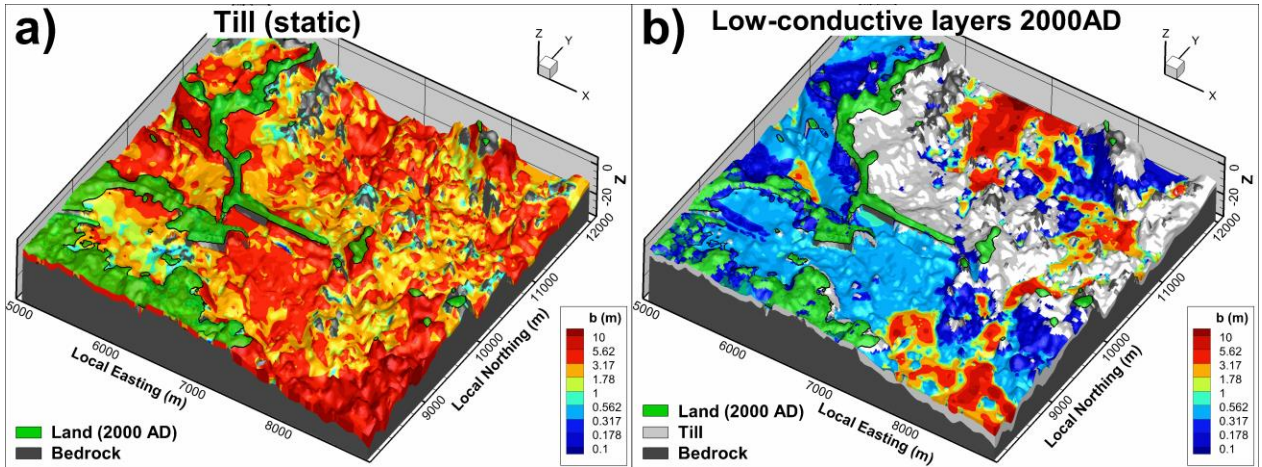le 2-2 in Follin 2008); these ranged from full coupling between fracture size and transmissivity (i.e., $\sigma_{stoch} = 0$; referred to as *correlated*) to a pure random parameterisation of fracture transmissivity (referred to as *uncorrelated* to fracture size). In the intermediate approach, referred to as *semi-correlated*, the stochastic component was assumed to be $\sigma_{stoch} = 1.0$ (or less, for sets with small variability in transmissivity), and the size parameters *a* and *b*, Eq. (1-1), were adjusted to preserve the total variability in fracture transmissivity as seen by a simulated borehole (see Appendix C in Follin 2008). In the SFR PFL-f data, the standard deviation of logarithmic transmissivity is typically less than 1.0, and therefore it was decided to employ a somewhat different approach. The total variance in fracture transmissivity as seen by simulated borehole exploration, σ^2_{tot}, is divided into two components: a deterministic (size-related) component, σ^2_{size}, and a stochastic component, σ^2_{stoch}, see Eq. (2-1).

$$\sigma^2_{tot} = \sigma^2_{size} + \sigma^2_{stoch} \qquad (2\text{-}1)$$

The original transmissivity parameterisation in Öhman et al. (2012) is fully deterministic, and hence $\sigma^2_{tot} = \sigma^2_{size}$. In the semi-correlated approach, the same total variance is assumed to consist of equally large contributions from the deterministic and stochastic components, i.e., $\sigma_{stoch} = \sigma_{size} = \sigma_{tot}/\sqrt{2}$ (see Table 2-1). Thus, the size parameters *a* and *b*, Eq. (1-1), must be adjusted to preserve the total variability in the semi-correlated fracture transmissivity 'as seen by simulated boreholes'. The size parameters were calibrated based on eight DFN realisations, which employ the following fracture-generation volumes (similarly to description in Appendix G of Öhman et al. 2012):

1) Large fractures (typically of side length L from 4 to 300 m) are generated in the entire SFR Regional domain
2) Medium-size fractures (typically of side length L from 0.5 to 4 m) are only generated in large cylinders that enclose each simulated sampling borehole (Figure 2-6)
3) Small fractures (side length L from 0.067 to 0.5 m) are generated in thin cylinders that enclose each simulated sampling borehole (Figure 2-6)

Fractures which are not connected to assumed hydraulic flow boundaries (deformation zones, SBA structures, and sea floor) are removed. The transmissivity of 24,570 fractures sampled in the core boreholes are used to calculate $\sigma_{tot} = \sigma_{size}$ of the deterministic transmissivity parameterisation (i.e., referred to as the original from Öhman et al. 2012), which in turn is used to provide a first estimate of $\sigma_{stoch} = \sigma_{tot}/\sqrt{2}$ (Table 2-1).
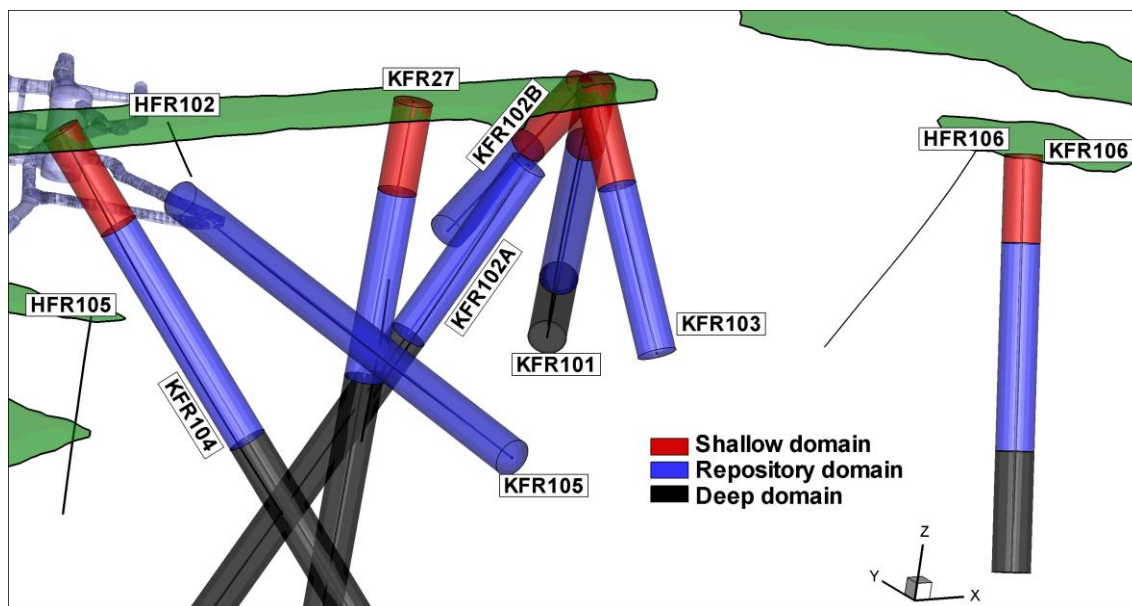
Figure 2-6. *Generation cylinders for medium-size fractures (4 ≥ L > 0.5 m). Similar cylinders are used for small fractures (0.5 ≥ L > 0.067 m), but are too thin for visibility.*

Table 2-1. Size-transmissivity parameterisation variants

Domain	No.	Set	Correlated model			Semi-correlated model		
			a	*b*	σ_{tot}	*a*	*b*	σ_{stoch}
Shallow	1	EW	2.1E-08	1.3	0.54	1.6E-08	1.32	0.38
	2	NE	1.8E-08	1	0.32	1.55E-08	0.95	0.22
	3	NW	5.3E-08	1.3	0.50	3.8E-08	1.27	0.36
	4	HZ	9.8E-08	1.32	1.03	6.5E-08	1.22	0.73
	5	Gd	2.1E-08	1.09	0.75	1.6E-08	1.09	0.53
Repository	6	EW	2.1E-09	1.1	0.57	1.75E-09	1.025	0.40
	7	NE	2.2E-09	1.3	0.55	2.1E-09	1.05	0.39
	8	NW	1.1E-08	1.1	0.63	8E-09	1.06	0.45
	9	HZ	8.5E-10	1.35	1.27	7.5E-10	1	0.89
	10	Gd	4E-09	0.8	0.63	2.6E-09	0.775	0.44
Deep	11	EW	3.6E-09	1.6	0.64	2.5E-09	1.35	0.46
	12	NE	1.9E-09	1	0.35	1.8E-09	0.93	0.24
	13	NW	4.7E-09	1.13	0.48	4.7E-09	1.14	0.34
	14	HZ	1.9E-09	1.15	0.64	1.5E-09	1.05	0.45
	15	Gd	2.7E-10	1.6	1.05	2.8E-10	1.32	0.74

Next, the size parameters *a* and *b*, Eq. (1-1), are adjusted – on a trial and error basis – to preserve the transmissivity statistics among fractures sampled in simulated borehole exploration (Table 2-1). This calibration is presented in more detail in Appendix D. Note that only fractures with transmissivity exceeding $T_{lim} = 2.5 \cdot 10^{-9}$ m^2/s is included in the comparative statistics. Note also, that in practise, the fractures included in regional-scale flow simulations are not truncated by T_{lim}, but by fracture size, depending on grid refinement (the fracture-size truncation ranges from 2 to 16 m). The codes used are in this calibration are [Semi-corr_DFN.F90] and [APPLY_Semi-corr_parameterisation_knwnf.f] (Appendix G).

2.5   HRD: Heterogeneity outside the SFR Regional domain

The sensitivity to HRD parameterisation in an extensive downstream area from SFR (Table 2-2; pink lines in Figure 2-7) is analysed based on five stochastic DFN realisations. A cut-and-paste approach is employed for the implementation of these realisations (Figure 2-7). First, the fractures of the "static" DFN (i.e., used in Öhman et al. 2014) inside a defined "generation domain" are removed (i.e., criterion in terms of fracture centres; Figure 2-7b). However, the fractures intersecting, either: 1) the SFR Regional domain, or 2) the "generation domain" are stored separately and referred to as "connectivity fringe" (pink structures in Figure 2-7b). This "connectivity fringe" has no particular role in flow simulations; it is only used during the removal of isolated fractures (along with other "static structures", such as deformation zones, SBAs, and Unresolved PDZs) prior to ECPM conversion.

Table 2-2. Fracture generation domain outside SFR (local coordinates[1])

Local easting (m)	Local northing (m)
9918	8019
12557	12148
7080	15649
4441	11520

1)   The xy-translation is = (1626000, 6692000).

Consideration of fracture size and the boundary between modelling domains

Following the DFN parameterisation that was used for the bedrock outside the Forsmark Fracture domains (FFMs; according to Appendix A in Öhman and Follin 2010), fractures are generated within the "generation domain" within the size interval side length = 25 to 1,000 m. It should be noted that the size cut off within the SFR Regional domain is considerably lower, 2 or 4 m (i.e., it may be argued to include shorter fractures outside the SFR Regional modelling domain). Five realisations of connected fracture networks are generated and merged with the static DFN in the surrounding domain (Figure 2-7c). The maximum side length of generated fractures is 1,000 m, and therefore the largest fractures can, theoretically, intersect disposal rooms of SFR1 (i.e., they can extend $1{,}000/2 \times \sqrt{2} = 707$ m into the SFR Regional domain).

The geological deformation-zone modelling by Curtis et al. (2010) focussed on magnetic anomalies and deformation zone intercepts with ground surface greater than 300 m. The SFR Local domain contains all modelled deformation zones with ground-surface trace lengths exceeding 300 m, while the SFR Regional domain only contains zones with trace lengths exceeding 1,000 m. Thus, the resolution level in the deterministic modelling is assumed to be 300 m; and the presence of undetected geological structures exceeding 300 m in trace lengths within the SFR Local domain is unlikely (i.e., such stochastic features are not allowed). It is confirmed by visual inspection that the five stochastic realisations do not extend more than 300 m into the SFR Regional domain (Figure 2-8; as the only exception, a deep fracture of R04 extends slightly more than 300 m into the SFR Regional domain, but below the SFR Local domain). Hence, none of

the five realisations stand out as unrealistic (Figure 2-8), based on visual comparison to the "static" DFN used in Öhman et al. (2014).
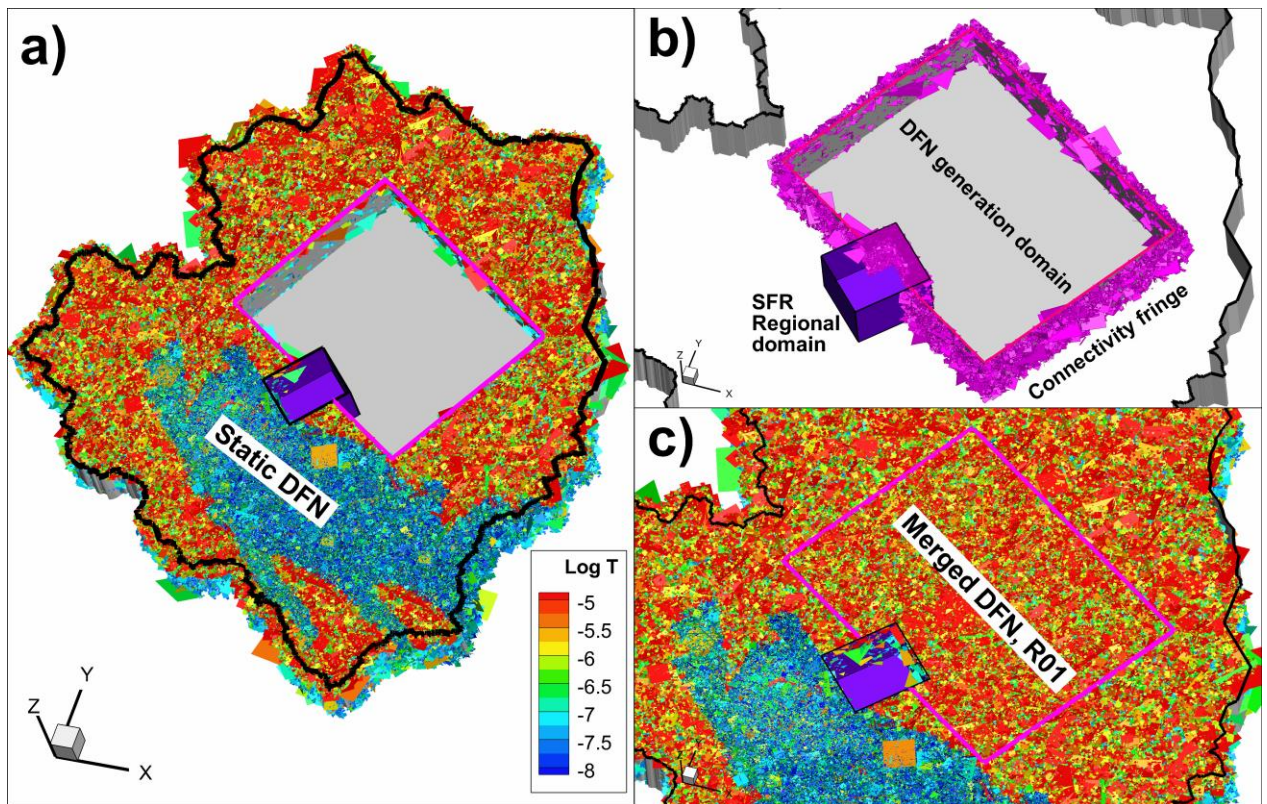

Figure 2-7. *DFN generation outside the SFR Regional domain (purple); a) static DFN parameterisation, b) fracture-generation domain (grey) and connectivity fringe (pink), and c) merged realisation, DFN R01.*

DokumentID
1578373, (1.0)

Sekretess
Öppen

Sida
32(165)

TD15 Complementary simulation cases in support of SR-PSU
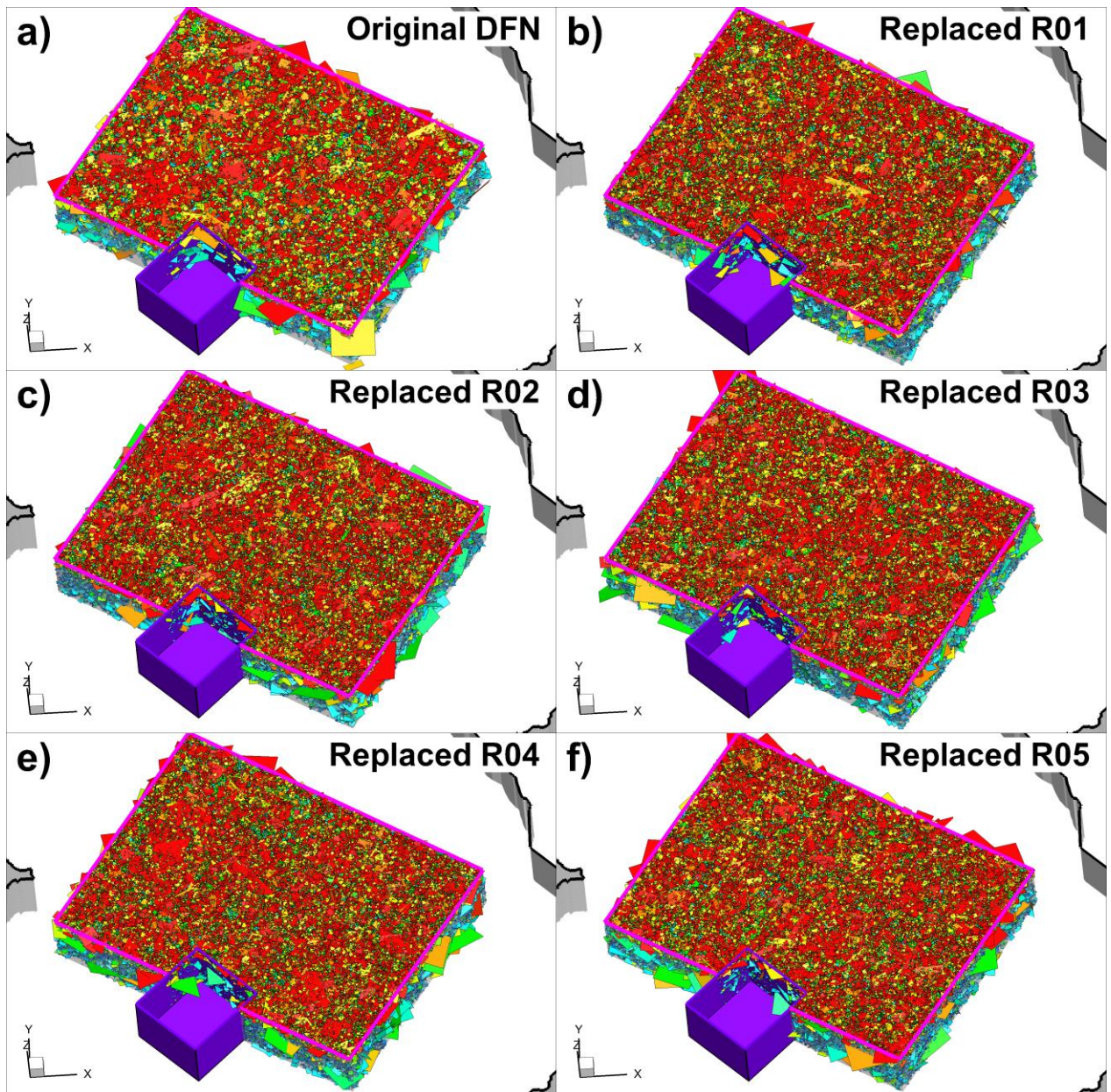
Figure 2-8. *DFN realisations addressing HRD heterogeneity outside the SFR Regional domain; a) the original "static" DFN used as reference to five stochastic realisations (b to f). SFR Regional domain (purple) and fracture-generation domain (pink).*

Note on fracture intensity

The generated DFN realisations have consistently higher fracture intensity, P_{32} (m^2/m^3), as compared to the replaced fractures in the "static" DFN (Table 2-3). However, closer inspection reveals that the discrepancy in fracture intensity is higher among small fractures (L ≤ 75 m) than it is for "medium-size fractures" (75 m < L ≤ 200 m; Table 2-3). This suggests that the discrepancy is caused by: 1) differences in the numerical sorting algorithm (the static DFN origins from SR-Site's "Heterogeneity Case", generated in ConnectFlow; (Joyce et al. 2010) and 2) included connectivity boundaries (i.e., many of the connecting geological structures associated to SFR were unavailable during SR-Site Forsmark; e.g., the extension of 5 deformation zones

outside the SFR Regional domain). The sorting algorithm in DarcyTools accounts for deformation-zone thickness, while it is not fully clear if ConnectFlow employs the central planes of deformation zones.

Table 2-3. Intensity ratio between static DFN and generated realisations[1]

Depth domain	Set	Size category		
		Small	Medium	Large
Shallow	EW	0.61	0.43	
	NE	0.53	0.97	
	NW	0.57	0.76	0.71
	Gd	0.43	0.57	0.74
	HZ	0.38	0.64	0.59
Repository	EW	0.68	0.48	
	NE	0.62	1.34	
	NW	0.60	0.93	0.53
	Gd	0.51	0.83	0.87
	HZ	0.41	0.77	0.85
Deep	EW	0.72	1.39	1.03
	NE	0.61	0.99	3.06
	NW	0.63	1.05	0.98
	Gd	0.54	1.00	1.10
	HZ	0.50	0.93	1.21
	Average	0.56	0.87	0.78

1) Calculated as ($P_{32, Static}/P_{32, Generated}$) for connected fracture networks, based on the first three DarcyTools realisations, R01 to R03. The "Medium" size category defined as 75 m < L ≤ 200 m, and remnant fractures are divided into Small and Large.

2.6 ECPM-scaling effects in model output (grid discretisation)

The ECPM conversion in the DarcyTools model setup is complex, including several types of structural input data combined with nested levels of refinement in the computational grid (Section 1.2.5; grid generation described in detail in Öhman et al. 2014). Thus, potential scaling effects that may affect the calculated performance measures in SR-PSU are analysed here.

The cell size in the DarcyTools model setup ranges from 1 m to 128 m (i.e., depending on the relative significance of geometrical resolution in the flow simulation; details provided in Öhman et al. 2014). In the key area for determining performance measures in SR-PSU (i.e., the particle-transport area; Figure 2-9a) the typical cell size is 8 m (Figure 2-10). However, it should be noted that the particle transport also involves smaller cells, in the proximity of the tunnel walls, as well as larger cells (i.e., a minor fraction of deeper and longer flow paths; grey bars in Figure 2-10). It was decided to refine the grid discretisation of the "particle-tracking area" in two steps (Table 2-4):

- Cell size of 4 m, and
- Cell size of 2 m

Note that the file management and computational demand grows substantially with number of cells (Table 2-4). The two refined grids are employed to setup the base-case scenario at 5000 AD (also referred to as case 1 in SR-PSU). Following the procedure in SR-PSU (details in Öhman et al. 2014), flow is solved and performance measures are determined by means of particle tracking. Thus, apart from refining the grid in the

SVENSK KÄRNBRÄNSLEHANTERING AB

PDF rendering: DokumentID 1578373, Version 1.0, Status Godkänt. Sekretessklass Öppen

"particle-tracking area", all other factors are kept identical to SR-PSU (see details on reference case in Section 2.2).

The subdomain for 4-m refinement is defined by an enclosed three-dimensional volume (i.e., a so-called DarcyTools object; Table 2-4). This volume contains the vast majority (but not necessarily all) of the trajectories in the reference-case particle tracking (Figure 2-9b). Flow is solved for the refined grid and the particle tracking is repeated in the refined grid (100,000 particles released). During this particle tracking, a list of traversed grid cells, which presently has the size 4 m, is being constructed [R_REFINEMENT_POINTS_2m_(SR-PSU_TD15).dat]. This list of cells is used, in a second step, to construct the 2-m grid refinement along preferential flow paths. The results of this study are presented in Section 3.6. A customised code is used for the identification of traversed fractures and DarcyTools grid cells outside the SFR Regional domain [TD15_Particle_tracking_OUTsideSFR].
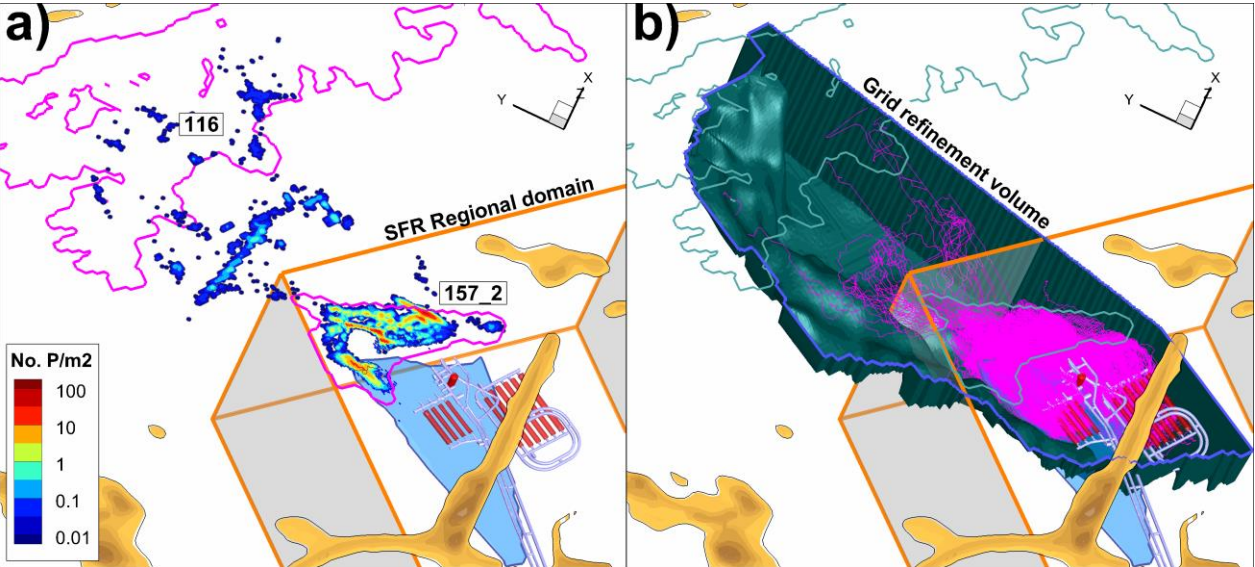
Figure 2-9. Subdomain for analysing potential ECPM scaling effects; a) particle exit locations in the 5000 AD base-case setup (contoured by density) in context of key biosphere objects (pink) and SFR Regional domain (orange), and b) grid-refinement volume (grey-green) defined based on particle trajectories (pink) .

Table 2-4. Number of grid cells with refinement scale

Case	Geometrical definition	No. Cells
Reference case (c. 8 m)	- Not refined -	6,307,256
Refinement 4 m	[R_REFINEMENT_VOLUME_4m_(SR-PSU_TD15).dat]	15,358,819
Refinement 2 m	[R_REFINEMENT_POINTS_2m_(SR-PSU_TD15).dat]	25,747,698

SVENSK KÄRNBRÄNSLEHANTERING AB

DokumentID
1578373, (1.0)

Sekretess
Öppen

Sida
35(165)

TD15 Complementary simulation cases in support of SR-PSU

Figure 2-10. Cell sizes in the particle-tracking area for three cases of grid refinement (base-case scenario, 5000 AD). The cell-size distribution reflects the population of cells traversed during tracking of 100,000 particles.

2.7   Transient inflow simulations

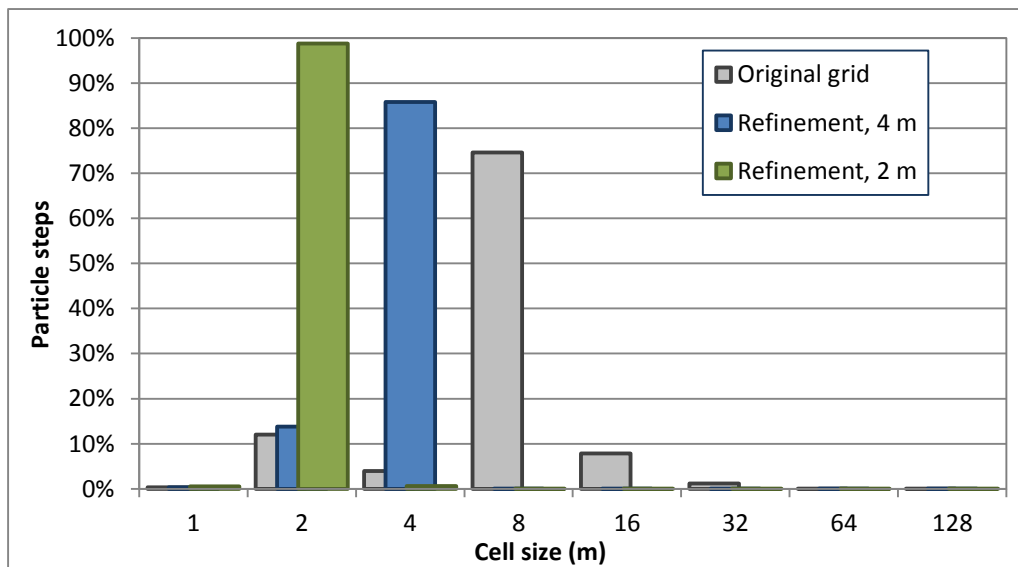Transient tunnel inflow is simulated over a 30 year period, where specific storage, S_s (-), is treated as a fitting parameter to represent the effective hydraulic diffusivity (i.e., $\alpha = K/S_s$) of the hydrogeological system. A low diffusivity implies that hydraulic conductivity, K, must be low in relation to the specific storage, S_s. Thus, for a fixed hydraulic conductivity parameterisation, K (m/s), high values of S_s are tested to mimic the slow hydraulic responses of a poorly connected fracture network (Figure 1-7). Thus, the fitted parameter does not necessarily reflect a realistic aquifer compressibility, but instead an effective modelling parameter which represents fracture-network connectivity (i.e., or lack thereof).

In order to simplify the model setup and to reduce simulation time, the transient tunnel inflow was simulated in a two-dimensional cross section (Figure 2-11). Head is prescribed along the top boundary, $H = \max(z_{sea}, z_{DEM})$, and no-flux is prescribed along the lateral and bottom boundaries (Figure 2-11). The tunnel walls are prescribed atmospheric pressure, $H = z$ m. The first year is solved by means of the smoothening hyperbolic time-step discretisation, after which the subsequent yearly time steps are solved. The inbuilt DarcyTools "sweep" command is used to allow iteration at each time step in order to establish convergence before proceeding to the next time step.

DokumentID
1578373, (1.0)

Sekretess
Öppen

Sida
36(165)

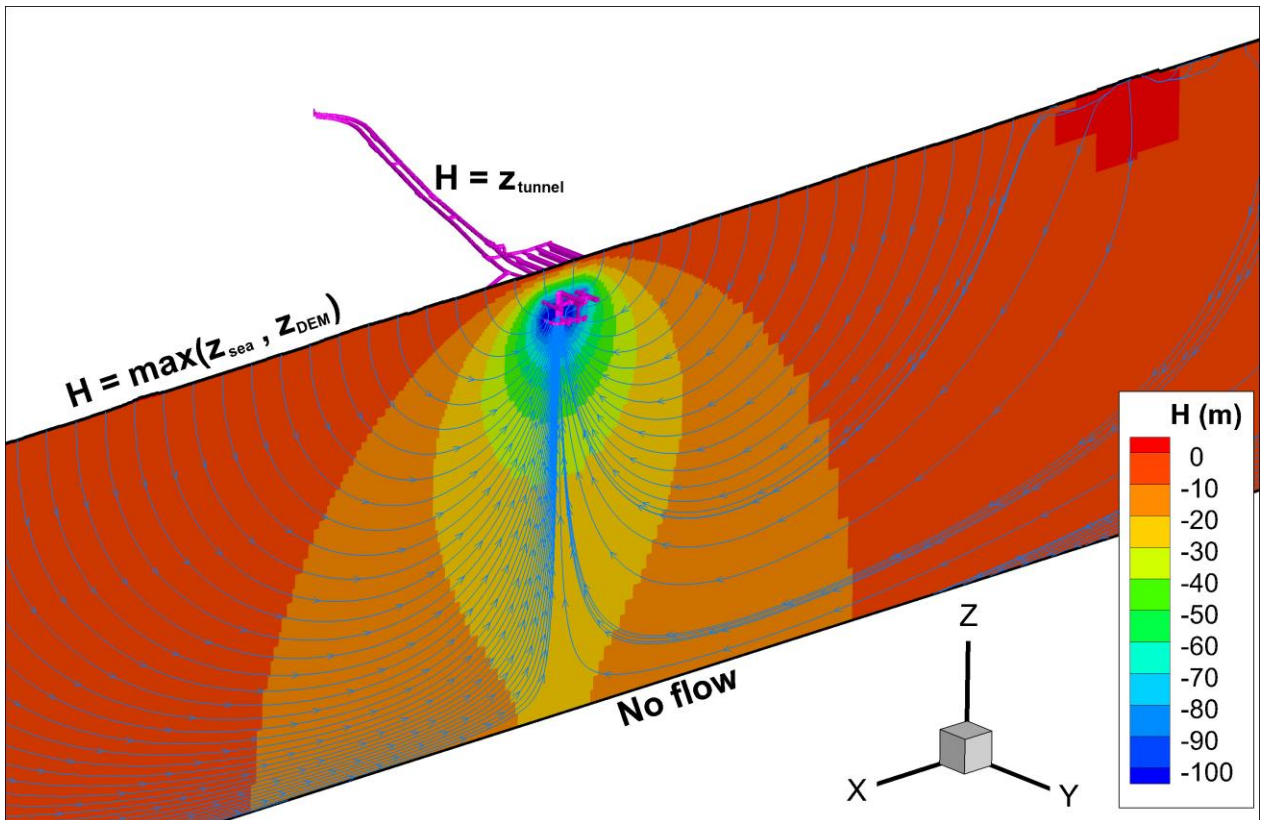TD15 Complementary simulation cases in support of SR-PSU

Figure 2-11. Setup for the 2D transient flow simulations, contoured by simulated head at the end of the 30 year period for Case 1 (Table 1-4) with uniform $K = 10^{-10}$ m/s. Note that the flow lines indicate flow direction only, but not the magnitude of flow.

A complication in the evaluation of transient inflow simulations is that SFR1 was constructed over a three-year long period, during which the tunnel was successively introduced as a sink to the surrounding rock (see discussion in Öhman et al. 2013). Four events are associated to hydraulic disturbances (Figure 3-40). The following data are unavailable for, which complicate comparison against simulations:

1) The tunnel construction phases are not available in detail (i.e., including grouting and bolting), hence the construction progress cannot be resolved accurately in simulations
2) It is difficult to identify an equivalent time reference for the initiation of tunnel inflow, which is representative for the starting point of simulations, i.e., $t = 0$,
3) the corresponding *initial inflow* during tunnel construction is unknown, i.e., what should be taken as the first, maximum tunnel inflow, prior to the first actual measurements.

Hence comparison to transient simulations must assume an initiation time point and the initial inflow at this point. For example, the data can be extrapolated backwards to one of the hydraulic reference events (e.g., penetration of ZFM871, for which the inflow is *assumed* to be 884 L/min; day 766 since official construction start). It must be kept in mind that although these assumptions are very crude, the significance of this simplification diminishes with time, and hence the focus should be on the late tail of inflow. Furthermore, purpose of these simulations is only to test under what premises the declining tunnel inflow can be related to low diffusivity.

The simulated transient inflow $Q(t)$ is normalised by its initial value, Q_{t0}:, in order to define a relative inflow value $[0 \ldots 1]$:

DokumentID
1578373, (1.0)

Sekretess
Öppen

Sida
37(165)

TD15 Complementary simulation cases in support of SR-PSU

$$Q_{\text{rel}} = \frac{Q(t)}{Q_{t0}}.$$

(2-2)

The purpose is to facilitate comparison to data, owing to two circumstances:

1) The scope of this study is not to perform a formal model calibration, or even to verify the parameterisation (i.e., this is rather complex due to the stochastic model components); instead the goal is to study premises for a low-diffusive hydrogeological system to reproduce the inflow data, which is approached in a sensitivity analysis of the parameter setting.

2) To reduce the computational time, the scoping simulations are reduced to a two-dimensional cross section (Figure 2-11). Consequently, the simulated inflow in a thin slice cannot be compared to the tunnel data in terms of absolute values.

3) The 3 year long construction period of SFR corresponds to a gradually introduced disturbance to the hydrogeological setting around SFR. It was decided not to account for this circumstance in the model setup. Thus, unlike the simulations, the inflow data lack of distinct time point for the initiation of the pressure disturbance, t_0 (discussed more below). A rudimentary method to account for this discrepancy is to assume that t_0 for inflow data refers to the penetration of ZFM871, while t_0 for simulations refer to the completion data for SFR (see Figure 3-40).

2.8 Alternative localisation of SFR3 (Forsmark lens)

Note on tunnel-flow algorithm

A consequence of the effort to avoid intersection with surrounding zones (Figure 1-5) is that the disposal rooms are aligned between the deformation zones, but not parallel to the general flow direction (i.e., nor is it fully aligned with SFR1 or the DarcyTools computational grid). This rotation implies a minor inconsistency against the planned localisation that is expected to have negligible effects in reality. However, particular hydrogeological conditions are known to cause numerical artefacts in the evaluation of simulated flow across disposal facilities. These conditions arise under saturated flow along a hydraulic conductor (e.g., the backfilled disposal rooms) that is non-aligned with the computational grid. Specific algorithms have been developed during SR-PSU to reduce these numerical artefacts (Appendix G). The so-called element method, where resultant Darcy velocity is calculated over the triangular elements of the tunnel geometry, is therefore applied in the tunnel-flow evaluation for the alternative localisation of SFR3 (i.e., method 3, SR-PSU TD10; Öhman 2013).

Merging DFN models in numerical implementation

The flow model is set up based on a combination of different types of structure input data, which consist of geometry (planes with two-dimensional thickness) and their hydraulic parameterisation (transmissivity). The geometrical data are of two types: deterministic (static geometry of deformation zones, sheet joints, and SBA structures) and stochastic (DFN realisations). The structural data refer to the two sites: SDM-PSU (SFR Regional domain), SDM-Site Forsmark (the tectonic lens). The relatively unchartered area outside the two sites is covered by a static DFN realisation (SR-Site extended heterogeneity case).

The following approach was taken to merge the DFN realisations that cover the alternative localisation with the SFR base case:

1) A cylindrical volume is defined around the alternative location of SFR3 (red cylinder in Figure 2-12; r = 1,300 m around the centre point (x, y) = 4900 m, 8600 m, defined in the local, non-rotated coordinate system). The cylindrical domain contains both Forsmark fracture domains (FFMs; orange in Figure 2-12c) and bedrock outside FFMs (green in Figure 2-12c).

SVENSK KÄRNBRÄNSLEHANTERING AB

2) The domain outside the cylinder is defined by the SFR base case (i.e., DFN R85 with the HCD base-case parameterisation, combined with the SR-Site extended heterogeneity case[6])

3) The cylindrical domain is defined by: 1) SR-Site's extended heterogeneity case outside FFMs (green in Figure 2-12c) and 2) stochastic realisations R01…R08 and R12 inside FFMS (orange in Figure 2-12c).

The DFN realisations are read from their original file format (i.e., ConnectFlow asc), converted to DarcyTools known-fracture format, and analysed in terms of tunnel-wall intersections by means of the two Fortran codes [Visualise_tunnel_intersections_2.F90] and [Read_Serco_fracts_IN_FFM-HOLE.F90] (Appendix G).
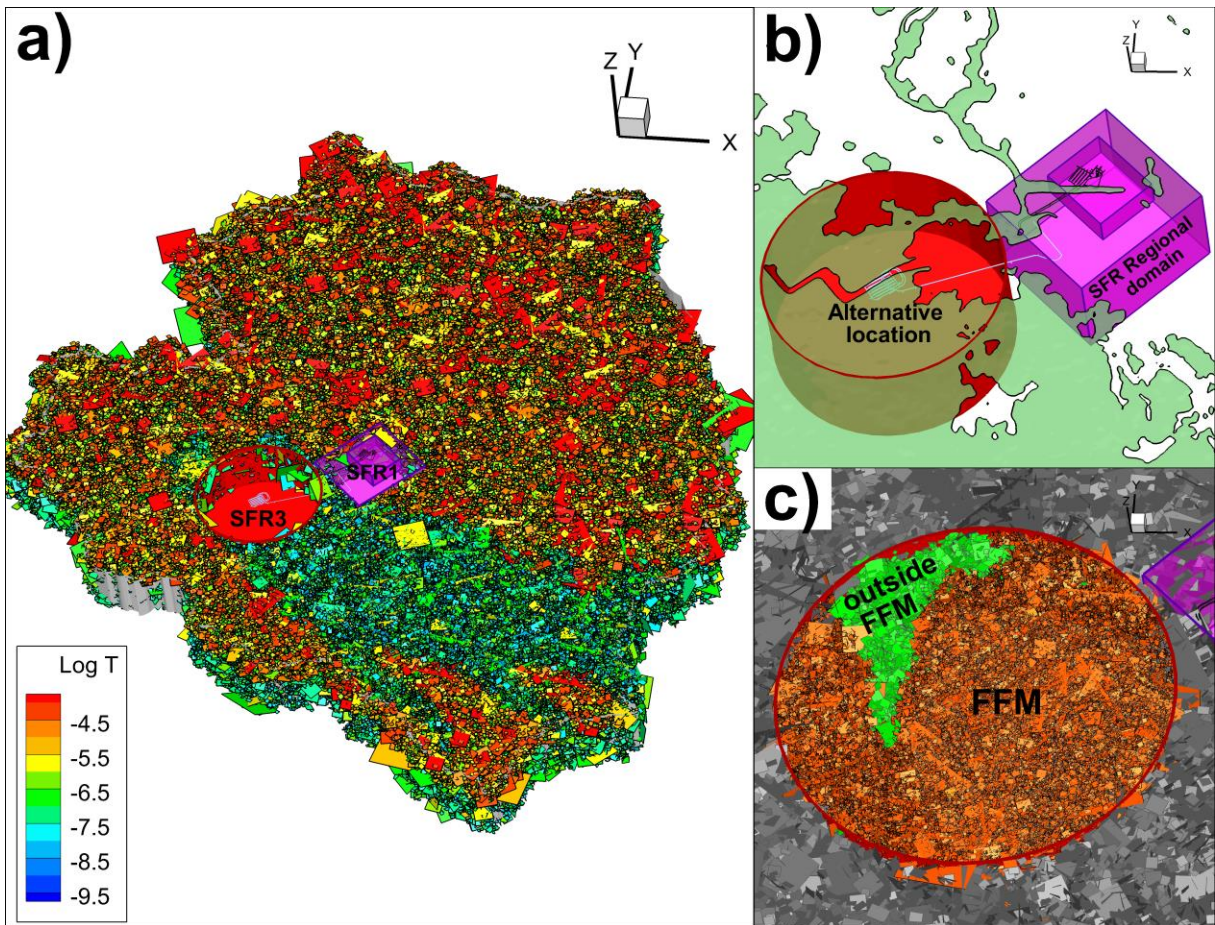
Figure 2-12. Merging of DFN models; a) subdomains around SFR1 and SFR3 embedded in SR-Site's extended heterogeneity case, b) repository subdomains in context of shoreline, and c) subdomain around alternative location of SFR3 divided into FFMs (orange) and bedrock outside FFMs (green).

Geometrical analysis of DFN realisations

The comparatively coarser resolution level in the deterministic deformation-zone modelling at SDM-Site Forsmark (i.e., minimum structure of 1,000 m; Section 1.2.7) necessitates particular emphasis to the variability range in the comparison between the two localisations. A strategy has therefore been suggested

---

[6] Based on the file SRS-FFM01-06_v4_alterFinal_nocpm_r1_sets1-65_all_96.asc, but extended according to SKBdoc ID 1395215

SVENSK KÄRNBRÄNSLEHANTERING AB

based on statistical exploration of hydraulic properties in nine DFN realisations to select three representative realisations that are implemented in flow simulations (Section 1.3.2).

Figure 2-13. Stochastic fracture intercepts for alternative location of SFR3 in the tectonic Forsmark lens in the studied DFN realisation.

Based on simulated exploration of tunnel-wall intersections of nine DFN realisations (e.g., Figure 2-14, Figure 2-15, and Figure 2-16) the following realisations were considered representative for covering the range of variability in hydraulic properties of the local host rock:

1) R03: representing the lower tail of bedrock transmissivity
2) R01: covering average rock
3) R06: representing the upper tail of bedrock transmissivity

It should be emphasised that analysis of a larger DFN ensemble is expected to have rendered a wider range of parameter variability, along with the identification of other realisations that are more representative of the end points in hydraulic heterogeneity of the host rock.

DokumentID
1578373, (1.0)

Sekretess
Öppen

Sida
40(165)

TD15 Complementary simulation cases in support of SR-PSU
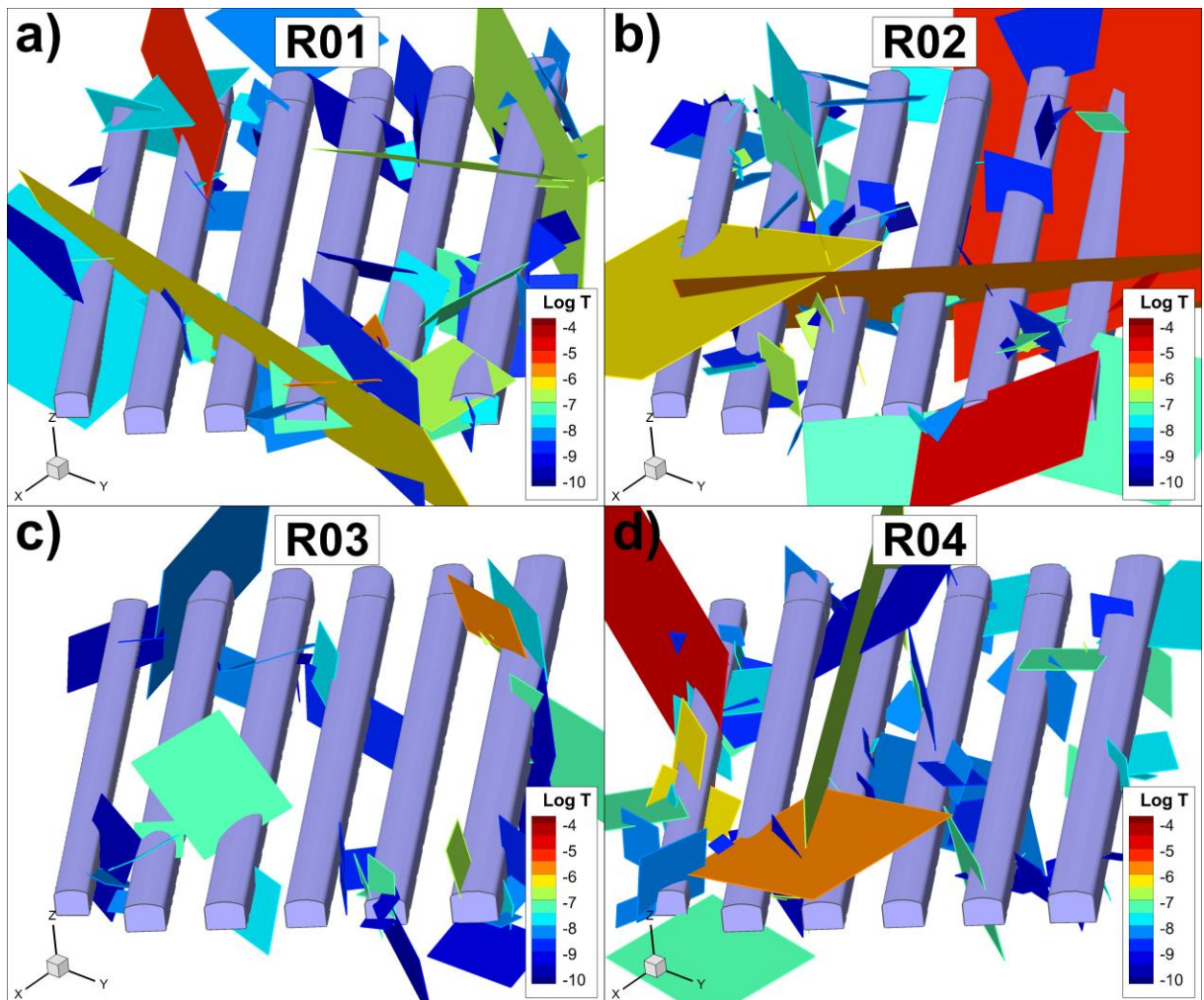
Figure 2-14. *Stochastic fracture intercepts for alternative location of SFR3 in the tectonic Forsmark lens; realisations R01 to R04.*

DokumentID
1578373, (1.0)

Sekretess
Öppen
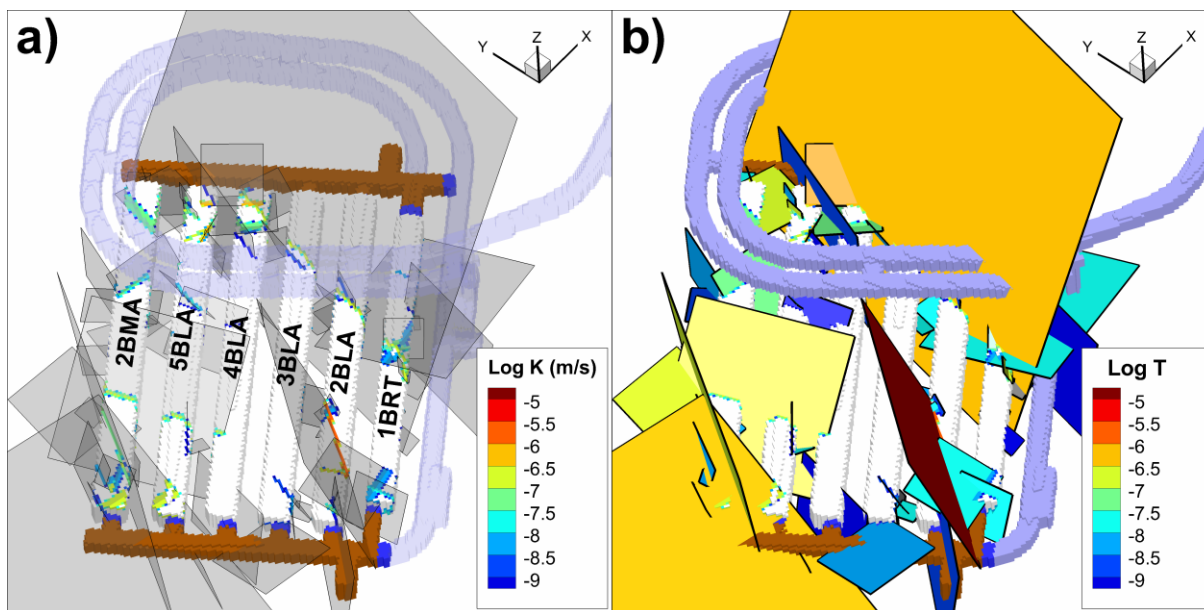
Sida
41(165)

TD15 Complementary simulation cases in support of SR-PSU
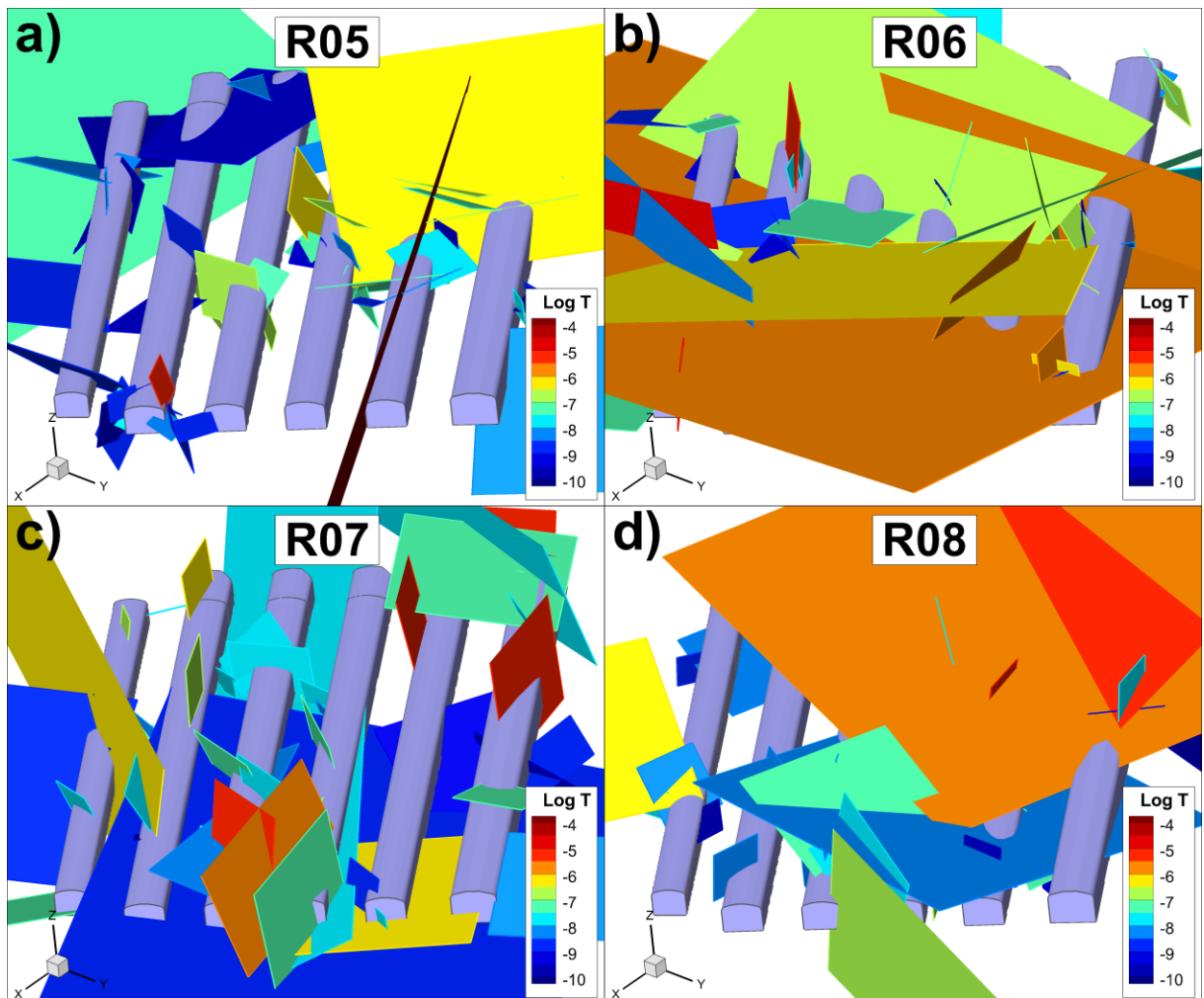
Figure 2-15. *Stochastic fracture intercepts for alternative location of SFR3 in the tectonic Forsmark lens; realisations R05 to R08.*

DokumentID
1578373, (1.0)

Sekretess
Öppen

Sida
42(165)

TD15 Complementary simulation cases in support of SR-PSU

Figure 2-16. Comparison between R01 versus remaining realisations to estimate the range of host-rock properties and to identify representative realisations; a) transmissivity distribution of sampled fracture intercepts (average per disposal room) and b) summed transmissivity of intersecting fractures per disposal room (ranges covered by geometric mean of the disposal rooms and their min/max values).

DokumentID
1578373, (1.0)

Sekretess
Öppen

Sida
43(165)

TD15 Complementary simulation cases in support of SR-PSU

3 Results

3.1 HSD parameterisation

3.1.1 Tunnel flow

The sensitivity analysis of the HSD parameterisation demonstrates an unexpected effect: the simulated tunnel flow is inversely proportional the hydraulic conductivity parameterisation, K_{HSD} (Figure 3-2). The two cases with lower HSD conductivity (i.e., cases 2 and 3 in Table 1-3) cause somewhat higher tunnel flow (on average 8% higher), as compared to the base case setting, while the high-conductive case (i.e., case 4 in Table 1-3) leads to lower tunnel flow (on average 30% less). This effect is somewhat counter-intuitive, and therefore the results are co-interpreted with the simulated groundwater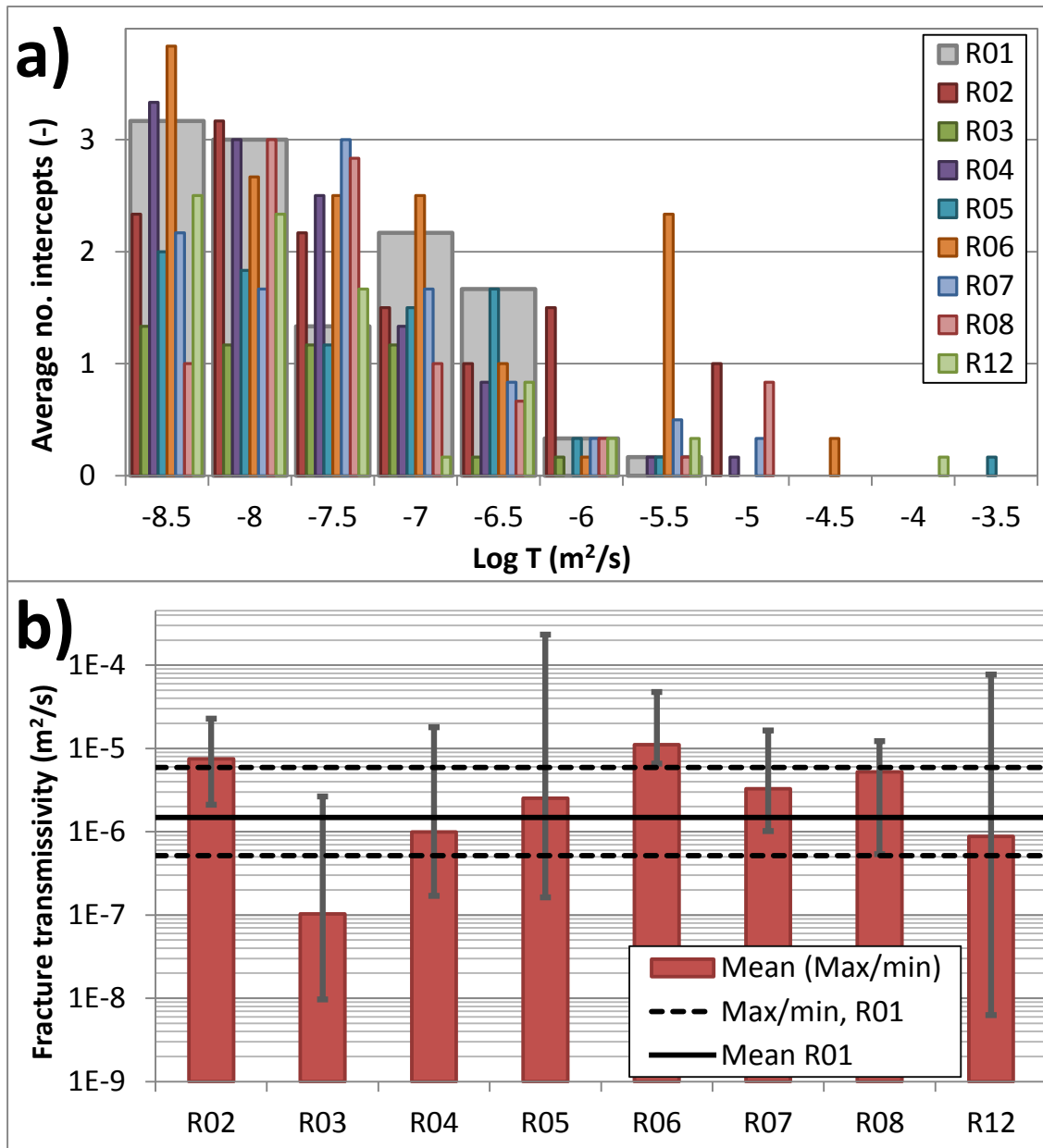 levels (Figure 3-6 and Figure 3-7) to gain a better understanding on the role of HSD in the large-scale flow simulations.

Conceptually, two roles of HSD can, depending on its hydraulic conductivity relative to the underlying bedrock, be considered in regional-scale flow. If the HSD is less permeable than the underlying bedrock, the HSD will constrain the bedrock infiltration, such that much of the net precipitation will be re-directed as runoff (Figure 3-1a). This would suggest a *direct* proportionality between HSD conductivity and flow rates in the bedrock (i.e., unlike the results demonstrated in simulations; Figure 3-2). If, on the other hand, HSD is more permeable than the underlying bedrock, and the regolith thickness is on par with the range of topographical gradients, the primary role of the HSD is to control the groundwater levels (i.e., hydraulic gradient) within the regolith deposits (Figure 3-1b). In other words, if the HSD is highly permeable, the groundwater levels in the regolith deposits may be drained in elevated parts of the domain and in turn reduce the hydraulic gradient in the underlying bedrock (Figure 3-1b). This effect is demonstrated in a simplified model setup where the role of HSD parameterisation on flow is studied in detail in a vertical cross section (Appendix F).
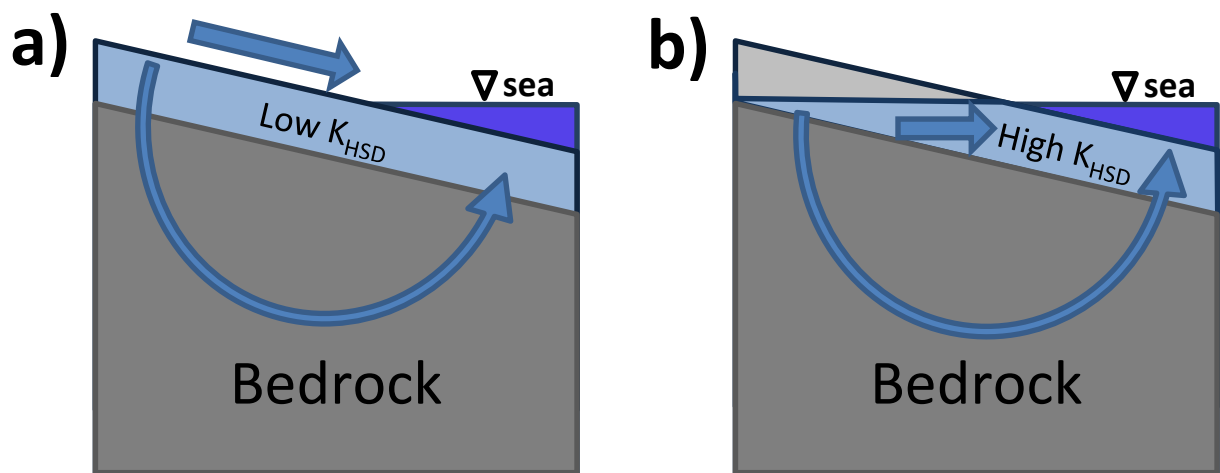
Figure 3-1. Conceptual endpoints of the role of HSD on regional-scale flow; a) low K_{HSD} upholds the hydraulic gradient in the underlying bedrock, but constrains the bedrock infiltration (flow), and b) high K_{HSD} drains the groundwater levels, which reduces the hydraulic gradient in the underlying bedrock.

Now, in the sensitivity analysis of HSD parameterisation, the low-conductive cases reduce the flow rates in the HSD layer, which leads to flooding the ground surface (Figure 3-6b and c). Flooding implies that the modelled net-precipitation exceeds infiltration and that the area has a large runoff component which is not explicitly resolved in the model. Instead, the recharge algorithm switches over to prescribed-head boundary

DokumentID
1578373, (1.0)

Sekretess
Öppen

Sida
44(165)

TD15 Complementary simulation cases in support of SR-PSU

conditions, H = z m (shown as pink-shaded in Figure 3-5b and c; see recharge algorithm in Öhman et al. 2014). Although the low K_{HSD} reduces flow in the regolith layers, its hydraulic conductivity still exceeds that of the underlying bedrock, and therefore the net effect is boosting the groundwater levels in the regolith layers without constraining the bedrock infiltration. As the result, lowered HSD conductivity leads to higher hydraulic gradients in the underlying bedrock and higher flow through disposal rooms, as compared to the base-case parameterisation.

The opposite holds for variant 4, where the groundwater level in the regolith is drained by the high hydraulic conductivity (Figure 3-7d). As the result, the groundwater levels can largely be solved under flux-boundary conditions, with maximum prescribed recharge 160 mm/yr (Figure 3-5d). The groundwater levels are smoothened out and comparatively less coupled to the local topography of ground surface, which in turn dampens the hydraulic gradients and declines the flow rates in the deeper rock (e.g., purple bars in Figure 3-2). This suggests that out of the two potential roles considered for the HSD, that is: 1) constraining the recharge to the underlying bedrock and 2) controlling the topographically driven hydraulic gradients, the simulation results indicate that the latter dominates for the hydrogeological setting at SFR (i.e., topography and the relative conductivities of HSD and bedrock). This effect is demonstrated in a simplified model setup in Appendix F.

To some extent the low groundwater levels in the high K_{HSD}-case could be exaggerated by the uncertainty in the applied recharge condition at the model top surface. As described in Öhman et al. (2014), the concept in the DarcyTools simulations is to assume a net precipitation (P-PET, mm/yr), of which part can recharge into the regolith, while the rest is overland runoff. This runoff is not modelled explicitly (i.e., it is excluded from simulations) and can therefore not re-infiltrate at some other point in the model. The DaryTools simulations assume a net precipitation of 160 mm/yr in all modelling cases, which is also the maximum local recharge. This value is based on previous water-balance modelling of meterorological and hydrological data in the Forsmark area, using the Mike-SHE software (DHI Software 2010), which rendered an effective annual net precipitation of c. 130 mm/yr (Mårtensson and Gustafsson 2010). A couple of aspects should be noted on this parameter:

1) The parameter is an effective catchment value (i.e., does not resolve spatial or temporal variation). In reality the evotranspiration (ET) is expected to exhibit spatial variation depending on local conditions (e.g., vegetation, topography, depth to groundwater, etc.). This motivates using a higher parameter value for *local maximum recharge* in DarcyTools simulations.
2) The parameter is based on a short period of meterorological and hydrological data (2005-2006), of which the first year is used for model initialision. Normally it is considered that a thirty-year period is required to capture the range of meteorological variance (i.e., to cover the range of dry-normal-wet years). The limited data period motivates using a higher parameter value for *local maximum recharge* in DarcyTools simulations.
3) SR-PSU addresses long-term safety, which implies climatological uncertainty in applying a present-day calibrated parameter to future scenarios. The climatological uncertainty applies to both precipitation and evotranspiration, as well as to how their spatial and temporal variability maps on to the annual, effective parameter. Furthermore, the effective parameter applies to a catchment that today is largely submerged under sea, which complicates hydrological calibration.

In summary, the assumed model parameter (P-PET)$_{max}$, which sets the upper bound for local recharge, is subject to several uncertainties, and particularly, it may be argued that the the low groundwater levels in the high K_{HSD}-case may lead to lower ET, which in turn suggests that the effects of HSD parameterisation are exaggerated.

TD15 Complementary simulation cases in support of SR-PSU

Also HSD case 6, which studies a potential contrast between terrestrial deposits and seafloor sediments at the time slice 2500 AD, demonstrates that a hydraulic-conductivity reduction in the uppermost layer of seafloor sediments may increase disposal-room cross flows slightly (Figure 3-3). This is not primarily associated to higher simulated groundwater level in the pier, as they are very similar to the base case (Figure 3-8). However, the widespread till layer is too permeable to constrain vertical flow across the bedrock surface, even if its hydraulic conductivity is reduced by an order of magnitude, and therefore, the impact of HSD case 6 is intimately related to local presence of low-permeable clay layers (Figure 2-5). The occurrence of clay is non-uniform and concentrated to basins sheltered from wave erosion, such as for example south of the SFR pier. Thus, the low-permeable clay layers above Singö deformation zone (i.e., south of the SFR pier; Figure 2-4) form a cap along the shoreline that upholds the pressure of the large-scale flow paths from elevated areas in the Forsmark inland. This causes HSD case 6 to re-direct groundwater discharge towards north of the SFR pier (Figure 2-5; Figure 4-11 in Öhman et al. 2014), and thereby slightly increasing tunnel flow.
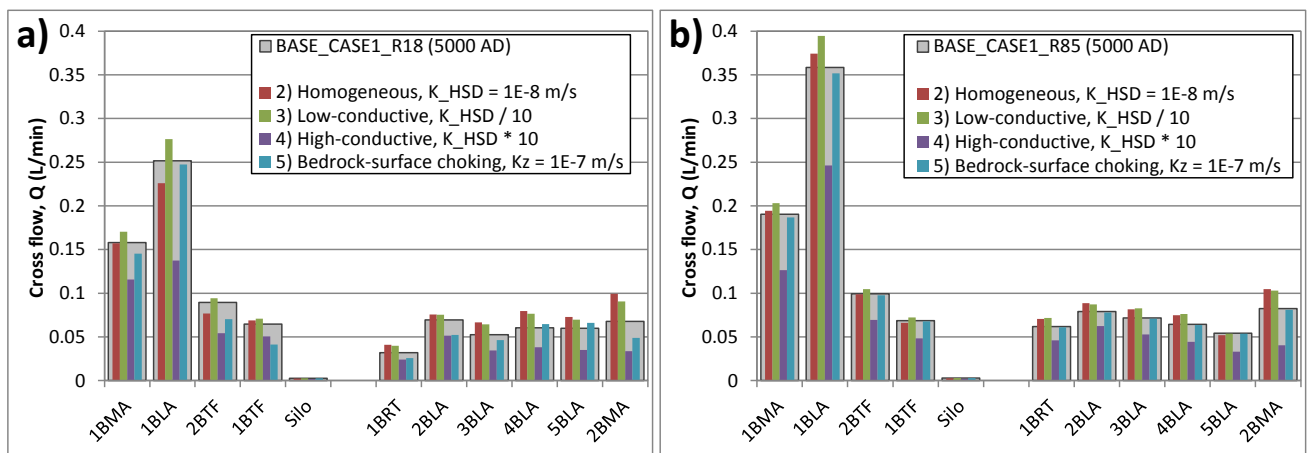
Figure 3-2. Simulated flow through disposal rooms in four HSD-parameterisation cases (variants 2 to 5; Table 1-3) compared to the base-case HSD setting (i.e., details in Öhman et al. 2014); a) the optimistic DFN realisation R18 and b) the pessimistic realisation R85.
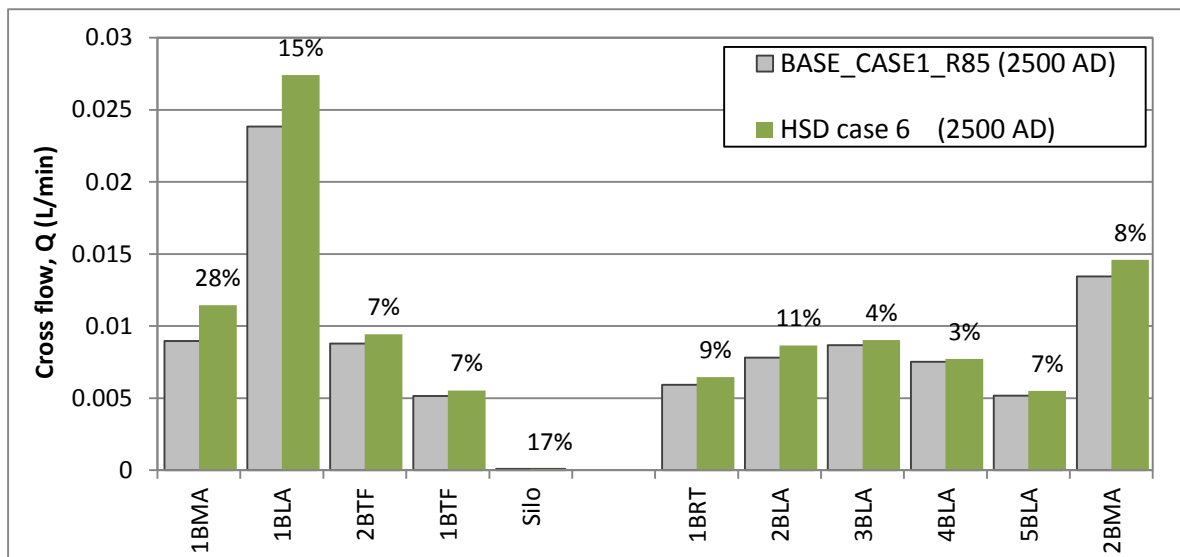
Figure 3-3. Simulated flow through disposal rooms for the HSD case assuming less permeable seafloor, at 2500 AD (HSD case 6; Table 1-3) compared to the base-case HSD setting (i.e., details in Öhman et al. 2014).

SVENSK KÄRNBRÄNSLEHANTERING AB

DokumentID
1578373, (1.0)

Sekretess
Öppen

Sida
46(165)

TD15 Complementary simulation cases in support of SR-PSU
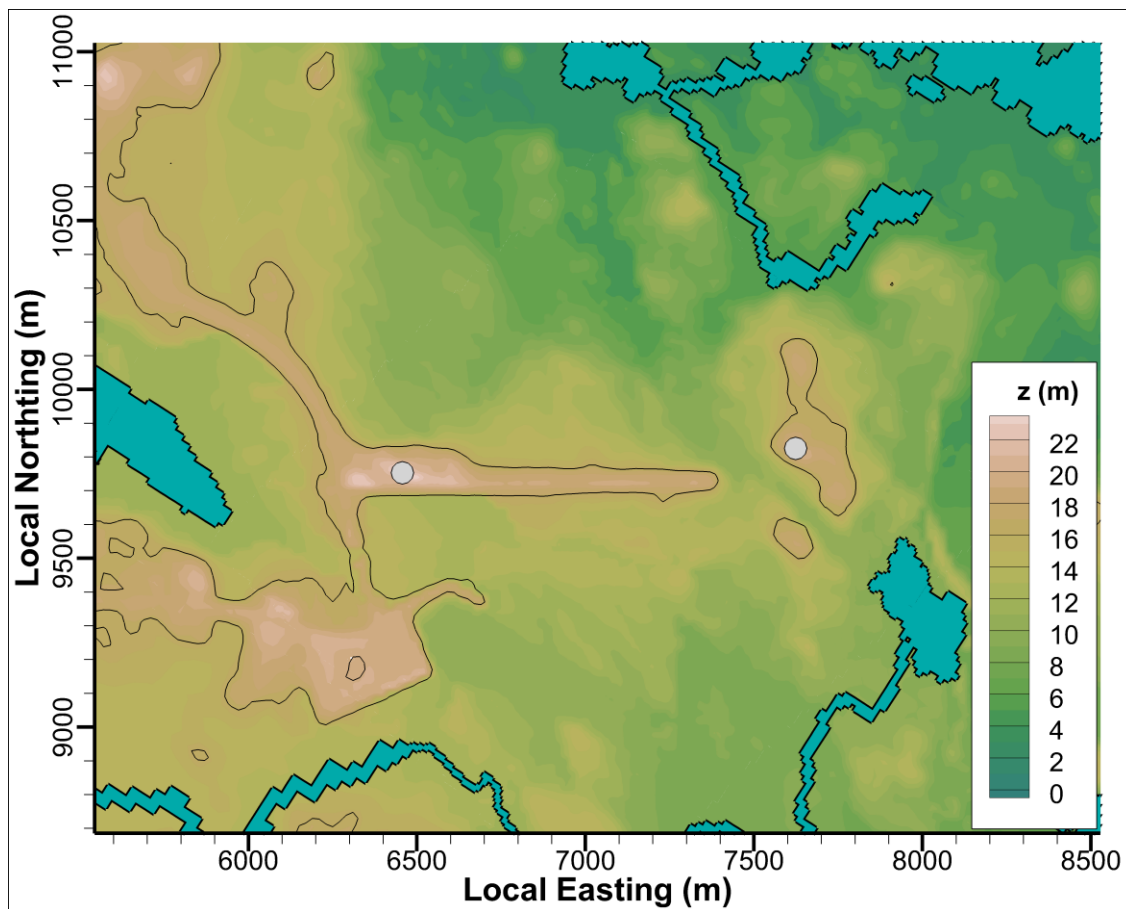
Figure 3-4. *Ground surface in the SFR near field emerged from the retreating sea, by 5000 AD, as the result of land uplift (contoured by elevation, z (m), above the sea). Pre-defined surface water (lakes and rivers) shown as blue-grey surfaces.*

DokumentID
1578373, (1.0)

Sekretess
Öppen

Sida
47(165)

TD15 Complementary simulation cases in support of SR-PSU
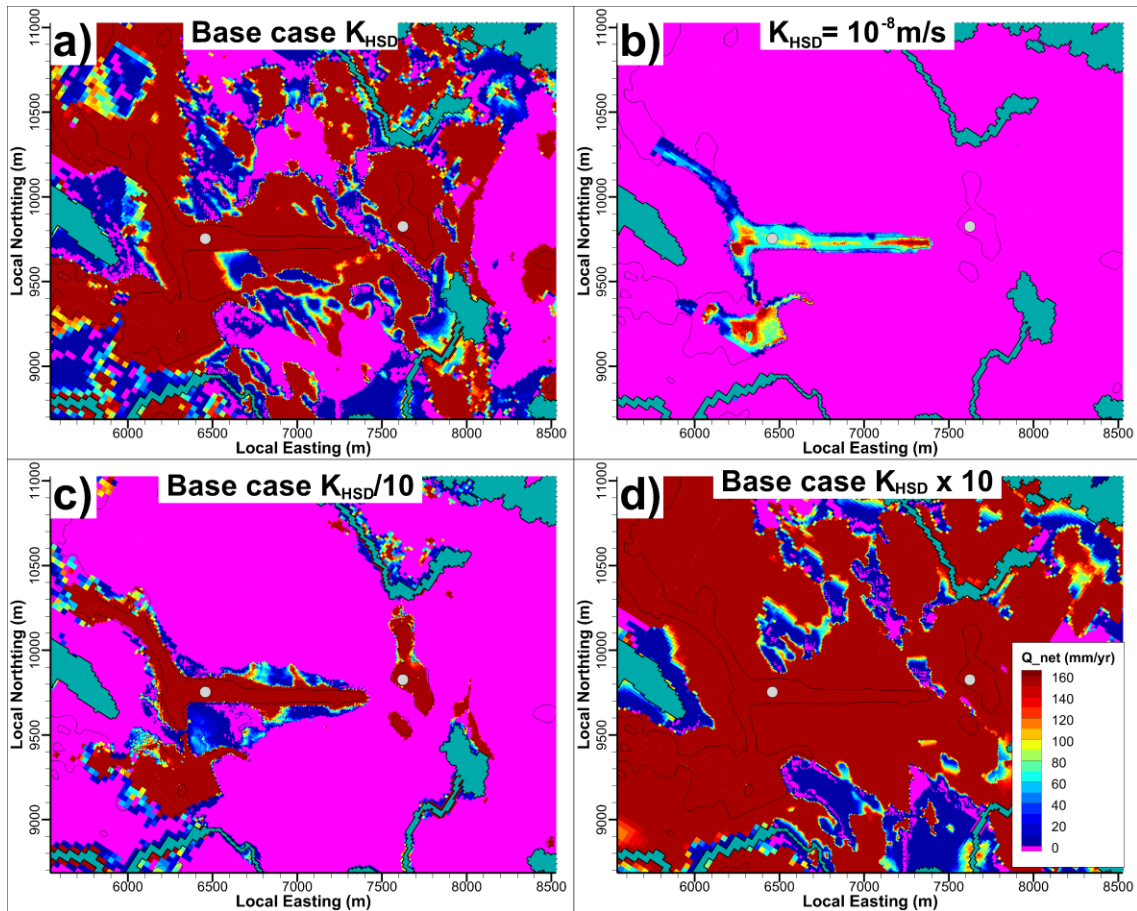
Figure 3-5. *Simulated local recharge at ground surface for HSD parameterisation variants 1 to 4 in Table 1-3. The principle of the mixed-boundary condition is to fit the recharge, Q_{net} (mm/yr), depending on the local hydrogeological settings. If flooding occurs, even for small Q_{net}, the boundary condition is locally switched into fixed-head, $H = z_{DEM}$ (pink surface).*

DokumentID
1578373, (1.0)

Sekretess
Öppen

Sida
48(165)

TD15 Complementary simulation cases in support of SR-PSU
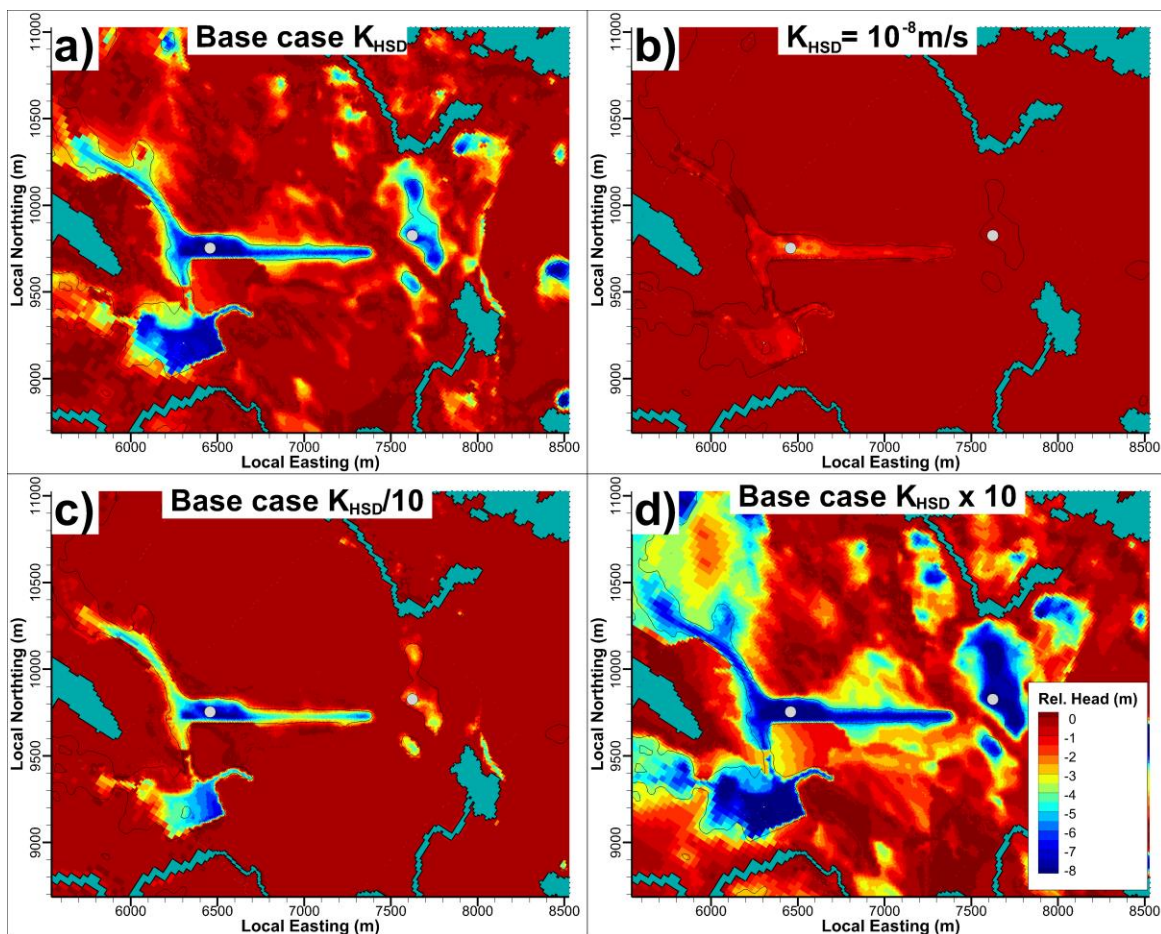
Figure 3-6. *Simulated relative ground-surface head, H - z_{DEM} (m), for HSD parameterisation variants 1 to 4 in Table 1-3. Less strictly speaking, the term relative head can be envisaged as "depth to groundwater"; more strictly, it is defined as simulated head in the uppermost cell layer, H (m), relative to local ground-surface elevation, z_{DEM} (m). Pre-defined surface-water objects (lakes and rivers) shown in blue-grey.*

DokumentID
1578373, (1.0)

Sekretess
Öppen

Sida
49(165)

TD15 Complementary simulation cases in support of SR-PSU
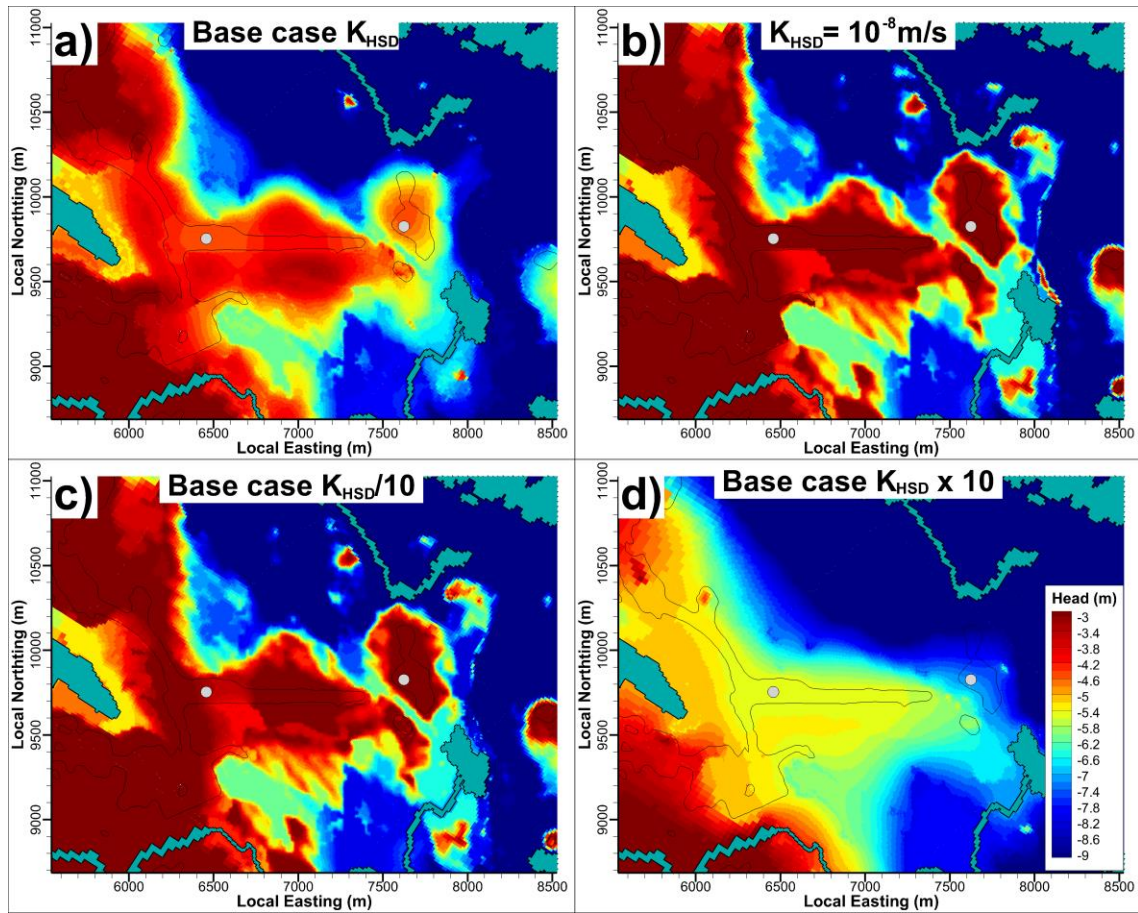
Figure 3-7. *Simulated head at ground surface for HSD parameterisation variants 1 to 4 in Table 1-3. Head is expressed in the fixed-bedrock reference (i.e., to avoid confusion from land uplift). Pre-defined surface-water objects (lakes and rivers) shown in blue-grey.*

TD15 Complementary simulation cases in support of SR-PSU
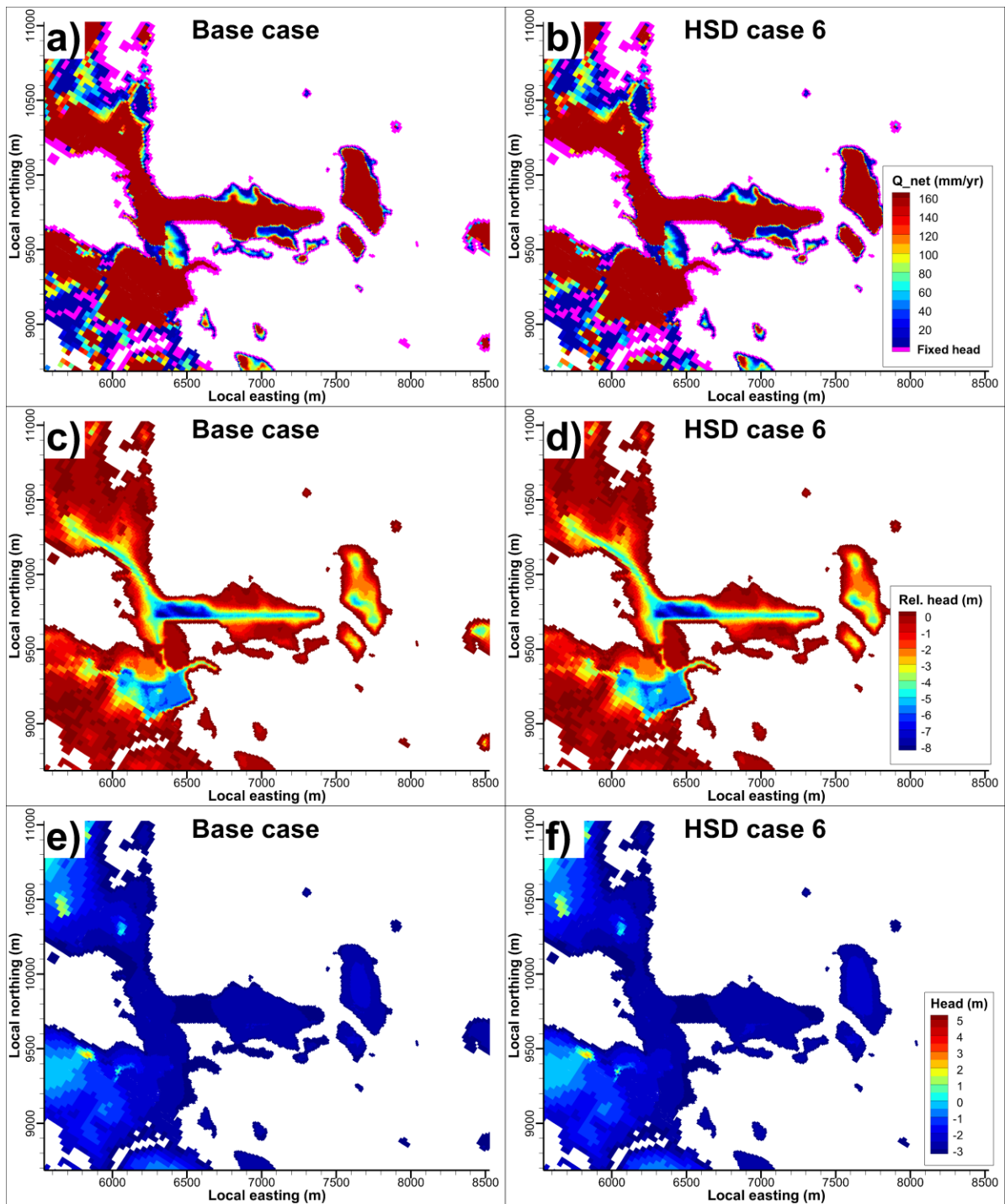
Figure 3-8. *Simulated ground-surface conditions for HSD case 6 compared to base case, at time slice 2500 AD.*

DokumentID
1578373, (1.0)

Sekretess
Öppen

Sida
51(165)

TD15 Complementary simulation cases in support of SR-PSU

3.1.2   Particle tracking

The two cases of low HSD conductivity have small effects on simulated performance measures (Table 3-1). The change has a negative sign for these two cases, implying that poorer performance measures are caclulated if the overlying regolith is low conductive. The reason for this is that low-conductive soil layers build up a higher groundwater level, which implies higher gradients in the underlying rock.

The groundwater levels are smoothened out in the highly conductive HSD case (variant 4), which reduces the hydraulic gradient and flow rates in the deeper rock. This implies longer travel time (median increases by +13% in the shallower SFR1, and +62% in the deeper SFR3). The simulated performance measures from particle tracking are presented in detail in (Figure 3-9 to Figure 3-13).

Table 3-1. Effect of HSD parameterisation on performance[1]

Performance measure	Facility	HSD case			
		2) $K_{HSD} = 10^{-8}$ m/s	3) Low K_{HSD}	4) High K_{HSD}	5) Bedrock-surface choke
Travel time	SFR1	-4%	-11%	13%	0%
	SFR3	-2%	-3%	62%	11%
F-quotient	SFR1	-9%	-12%	14%	-6%
	SFR3	-9%	-7%	54%	7%
Path length	SFR1	-6%	-6%	-8%	0%
	SFR3	2%	2%	15%	5%

1)   Expressed as change in median value, relative to default HSD parameterisation (HSD-case 1)

SVENSK KÄRNBRÄNSLEHANTERING AB

DokumentID
1578373, (1.0)

Sekretess
Öppen

Sida
52(165)

TD15 Complementary simulation cases in support of SR-PSU
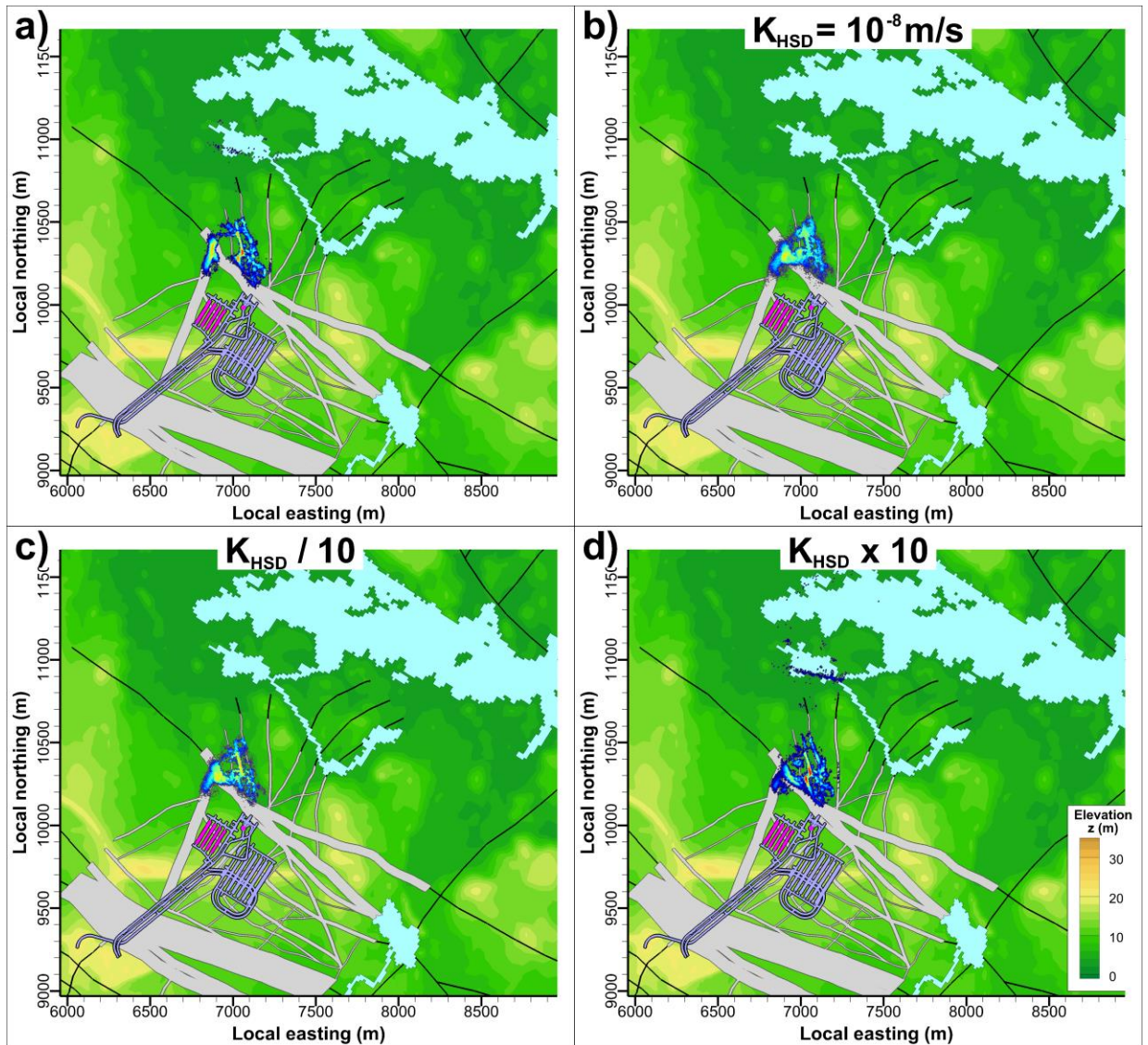
Figure 3-9. *Sensitivity to HSD parameterisation in particle tracking. Particle exit locations from SFR1 compared for alternative HSD parameterisations, BASE_CASE1_DFN_R85.*

DokumentID
1578373, (1.0)

Sekretess
Öppen

Sida
53(165)

TD15 Complementary simulation cases in support of SR-PSU
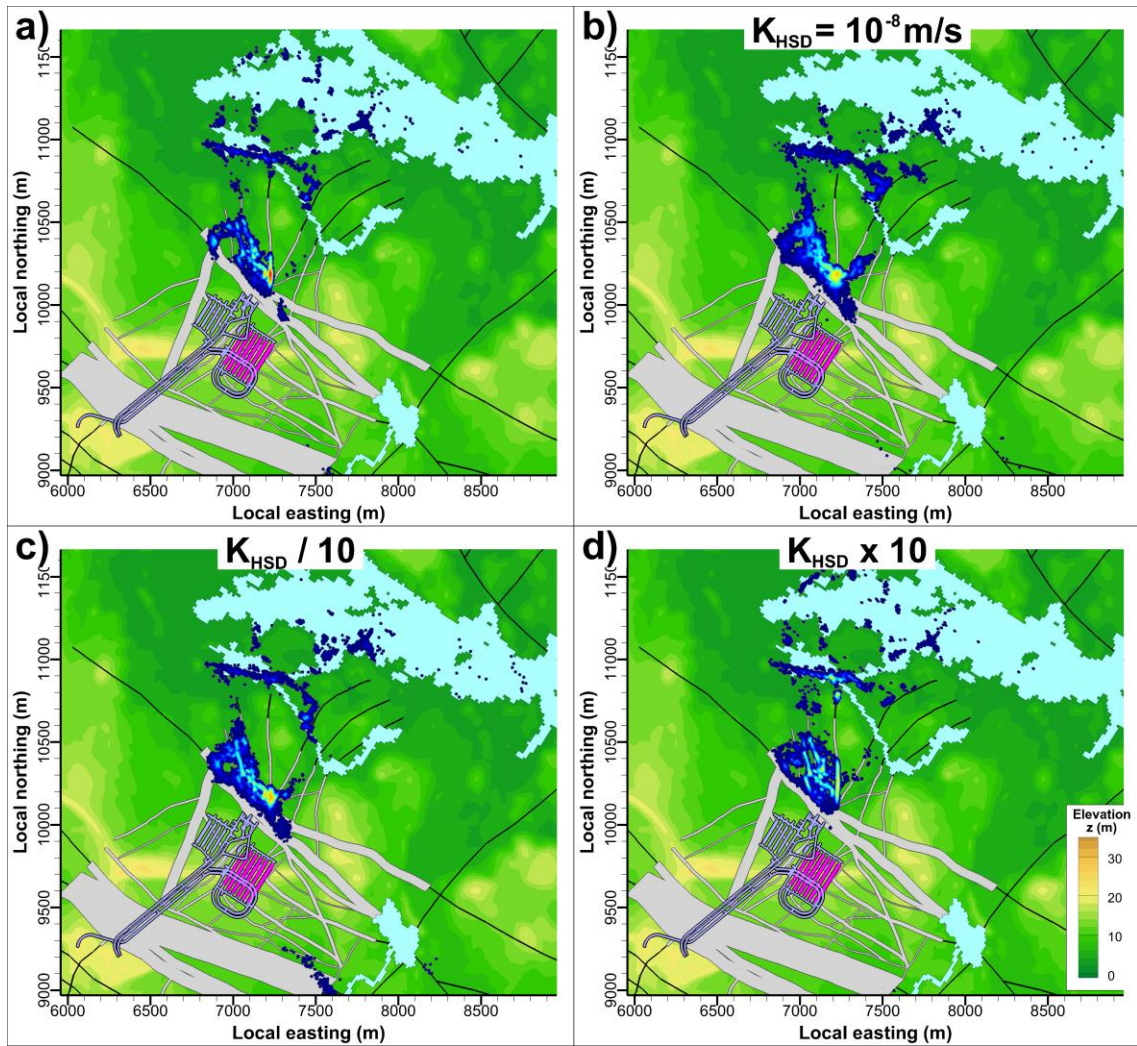
Figure 3-10. Sensitivity to HSD parameterisation in particle tracking. Particle exit locations from SFR3 compared for alternative HSD parameterisations, BASE_CASE1_DFN_R85.

DokumentID
1578373, (1.0)

Sekretess
Öppen

Sida
54(165)

TD15 Complementary simulation cases in support of SR-PSU
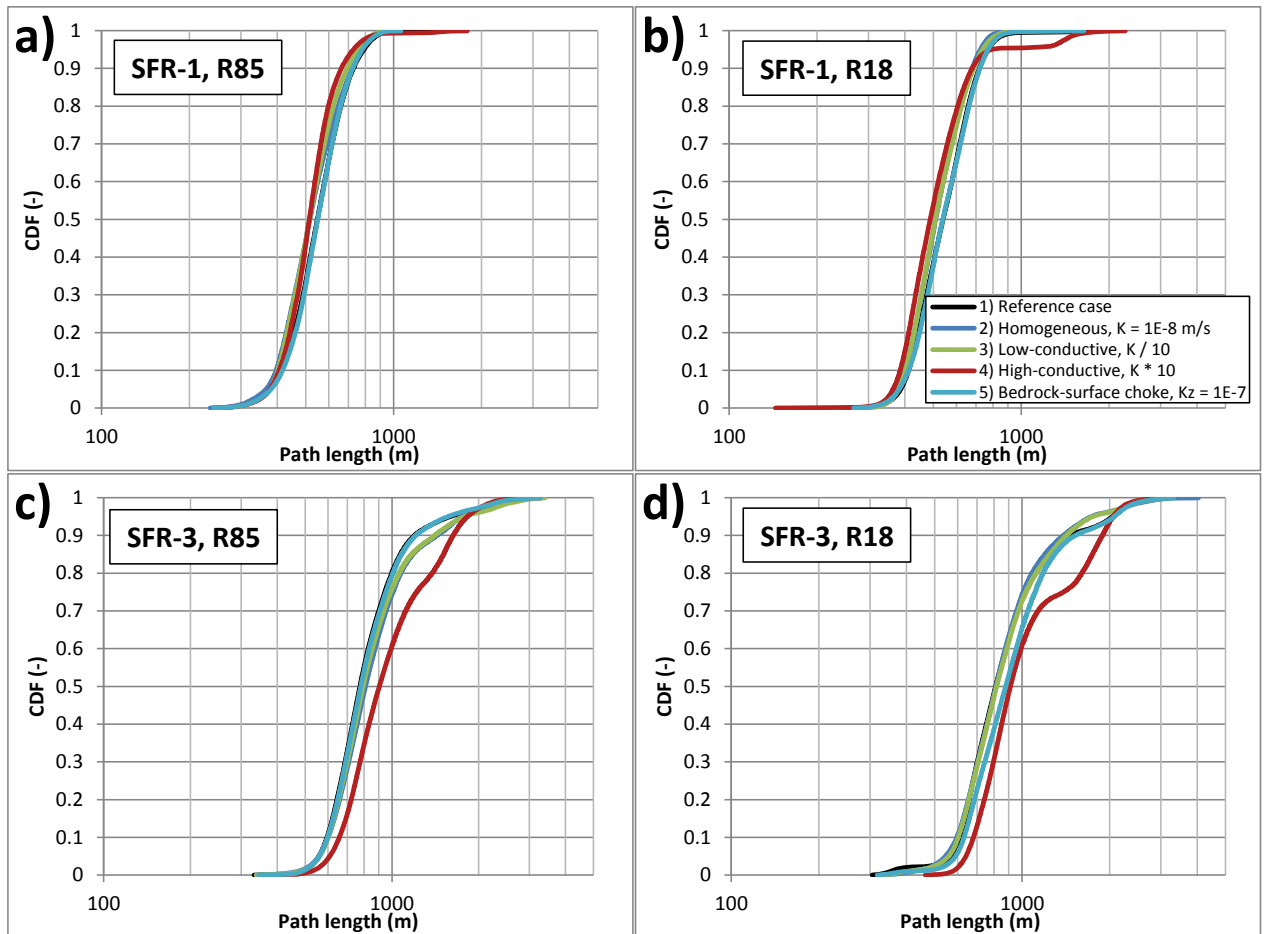
Figure 3-11. Sensitivity in simulated path length to HSD-parameterisation alternatives.

DokumentID
1578373, (1.0)

Sekretess
Öppen

Sida
55(165)

TD15 Complementary simulation cases in support of SR-PSU
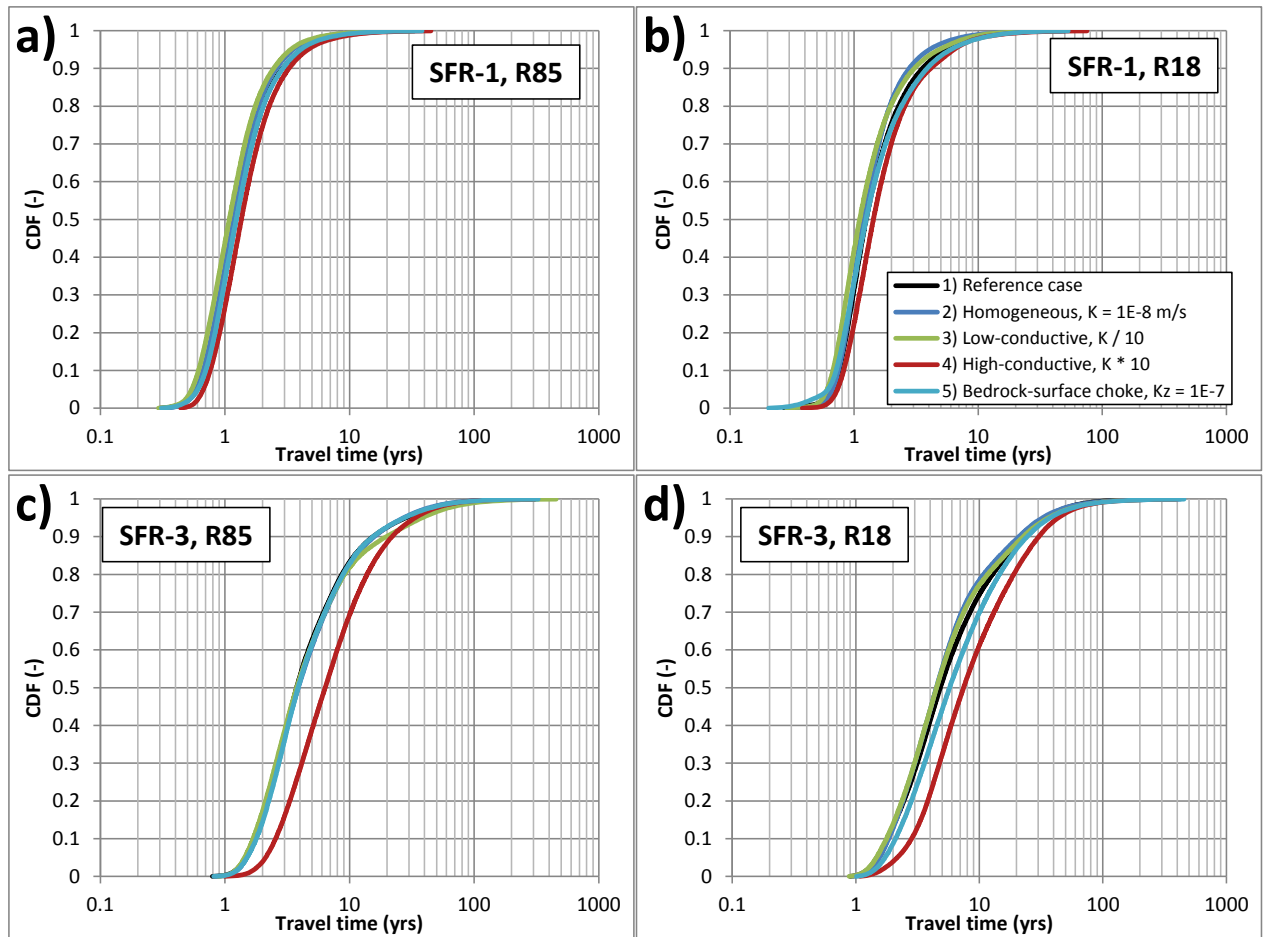
Figure 3-12. Sensitivity in simulated travel time to HSD-parameterisation alternatives.

DokumentID
1578373, (1.0)

Sekretess
Öppen

Sida
56(165)

TD15 Complementary simulation cases in support of SR-PSU
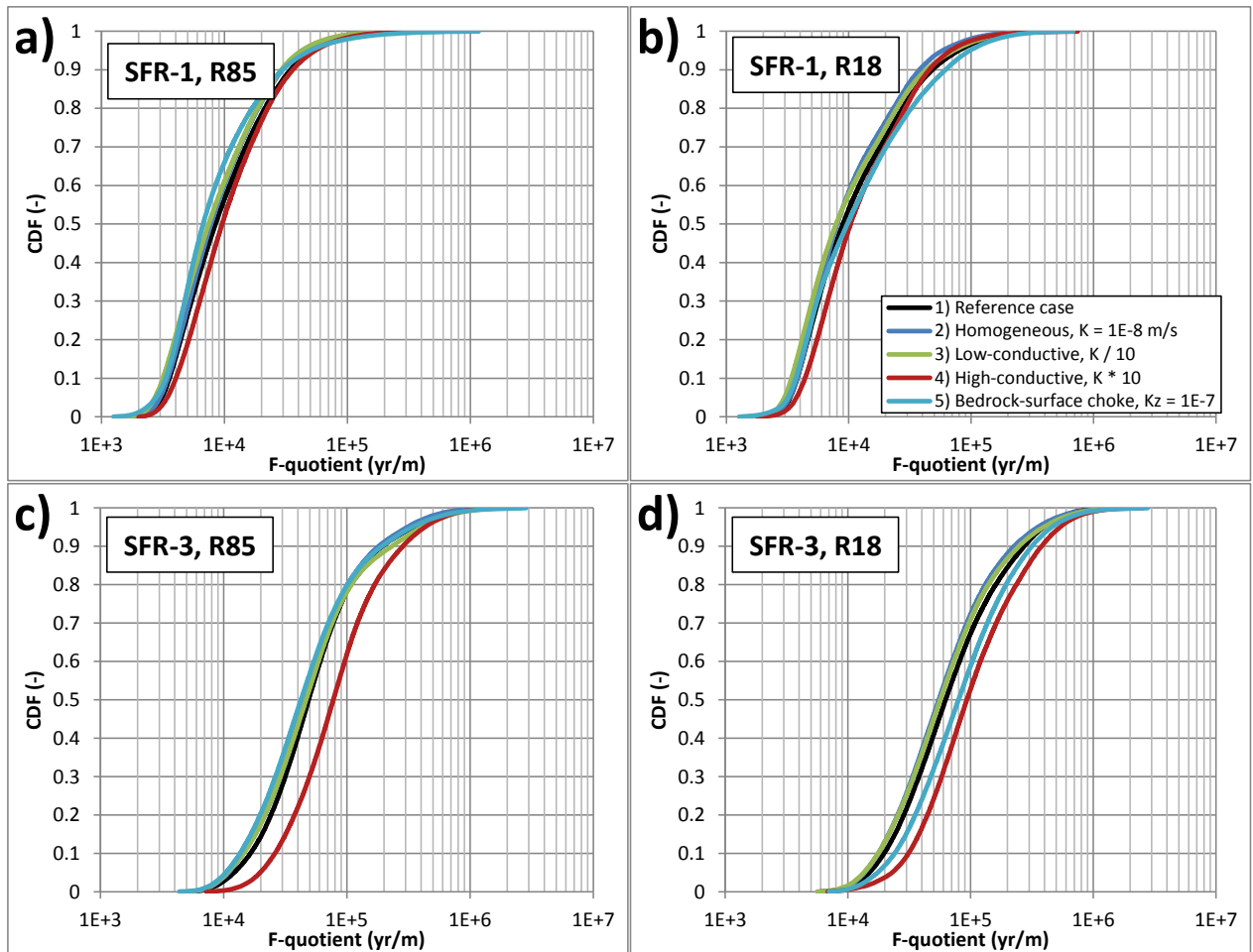
Figure 3-13. *Sensitivity in simulated F-quotient to HSD-parameterisation alternatives.*

3.2 HCD parameterisation (role of historic packer data)

Historic short-term, packer-test data represent local hydraulic properties of the surrounding rock mass. In case the flowing fracture system is compartmentalised, the use of local hydraulic data may result in overestimation of the effective transmissivity of large-scale flow paths (e.g., deformation zones). Thus, data-based HCD parameterisation is subject to an uncertainty concerning if the representative scale of data relative to the modelled structure (i.e., particularly regarding the historic packer data, as discussed in Appendix A of Öhman et al. 2013). The significance of this uncertainty is evaluated by comparing the performance measures of the original data-based HCD parameterisation (Table 1-1) versus those in the reference case.

The transmissivity parameterisation of the key zones surrounding SFR (i.e., ZFM871, ZFMNW0805, ZFMWNW0001) is between 2.5 and 10 times higher in the original data-based parameterisation, as compared to the final, revised HCD parameterisation (Table 1-1). The results demonstrate that – even if the individual flow magnitudes are redistributed somewhat between the different disposal rooms – the effect is negligible in terms of total flow across the facilities (Figure 3-14; the net effect is less than 1%).
Likewise, visual inspection of particle exit locations suggests that the HCD parameterisation also has negligible effect on particle tracking (Figure 3-15).

TD15 Complementary simulation cases in support of SR-PSU
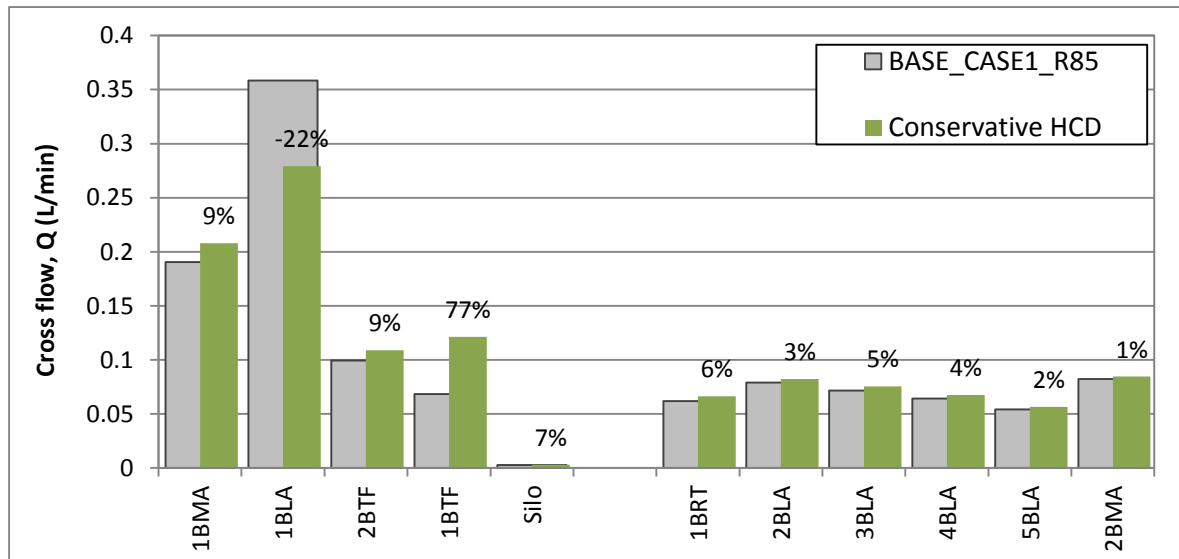
Figure 3-14. Disposal-room cross flows for conservative HCD parameterisation (Table 1-1) compared against base case.

DokumentID
1578373, (1.0)

Sekretess
Öppen

Sida
58(165)

TD15 Complementary simulation cases in support of SR-PSU
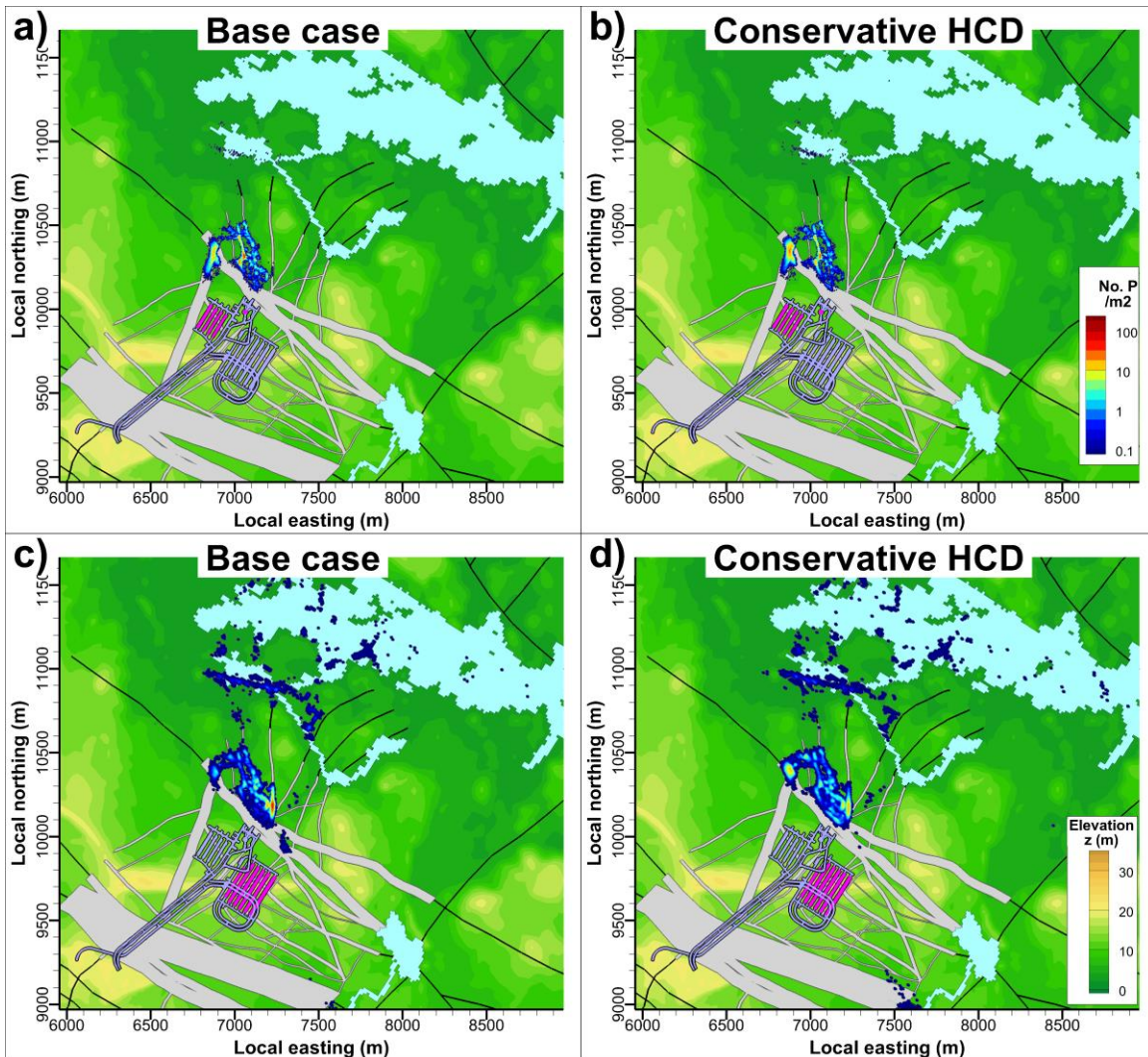
Figure 3-15. Sensitivity of exit locations to HCD parameterisation. The base-case parameterisation (SR-PSU in Table 1-1) is compared against the alternative based on historic packer data (referred to as conservative HCD parameterisation). Distribution of exit locations from SFR 1 (pink-shaded) shown in a) and b), while the exit locations from SFR 3 (pink-shaded) are shown in c) and d).

3.3   HRD: Size-transmissivity correlation in DFN model

The transmissivity parameterisation of the semi-correlated approach is compared against the original DFN parameterisation (i.e., the correlated approach) to verify that it is statistically consistent to its original setting, as seen by simulated borehole exploration and truncated below $T_{lim} = 2.5 \cdot 10^{-9}$ m^2/s (Appendix D). The semi-correlated parameterisation is demonstrated for fractures that intersect the disposal rooms of SFR1 and SFR3 (Figure 3-16). Note how the two sub-horizontal fractures A and B, of equal size and of the same set, parameterised as $T = 3 \cdot 10^{-7}$ m^2/s in its original setting, range from $2 \cdot 10^{-9}$ m^2/s to $3 \cdot 10^{-6}$ m^2/s in the semi-correlated parameterisation.

The semi-correlated parameterisation is verified further by means of simulated-borehole exploration (Appendix D), in terms of:
   1)   cross plots between sampled fracture transmissivity and size

DokumentID
1578373, (1.0)

Sekretess
Öppen

Sida
59(165)

TD15 Complementary simulation cases in support of SR-PSU

2) statistical distributions of sampled fracture transmissivity, and
3) transmissivity distributions of a full DFN realisation (i.e., c. 6,000,000 fractures).
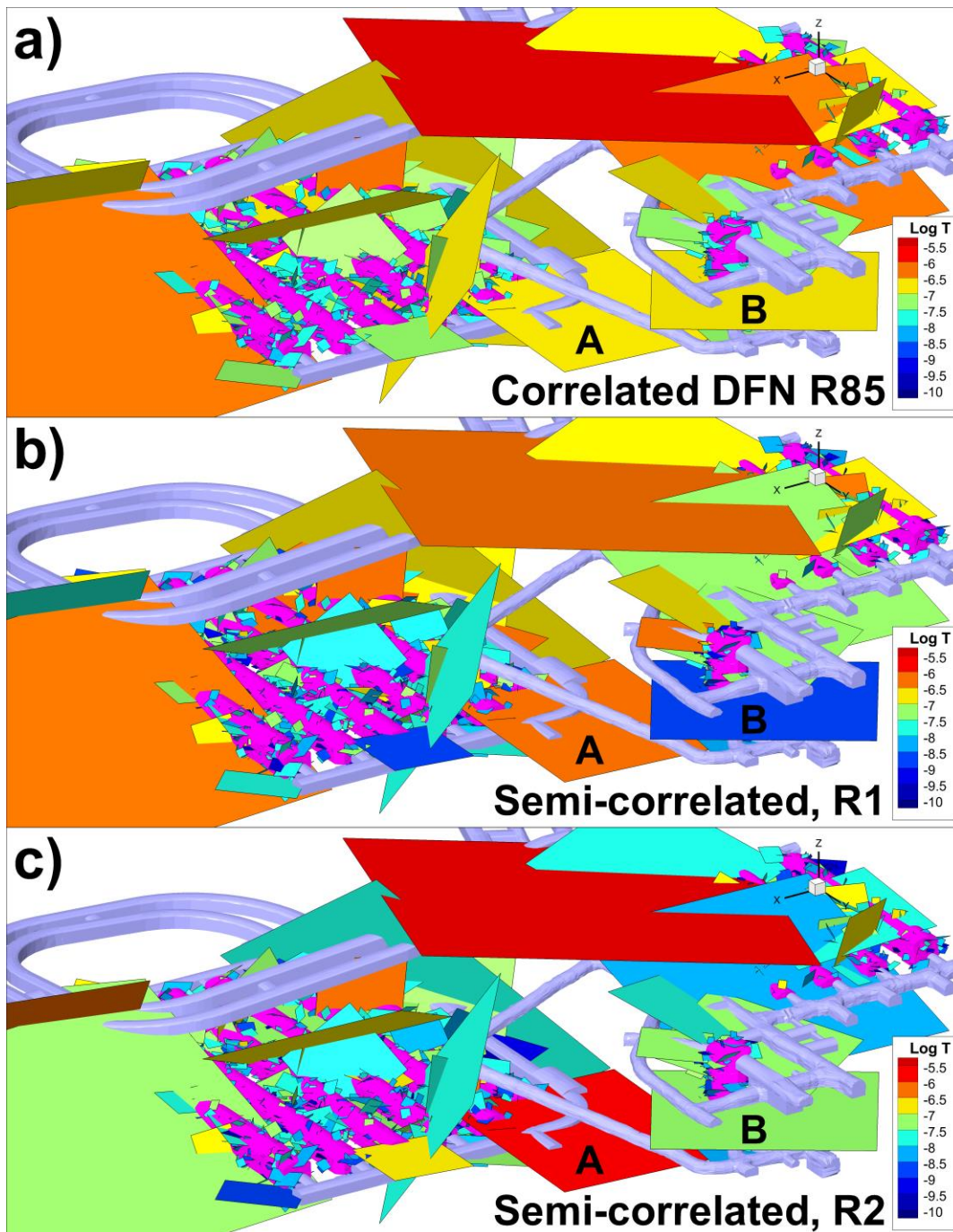
Figure 3-16. *Demonstration of the semi-correlated approach for fractures that intersect the disposal rooms; a) the original, deterministic size-transmissivity parameterisation of DFN R85, versus two parameterisation realisations that include a stochastic component, b) and c).*

DokumentID
1578373, (1.0)

Sekretess
Öppen

Sida
60(165)

TD15 Complementary simulation cases in support of SR-PSU

3.3.1   Disposal-room cross flow

All disposal rooms in SFR are expected to be intersected by the type of large fractures that dominate the hydraulic connection of regional-scale flow paths (e.g., Figure 3-16). Hence, the correlated approach is expected to be the most pessimistic parameterisation, as "*large fractures do not only form the most connected flow paths, but are also the most transmissive*".

Along with expectations, the effect of semi-correlated parameterisation on simulated disposal-room flow is small (Figure 3-17). The net effect is about -10%, although at the scale of individual disposal rooms the crossflow typically ranges from -30 to +15% (Figure 3-18).
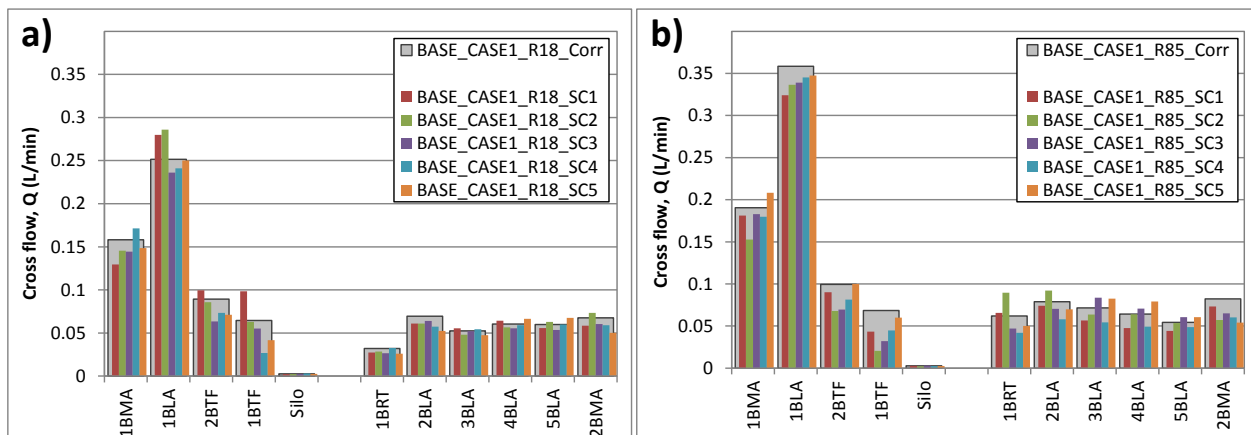
Figure 3-17. Effect of semi-correlated transmissivity parameterisation evaluated in terms of disposal-room flow for two DFN realisations; a) DFN R18 and b) DFN R85.
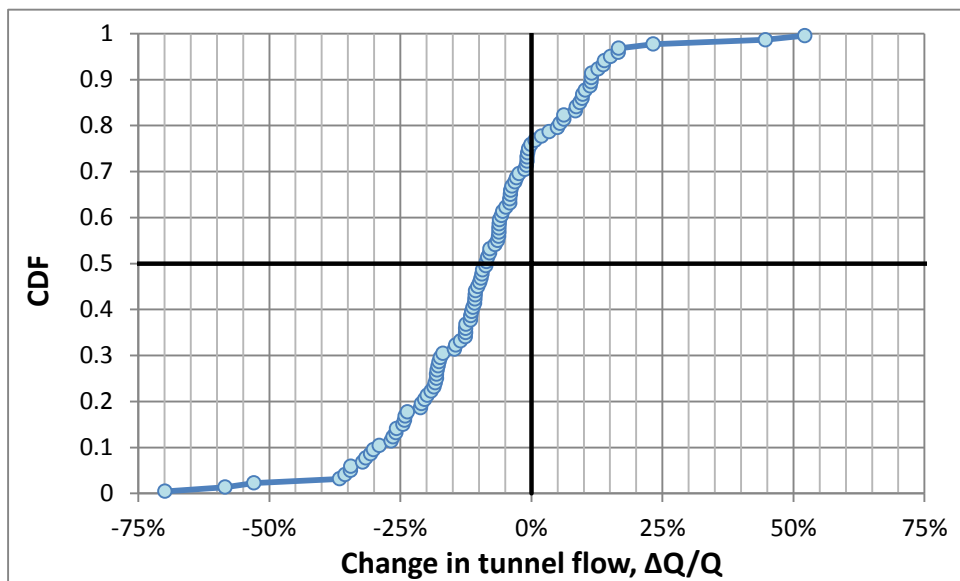
Figure 3-18. Effect of semi-correlated DFN parameterisation on disposal-room flow. The effect is evaluated on basis of individual disposal rooms (11), examined parameterisation realisations (5; SC1 to SC5), and two DFN realisations (R85 and R18).

SVENSK KÄRNBRÄNSLEHANTERING AB

DokumentID
1578373, (1.0)

Sekretess
Öppen

Sida
61(165)

TD15 Complementary simulation cases in support of SR-PSU

3.3.2 Particle-tracking performance

The effect of the semi-correlated DFN parameterisation on the simulated performance measures is small (Table 3-2). Note that the net effect is typically slightly improved performance (i.e., longer paths, longer travel time, and higher F-quotient). The effect on performance measures is demonstrated for the two DFN realisations, R85 and R18, and the two facilities, SFR1 and SFR3, separately (Figure 3-19 to Figure 3-21).

Table 3-2. Average effect[1] on simulated performance measures

	SFR1	SFR3
Path length, L (m)	1.0%	1.8%
Travel time, t (yrs)	3.5%	5.6%
F-quotient, F (yr/m)	13.0%	9.1%

1) Average difference in median value, as evaluated based on 5 realisations of semi-correlations of DFN R85 and DFN R18, (bedrock case 1 and 2 in Öhman et al. (2014)) compared to their original parameterisation (i.e., correlated size-transmissivity).
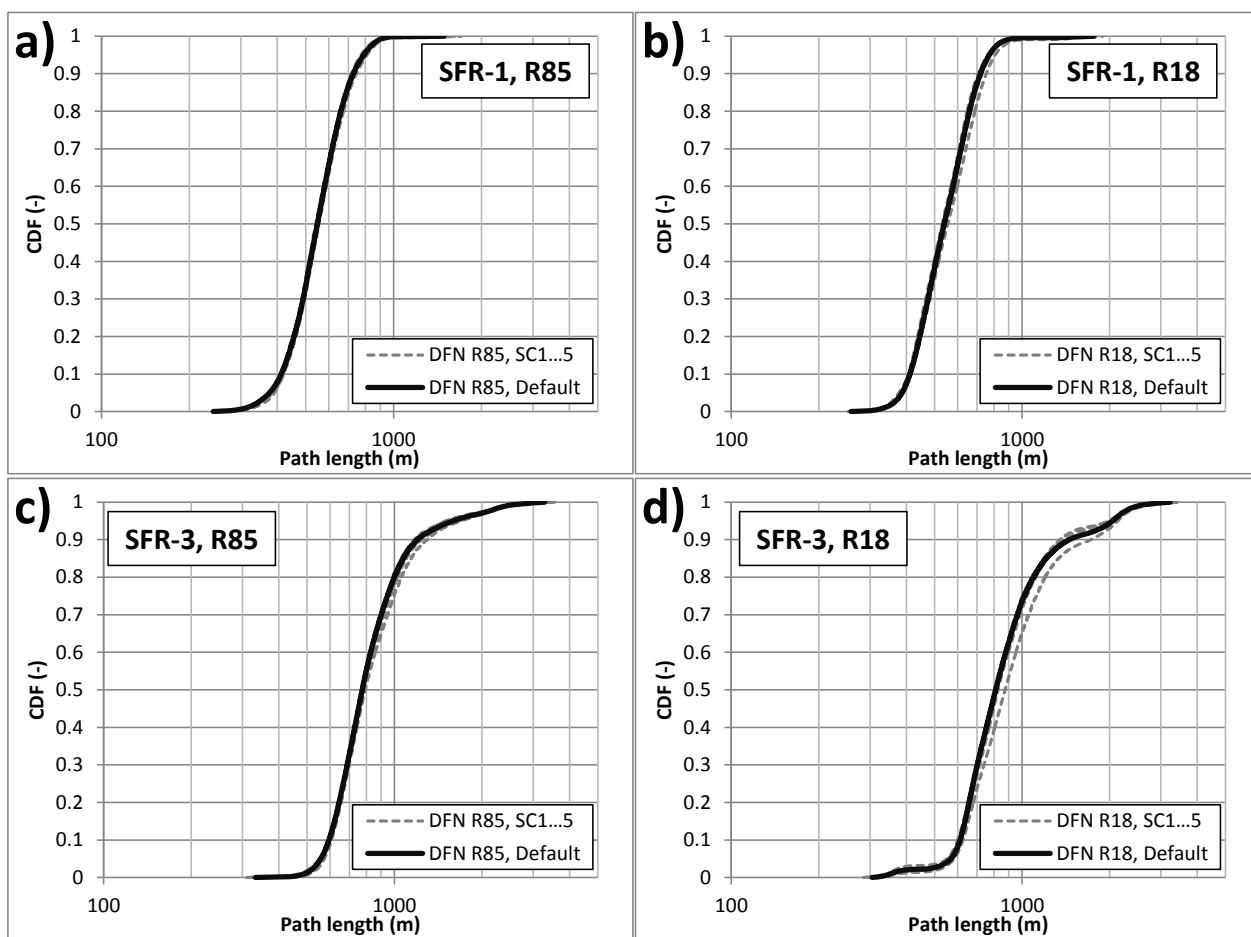
Figure 3-19. Effect of semi-correlated DFN parameterisation on simulated performance measures.

DokumentID
1578373, (1.0)

Sekretess
Öppen

Sida
62(165)

TD15 Complementary simulation cases in support of SR-PSU
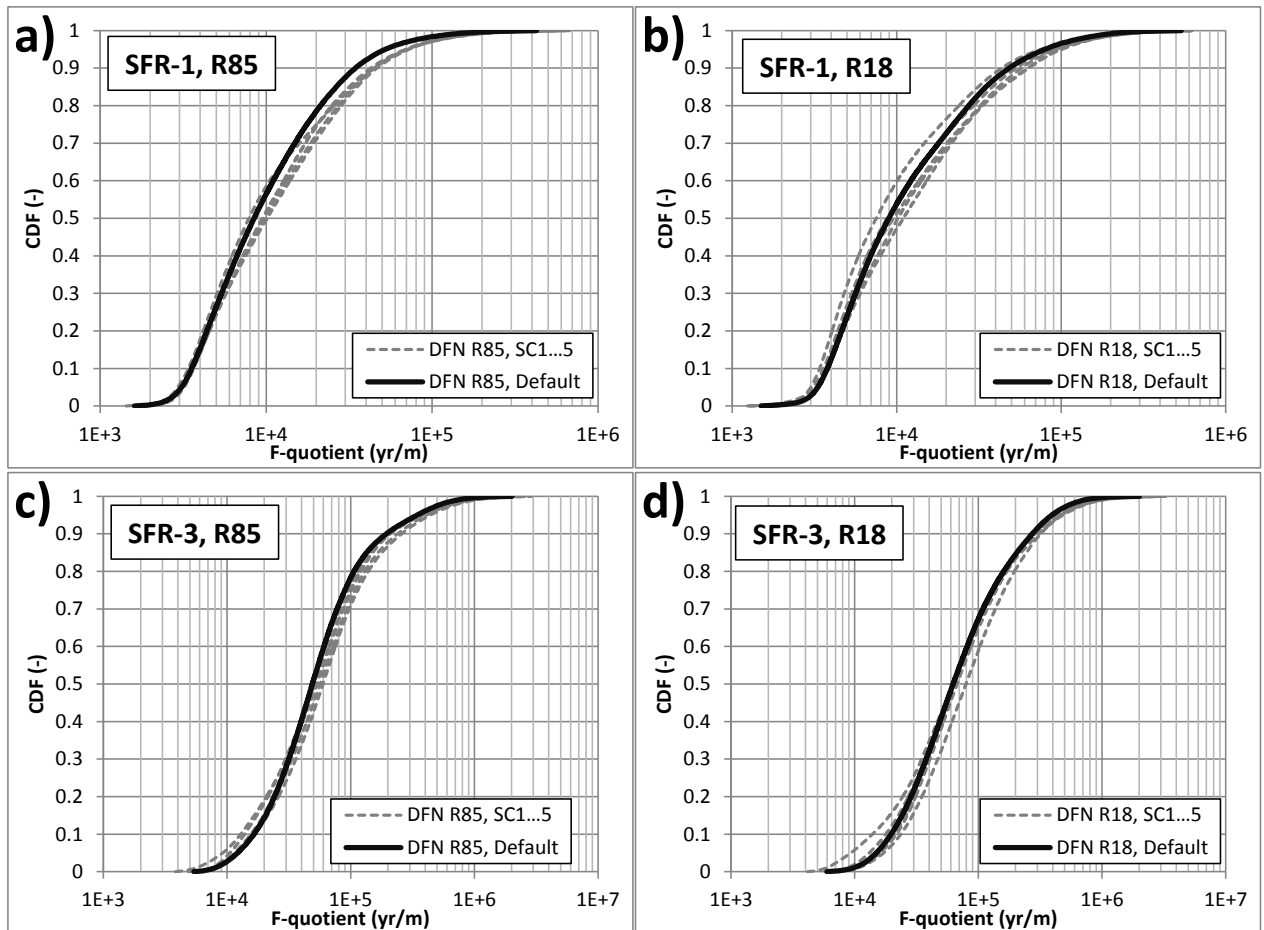
Figure 3-20. Effect of semi-correlated DFN parameterisation on simulated performance measures.
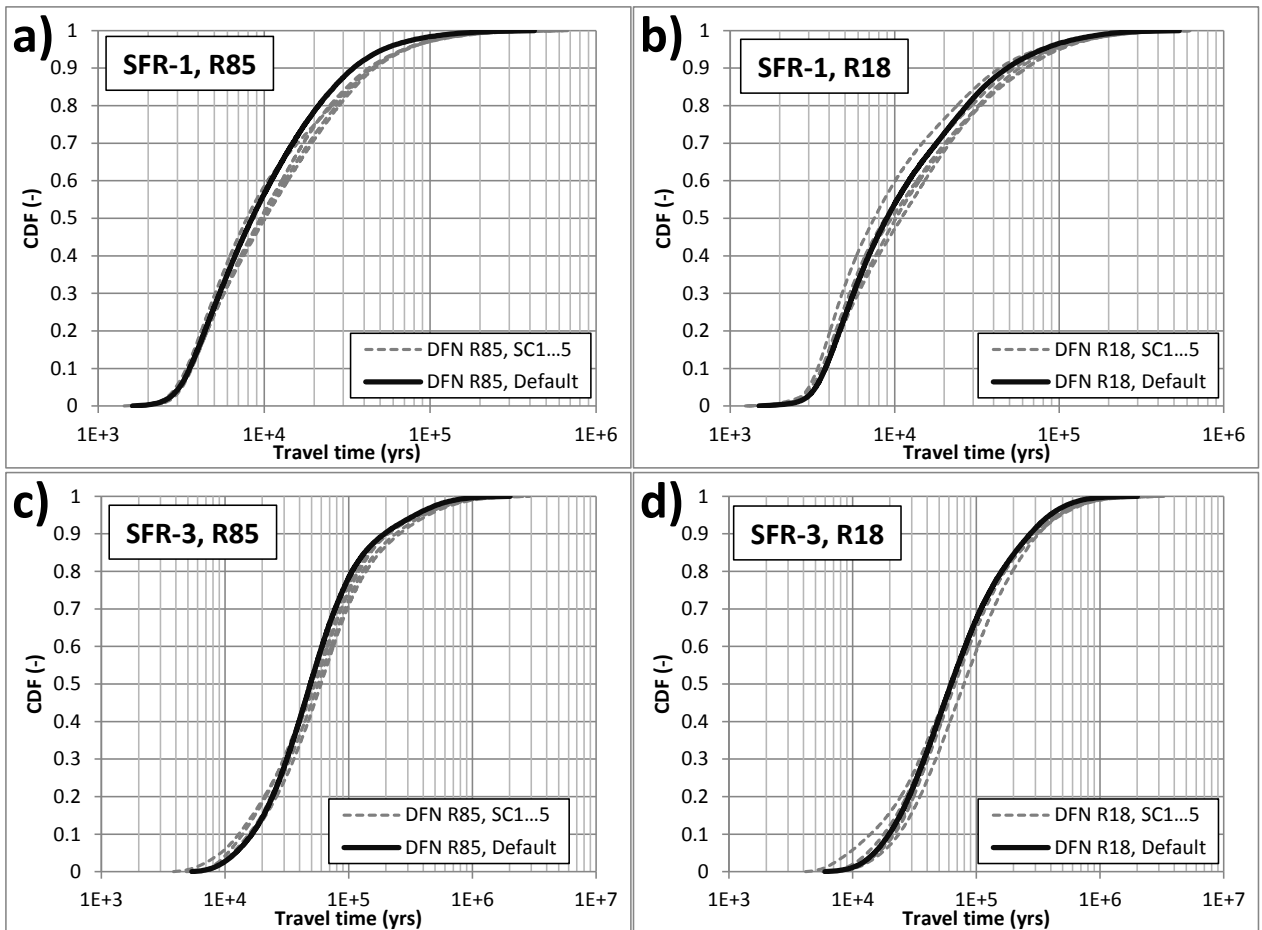
Figure 3-21. Effect of semi-correlated DFN parameterisation on simulated performance measures.

3.4   HRD: Heterogeneity outside SFR Regional domain

The Hydraulic Rock-mass Domain (HRD) parameterisation outside the SFR Regional domain was based on a single DFN realisation in SR-PSU (i.e., TD11; Öhman et al. (2014) and Odén et al. (2014)). Thus, although the HRD parameterisation outside the SFR Regional domain reflect hydraulic heterogeneity resulting from structures/fractures that fall below the resolution of deterministic modelling (maximum side length, or ground-surface intercept of 1,000 m), the sensitivity to structural channelling was not fully accounted for, as its stochastical heterogeneity was kept *static* in the TD11 (Öhman et al. 2014) sensitivity analysis. This section is therefore devoted to evaluate the uncertainty component arising from a stochastic representation of the fracture network outside the SFR Regional domain (geometrical and hydraulic properties). This is evaluated by comparing performance measures of the static DFN realisation, used in TD11 and Odén et al. (2014) versus those from five stochastic DFN realisations, as illustrated in Figure 2-7 and Figure 2-8. All simulations in this particular study employ the same model scenario: a) time-slice 5000 AD and b) base-case parameterisation inside the SFR Regional domain (i.e., referred to as Case 1 in TD11, with homogeneous HCD and DFN R85).

DokumentID
1578373, (1.0)

Sekretess
Öppen

Sida
64(165)

TD15 Complementary simulation cases in support of SR-PSU

3.4.1   Analysis of performance measures

The quantified performance measures are: disposal-room cross flow (Figure 3-22), exit locations (Figure 3-24 and Figure 3-25), and particle-trajectory statistics (Figure 3-26). At the more detailed level, the observed effects are put in context of the parameterised flowing fracture network (Figure 3-27 to Figure 3-32). A probabilistic analysis is also undertaken to determine the risk of DFN realisations with anomalous exit locations (Appendix E).

The effects from stochastic HRD parameterisation outside the SFR Regional domain are negligible in simulated disposal-room cross flow (Figure 3-22). The reason for this is that, although the parameterisation outside the SFR Regional domain affects distant downstream flow paths (as demonstrated later; Figure 3-27 to Figure 3-32), the disposal-room flow is primarily controlled by the nearfield parameterisation (i.e., HCD and HRD inside the SFR Regional domain). Thus, as the parameterisation inside the SFR Regional domain is kept constant, the impact on simulated disposal-room is very small, compared to the impact on particle tracking results.

Figure 3-22. Sensitivity of tunnel flow to stochastic HRD parameterisation outside SFR Regional domain; static parameterisation employed in SR-PSU (grey bars) compared to DFN realisations, R01 to R05.

Exit locations

Tracking released particles from disposal rooms of SFR1 and SFR3 demonstrates that most trajectories terminate inside the SFR Regional domain (i.e., exit location defined as the point of discharge across the bedrock surface). More precisely, less than one percent (0.1%) of the exit locations from SFR1 occurs inside the SFR Regional domain, while the corresponding fraction for SFR3 is 5% (i.e., owing to its deeper location, which cause longer flow paths). Based on this observation, the analysis of stochastic heterogeneity in HRD parameterisation outside SFR Regional domain was not prioritised within SR-PSU. However, analysis of the studied five realisations here (Figure 2-7 and Figure 2-8) demonstrates that:

- Most realisations have little or no effect on exit locations (4 out of 5 do not affect exit locations from SFR1, while an increasing fraction of exit locations from SFR3 is observed outside the SFR Regional domain; Figure 3-23)
- Up to 50% of the particles can exit outside the SFR Regional domain (i.e., R02 in Figure 3-23)

SVENSK KÄRNBRÄNSLEHANTERING AB

DokumentID
1578373, (1.0)

Sekretess
Öppen

Sida
65(165)

TD15 Complementary simulation cases in support of SR-PSU

- Irrespectively of stochastic DFN realisation, the general pattern of exit locations exhibits strong correlation to topographical depressions (Figure 3-24 and Figure 3-25) as well as ground-surface intercepts of the flowing fracture network (Figure 3-27 to Figure 3-32).
- In spite of migrated exit locations and extended path lengths, the effects in key performance measures, advective travel time and F-quotient, are very small (Figure 3-26)
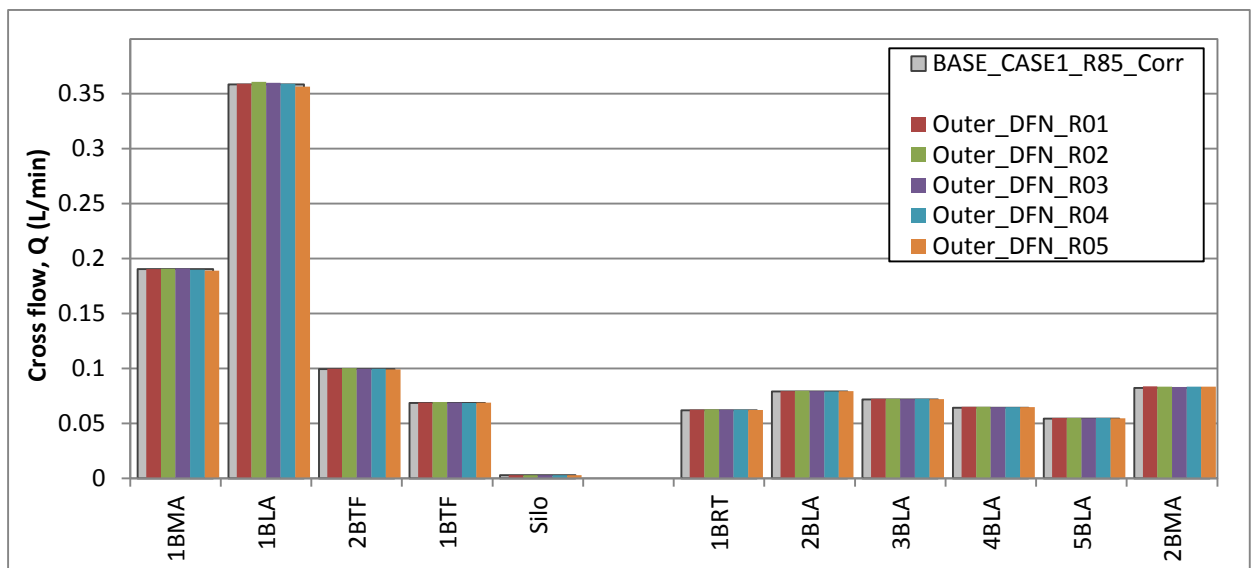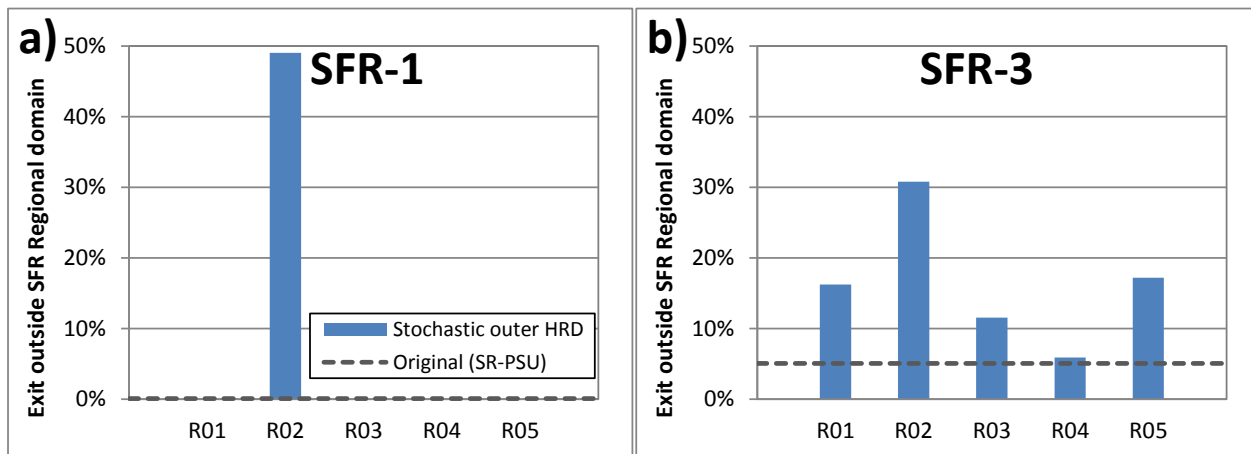

Figure 3-23. *Sensitivity of tunnel flow to stochastic HRD parameterisation outside SFR Regional domain; static parameterisation employed in SR-PSU (grey bars) compared to DFN realisations, R01 to R05.*

DokumentID
1578373, (1.0)

Sekretess
Öppen

Sida
66(165)

TD15 Complementary simulation cases in support of SR-PSU
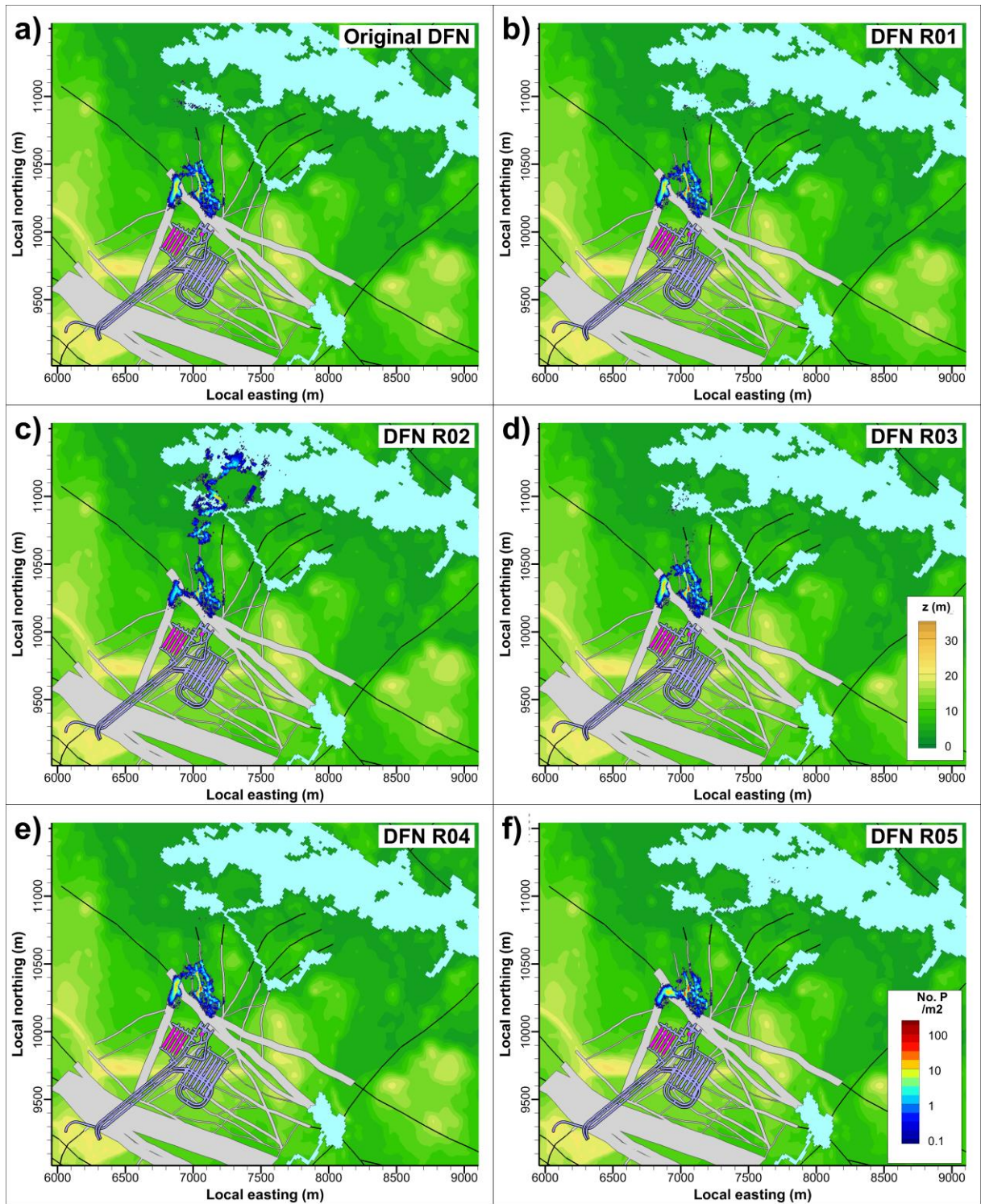
Figure 3-24. Density in particle-exit locations from SFR1 (pink shaded), depending on stochastic parameterisation of the heterogeneous HRD outside the SFR Regional domain; a) the original, static DFN realisation used in SR-PSU (i.e., Öhman et al. (2014) and Odén et al. (2014)), compared against realisations R01 to R05 (Figure 2-7).

DokumentID
1578373, (1.0)

Sekretess
Öppen

Sida
67(165)

TD15 Complementary simulation cases in support of SR-PSU
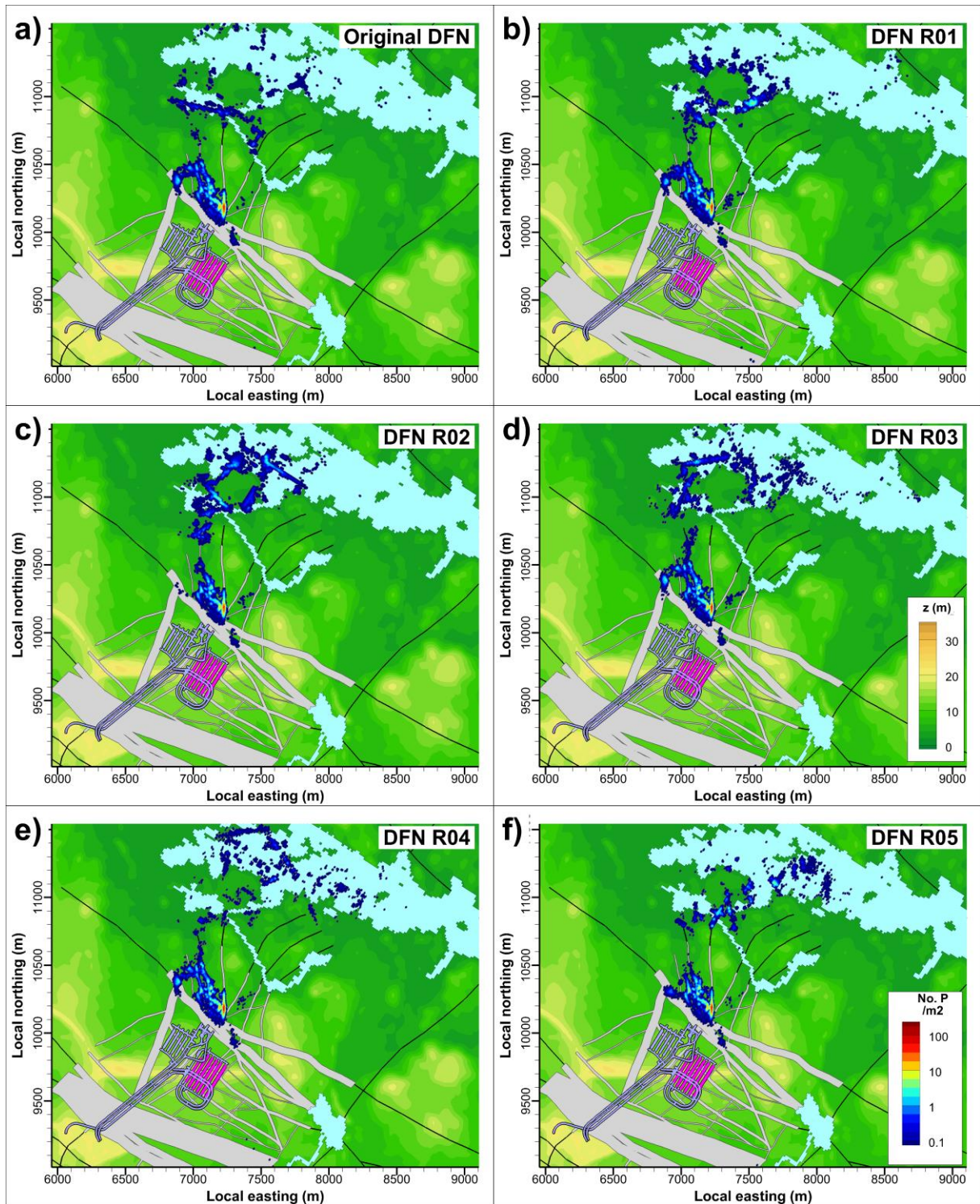
Figure 3-25. *Density in particle-exit locations from SFR3 (pink shaded), depending on stochastic parameterisation of the heterogeneous HRD outside the SFR Regional domain; a) the original, static DFN realisation used in SR-PSU (i.e., Öhman et al. (2014) and Odén et al. (2014)), compared against realisations R01 to R05 (Figure 2-7).*

DokumentID
1578373, (1.0)

Sekretess
Öppen

Sida
68(165)

TD15 Complementary simulation cases in support of SR-PSU

***Figure 3-26.** Sensitivity to channelling of fractures below the resolution for deterministic modelling, quantified in terms of performance measures for DFN realisation, R01 to R05.*

DokumentID
1578373, (1.0)

Sekretess
Öppen

Sida
69(165)

TD15 Complementary simulation cases in support of SR-PSU

3.4.2   Inspection of flow paths outside the SFR Regional domain

Simulation results indicate that, although the channelling of structures outside SFR Regional domain has a minor impact on cumulative performance measures, a substantial fraction of the exit locations can be re-directed to downstream biosphere objects (Section 3.4.1). Therefore, the flow paths which cross the SFR Regional-domain boundary in DFN realisations R01 to R05 are analysed in detail. In particular, DFN realisation R02 has the most dramatic effect on the re-location of exist locations, and therefore the goal of this study is to:

1) infer the cause to this effect,
2) to judge if the phenomenon is realistic, and
3) judge the risk of occurrence

Inspection demonstrates that the re-direction of exit locations in R02 are primarily caused by a single, large fracture (red plane in Figure 3-29), which extends more or less from the junction of ZFMNNE0869 and ZFMNW0805 (white arrow in Figure 3-33) and to Charlie's lake (Biosphere object 116). The fracture is sub-horizontal and follows the bedrock surface at depths ranging from 0 to 40 m. Via the intersections of steeply dipping fractures, the sub-horizontal fracture is hydraulically connected to the ground surface (Figure 3-34b) at lower terrain than in Biosphere 157_2; thus the flow paths are re-directed towards the point of minimum potential (lowest ground surface).

It should be noted that the large fracture in DFN R02 does not extend far into the SFR Regional domain (see 300 m respect distance in Figure 3-33); in fact, it does not cross south of ZFMNW0805A/B. This type of shallow, sub-horizontal fractures, seemingly unrelated to deformation zones, is observed in the SFR investigations (Öhman et al. 2012). Furthermore, little is known about the bedrock characteristic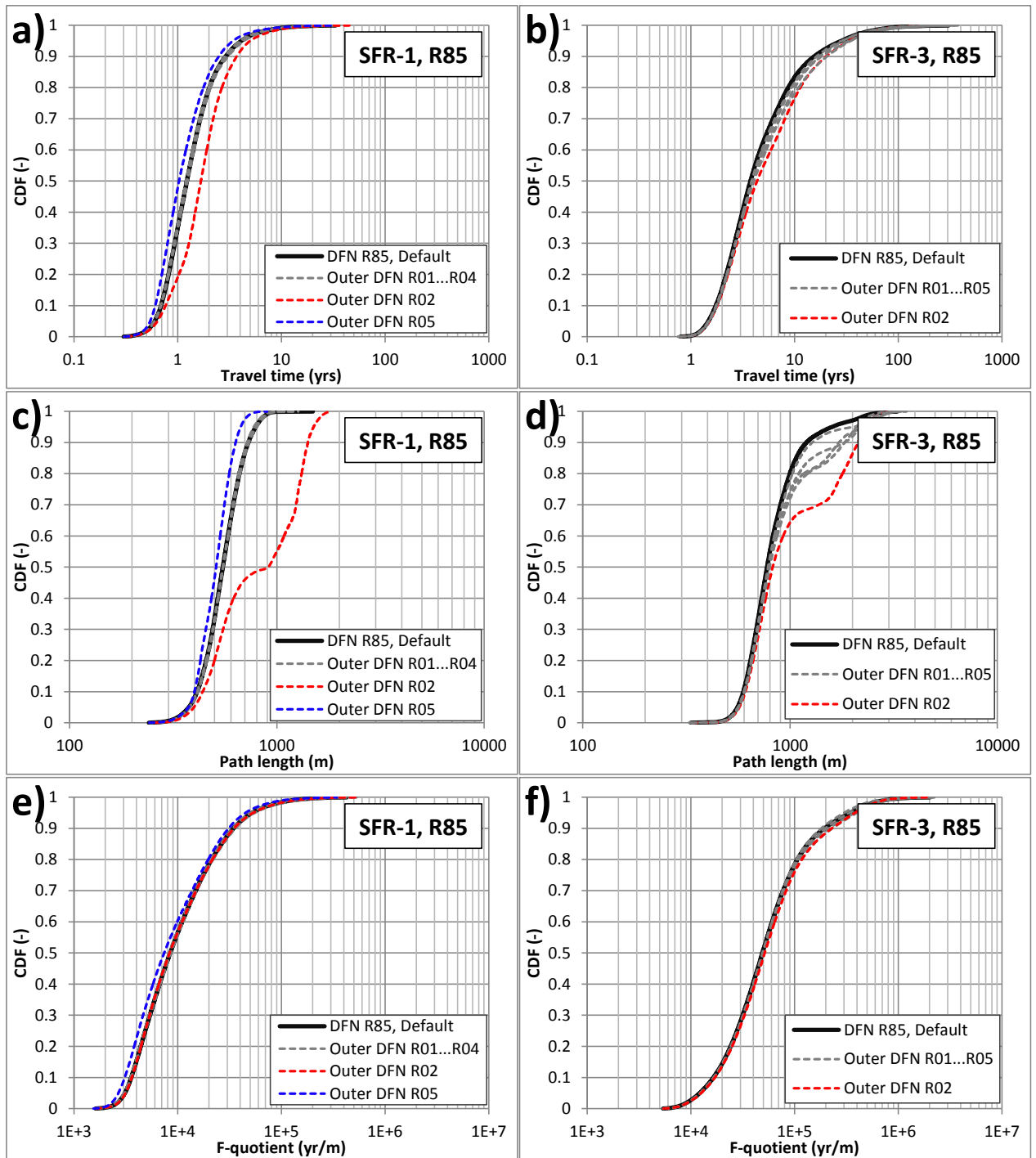s north of ZFMNW0805A/B. Therefore, the occurrence of this type of structures cannot be dismissed as "unrealistic". Based on the ensemble of realisations studied here (six realisations), the occurrence of this phenomenon must be estimated as once per every 6 realisations ≈ a frequency of occurrence of 17%. However, the studied ensemble is too small to provide a realistic representation of stochastic variability, and therefore this risk estimation is highly uncertain.

Therefore, a probabilistic/geometric DFN analysis has been undertaken to provide a better-funded estimate of the occurrence of the phenomenon observed in DFN R02 (Appendix E). A set of hydrogeological traits are defined, which are assumed indicative of stochastic structures with potentially a dramatic impact on particle trajectories outside the SFR Regional domain. A large ensemble of DFN realisations is generated (1,000 realisations) and analysed in terms of the pre-defined hydrogeological identification traits, in order to estimate the frequency of occurrence of the type of stochastic structures that may dramatically re-direct a substantial fraction of the discharging flow from SFR (i.e., the type of structures found in DFN R02). As the outcome, the risk of this phenomenon is estimated to be considerably rarer than 1/6 (the frequency of occurrence is estimated to ≈ 1.4%).

DokumentID
1578373, (1.0)

Sekretess
Öppen

Sida
70(165)

TD15 Complementary simulation cases in support of SR-PSU

Figure 3-27. Sensitivity to DFN outside SFR Regional domain in particle tracking: Static DFN realisation. Release disposal room (red), biosphere objects (pink line), SFR Regional domain (orange lines), particle trajectories (grey lines), exit-location density (contoured in a and b), ground-surface fracture intercepts (black lines, in c and d), trajecting fractures (contoured by transmissivity in c and d)

DokumentID
1578373, (1.0)

Sekretess
Öppen

Sida
71(165)

TD15 Complementary simulation cases in support of SR-PSU

Figure 3-28. *Sensitivity to DFN outside SFR Regional domain in particle tracking: realisation R01. Release disposal room (red), biosphere objects (pink line), SFR Regional domain (orange lines), particle trajectories (grey lines), exit-location density (contoured in a and b), ground-surface fracture intercepts (black lines, in c and d), trajecting fractures (contoured by transmissivity in c and d).*

DokumentID
1578373, (1.0)

Sekretess
Öppen

Sida
72(165)

TD15 Complementary simulation cases in support of SR-PSU

Figure 3-29. *Sensitivity to DFN outside SFR Regional domain in particle tracking: realisation R02. Release disposal room (red), biosphere objects (pink line), SFR Regional domain (orange lines), particle trajectories (grey lines), exit-location density (contoured in a and b), ground-surface fracture intercepts (black lines, in c and d), trajecting fractures (contoured by transmissivity in c and d).*

DokumentID
1578373, (1.0)

Sekretess
Öppen

Sida
73(165)

TD15 Complementary simulation cases in support of SR-PSU

Figure 3-30. *Sensitivity to DFN outside SFR Regional domain in particle tracking: realisation R03. Release disposal room (red), biosphere objects (pink line), SFR Regional domain (orange lines), particle trajectories (grey lines), exit-location density (contoured in a and b), ground-surface fracture intercepts (black lines, in c and d), trajecting fractures (contoured by transmissivity in c and d).*

DokumentID
1578373, (1.0)

Sekretess
Öppen

Sida
74(165)

TD15 Complementary simulation cases in support of SR-PSU
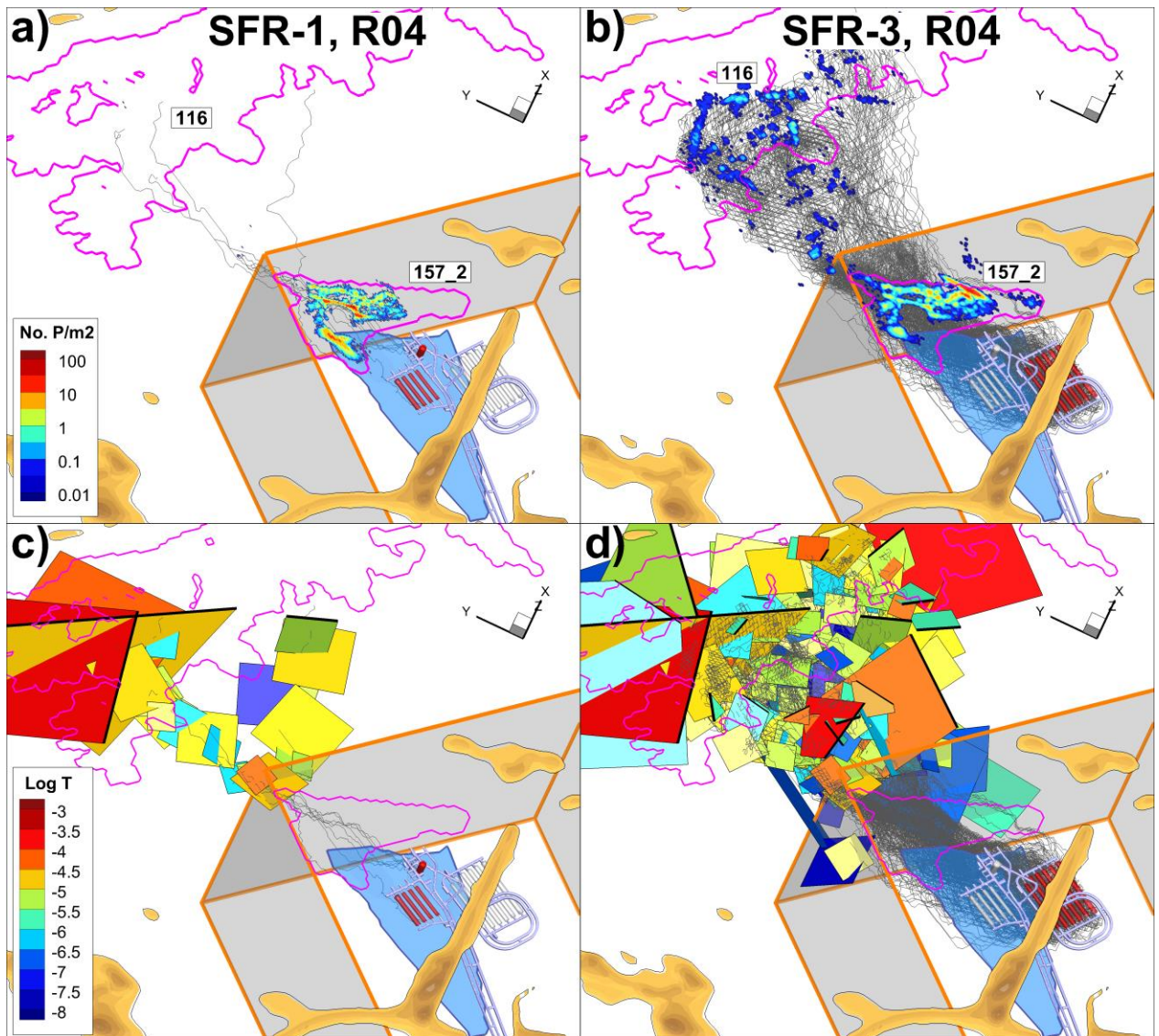
Figure 3-31. *Sensitivity to DFN outside SFR Regional domain in particle tracking: realisation R04. Release disposal room (red), biosphere objects (pink line), SFR Regional domain (orange lines), particle trajectories (grey lines), exit-location density (contoured in a and b), ground-surface fracture intercepts (black lines, in c and d), trajecting fractures (contoured by transmissivity in c and d).*

DokumentID
1578373, (1.0)

Sekretess
Öppen

Sida
75(165)
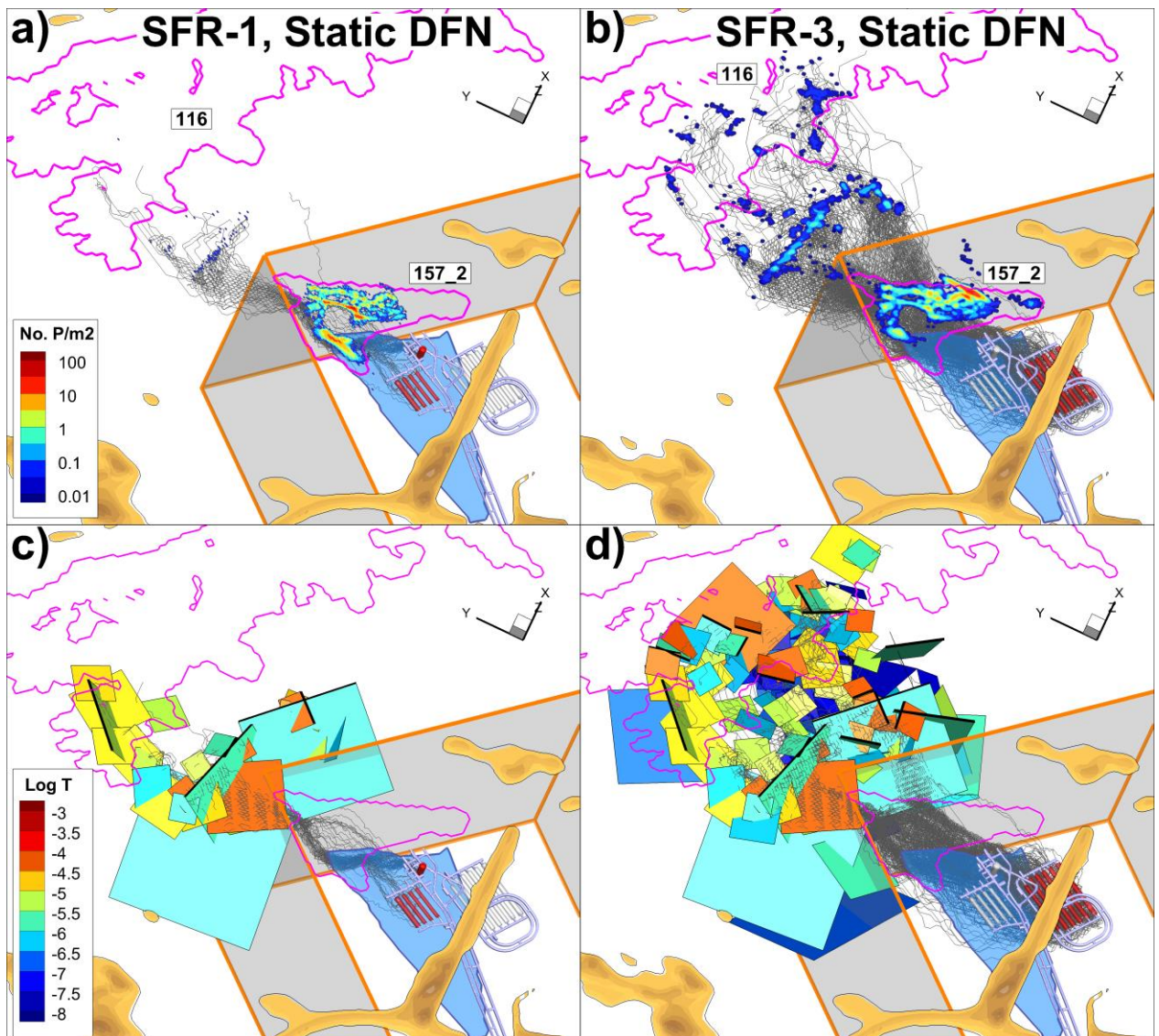
TD15 Complementary simulation cases in support of SR-PSU
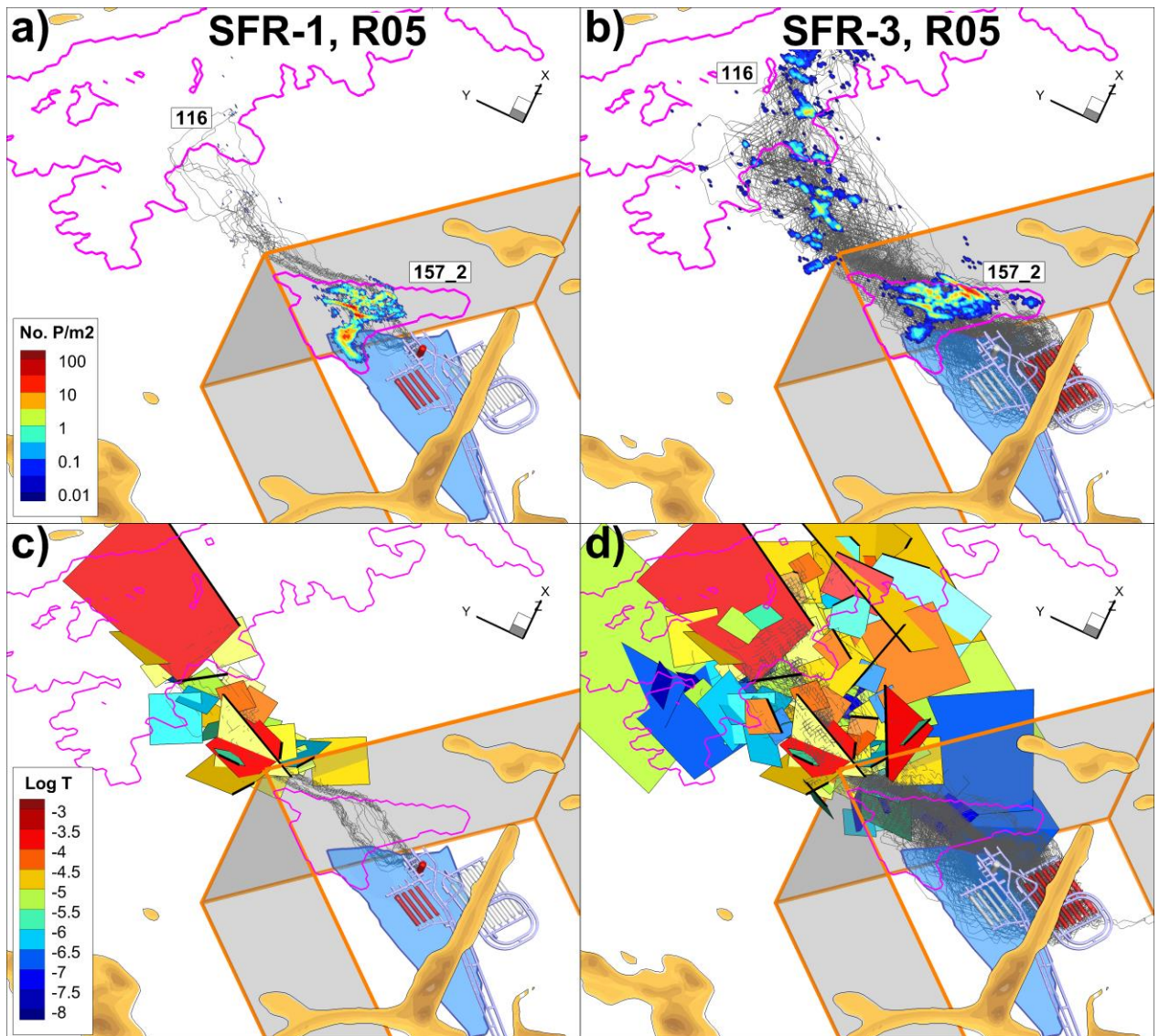
Figure 3-32. Sensitivity to DFN outside SFR Regional domain in particle tracking: realisation R05. Release disposal room (red), biosphere objects (pink line), SFR Regional domain (orange lines), particle trajectories (grey lines), exit-location density (contoured in a and b), ground-surface fracture intercepts (black lines, in c and d), trajecting fractures (contoured by transmissivity in c and d).
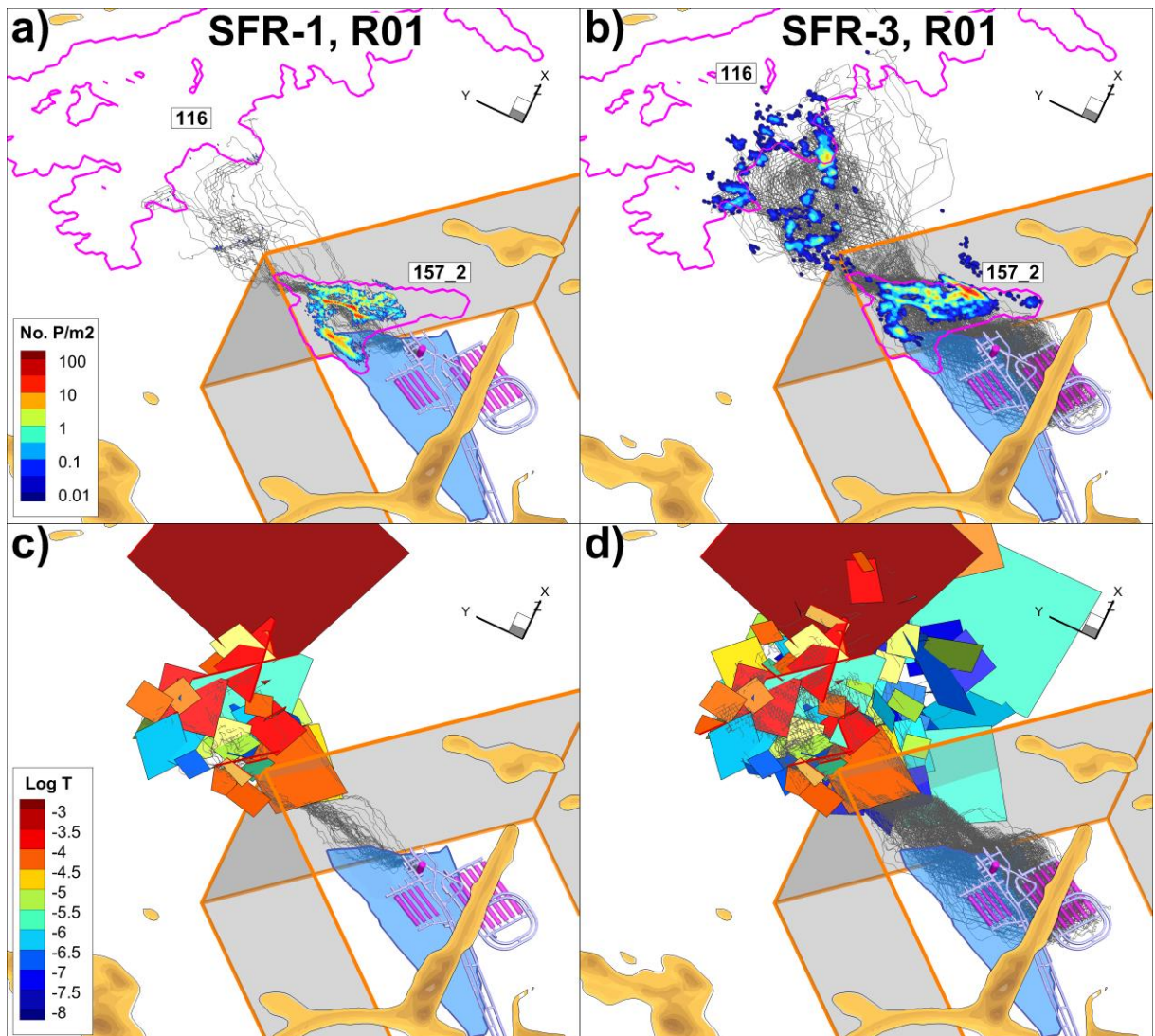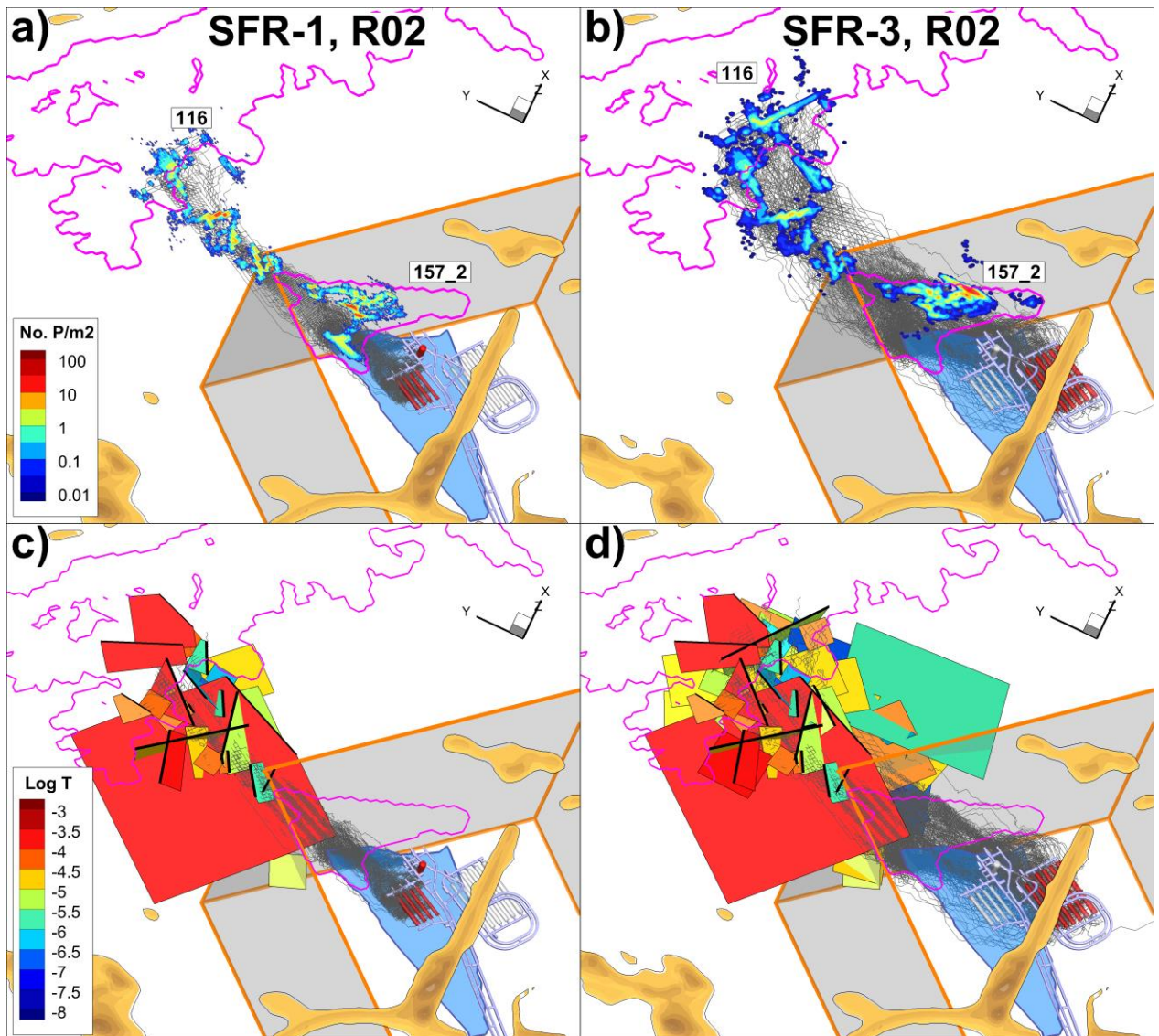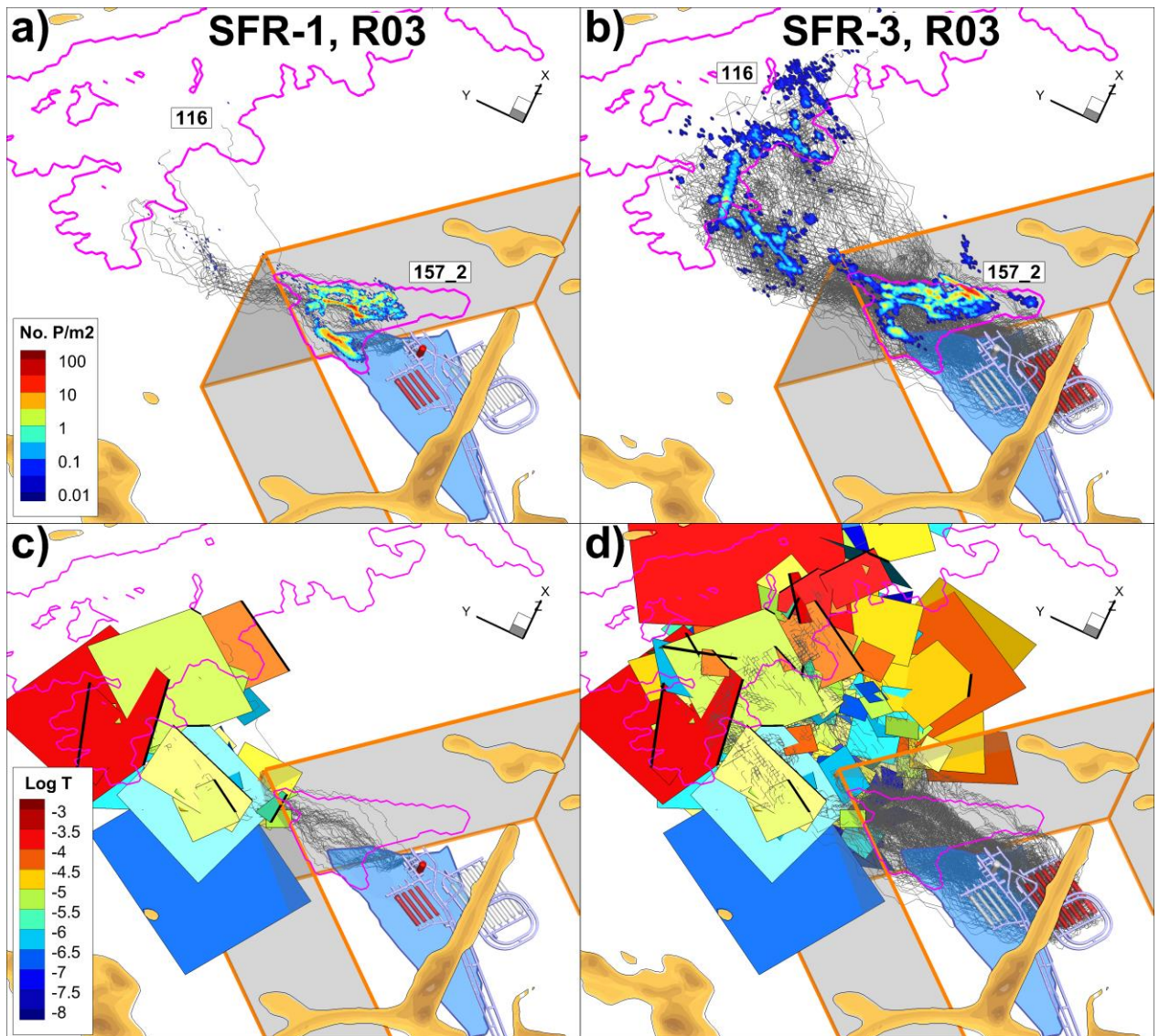
DokumentID
1578373, (1.0)

Sekretess
Öppen

Sida
76(165)

TD15 Complementary simulation cases in support of SR-PSU
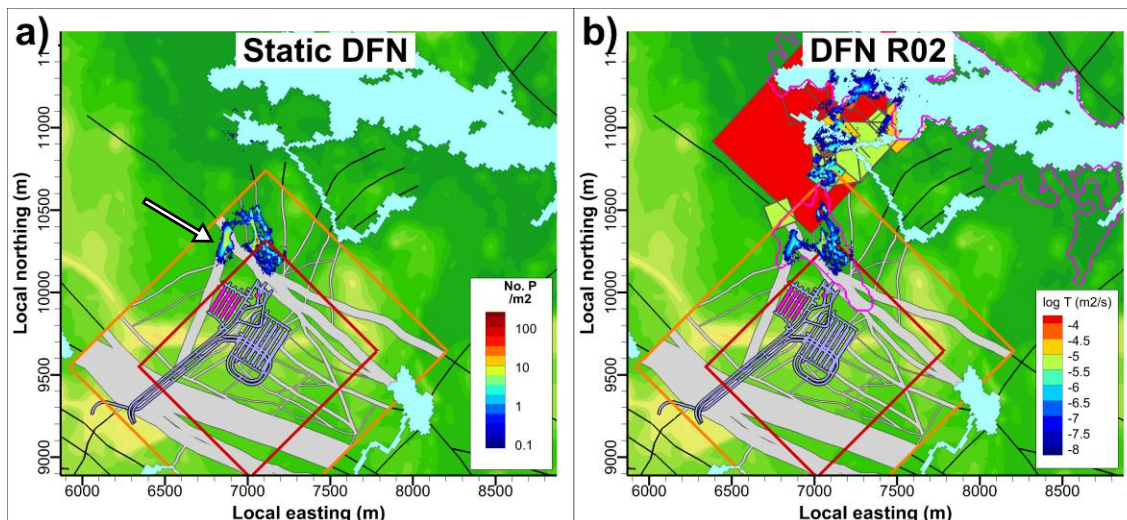
Figure 3-33. Detailed analysis of sensitivity to DFN outside SFR Regional domain; a) the discharging flow paths from SFR1 to ZFMNNE0869 (white arrow) can be re-directed by b) large sub-horizontal fractures (red plane). A 300 m respect distance (red line) to the SFR Regional domain (orange line) provided for spatial reference.
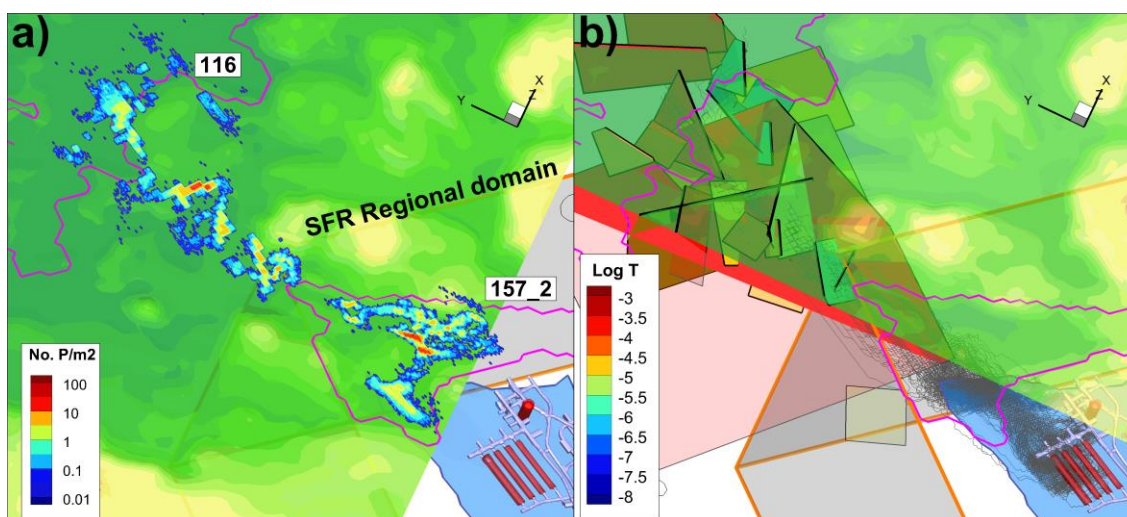
Figure 3-34. Three-dimensional visualisation of the structure re-directing flow paths in DFN R02.

3.4.3 Particle exit in terms of biosphere objects

The evaluation of HRD heterogeneity outside the SFR Regional domain (Section 3.4.2) demonstrates that stochastic DFN realisations can displace particle exit locations between the terrestrial biosphere object 157_2 and the lake object 116 (also referred to as Charlie's lake; see Figure 1-8). In particular, DFN realisation R02 stands out with the largest effect on the re-localisation of particles (see Section 3.4.2). The particle re-location of DFN R02 is also evaluated in terms of modelled biosphere objects (Figure 1-8, Table 3-3, and Table 3-4). The anomalous fraction of particles reaching object 157_1 in DFN R02 is accompanied with an overall increase in discharge to the biosphere object (Table 3-5), which indicates that the drastic increase in particle transport to object 157_1 is somewhat dampened by dilution (c. a factor of 4).

Table 3-3. Effect of HRD heterogeneity on particle exit to biosphere (Figure 1-8).

TD15 Complementary simulation cases in support of SR-PSU

	DFN outside SFR regional domain	Fraction of particle exit per biosphere object (%)					
		157_2	157_1	116	159	121_2	121_1
SFR1	**Static DFN**	**99.9**	**0.1**	**0.0029**			
	DFN_R01	99.9	0.039	0.021			
	DFN_R02	*51.9*	*37.9*	*10.2*			
	DFN_R03	99.9	0.1	0.0049			
	DFN_R04	100	0.008	0.0015			
	DFN_R05	100	0.019	0.011			
SFR3	**Static DFN**	**95.7**	**3.0**	**0.7**	**0.60**	**0.011**	**0.0009**
	DFN_R01	84.2	5.1	10.6	0.0052	0.0099	0.0013
	DFN_R02	*70.6*	*13.9*	*15.4*	*0.0035*	*0.0089*	*0.0012*
	DFN_R03	89.5	2.8	7.6	0.015	0.0094	0.0010
	DFN_R04	94.2	0.7	5.1	0.0038	0.0093	0.0014
	DFN_R05	83.1	8.6	8.3	0.0081	0.010	0.0015

Table 3-4. Detailed particle exit to biosphere objects, DFN R02[1] (Figure 1-8).

Set up	Particle release (%)	Fraction of particle exit per biosphere object (%)					
		157_2	157_1	116	159	121_2	121_1
Static DFN							
SFR1	**100**	**99.9**	**0.09**	**0.003**			
1BMA	31.7	31.7	0.01	0.0002			
1BLA	20.6	20.6	0.01	0.0004			
2BTF	16.1	16.1	0.01				
1BTF	14.5	14.5	0.01	0.0002			
Silo	17.0	17.0	0.06	0.002			
SFR3	**100**	**95.7**	**3.1**	**0.67**	**0.60**	**0.01**	**0.001**
1BRT	12.8	12.6	0.21	0.02	0.02		
2BLA	16.9	16.5	0.36	0.03	0.06		
3BLA	16.6	16.0	0.46	0.05	0.14		
4BLA	16.5	15.9	0.45	0.09	0.12		
5BLA	16.3	15.4	0.58	0.17	0.10	0.0005	
2BMA	20.9	19.4	0.97	0.31	0.17	0.01	0.001
DFN, R02							
SFR1	**100**	**51.9**	**37.8**	**10.2**			
1BMA	31.2	10.8	16.10	4.32			
1BLA	20.3	8.9	9.04	2.36			
2BTF	16.1	9.2	5.49	1.44			
1BTF	14.7	10.1	3.58	0.96			
Silo	17.6	12.9	3.61	1.09			
SFR3	**100**	**70.6**	**13.9**	**15.4**	**0.0035**	**0.01**	**0.001**
1BRT	12.6	7.8	3.30	1.43			
2BLA	16.7	10.8	3.60	2.29			
3BLA	16.6	10.3	2.68	3.62			
4BLA	16.7	12.2	1.69	2.80	0.0001		
5BLA	16.5	13.2	1.15	2.12	0.001	0.001	
2BMA	21.0	16.3	1.52	3.16	0.003	0.01	0.001

1)   DFN realisation outside SFR regional domain

DokumentID
1578373, (1.0)

Sekretess
Öppen

Sida
78(165)

TD15 Complementary simulation cases in support of SR-PSU

Table 3-5. Effect of outer HRD heterogeneity on biosphere-object discharge.

Set up	Bedrock discharge[1], q (mm/yr)					
	157_2	157_1	116	159	121_2	121_1
TD11, Static DFN	*79.6*	*20.7*	*27.9*	*52*	*43.3*	*118.7*
TD15, Static DFN	**79.5**	**20.84**	**28.1**	**52.4**	**44.16**	**118.9**
TD15, DFN_R01	79.48	25.68	47.42	78.05	43.51	103.51
TD15, DFN_R02	63.57	77.33	33.90	52.71	44.08	103.19
TD15, DFN_R03	86.69	20.29	41.44	46.98	44.18	106.43
TD15, DFN_R04	78.98	42.47	45.87	79.78	43.73	104.47
TD15, DFN_R05	94.39	36.33	48.63	57.19	43.52	104.70

1) Colour-coded relative to the static DFN case (blue = lower, red = higher)

3.5 Deterministic SBA structures

The performance measures for SFR1 are not very sensitive to the existence of the deterministically modelled SBAs; neither in terms of cross flow through the disposal rooms (Figure 3-35), nor in exit locations (Figure 3-36; Table 3-6). This is in line with expectations, as the SBA-structures are not associated to flow paths for the existing SFR1 (see discussion on model exercise M4 in Öhman et al. 2013), and the SBA structures were intentionally avoided in the localisation of the extension SFR3.

The planned extension, SFR3, is comparatively more affected by the presence of SBA structures, which is due to its deeper location, closer to the wedge between NNW1034 and NW0805. The largest effect from not including SBA structures is a 31% reduction of flow in 2BMA, which is located closest to the structures SBA1-6, and the wedge between NNW1034 and NW0805 (Figure 3-35). Moreover, the SBA structures (primarily the underlying SBA6) tend to re-direct the deeper particle trajectories upwards, towards biosphere object 157_2. This is demonstrated by the setup without SBA structures, where the fraction of released particles reaching the more remote biosphere objects 157_1 and 116 is slightly larger (i.e., in total, the SBA affect 2% of the particles released to SFR3; Table 3-6). Specifically for 2BMA, the SBA structures re-direct c. 10% of its released particles (Figure 3-37).

DokumentID
1578373, (1.0)

Sekretess
Öppen

Sida
79(165)

TD15 Complementary simulation cases in support of SR-PSU
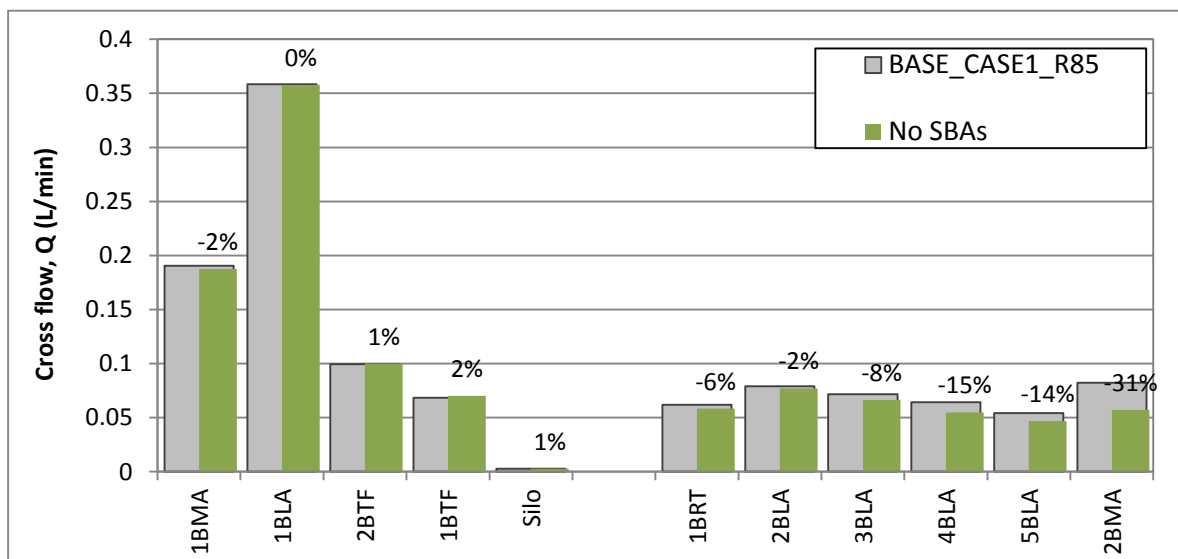
Figure 3-35. *Significance of deterministically modelled SBA on disposal-room cross flows; base case, 5000 AD compared against a setup without SBAs.*
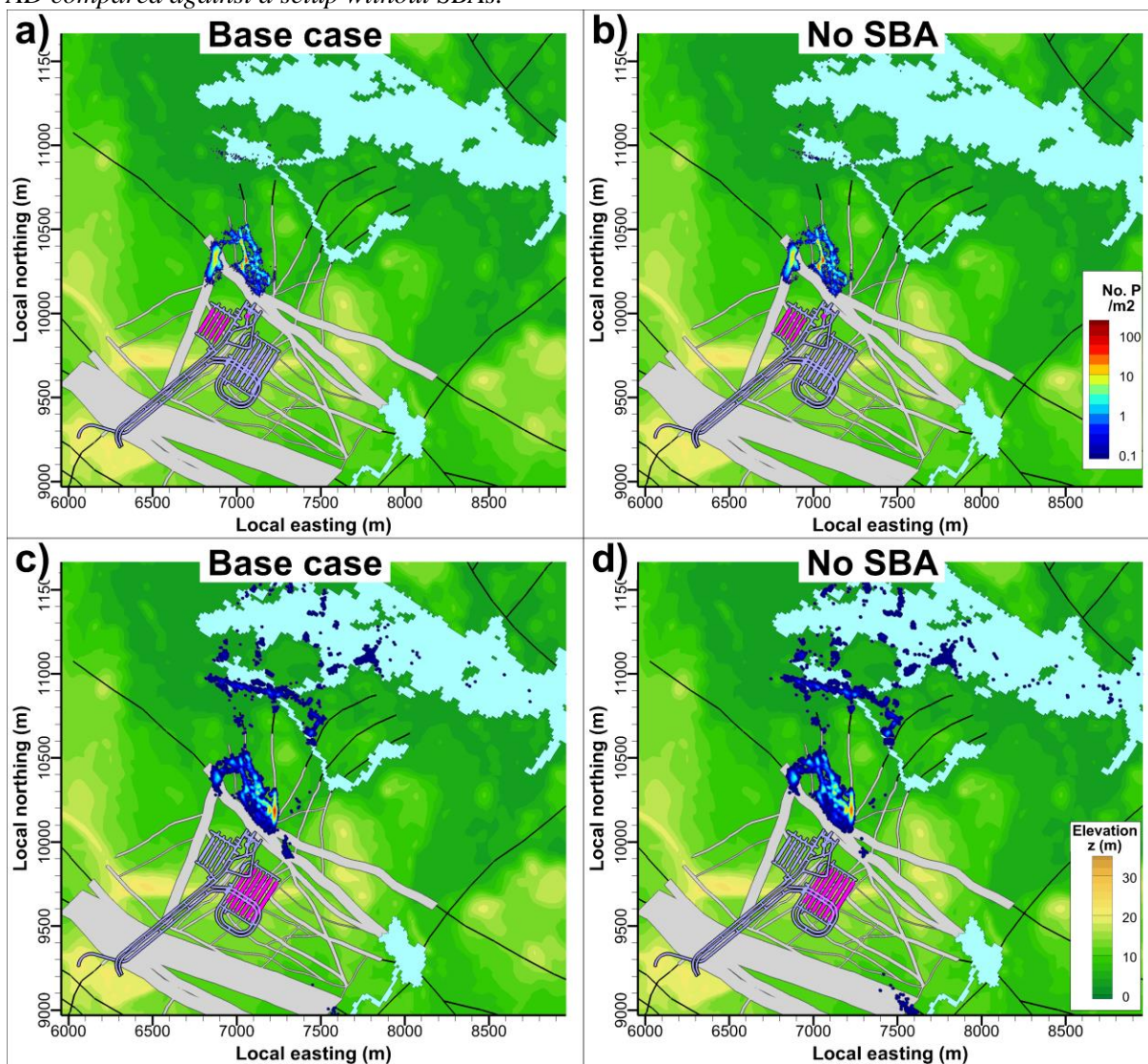
Figure 3-36. *Significance of SBAs for exit locations; setup without deterministically modelled SBAs compared against base case. Classified in terms of biosphere objects in Table 3-6.*

Table 3-6. Role of deterministic SBA structures for particle exit locations (Figure 1-8).

Set up	Particle release (%)	Fraction of particle exit per biosphere object (%)					
		157_2	157_1	116	159	121_2	121_1
Base case							
SFR1	**100**	**99.9**	**0.09**	**0.003**			
1BMA	31.7	31.7	0.01	0.0002			
1BLA	20.6	20.6	0.01	0.0004			
2BTF	16.1	16.1	0.01				
1BTF	14.5	14.5	0.01	0.0002			
Silo	17.0	17.0	0.06	0.002			
SFR3	**100**	**95.7**	**3.1**	**0.67**	**0.60**	**0.01**	**0.001**

TD15 Complementary simulation cases in support of SR-PSU

1BRT	12.8	12.6	0.21	0.02	0.02		
2BLA	16.9	16.5	0.36	0.03	0.06		
3BLA	16.6	16.0	0.46	0.05	0.14		
4BLA	16.5	15.9	0.45	0.09	0.12		
5BLA	16.3	15.4	0.58	0.17	0.10	0.0005	
2BMA	20.9	19.4	**0.97**	0.31	0.17	0.01	0.001
No SBA							
SFR1	**100**	**99.9**	**0.1**	**0.004**			
1BMA	31.6	31.6	0.01	0.0003			
1BLA	20.6	20.6	0.01	0.0002			
2BTF	16.1	16.1	0.01	0.0004			
1BTF	14.5	14.5	0.01	0.0005			
Silo	17.1	17.1	0.05	0.0025			
SFR3	**100**	**93.4**	**4.5**	**1.0**	**0.9**	**0.1**	**0.0083**
1BRT	12.8	12.6	0.19	0.01	0.02		
2BLA	16.9	16.5	0.32	0.02	0.05		
3BLA	16.7	16.0	0.52	0.05	0.17		
4BLA	16.6	15.8	0.55	0.07	0.18		
5BLA	16.3	15.4	0.63	0.11	0.17	0.0033	0.0002
2BMA	20.6	17.1	**2.28**	0.77	0.37	0.11	0.008
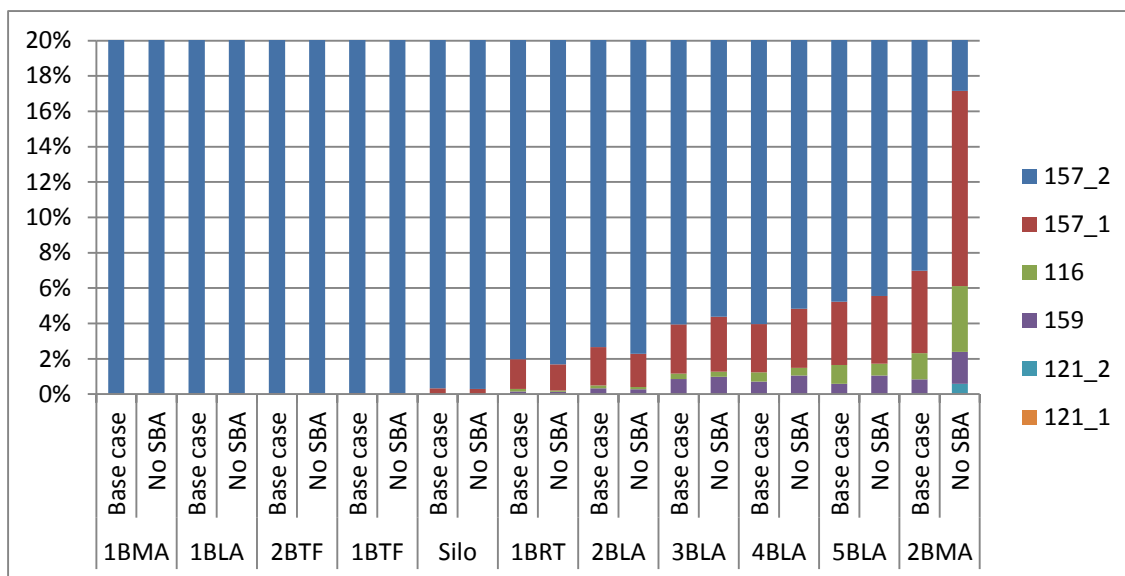
Figure 3-37. Significance of SBA for exit locations; shown as stacked distributions (normalised) of exit locations from individual disposal facilities to biosphere objects. The stacked histograms are normalised per disposal room (to a total of 100%), while the y-axis is truncated in order to resolve the re-distribution of exit locations at the detailed level.

3.6　ECPM-scaling effects in model output (grid discretisation)

Simulations demonstrate that improving the grid refinement leads to a reduction in disposal-room cross flows by on average c. 20% (Figure 3-38). The reduction in simulated flow is rather consistent among disposal rooms. Further grid refinement, from cell size 4 m to 2 m, has only minor impact on simulated flow. This suggests that the exaggerated flow connectivity in ECPM upscaling – as compared against a true DFN

SVENSK KÄRNBRÄNSLEHANTERING AB

simulation – is at least 20%, but probably not much larger than that. The demonstrated phenomenon that simulated flow depends on grid resolution can be explained as follows:

1) The resemblance between geometrical ECPM upscaling and its underlying fracture network is limited by grid discretisation, which tends to exaggerate the hydraulic connectivity of its underlying DFN,
2) A higher grid resolution resolves the physical gaps between fractures in the DFN to a higher degree, and hence it better honours local bottlenecks in hydraulic connectivity along flow paths.

It should be pointed out that ECPM upscaling is typically a practical necessity in large-scale simulations, owing to computational limitations, and its drawback of exaggerated flow connectivity may be acceptable as it is often perceived as conservative in risk assessment.
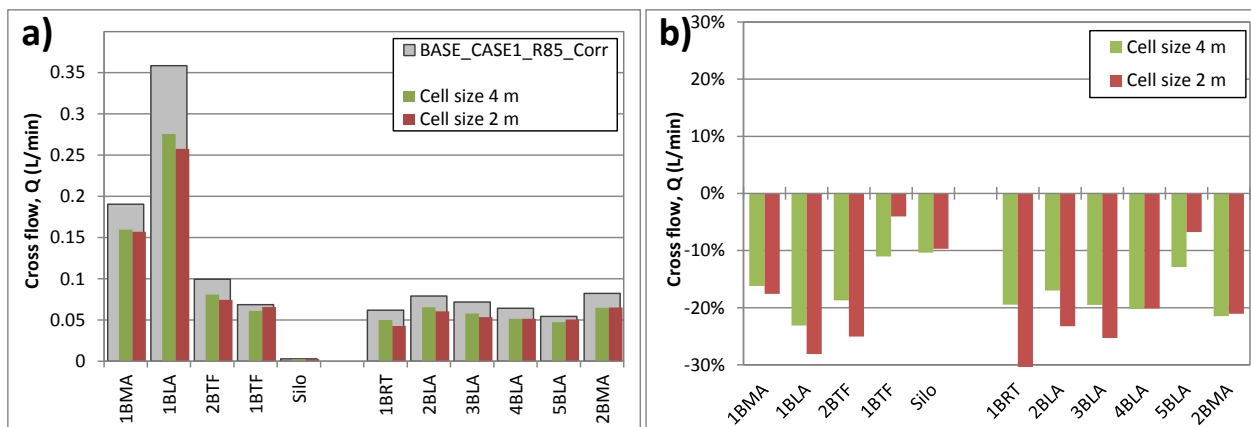
Figure 3-38. Sensitivity to ECPM scaling effects in disposal-room flow calculations.

The particle-tracking performance measures are comparatively less sensitive to ECPM scaling effects (Figure 3-39). The largest effect is a c. 10% reduction in travel times for SFR1 (Figure 3-39a), which is probably associated to the 20% reduction in flow. In particular, the refined discretisation has only minute effects on the distribution of tracked path lengths (Figure 3-39c and d), which signifies that the grid discretisation in SR-PSU does not conceal artificially connected large-scale flow paths that are of key significance to the performance assessment.

Note that a higher grid discretisation reduces the tendency to include nearby non-connected fractures within the property-averaging control volume, leading to an improved distinction between preferential flow paths and the less connected/conductive bedrock, which in turn makes the ECPM approach more similar to its DFN analogy. One of the benefits is that the traversed ECPM properties during particle tracking are more representative of the actual flow path, as the property contribution from undue fractures declines with refined resolution (i.e., smaller cell-control volumes).

ECPM upscaling renders conservative performance measures (at least 20% exaggerated flow across disposal rooms), although the scaling effects are small relative to other sources of heterogeneity and conceptual uncertainty.

SVENSK KÄRNBRÄNSLEHANTERING AB

DokumentID
1578373, (1.0)

Sekretess
Öppen

Sida
82(165)

TD15 Complementary simulation cases in support of SR-PSU
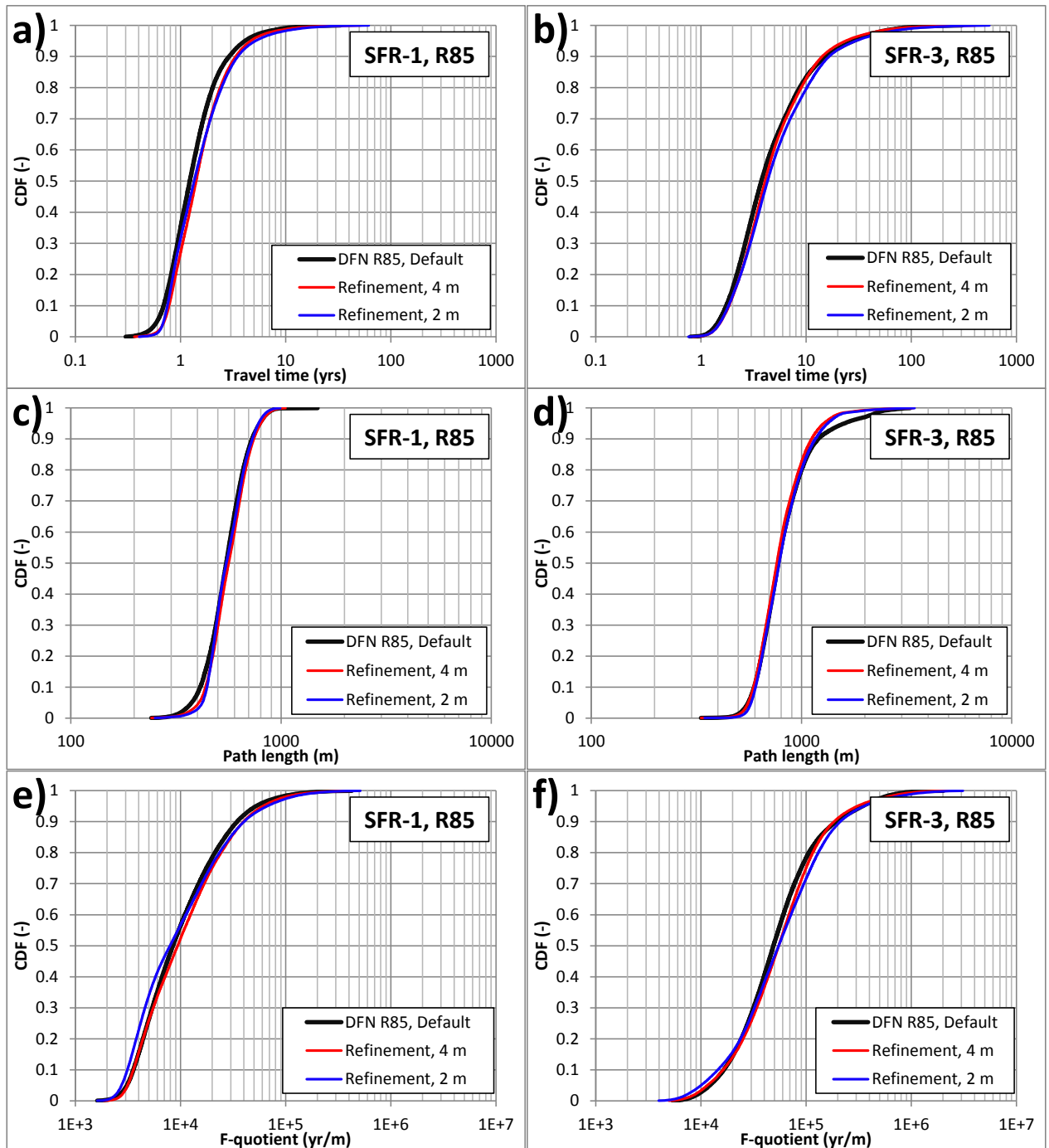
Figure 3-39. Sensitivity to ECPM scaling effects in particle-tracking performance measures.

3.7 Transient simulation of tunnel inflow and drawdown

This section presents the results of the two-dimensional transient simulations of tunnel inflow since the construction of SFR (c. a 30 year period). Here, the declining trend in tunnel inflow and the falling head in monitored borehole sections (see Öhman et al. 2012) is modelled as a slowly responding hydrogeological system, where the sensitivity to diffusivity, $\alpha = K/S_s$, is studied by elaborating the parameterised apparent

DokumentID
1578373, (1.0)

Sekretess
Öppen

Sida
83(165)

TD15 Complementary simulation cases in support of SR-PSU

specific storage, S_S (m^{-1}), relative to a given hydraulic-conductivity parameterisation, K (m/s). Two hydraulic-conductivity parameterisations are compared: a homogeneous case (Section 3.7.1) and a heterogeneous case (Section 3.7.2). The transient simulation sequences are evaluated in terms of both: 1) tunnel inflow and 2) drawdown. Since a simplified 2D setup is employed, the simulated drawdown is not matched against exact borehole data, but evaluated in general terms based on borehole-data observations, namely: 1) a substantial magnitude in drawdown (i.e., on the order 30 to 100 m) and 2) still in a transient state (head declining by c. 1 m/yr).

3.7.1 Case 1: Homogeneous parameterisation

The homogeneous model setup reflects apparent, effective large-scale properties (i.e., both K and S_S). The hydraulic conductivity, K, is set uniformly to 10^{-10} m/s (which is representative of the Silo; Öhman et al. 2013), while the sensitivity to apparent specific storage, S_s (m^{-1}), is analysed within a span over several many orders of magnitude to reproduce the ongoing decline of flow after 30 years (Figure 3-40). The sequence of normalised inflow can be reproduced for an apparent specific storage of $S_s = 0.03$ m^{-1} (Figure 3-41). This value is out of realistic bounds for aquifer storage, even if the fitted parameter is envisaged as an apparent entity signifying a very slow (low-diffusive) system arising from poor fracture connectivity. The simulations demonstrate that the observed history of declining tunnel inflow resembles the transient response of an exceptionally slowly responding system (i.e., poorly connected fracture system, as indicated by a high apparent specific storage). This pinpoints the difficulty in inferring a singular cause, or ruling out potential causes (i.e., such as gradually developing flow resistances), to the observed phenomenon.

It should be noted that the simulations do not assume tunnel-wall skin (i.e., bedrock hydraulic conductivity is set to homogeneously 10^{-10} m/s). It may be expected that introducing a flow resistence in the tunnel wall would have led to a somewhat lower apparent storativity reproducing the inflow history (Jan-Erik Ludvigson, pers. com.).
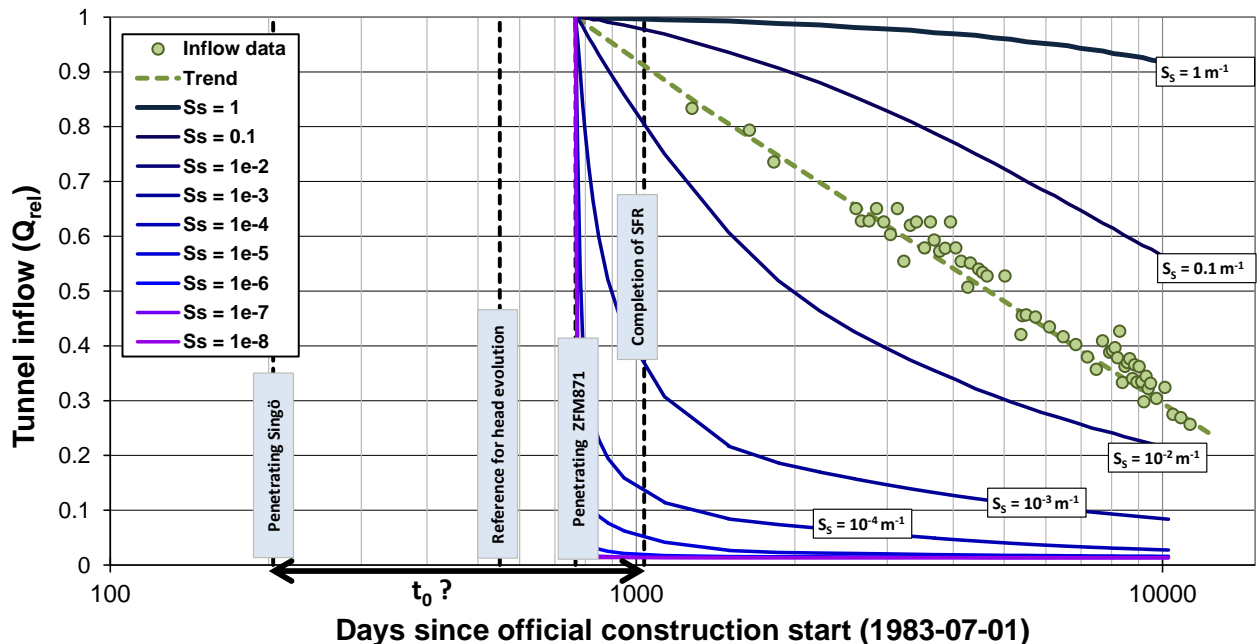

Figure 3-40. Simulated transient inflow in the homogeneous case; uniform hydraulic conductivity, K = 10^{-10} m/s, and variable specific storage, S_S (m^{-1}). The role of hydraulic diffusivity is elaborated by varying the specific storage.

DokumentID
1578373, (1.0)

Sekretess
Öppen

Sida
84(165)

TD15 Complementary simulation cases in support of SR-PSU
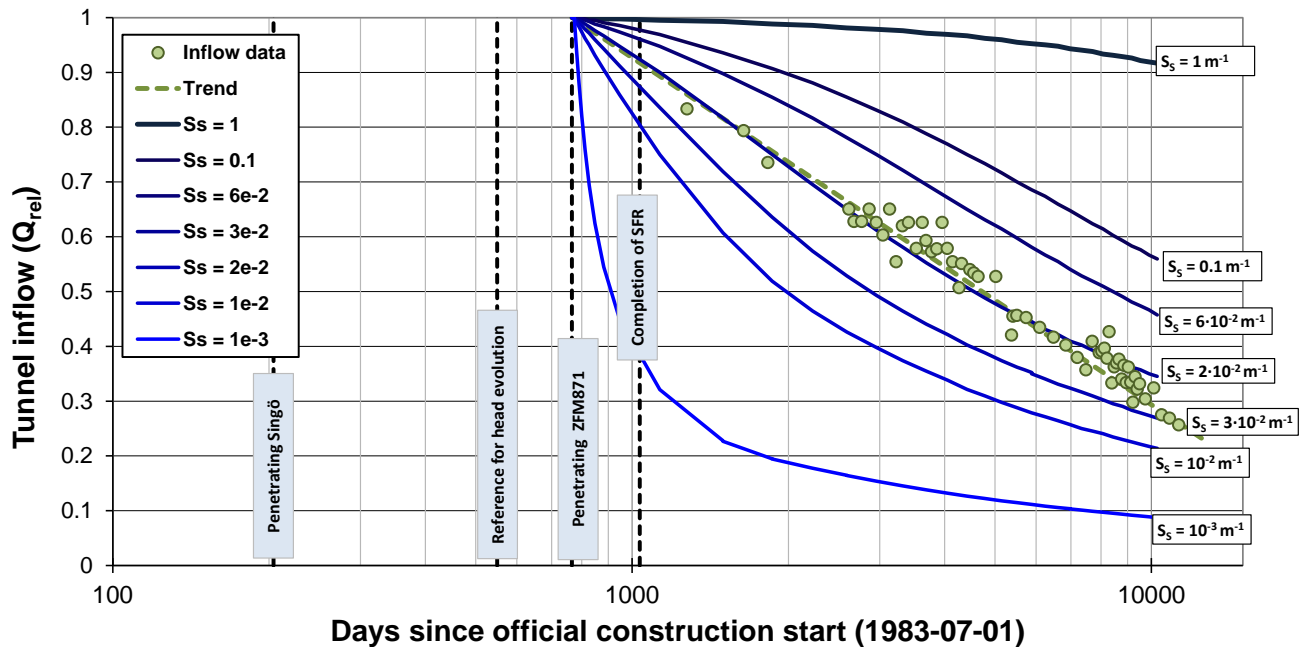
Figure 3-41. Fine-tuned transient inflow in the homogeneous case; uniform hydraulic conductivity, K = 10^{-10} m/s, and variable specific storage, S_S (m^{-1}).

The role of apparent specific storage, S_s (m^{-1}), is also demonstrated in the appearance of simulated drawdown. Very high settings ($S_s \geq 10^{-2}$ m^{-1}) cause a too slow development of drawdown, leading to an underestimation in magnitude, even at the end of the 30 year period. Low settings ($S_s \leq 10^{-5}$ m^{-1}; in the realistic range of physical aquifer storage) cause the drawdown to develop too fast, with almost stationary head at the end of the 30-year period. Values in the range 10^{-4} to 10^{-3} m^{-1} render the best resemblance to drawdown data (i.e., both realistic magnitudes and still meter-scale decline at the end of the period; Figure 3-42).

The sensitivity to apparent specific storage, in terms of large-scale head field, appears to take on its maximum at c. $S_s = 10^{-4}$ m^{-1} (Figure 3-43).
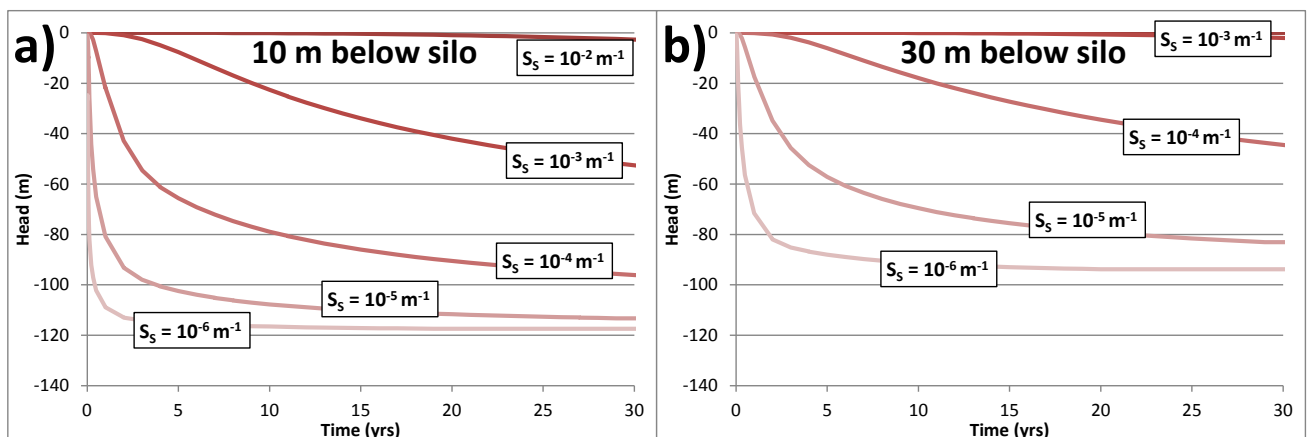
Figure 3-42. Simulated transient drawdown below the Silo in the homogeneous case; uniform hydraulic conductivity, K = 10^{-10} m/s, and variable specific storage, S_S (m^{-1}).

DokumentID
1578373, (1.0)

Sekretess
Öppen

Sida
85(165)

TD15 Complementary simulation cases in support of SR-PSU

Figure 3-43. *Close-up of simulated head after 30 years of inflow in the homogeneous case ($K = 10^{-10}$ m/s). The role of hydraulic diffusivity is elaborated by varying the specific storage.*

TD15 Complementary simulation cases in support of SR-PSU

3.7.2 Case 2: Heterogeneous parameterisation

The second model case demonstrates the role of diffusivity in a model case of heterogeneous parameterisation (upscaled ECPM properties from an underlying fracture network, $S_{s,ECPM}$ and K_{ECPM}). The ECPM parameterisation employs a minimum specific-storage value of $S_{S,ECPM} = 10^{-7}$ m^{-1}, and a default setting for fractures, $S_{S,Fract} = 10^{-6}$ m^{-1}. The storage from fractures is small compared to the storage from deformation zones (Figure 3-44b).
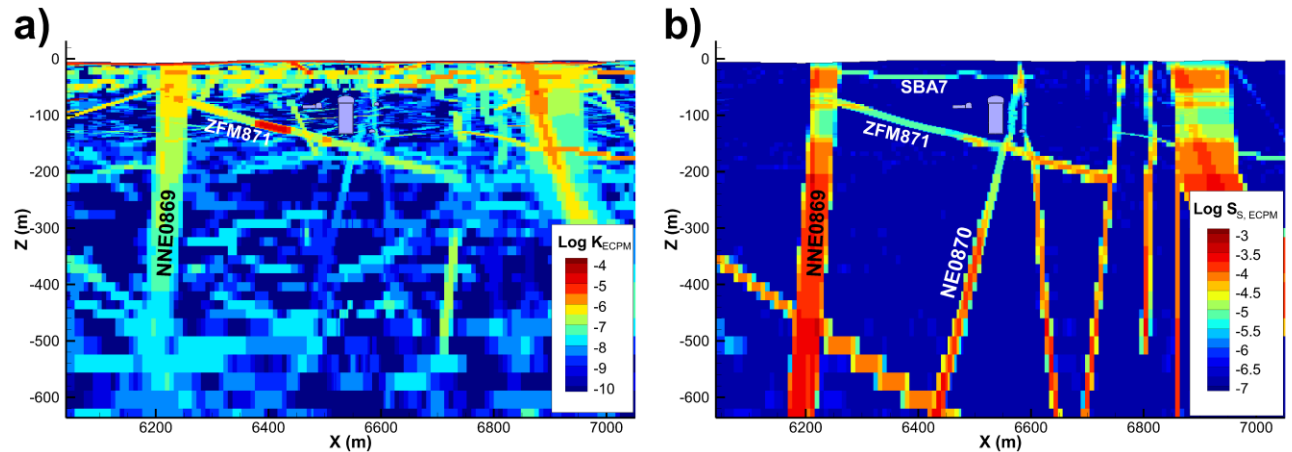
Figure 3-44. *Close-up of ECPM parameterisation in the heterogeneous case; a) K_{ECPM} and b) $S_{S,ECPM}$, upscaled from deformation zones and an underlying fracture network.*

The role of diffusivity in this model case is examined by the introduction of a global scaling-factor, F (-), which is used to elaborate the diffusitivity over a wide range. F is varied from 1 to 10^{7}, such that $\alpha \propto F^{-1}$ (by $S_s = S_{s,ECPM} \times \sqrt{F}$, and $K = K_{ECPM} / \sqrt{F}$; Table 1-4). The simulated inflow in the heterogeneous case declines rapidly over the first years, after which it stabilises to a more-or-less constant level (Figure 3-45).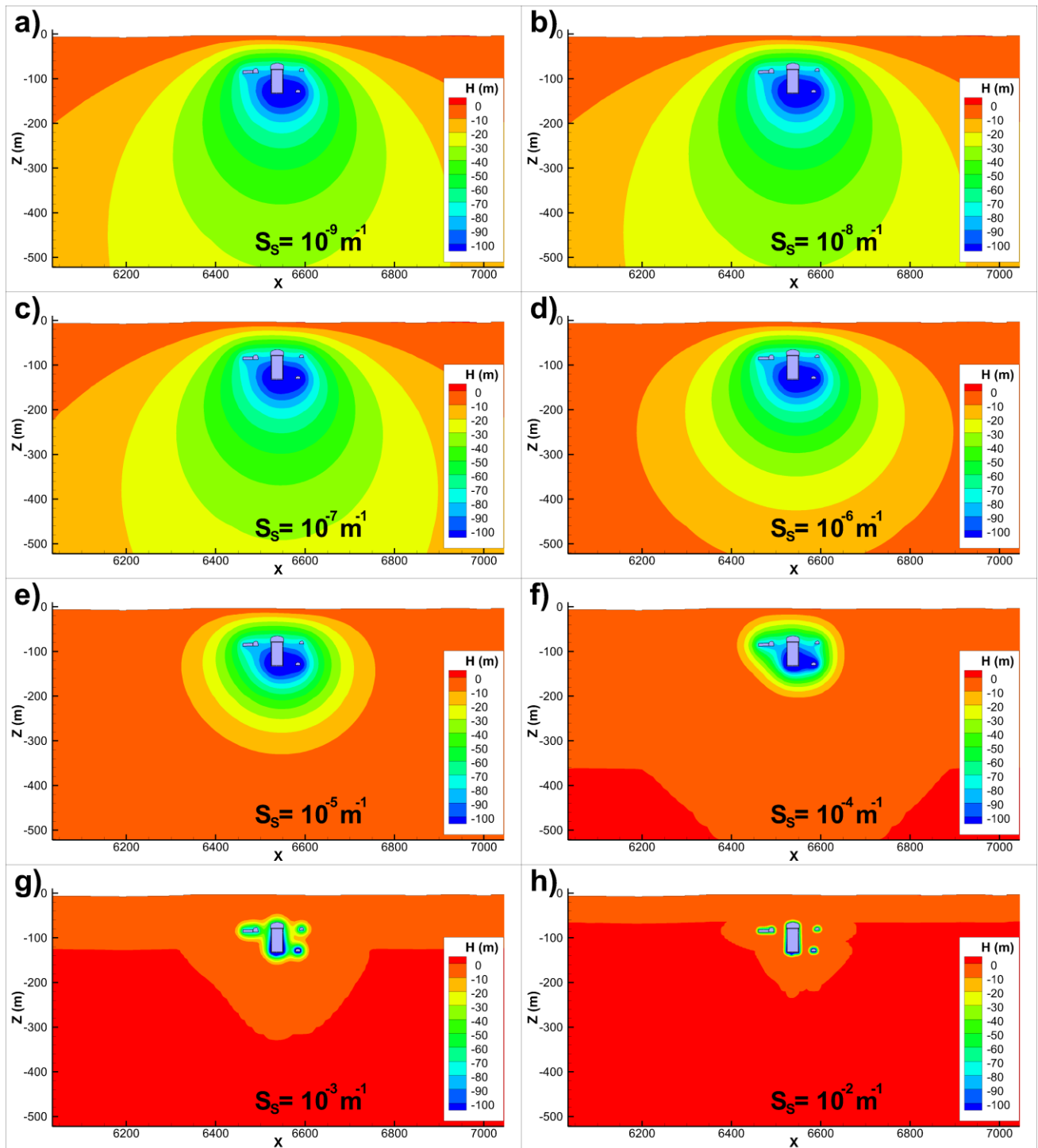 Thus, the the appearance in simulated inflow cannot reproduce the logarithmic trend in inflow data (i.e., linear trend in a logarithmic time scale) over the studied 30 year period. One reason for this may be that no tunnel-wall skin is implemented. Another reason could be that – irrespectively of the rescaling factor – the relationship between the connectivity and transmissivity is largely determined by the geometrical structure in the ECPM realisation (i.e., reflecting the deformation-zone geometry), and hence more difficult to fine-tune by means of macroscopic calibration knobs (such as the scaling factor mimicking fracture connectivity). The influence of the geometrical structure in the ECPM parameterisation can be observed in the uneven pattern in simulated drawdown (Figure 3-47). For example, the drawdown propagates via ZFMNE0870 below the silo, with very similar magnitudes at 10 m depth and 30 m depths below the silo (Figure 3-46; compare to the homeogeneous case, Figure 3-42).

DokumentID
1578373, (1.0)

Sekretess
Öppen

Sida
87(165)

TD15 Complementary simulation cases in support of SR-PSU
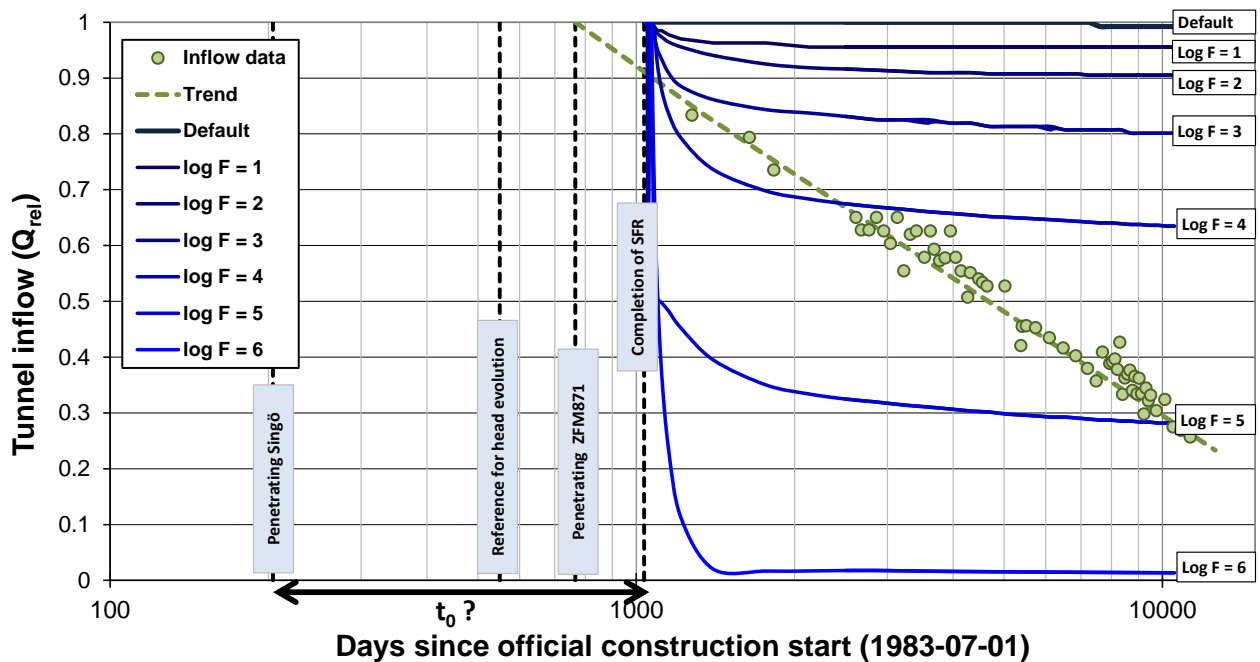
Figure 3-45. *Simulated transient inflow for heterogeneous case (upscaled K_{ECPM} and $S_{s,ECPM}$); diffusivity elaborated by scaling factor, F.*
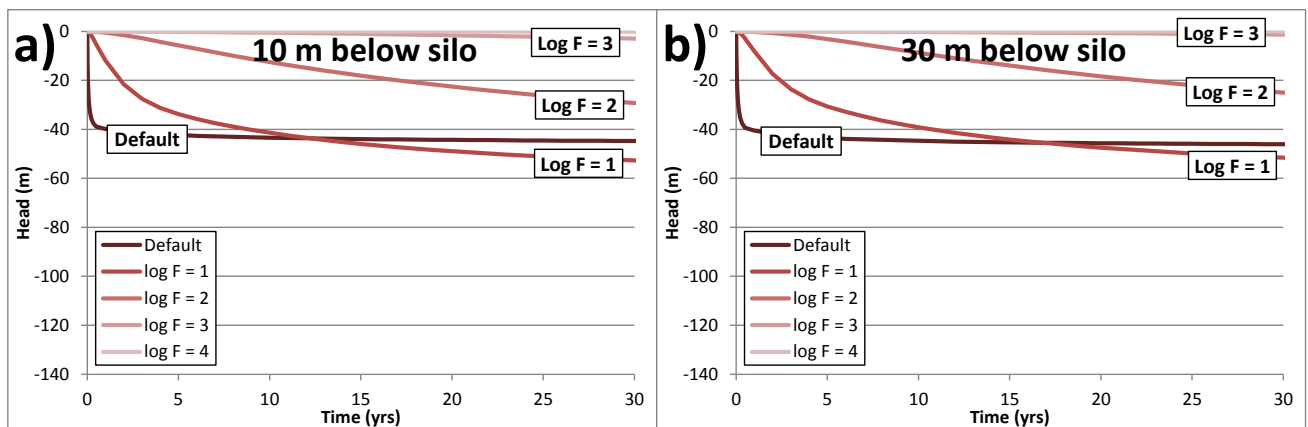
Figure 3-46. *Simulated transient head for heterogeneous case (upscaled K_{ECPM} and $S_{s,ECPM}$); diffusivity elaborated by scaling factor, F.*

DokumentID
1578373, (1.0)

Sekretess
Öppen

Sida
88(165)

TD15 Complementary simulation cases in support of SR-PSU

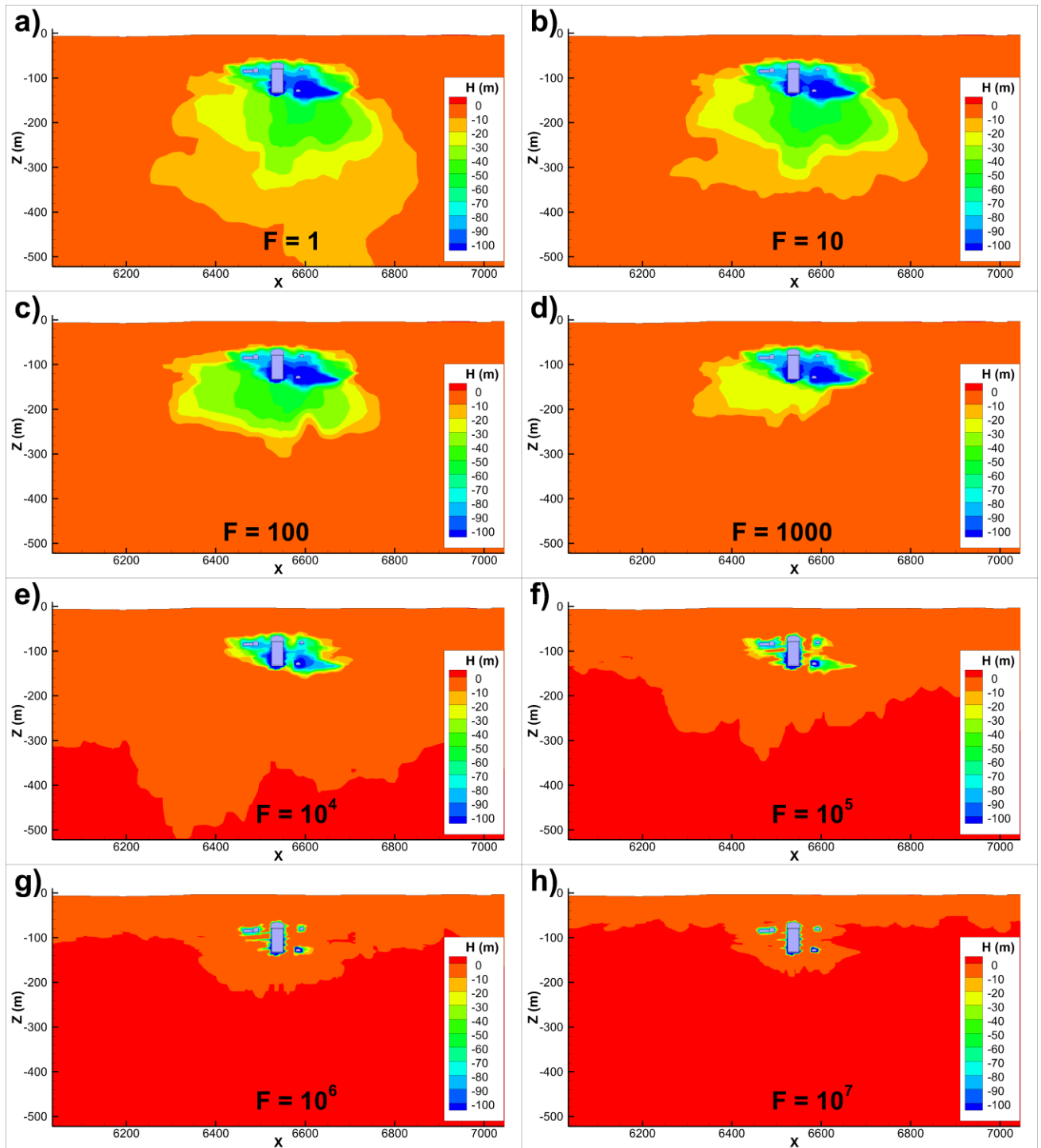***Figure 3-47.*** *Close-up of simulated head after a 30 year inflow period for a heterogeneous case (upscaled K_{ECPM} and $S_{s,ECPM}$). Different hydraulic diffusivity levels are imposed by a scaling factor, F (-), such that $S_s = S_{s,ECPM} \times \sqrt{F}$, and $K = K_{ECPM} / \sqrt{F}$.*

DokumentID
1578373, (1.0)

Sekretess
Öppen

Sida
89(165)

TD15 Complementary simulation cases in support of SR-PSU

3.8 Alternative localisation of SFR3 (Forsmark lens)

3.8.1 Disposal-room flow

The flow simulations confirm a reasonable correlation between statistical exploration of tunnel-wall transmissivity (Section 2.8) and simulated disposal room cross flow (Figure 3-48), which suggests that the selected three realisations are sufficiently representative for covering the span disposal-room crossflow of the wider ensemble (here, nine DFN realisations).
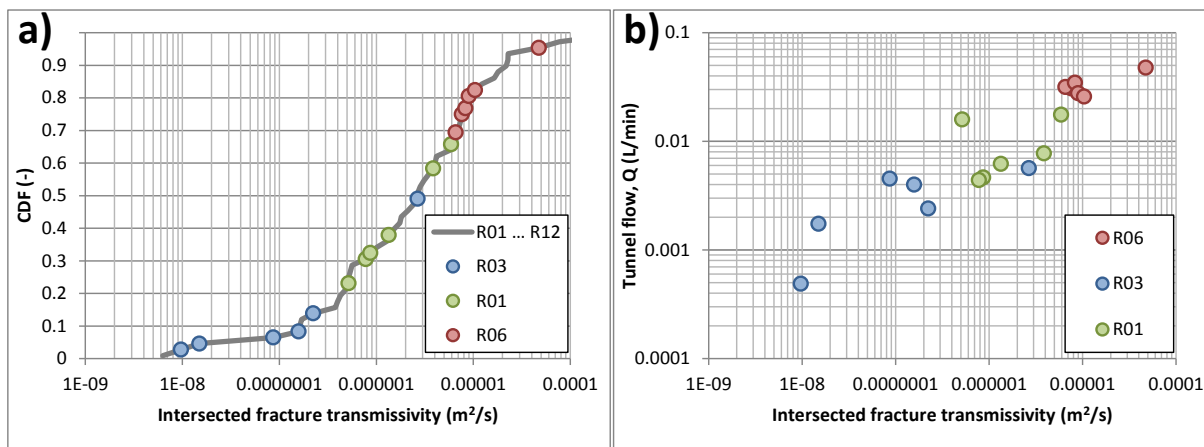

Figure 3-48. Range of variability in the local host rock outside deformation zones (HRD); a) sampled fracture transmissivity intercepts per disposal room (estimated from six disposal rooms and nine DFN realisations), and b) relation between intersected fracture transmissivity and simulated disposal-room crossflow (here 2000AD).

As stated earlier, all tunnel-flow calculations are based on a vector-based method, referred to as method 3 in PM to SR-PSU-TD10 (Öhman 2013). More precisely, a customised FORTRAN code is used for these calculations [Get_flows_SFR3_in_LENSE.f] (Appendix G). The simulated disposal-room crossflows for the three realisations are compared against the 17 bedrock cases in SR-PSU-TD11 (Öhman et al. 2014). The comparison is made for three time slices: 2000AD, 2500AD, and 5000AD. The following can be concluded:

1) The span of variability (whiskers in Figure 3-49) reflects the resolution of the underlying deterministic structural model; the alternative location has larger a stochastic model component (a resolution level of 1,000 m, as compared to 300 m applied in PSU), which is manifested by larger variability spans. Probably, variability span is underestimated for the alternative location, as it is limited to a few realisations.
2) The settings of the alternative location has matured further towards the stationary conditions of a terrestrial state (i.e., owing to its location below emerged ground surface, it is less affected by shoreline retreat than the applied location is; Figure 3-49).
3) in the applied location for SFR3 (i.e., inside the SFR Regional domain) the crossflows are lower during its current flow regime, which is characterised by its location below sea. As the flow field develops into stationary terrestrial conditions, the crossflows in the applied location exceed those in the alternative location (i.e., inside the Forsmark lens). One reason for this is that – in contrast to the alternative location – the applied localisation of SFR3 could not circumvent intersection of deformation zones, as they are more abundant in the highly resolved structural model of the SFR Regional domain.

SVENSK KÄRNBRÄNSLEHANTERING AB

DokumentID
1578373, (1.0)

Sekretess
Öppen

Sida
90(165)

TD15 Complementary simulation cases in support of SR-PSU
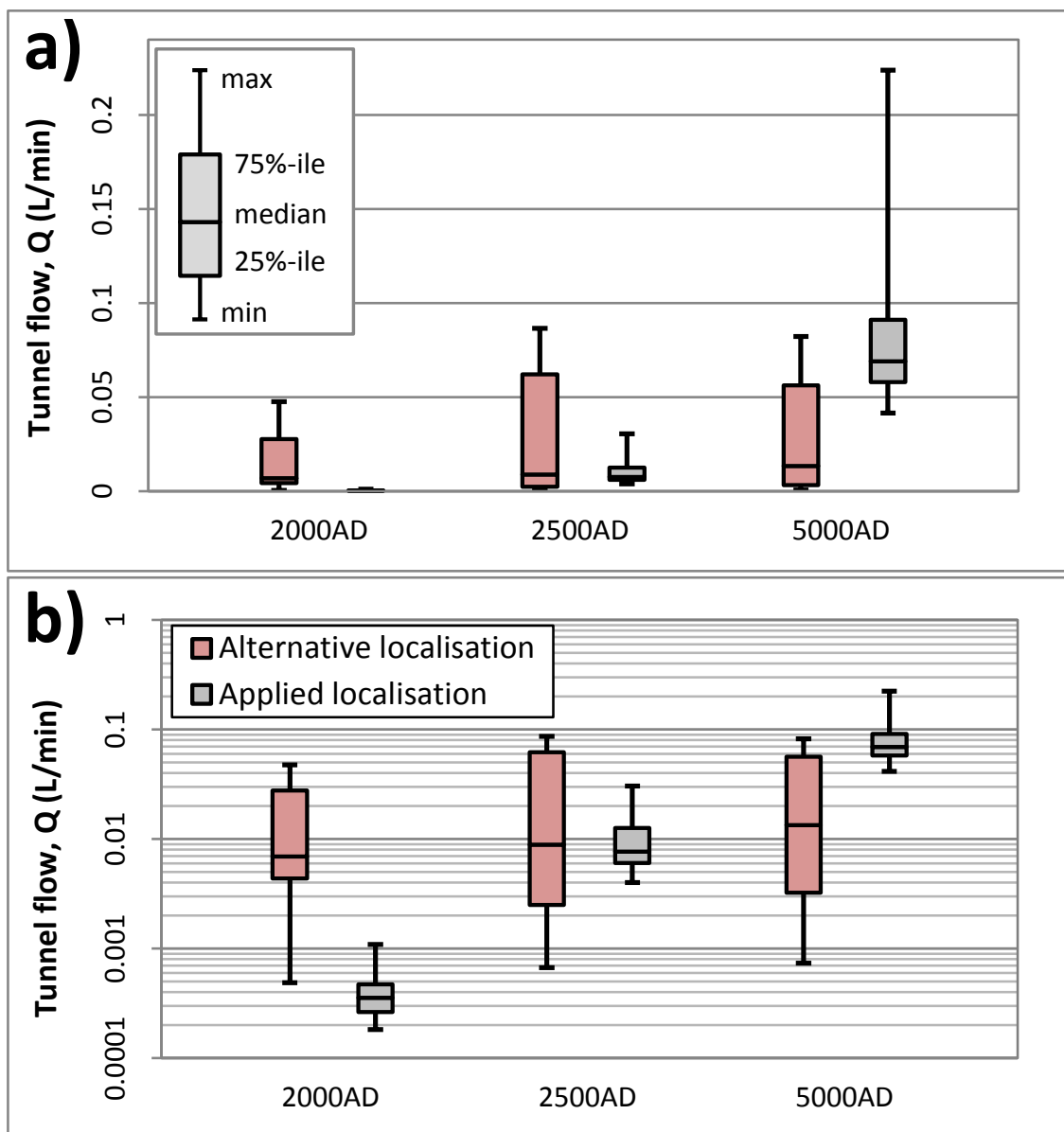
Figure 3-49. *Comparison of simulated disposal-room crossflow of the two localisation alternatives; a) linear scale and b) logarithmic scale. Note that the variability span of the alternative location is probably underestimated owing to the limited set of DFN realisations.*

3.8.2   Particle tracking

Particle tracking demonstrates that very few flow paths from the alternative SFR3 localisation pass across the Singö deformation zone (c. 0.5%; Table 3-7). Instead, most paths exit via the Singö deformation zone, west of the SFR regional domain (92%, biosphere object 118), or in Asphällsfjärden, south of the Singö deformation zone (7%, biosphere object 120; Figure 3-50d).

SVENSK KÄRNBRÄNSLEHANTERING AB

DokumentID
1578373, (1.0)

Sekretess
Öppen

Sida
91(165)

TD15 Complementary simulation cases in support of SR-PSU
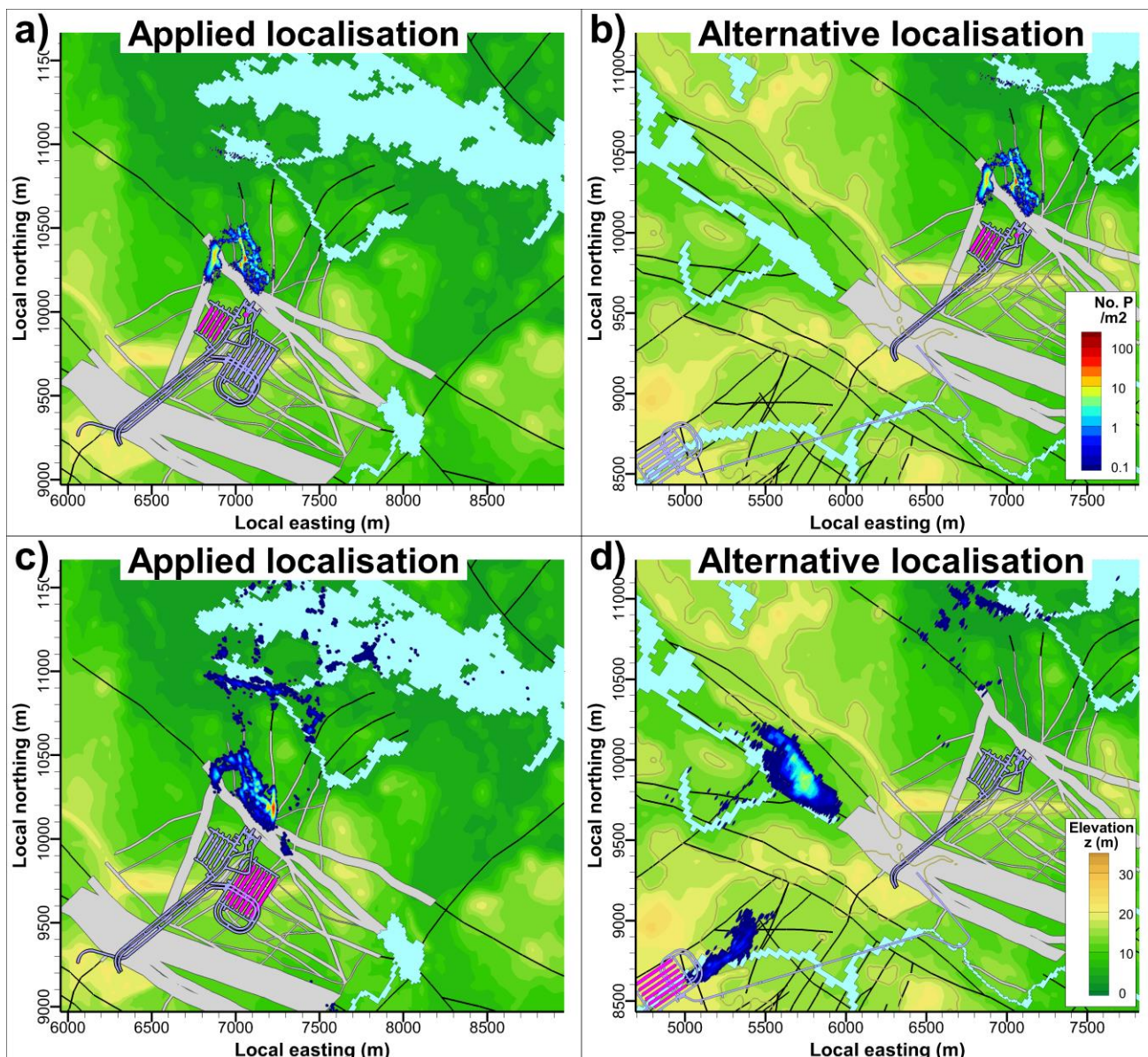
Figure 3-50. *Exit locations depending on localisation of SFR 3. Applied localisation in the SFR Regional domain compared to its alternative localisation in the geological lens of Forsmark (R01). Exit locations from SFR 1 (pink-shaded) shown in a) and b), while exit locations from SFR 3 (pink-shaded) shown in c) and d).*

Table 3-7. Particle-exit from SFR3 to biosphere objects (5000 AD); applied location compared to alternative location.

Location	Particle release (%)	Fraction of particle exit per biosphere object (%)								
		157_2	157_1	116	159	121_2	121_1	118	120	117
Applied	**100**	**95.7**	**3.1**	**0.67**	**0.60**	**0.01**	**0.001**			
1BRT	13	12.6	0.21	0.02	0.02					
2BLA	17	16.5	0.36	0.03	0.06					

DokumentID
1578373, (1.0)

Sekretess
Öppen

Sida
92(165)

TD15 Complementary simulation cases in support of SR-PSU

3BLA	17	16.0	0.46	0.05	0.14					
4BLA	17	15.9	0.45	0.09	0.12					
5BLA	16	15.4	0.58	0.17	0.10	0.0005				
2BMA	21	19.4	0.97	0.31	0.17	0.01	0.001			
Alternative	**100**	**0.01**	**0.3**	**0.2**				**92**	**7**	**0.001**
1BRT	12	0.001	0.01	0.01				11	1.4	
2BLA	17	0.003	0.05	0.02				15	1.8	
3BLA	17	0.003	0.07	0.03				14	3.0	
4BLA	16	0.003	0.09	0.05				15	0.6	
5BLA	17		0.05	0.03				16	0.4	
2BMA	21	0.001	0.05	0.04				21	0.1	0.001

SVENSK KÄRNBRÄNSLEHANTERING AB

DokumentID
1578373, (1.0)

Sekretess
Öppen

Sida
93(165)

TD15 Complementary simulation cases in support of SR-PSU

4   Summary

This report addresses remaining issues that have been identified in the hydrogeological modelling of SDM-PSU. These have been identified during review by the regulating Swedish Radiation Safety Authority, Strålsäkerhetsmyndigheten (SSM), and/or in a complementary inventory undertaken by Svensk Kärnbränslehantering AB (SKB; compiled in Appendix A). Based on the nature of modelling issues, they have been addressed, either by means of:

1) Complementary field investigations, undertaken to *resolve* or *reduce* uncertainties (summarised in Appendix B and C),
2) Numerical sensitivity analysis, to *quantify the significance* of modelling uncertainties in SR-PSU by means of flow simulations, or
3) Conceptual flow modelling, to *demonstrate* an alternative conceptual interpretation to the declining tunnel inflow to SFR1.

The issues identified as key modelling uncertainties (Sections 1.2 and 1.3) were addressed by means of flow simulations to evaluate the significance in terms of performance measures (Section 1.4). With a few exceptions, all flow simulations employ the same model scenario: a) time-slice 5000 AD and b) base-case parameterisation inside the SFR Regional domain (i.e., referred to as Case 1 in Öhman et al. (2014), with homogeneous HCD and DFN R85).

4.1   Complementary field investigations

Confidence-building in SBA structures (directed interference tests)

Five interference tests have been conducted to elucidate the modelled extension and parameterisation of SBA structures SBA1 to SBA6 (Appendix B). With the exception of SBA1, the tests confirm the modelled structures, particularly SBA6. The de-installation and re-installation of the packed-off monitoring system in KFR27 was found to cause large-scale, long-term trends in intercepts associated to SBA6, which signifies the hydrogeological role of SBA6, propagating remote drawdown from ZFM871 via an open borehole section in KFR27. Another important observation is that no responses have been observed across the Central Block (i.e., in KFR104, HFR105, HFM35, HFM34, or KFM11A). The outcome of the interference tests suggests a few minor revisions of the deterministically modelled SBA structures. One notion may be combining SBA1, SBA2, and SBA3 to a larger structure SBA1-3, which is updated based on the information from the observed interferences.

Occurrence of hydraulic chokes (overlapping PSS tests)

Overlapping short-term, double-packer tests (PSS) have been conducted in two boreholes (KFR27 and KFR105) to supplement the existing PFL data from the recent PSU site investigation (2008-2009). The purpose was to evaluate the occurrence of *hydraulic chokes*, but also to demonstrate if PFL-logging under atmospheric conditions has caused a systematic underestimation of transmissivity (Appendix C). The occurrence of *hydraulic chokes* is manifested by a discrepancy in hydraulic properties related to test duration; where the transmissivity evaluated from short-term transient tests (PSS) exceed that from pseudo-stationary tests (PFL). PFL-logging a borehole drilled from subsurface under atmospheric conditions (i.e., KFR105) implies a dramatic drawdown, which may underestimate hydraulic properties (e.g., due to turbulence, gas-bubble formation, hydro-mechanical fracture closure, and missing drained fractures).

The outcome is studied as the ratio, T_{PSS}/T_{PFL}. A clear difference is demonstrated between the two boreholes; most sections of KFR27 exhibit consistency between PSS and PFL data (i.e., the ratio contained within an order of magnitude), whereas the presence of hydraulic chokes is demonstrated in 8/96 sections (i.e., one being the SBA6 intercept). Along with expectations, KFR105 exhibits a systematic discrepancy between PSS

DokumentID
1578373, (1.0)

Sekretess
Öppen

Sida
94(165)

TD15 Complementary simulation cases in support of SR-PSU

and PFL data (median ratio $T_{PSS}/T_{PFL} = 4$). Thus, the interpretation of the *Central Block* as less transmissive and less connected, compared to its bounding belts has, to some extent, been exaggerated by inappropriate test conditions in KFR105, However, the interpretation is still supported by KFR104. Overall, the evidence of compartmentalisation in PSS data (frequency of $T_{PSS}/T_{PFL} >10 \approx 10\%$, frequency of interpreted no-flow boundaries: $\approx 20\%$) is less than expected (Öhman et al. 2012).

4.2   Numerical sensitivity analysis

Sensitivity to HSD parameterisation

The sensitivity to HSD parameterisation (i.e., hydraulic conductivity of regolith layers) was evaluated by five HSD parameterisation variants (listed in Table 1-3) compared against the base-case setup. Simulations demonstrate that bedrock infiltration is not limited by the the hydraulic conductivity of the regolith (not even in the low K_{HSD} case), but instead it is limited by the vertical hydraulic conductivity of the bedrock. Therefore, the main effect of varying K_{HSD} appear in the gradients of simulated groundwater levels, where the low-conductive HSD case raises the groundwater level close to ground surface (closely following topographical gradients), while the high-conductive HSD case renders a "smoothened" groundwater table that is more de-coupled from local topographical gradients. This leads to a somewhat counter-intuitive result, where the low-conductive HSD case increases the flow rates in the disposal rooms of SFR1 and SFR3 (i.e., inverse proportionality), arising from stronger hydraulic gradients in the underlying (less permeable) bedrock. This phenomenon is only expected to occur in the situation where HSD conductivity does not constrain bedrock infiltration (i.e., if $K_{HSD} > K_{HRD}$). Note that, in a different situation, where HSD controls bedrock infiltration (i.e., $K_{HSD} < K_{HRD}$), the bedrock flow rates are expected to be directly proportional to HSD conductivity.

Also HSD case 6, which studies a potential contrast in properties between terrestrial deposits and seafloor sediments, demonstrates that a hydraulic conductivity reduction in the uppermost layer of seafloor sediments may increase disposal-room cross flows somewhat. This is not primarily associated to higher simulated groundwater level in the pier, but rather to the local presence of low-permeable clay layers south of the SFR pier. Thus, the low-permeable clay layers above Singö deformation zone (i.e., south of the SFR pier) form a cap along the shoreline that upholds the pressure of the large-scale flow paths from elevated areas in the Forsmark inland and thereby slightly increasing tunnel flow.

The simulations indicate that the performance measures of simulated particle trajectories are not particularly sensitive to HSD parameterisation. As the HSD conductivity is varied by an order of magnitude, the magnitude of the effect on particle-performance measures is on the order of a few percent. The maximum effect is determined to be 62% in SFR3 for the high-HSD conductivity case; however, this result is expected to be artificially exaggerated by the fact that the net precipitation (P-PET) was kept constant in all HSD cases. In reality, the net precipitation is expected to be larger in a case with higher HSD parameterisation, which would dampen the effects on performance measures.

Sensitivity to historic data support in HCD parameterisation

Historic packer-test data of short test duration represent local hydraulic properties of the surrounding rock mass. In case the flowing fracture system is compartmentalised, the use of local hydraulic data may overestimate the effective transmissivity of large-scale flow paths (e.g., deformation zones). Thus, data-based HCD parameterisation is subject to a conceptual uncertainty concerning the representative scale of data relative to the modelled structure (i.e., referring to the historic packer data). The significance of this uncertainty is evaluated by comparing the original data-based HCD parameterisation versus the re-assessed HCD parameterisation (Table 1-1). The simulations demonstrate that – even if the flow magnitudes redistribute among the disposal rooms – the net effect is negligible in terms of total flow across the facilities.

DokumentID
1578373, (1.0)

Sekretess
Öppen

Sida
95(165)

TD15 Complementary simulation cases in support of SR-PSU

Likewise, the uncertainty in HCD parameterisation has negligible effect on particle tracking and their exit locations.

Sensitivity to size-transmissivity correlation in the DFN model

Two model approaches for the correlation between fracture size and fracture transmissivity in the DFN model are compared; the two variants are referred to as the *correlated* (employed in PSU) and the *semi-correlated* (alternative variant used in SR-Site Forsmark) approaches. The correlated transmissivity model is the more pessimistic model for SR-PSU as the disposal rooms are intersected by several fractures (numerous small and few large) and "*large fractures do not only form the longest connected flow paths, but also the most transmissive paths*". Nevertheless, the effect of semi-correlated parameterisation is small, both in terms of disposal-room flow and in terms of retention properties along particle trajectories (i.e., the magnitude is typically on the order of 10%, or so).

Sensitivity to HRD heterogeneity outside the SFR Regional domain

The sensitivity analysis to model uncertainty/heterogeneity in SR-PSU was constrained to addressing the parameterisation inside the SFR Regional domain (i.e., TD11; Öhman et al. (2014) and Odén et al. (2014)). Based on an analysis of particle exit locations, the model performance was assumed to be rather insensitive to the parameterisation in peripheral parts of the model domain, and therefore the Hydraulic Rock-mass Domain (HRD) outside the SFR Regional domain was parameterised based on a single (static) DFN realisation. In this study, the validity in such an assumption was tested by comparing the performance measures of the static DFN realisation, used in TD11 SR-PSU (i.e., Öhman et al. 2014), versus five stochastic realisations of the rock mass outside the SFR Regional domain. The simulations demonstrated that the disposal-room flow is indeed primarily controlled by the nearfield parameterisation (i.e., HCD and HRD inside the SFR Regional domain) and therefore the introduction of stochastic realisations has largely no impact on tunnel flow in the facilities. Under normal circumstances, the peripheral HRD parameterisation has negligible impact on simulated particle trajectories from SFR1 (and their exit locations to the biosphere), but tends to re-direct somewhat more particles from SFR3 outside the SFR Regional domain (i.e., the fraction increases from 5% to 15%).

However, the simulations also demonstrate that the occurrence of large SBA-type fractures outside the SFR Regional domain can – under particular circumstances – serve as a pivot that dramatically re-directs flow paths to downstream biosphere objects 157_1 and 116. A probabilistic analysis suggests that the risk of this event (i.e., the frequency of occurrence for this type of fractures with dramatic impact on exit locations outside the SFR Regional domain) is small (c. 1%; Appendix E). In spite of the dramatically displaced exit locations (and extended path lengths), the effects in terms of key performance measures, advective travel time and F-quotient, are negligible.

Sensitivity to deterministic SBA structures

The uncertainty in deterministically modelled SBA structures has been addressed the light of stochastic variability in the DFN model (Section 1.2.4). The primary role of the deterministically modelled SBA structures is to honour detailed anomalous hydrogeological data in the vicinity of the planned SFR extension, which are relevant for the emplacement of the SFR extension. As the result, it has been possible to adapt the design of SFR3 so as to avoid direct intersection with the SBA structures, which in turn diminishes their role in model performance. Furthermore, it has been demonstrated that the hydrogeological properties of SBA structures have a duplicate representation in the SDM (i.e., covered by deformation zones, Unresolved PDZs and the stochastic variability of DFN realisations, or its underlying data are of a type that is not normally included in the model); this means that from a methodological modelling perspective, the deterministical SBA

DokumentID
1578373, (1.0)

Sekretess
Öppen

Sida
96(165)

TD15 Complementary simulation cases in support of SR-PSU

structures can be removed without underrepresenting the hydrogeological data of the site. Simulations demonstrate that not including the SBA structures only affects the performance measures of 2BMA; its cross flow reduces by c. 31% and about 10% of its particle trajectories are re-directed to downstream biosphere objects. In summary, recent field investigations have reinforced the model representation of SBA structures (Appendix B), while numerical modelling has demonstrated that their role is small, provided direct intersection with the tunnel facility can be avoided.

Sensitivity to ECPM scaling effects (grid discretisation)

DarcyTools employs a geometrical upscaling approach to transfer the properties of an underlying fracture network to its computational grid (as opposed to hydraulic upscaling), and as such, the grid discretisation affects the flow connectivity in the ECPM grid (i.e., refers to connectivity of preferential paths, as all grid cells are geometrically connected). The benefit of ECPM upscaling is a dramatic reduction in computational load (i.e., and typically necessary due to computational limitations). Simulations demonstrate that improving the grid refinement reduces the disposal-room cross flows by c. 20%. Further grid refinement, to a cell size of 2 m, has only minor impact on simulated flow, which suggests that the exaggerated flow connectivity in ECPM upscaling – as compared against a true DFN simulation – is probably not much larger than 20%. However, exaggeration of flow is often perceived as conservative in risk assessment, and therefore the drawbacks of overrepresented connectivity in ECPM can be considered acceptable in context of its merits. The particle performance measures are comparatively less sensitive to ECPM scaling effects (at the most, c. 10% reduction in travel time).

4.3   Complementary simulations

Transient (2D) simulations of declining tunnel inflow

Different phenomena have been suggested to explanain the trend of declining inflow to SFR1 (Öhman et al. 2013). Preceding simulations, in SDM-PSU, have assumed that this trend reflects a gradual developing flow resistance, as the rock-mass is affected by the open-tunnel conditions (i.e., referred to as skin effect, but the resistance may propagate well beyond the tunnel wall). This study considers an alternative explanation, where an analogy is made between the long-term trends in flow and pressure data observed around the open facility and the typical flow-pressure history observed during hydraulic constant-head tests in low-diffusive environments (Figure 1-3; Figure 1-7). Thus, the declining tunnel inflow is assumed to reflect transient aquifer-storage effects of a very slow-responding hydrogeological system, where the apparent hydraulic diffusivity is defined by $\alpha = K_{ECPM}/S_s$. Here, S_s (m^{-1}), is envisaged as *apparent specific storage*, which is combined of two components: 1) the *material* property of the aquifer and 2) an *equivalent* property reflecting limitation in connectivity (Figure 1-7). The role of hydraulic diffusivity in tunnel inflow and propagation of drawdown is analysed by varying S_s over several orders of magnitude to mimic the slow hydraulic responses of a poorly connected fracture network.

The appearance of transient tunnel inflow in a poorly connected flowing fracture system is very similar to that arising from gradually developing flow resistances (i.e., which are not necessarily confined to the proximity of the tunnel wall), which makes the two potential causes to transient trends difficult to differentiate. The goal here is to examine if poor flow connectivity can provide a single-handed explanation to the declining tunnel inflow, and therefore tunnel-wall skin is *not* applied in these simulations. Two cases are considered: a homogeneous case and a heterogeneous case (based on ECPM upscaling from an underlying fracture network).

The model setup is simplified by a two-dimensional onset, in which the 30 year period of transient inflow is simulated in terms of normalised flow, Eq. (2-2). Simulations demonstrate that the pattern in declining inflow

DokumentID
1578373, (1.0)

Sekretess
Öppen

Sida
97(165)

TD15 Complementary simulation cases in support of SR-PSU

can be reasonably well reproduced in the homogeneous case. However, the fitted apparent specific storage is exceptionally high, $S_s = 0.03$ m^{-1}, which is is outside the range of credible values for a confined aquifer. This suggests that the observed trend in inflow cannot be explained by transient storage effects of a poorly connected fracture alone, but is probably a combined phenomenon, which also includes gradual development of flow resistances over time (i.e., as dicussed in Öhman et al. 2012). Simulations in a heterogeneous model setup could not reproduce the pattern in declining tunnel inflow, which suggests that the pattern in tunnel inflow is also affected by structural geometry (i.e., adds the complexity of flow dimensions, which is not well assessed in a 2D cross section).

In summary, the results suggest that:
1) the observed trends in borehole drawdown can be associated to transient behaviour of the poor communication observed in the field (e.g., Figure 1-6), but that
2) the observed trend in tunnel inflow probably reflects a combined effect between a poorly connected fracture system and gradually developing flow resistances.

Alternative localisation of SFR3 (Forsmark lens)

The most notable difference between the compared localisations of SFR3 concerns the sensitivity to shoreline retreat. As thoroughly discussed in Öhman et al. (2014), the hydrogeological setting of the planned localisation (i.e., inside the SFR Regional domain) changes significantly over the next couple of thousand years), while at the alternative location, in the Forsmark lens, it has already stabilised to more-or-less stationary conditions.

The spatial resolution in the deterministically modelled geological structures differs between the two locations (i.e., the size cut-off between stochastic and deterministic representation of geological structures). This causes a bias in the comparison between the two alternatives, as the uncertainty is higher in the modelled performance of the alternative location (i.e., requiring the analysis of a larger ensemble of DFN realisations). The alternative location of SFR3 significantly reduces the risk of interaction with the existing facility SFR1, as few flow paths emerge across the Singö deformation zone.

This study has neither addressed the practical aspects of constructing and operating SFR3 at the alternative location, nor aspects of long-term safety that may affect the deep repository for spent nuclear fuel.

SVENSK KÄRNBRÄNSLEHANTERING AB

DokumentID
1578373, (1.0)

Sekretess
Öppen

Sida
98(165)

TD15 Complementary simulation cases in support of SR-PSU

References

Carlsson L, Carlsten S, Sigurdsson T, Winberg A, 1985. Hydraulic modelling of the final repository for reactor waste (SFR). Compilation and conceptualization of available geological and hydrogeological data. Edition 1. SKB SFR 85-06, Svensk Kärnbränslehantering AB.

Cooper H H, Jacob C E, 1946. A generalized graphical method for evaluating formation constants and summarizing well-field history. Eos, Transactions of the American Geophysical Union 27, 526–534.

Curtis P, Markström I, Petersson J, Triumf C-A, Isaksson H, Mattsson H, 2011. Site investigation SFR. Bedrock geology. SKB R-10-49, Svensk Kärnbränslehantering AB.

DHI Software, 2010. MIKE SHE – User Manual. Hørsholm, Denmark: DHI Water, Environment & Health.

Harrström J, Hedberg S, Öhman J, 2017. Hydraulic Interference Tests in KFR27, KFR103, and KFR105**.** Site investigation SFR. SKB P-17-20, Svensk Kärnbränslehantering AB.

Holmén J G, Stigsson M, 2001. Modelling of future hydrogeological conditions at SFR. SKB R-01-02, Svensk Kärnbränslehantering AB.

Hurmerinta E, Väisäsvaara J, 2009. Site investigation SFR. Difference flow logging in boreholes KFR104 and KFR27 (extension). SKB P-09-20, Svensk Kärnbränslehantering AB.

Follin S, 2008. Bedrock hydrogeology Forsmark. Site descriptive modelling, SDM-Site Forsmark. SKB R-08-95, Svensk Kärnbränslehantering AB.

Follin S, Levén J, Hartley L, Jackson P, Joyce S, Roberts D, Swift B, 2007. Hydrogeological characterisation and modelling of deformation zones and fracture domains, Forsmark modelling stage 2.2. SKB R-07-48, Svensk Kärnbränslehantering AB.

Joyce S, Simpson T, Hartley L, Applegate D, Hoek J, Jackson P, Swan D, Marsic N, Follin S, 2010. Groundwater flow modelling of periods with temperate climate conditions – Forsmark. SKB R-09-20, Svensk Kärnbränslehantering AB

Ludvigson J-E, Hjerne C, 2014. Detailed analysis of selected hydraulic interference tests and review of new test analysis methods. SKB R-10-73, Svensk Kärnbränslehantering AB.

Meier P M, Carrera J, Sanchez-Vila X, 1998. An evaluation of Jacob ' s method for the interpretation of pumping tests in heterogeneous formations. Water Resources Research 34, 1011–1025.

Mårtensson E, Gustafsson L-G, 2010. Hydrological and hydrogeological effects of an open repository in Forsmark. Final MIKE SHE flow modelling results for the Environmental Impact Assessment. SKB R-10-18, Svensk Kärnbränslehantering AB.

Odén M, Follin S, Öhman J, Vidstrand P, 2014. SR-PSU Bedrock hydrogeology. Groundwater flow modelling methodology, setup and results. SKB R-13-25, Svensk Kärnbränslehantering AB.

DokumentID
1578373, (1.0)

Sekretess
Öppen

Sida
99(165)

TD15 Complementary simulation cases in support of SR-PSU

Pekkanen J, Pöllänen J, Väisäsvaara J, 2008. Site investigation SFR. Difference flow logging in boreholes KFR101 and KFR27. SKB P-08-98, Svensk Kärnbränslehantering AB.

Rhén I (ed), Gustafson G, Stanfors R, Wikberg P, 1997. Äspö HRL – Geoscientific evaluation 1997/5. Models based on site characterization 1986–1995. SKB TR 97-06, Svensk Kärnbränslehantering AB.

Sánchez-Vila X, Meier P M, Carrera J, 1999. Pumping tests in heterogeneous aquifers: An analytical study of what can be obtained from their interpretation using Jacob's method. Water Resources Research 35, 943. doi:10.1029/1999WR900007

SKB, 2013. Site description of the SFR area at Forsmark at completion of the site investigation phase. SDM-PSU Forsmark. SKB TR-11-04, Svensk Kärnbränslehantering AB.

SKB, 2014. Safety analysis for SFR. Long-term safety. Main report for the safety assessment SR-PSU. SKB TR-14-01, Svensk Kärnbränslehantering AB.

Svensson U, Ferry M, Kuylenstierna H-O, 2010. DarcyTools version 3.4 – Concepts, methods and equations. SKB R-07-38, Svensk Kärnbränslehantering AB.

Väisäsvaara J, 2009. Site investigation SFR. Difference flow logging in borehole KFR105. SKB P-09-09, Svensk Kärnbränslehantering AB.

Walger E, Ludvigson J-E, Gentzschein B, 2010. Site investigation SFR. Evaluation of selected interference tests and pressure responses during drilling at SFR. SKB P-10-43, Svensk Kärnbränslehantering AB.

Walker D D, Roberts R M, 2003. Flow dimensions corresponding to hydrogeologic conditions. Water Resources Research 39, 1349. doi:10.1029/2002WR001511

Öhman J, 2013. TD10- SFR3 adaptation to hydrogeological conditions. SKBdoc 1395215 ver 1.0, Svensk Kärnbränslehantering AB.

Öhman J, 2014. TD08- SFR3 effect on the performance of the existing SFR1. SKBdoc 1395214 ver 2.0, Svensk Kärnbränslehantering AB.

Öhman J, Follin S, 2010. Site investigation SFR. Hydrogeological modelling of SFR. Model version 0.2. SKB R-10-03, Svensk Kärnbränslehantering AB.

Öhman J, Bockgård N, 2013. TD05-Effects in ECPM translation. SKBdoc 1395200 ver 1.0, Svensk Kärnbränslehantering AB.

Öhman J, Odén M, 2017. TD-14 Complementary simulation cases in support of SR-PSU. SKBdoc 1496921 ver 1.0, Svensk Kärnbränslehantering AB.

Öhman J, Bockgård N, Follin S, 2012. Site investigation SFR. Bedrock hydrogeology. SKB R-11-03, Svensk Kärnbränslehantering AB.

Öhman J, Follin S, Odén M, 2013. Site investigation SFR. Bedrock hydrogeology – Groundwater flow modelling. SKB R-11-10, Svensk Kärnbränslehantering AB.

Öhman J, Follin S, Odén M, 2014. SR-PSU Hydrogeological modelling. TD11 – Temperate climate conditions. SKB P-14-04, Svensk Kärnbränslehantering AB.

A. Appendix

Inventory of significant uncertainties

An inventory of uncertainties in the bedrock hydrogeological model identified by Öhman et al. (2012), showing whether and how these have been accounted for in the hydrogeological modelling for SR-PSU, and with an accounting of the expected consequences in terms of uncertainties in safety assessment calculations, for the uncertainties that have not been explicitly addressed.

Note that some issues may be of conceptual type (data inference is inconclusive or contradictory), technical type (the numerical methods may be unfeasible or inappropriate), or lacking data support.

Table A-1. Comparison of uncertainties/issues raised in bedrock hydrogeology report (SKB-11-03) versus handling in the SDM-PSU main report (SKB TR-11-04 Section 7.6).

Issue	As raised in Öhman et al. (2012)	Handling in SDM-PSU main report	Handling in SR-PSU	Expected consequences (if evaluated in SR-PSU)
Hydraulic properties of HCDs	ENE to NNE and WNW to NW sets of deformation zones within the Central block are highly heterogeneous with local high-T channels;	No remarks on the significance of these inferences were found in this preliminary-stage review.	Homogeneous and heterogeneous HCD variants are compared in bedrock cases of sensitivity analyses (TD08, TD10, and TD11). Assumed heterogeneity scale: 100 m. In conditioned bedrock cases (e.g. base case), the key zones for SFR3 are low-transmissive at tunnel intercepts in the Central block	Possibly, the role of deformation zones as deterministic flow paths is overestimated
Connectivity of HCDs	Evidence of heterogeneous contact between ZFM871 and steeply dipping zones and indications of internal heterogeneity and/or discontinuity in ZFMNW0805B (e.g., remnant historic groundwater types and drawdown).	Discontinuous or poor connection between ZFMNW0850B and ZFM871 explored in open-tunnel simulations (Öhman et al. 2013).	Not addressed specifically in SR-PSU (apart from heterogeneous HCD variants, see above)	The hydraulic connection between ZFM871 and steeply dipping zones (ZFMNW0805A/B and ZFMNNE0869) has a key role in downstream flow paths from SFR1. Possibly, their role as deterministic flow paths is overestimated relative to the stochastic DFN. Irrespectively of HCD flow paths, the topographical conditions are still expected to concentrate particle exit locations to biosphere object 157_2 (as demonstrated by 'the homogeneous bedrock case' in TD10).
Role of HCD and HRD in hydraulic connectivity	The hydraulic contrast between HRD and steeply dipping HCD appears subordinate to the lateral contrast in hydraulic data (i.e., the central block compared to the Northern Boundary belt; p. 90, p. 95)	Hydraulic data inside deformation-zone intercepts modelled as deterministic structures (i.e., known, large-scale geometry).	Hydraulic data inside deformation-zone intercepts modelled as deterministic structures. "*the sub-horizontal to gently dipping structures above −200 m elevation, including minor zones and discrete fractures, make a much more significant contribution to the pattern of local groundwater flow in the*	Possibly, the role of steeply-dipping deformation zones (i.e., deterministic flow paths) has been overestimated in the hydrogeological modelling (i.e., relative to SBA structures), leading to conservative predictions, but perhaps underestimated uncertainty in the geometry of flow-paths.

PDF rendering: DokumentID 1578373, Version 1.0, Status Godkänt, Sekretessklass Öppen

DokumentID
1578373, (1.0)

Sekretess
Öppen

Sida
102(165
)

TD15 Complementary simulation cases in support of SR-PSU

		upper part of the bedrock than the steeply dipping deformation zones."		
HCD depth trend	Insufficient data support to evaluate HCD depth trend (p. 85, 86, 116). Maximum-transmissivity analysis biased by declining borehole coverage with depth.	*"Scarce data at depth lead to uncertainty in depth trend analyses. Also, a depth trend fitted to maximum transmissivity may be artificially exaggerated, as a smaller sample size reduces the probability of finding large values (particularly in such highly skewed distributions as log-normal or power law). Nevertheless, the hydraulic data at SFR suggest the existence of a depth trend. Due to data limitations, the HCD depth trend for SDM-Site Forsmark (Follin 2008) was accepted as valid for the hydrogeological model for SFR."*	Significance of HCD depth trend evaluated in sensitivity analysis (TD11)	The assumed depth trend is conservative (i.e., yields higher tunnel flow; TD10 and TD11) owing to the unusual circumstance of deep, long intercepts of the two key zones for SFR3 (ZFMWNW0835 and ZFMENE3115),
Hydraulic parameterisation of HCDs	"Sub-parallel borehole intercepts" implies long test intervals compared to true thickness, which may lead to unrepresentative characterisation (p. 87).	Hydraulic data inside deformation-zone intercepts modelled as deterministic structures (irrespectively of intercept length).		Overestimated transmissivity in ZFMWNW0835 and ZFMENE3115 may exaggerate tunnel flow (SFR3)
Local conditioning of HCDs	Range of conditioning hydraulic data. Relevant issue as intercepts in the vicinity of SFR3 are unusually low-transmissive.	SFR1 intercepts conditioned based on grouting information in Base case. SFR3 intercepts conditioned as low-transmissive in Base case	SFR3 intercepts conditioned as low-transmissive in Base case (Fig 4-8 in Öhman et al. 2014). Significance evaluated by comparing conditioned and non-conditioned cases in sensitivity analysis (TD10, TD11)	
Spatial extension of ZFM871	ZFM871 terminated based on geological concepts, rather than data support. Borehole data north of ZFMNW0805A discussed in Appendix A, Öhman et al. (2013). Anomalous drawdown southeast of ZFMENE3115 discussed in pp 72–73 in Öhman et al. (2012)	ZFM871 has been modelled to terminate against zones ZFMENE3115, ZFMNNE0869, ZFMNW0805A/B and ZFMWNW1035 (p. 100)	Significance of ZFM871extension evaluated in sensitivity analysis (TD08)	An extended geometry of ZFM871 has minor impact on disposal-room flow, interactions and exit locations. A probably reason for this is that particle trajectories from SFR1 are "cornered in" by the topographical depression at the junction of the discharging zones ZFMNNE0869 and ZFMNW0805A/B
Sediment choking	Seafloor sediments hypothesised as potentially constraining inflow under open-tunnel conditions (p. 79 and Model exercises in Öhman et al. 2013)	"*The regolith potentially has an important role in controlling the contact between the sea (positive flow boundary) and the underlying bedrock.*" (p. 79)	Significance of HSD parameterisation evaluated in sensitivity analysis (TD15)	Minor impact on tunnel flow. Its primary role is not constraining bedrock recharge, but instead the balance between runoff and groundwater levels, which controls the hydraulic gradient in deep rock
Generality in HSD parameterisation	Validity in transferring HSD parameterisation from Forsmark land to SFR seafloor (Calibrated effective conductivity is subject to local	"Although it has not been explicitly confirmed, these effective parameters are assumed to be valid for offshore	Significance of HSD parameterisation evaluated in sensitivity analysis (TD15)	Minor impact on tunnel flow

SVENSK KÄRNBRÄNSLEHANTERING AB

TD15 Complementary simulation cases in support of SR-PSU

	topographical and hydrological conditions). Terrestrial properties may differ from submerged (soil formation processes, p. 77).	marine sediments at SFR as well. It is possible that the hydraulic conductivity on land is somewhat enhanced due to frost heave, worm holes, tree roots, etc. Uncertainties … will be handled in the SR-PSU …"		
Hydraulic properties of HRD	Base-case parameterization is provided in Table 6-2; alternative parameterization including KFR106 is provided in Table G-7. Possible depletion of Hydro-DFN model by deterministic treatment of SBA structures is mentioned on p. 108 but not investigated.	No remarks on the significance of these inferences were found this preliminary-stage review.	Only the base-case parameterisation (Table 6-2) propagated to SR-PSU.	This is a misunderstanding. The text on p. 108 is perhaps not fully clear. Deterministic modelling of SBA-type data implies its geometry is assumed to be 'known', and it is therefore given a 'static geometrical representation'. The truth is that its geometry is not deterministically known, and compared to the geological HCD modelling, the modelled SBA structures are highly uncertain. Therefore, deterministic handling of SBA-type data means 'depleting' the upper-tail data from the hydro-DFN (i.e., stochastic representation), which implies a risk of underrepresenting the geometrical uncertainty in occurrence and spreading of such data. In spite of this, the deterministic approach is defendable, as the alternative (stochastic handling via the DFN) is considered to be inappropriate (it is also subject to unsupported assumptions and model simplifications). Furthermore, the conditioning information on absence of SBA structures, provided by several boreholes and the existing SFR, is difficult to honour via a DFN approach. The geometrical inference of Unresolved PDZs is considered to be a midway approach to represent this type of data.
DFN size-distribution	The fracture size distribution is recognised as the most uncertain DFN parameter (p. 109); during the *calibration*, most data are assumed to be small, unconnected or low-transmissive fractures (i.e., negligible for regional-scale simulations); thus, *simulations* rely on an extrapolation of the upper tail (which is highly uncertain, due to limited or no data support). Two alternative size-distribution concepts are presented in Table 6-2	*"Power-law scaling also leads to particular uncertainty in the maximum size/transmissivity, which is related to available borehole length"* Both size-distribution concepts presented (Appendix 5)	Only the "Connectivity Analysis" concept is used in SR-PSU	The alternative, Tectonic continuum approach, includes large, low-transmissive, steeply-dipping fractures, which is expected to "raise the background conductivity"

TD15 Complementary simulation cases in support of SR-PSU

DFN size-distribution	The minimum mapped fracture size is assumed to be equal to borehole radius, $r_0 = r_{bh}$. Alternative inference suggested in Appendix H of Öman and Follin (2010).	"$r_0 = r_{bh}$" (Appendix 5)	Only the "$r_0 = r_{bh}$" concept used	The alternative is expected to produce a more homogeneous parameterisation (less dominance of few, large, highly-transmissive fractures). It should also be noted that the ECPM upscaling in DarcyTools has a 'homogenising effect', depending on grid-cell resolution.
DFN size-transmissivity	Fracture size is assumed correlated to PFL-f transmissivity, such that DFN connectivity reflects the discrepancy between open-fracture frequency and PFL-anomaly frequency in boreholes. Although it is realistic to expect a certain degree of correlation between size and transmissivity, two issues are raised: • PFL transmissivity is an apparent value, that is not necessarily intrinsic to the tested fracture (bottleneck along flow path) • The model representation (homogeneous parameterisation) becomes unrealistic for large fractures	"*The key uncertainties of the DFN parameterisation are related to the conceptual methodology where fracture size is coupled to measured transmissivity (i.e. apparent transmissivity)."* *"Power-law scaling also leads to particular uncertainty in the maximum size/transmissivity, which is related to available borehole length"*	Irrespectively if it is realistic, or not, the correlated size-transmissivity model is considered to be "conservative" (causing high tunnel flows), and is therefore used in TD08, TD10, and TD11. Test simulations indicate that the semi-correlated size-transmissivity relationship has negligible effect on simulated tunnel flow (see TD15).	Although weaknesses are apparent in the numerical representation of PFL-f data, it is not clear how this technical issue can be resolved.
Boundary of HRD domains for DFN model	Note on p. 109 that the boundary between the repository and deep domains may be need to be reconsidered once the depth of the SFR extension has been decided.	No remarks on this topic were found this preliminary-stage review.	The HRD depth domains were defined based on the depth of the existing SFR, as the depth of its planned extension was not decided during SDM-PSU. However, the planned depth of the extension (-117 to -135 m) falls within the depth interval of the existing SFR (-69 to -133 m). Therefore, the HRD depth domains have not been revised.	The planned depth of the extension does not motivate revising the HRD depth domains.
SBA structures	SBA8 is regarded as uncertain and not included in final model.	Eight SBA structures mentioned. No specific remarks on handling of uncertain structures such as SBA8.	The grounds for handling SBA8 have been reconsidered during SR-PSU. SBA8 is not based on the PFL-f data that form the basis of the hydro-DFN, and as such, its inclusion in flow modelling allows honouring deterministic information from the SFR facility without affecting the hydro-DFN (i.e., not 'depleting' its data support).	In spite of its uncertainty, it is difficult to motivate exclusion of SBA8. Inclusion of SBA8 is expected to have a minor effect on flow simulations.

SVENSK KÄRNBRÄNSLEHANTERING AB

TD15 Complementary simulation cases in support of SR-PSU

Hypothesized absence of SBA structures in the Central Block below -60 m	Motivated by data from HFR101, KFR104 and KFR105, but not confirmed.	Not discussed.	Difficult to confirm without support from additional borehole (i.e., cannot be resolved by data analysis or simulations, alone). The *significance* of the hypothesised lateral contrast can be evaluated in a sensitivity analysis of flow simulations (e.g., apply the DFN parameterisation in Table G-7 as an alternative to Table 6-2).	
Reliance on PFL-f data	Analysis relies exclusively on PFL-f data which are believed to be subject to "hydraulic choking" effects; packer test (PSS) data not available (p. 115) or not utilized due to questions about quality (p. 117).	Dependence of hydrogeological DFN model on PFL-f data noted (p. 180, 4th bullet) but discussion is limited to effects of transmissivity censoring.	Complementary PSS tests are carried out in KFR27 and KFR105.	
Limited scope of interference tests	Intercepts of interpreted SBAs and unresolved PDZs have not been evaluated by interference tests.	Additional interference tests are discussed in relation to issue of declining inflows to existing SFR excavations.	Complementary interference tests have been carried out (2015/2016) in KFR27, KFR103 and KFR105, targeting SBA intercepts and Unresolved PDZs.	
Possible lateral trends in HRD.	Indications of possible trends especially in PFL-f transmissivity observed between the Central block and N/S boundary belts (p. 116). Various alternatives suggested in Section 5.6.	Possible lateral trends are mentioned as an uncertainty (p. 180).	The complementary PSS tests and interference tests may resolve hypothesised 'PFL-choking'.	
Use of "old" data from the existing SFR	Older data seem to result in higher transmissivities of deformation zones, but only used as complementary data in SDM-SFR. Only core-drilled boreholes surveyed by PFL-f method used in SDM-SFR.	Historic and recent data noted to be of different quality and test types, and reflect different stages of the SFR disturbance; this complicates the use of a single model for different sub-domains. No discussion of plans for re-testing old boreholes.	SKB has no plans for re-testing old boreholes. Possibly, the historic transmissivity data can be compared against simulated borehole sampling	
Time-dependent decrease in inflow to existing SFR excavations	Alternative explanations raised but not quantified.	Acknowledged in general terms, but stated that of the possible reasons "probably all of them are reversible." Suggested that further analysis of interference tests could shed light on this issue but due to short duration of these tests, calibration of storativity is a key issue. Longer-duration interference tests are mentioned as a way to provide more robust data but no plans to conduct such tests are indicated.	The declining inflow has been simulated as a transient constant-head condition, in a 2D cross section, to quantify the apparent storativity term (TD15). It is also possible to model unsaturated tunnel inflow in DT using van-Genuchten relationship	
Uncertainties in SFR inflow measurements due to ventilation	Scoping calculations indicate significant impact of ventilation air.	Uncertainty acknowledged as +/- 30 liters per minute, depending on the season. No plans for measurements indicated.	HCD parameterisation based on borehole data. Uncertainty due to ventilation assumed subordinate to e.g., depth trend and connectivity	The net effect of seasonal variation in ventilation contribution/loss is expected to balance out in annual inflow data (i.e., assumed subordinate to uncertainty regarding skin effects, grouting, and transient

SVENSK KÄRNBRÄNSLEHANTERING AB

DokumentID
1578373, (1.0)

Sekretess
Öppen

Sida
106(165
)

TD15 Complementary simulation cases in support of SR-PSU

				development). Tunnel-inflow simulations given less weight in confidence-building of SDM-PSU due to uncertainty regarding skin effects and transient development.
Kinematic porosity	Not discussed in SDM-PSU. Key property for calculating travel time. Applied on grid-cell basis (i.e., not resolving flowing fractures explicitly), assuming an empirical transport-aperture relation.	Not discussed in SDM-PSU	Significance of porosity parameterisation evaluated in sensitivity analysis (TD08)	The applied concept renders short particle travel time (i.e., pessimistic).

DokumentID
1578373, (1.0)

Sekretess
Öppen

Sida
107(165
)

TD15 Complementary simulation cases in support of SR-PSU

B.   Appendix

Complementary interference tests of SBA structures

This appendix presents an overview of the results of five interference tests conducted with the purpose to respond to Strålsäkerhetsmyndighetens (SSM)'s request for supplements[7]. A more comprehensive description of the execution, results, and analyses is documented in Harrström et al. (2017).

Introduction

Based on various hydrogeological support (e.g., extrapolation of anomalous PFL-f data, radar reflectors, and geology) identified borehole responses in SDM-PSU (Figure 4-21 to Figure 4-27 in Öhman et al. 2012), could be deterministically modelled in terms of so-called Shallow-Bedrock Aquifer (SBA) structures (see Appendix B and H in Öhman et al. 2012; Figure B-1). However, the responses monitored during the successive drilling of boreholes resulted in an incomplete response matrix (i.e., not all boreholes had been drilled, or their monitoring equipment had not yet been installed). Thus, the deterministically modelled SBA structures relied on a number of assumed hydraulic connections, (i.e., not yet been confirmed by interference tests). Furthermore, drilling responses are not suitable for hydraulic characterisation of the connecting structures.

The existence and the hydraulic properties of the deterministically modelled Shallow-Bedrock Aquifer (SBA) structures was therefore confirmed by four complementary interference tests, conducted from the autumn 2015 to the spring 2016 (Table B-1). The purpose of the tests was to: confirm the existence, provide additional information on their spatial extent, and characterisation of hydraulic properties. The tests were set up based in context of the prevailing interpretation of SBA structures.

 A fifth interference test was also undertaken in the Central Block to test its potential existence of hydraulic connections to the SBA structures (i.e., or, lack thereof). It should be noted that hydraulic responses from drilling and controlled disturbances in KFR105 have been analysed during SDM-PSU; however, the existing data were subject to uncertainty owing to unfavourable testing conditions.

Table B-1. Complementary interference tests of SBA structures[1]

Test	Structure	Borhole	Interval From (m)	To (m)	Pump start	Duration day (hrs:min)	Non-operative boreholes[2]
1	SBA1	KFR27	47	57	2015-12-09	4 (18:20)	KFR102B, KFR103
2	SBA6	KFR27	189.4	194.4	2016-02-23	2 (21:02)	KFR103
3	SBA2-3	KFR103	83.5	93.5	2016-04-01	2 (21:23)	
4[3]	SBA4-5 (SBA6)	KFR103	177	187	2016-04-07	3 (22:16)	
5	Central block	KFR105	120	137	2016-04-26	3 (02:16)	

1) Details given in Harrström et al. (2017)
2) The installed measurement system was out of order due to corrosion. Hence it was not possible to detect potential responses in these boreholes.
3) The pumped borehole intercept has been interpreted as intercepted by SBA4-5. The primary objective of the test is to examine if KFR103 is hydraulically connected to SBA6, as the borehole instrumentation was not operative during the two preceding tests 1 and 2 (due to corrosion of the equipment).

---

[7] Begäran om komplettering av ansökan om utökad verksamhet vid SFR – hydrogeologi (SSM2015-725-40)
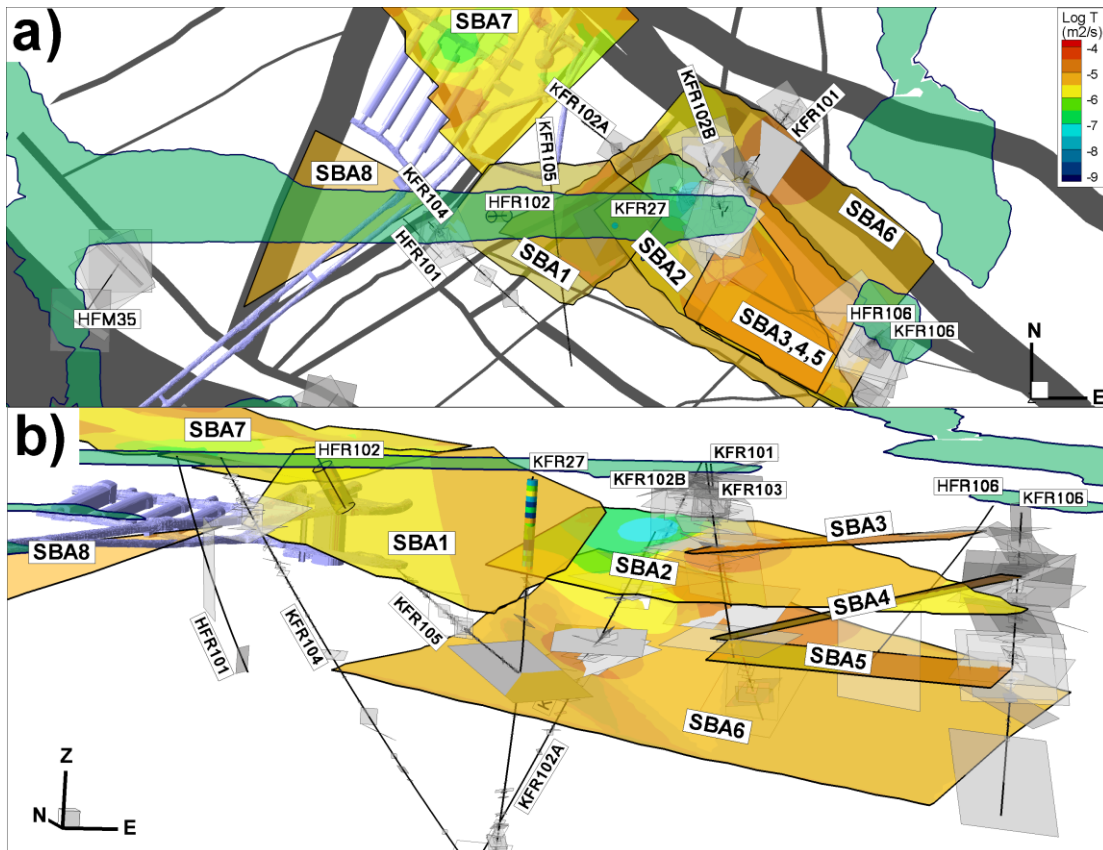
DokumentID
1578373, (1.0)

Sekretess
Öppen

Sida
108(165
)

TD15 Complementary simulation cases in support of SR-PSU

Figure B-1. *Deterministically modelled Shallow-Bedrock Aquifer (SBA) structures; a) top view, and b) view from southwest.*

De-trending influence from sea and air-pressure

The interference tests are conducted below the Baltic Sea and are therefore severely affected by fluctuations in both sea level and air pressure (see Öhman et al. 2012; Figure B-2). The fluctuations are at decimetre-scale (Figure B-3), which complicates the distinction between response and non-response for the applied response criterion, dp = 0.1 m. The influence from sea and barometric pressure depends on the depth of the borehole sections: the uppermost sections (unconfined) are considerably more affected by sea-level fluctuations than deeper sections of the same borehole. The deep sections are on the other hand negatively correlated to air pressure, owing to an underlying assumption on full barometric efficiency in the conversion from monitored pressure levels to head (i.e., involving subtraction by the momentaneous air pressure data). The correlation to air pressure is weak in the uppermost borehole sections, indicating that they are subject to full barometric efficiency, which is properly removed. The deeper sections only exhibit half the barometric efficiency and therefore the full barometric efficiency subtraction imposes a negative correlation of 0.5. It should be noted that although the sea level itself is partly correlated to the air pressure (mesoscale weather systems), it is also affected by the prevailing wind conditions. The interpretation of responses was made in two steps:

1) Raw-data analysis (with manual consideration to recognised patterns in sea and air pressure)
2) Analysis of de-trended data, where the noise from sea and air pressure have been reduced by means of multiple regression (Figure B-4)

DokumentID
1578373, (1.0)

Sekretess
Öppen

Sida
109(165
)

TD15 Complementary simulation cases in support of SR-PSU
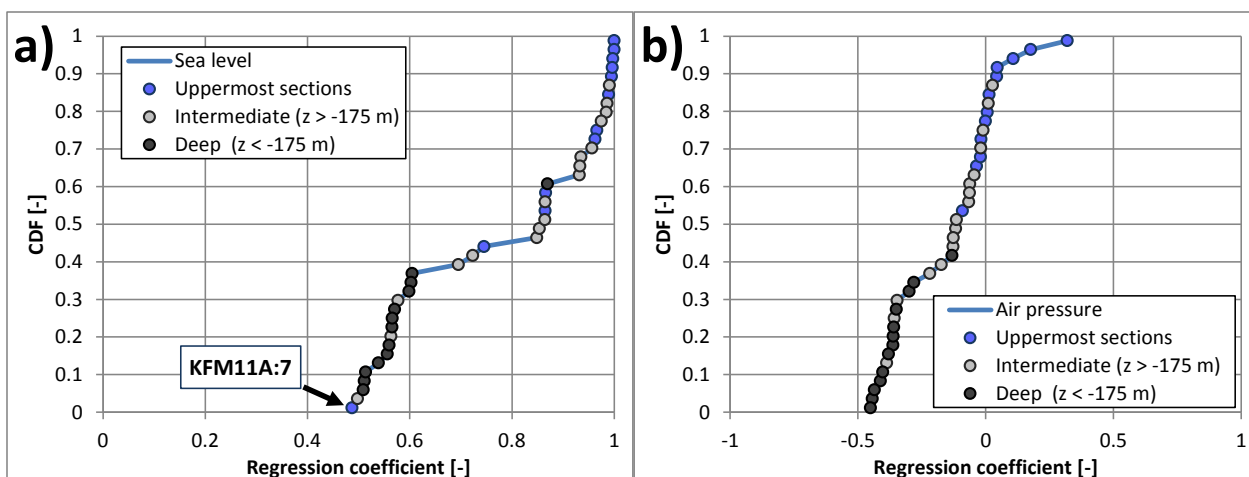

Figure B-2. *Regression coefficients between monitored head and fluctuation in sea level and air pressure.*
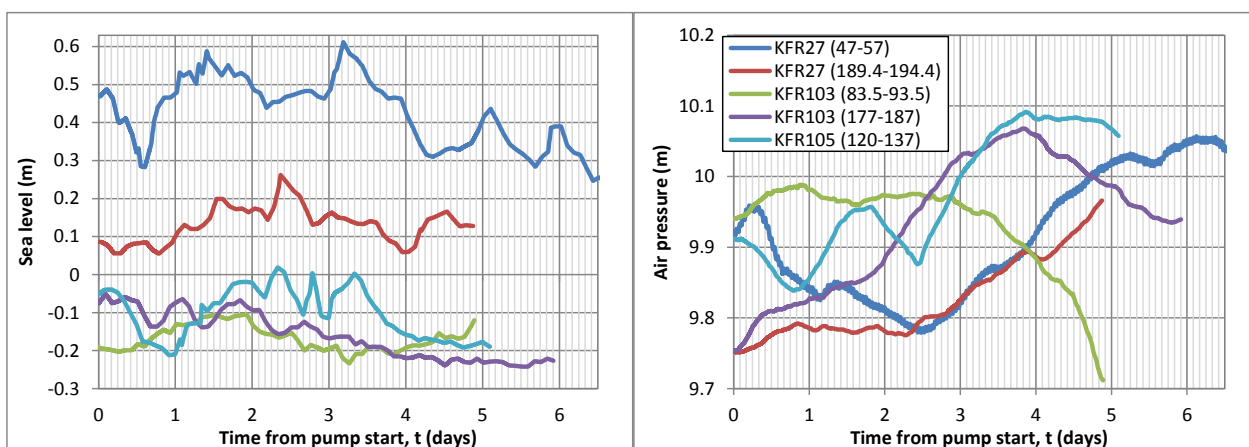

Figure B-3. *Sea and air-pressure fluctuations during the five interference tests.*

DokumentID
1578373, (1.0)

Sekretess
Öppen

Sida
110(165
)

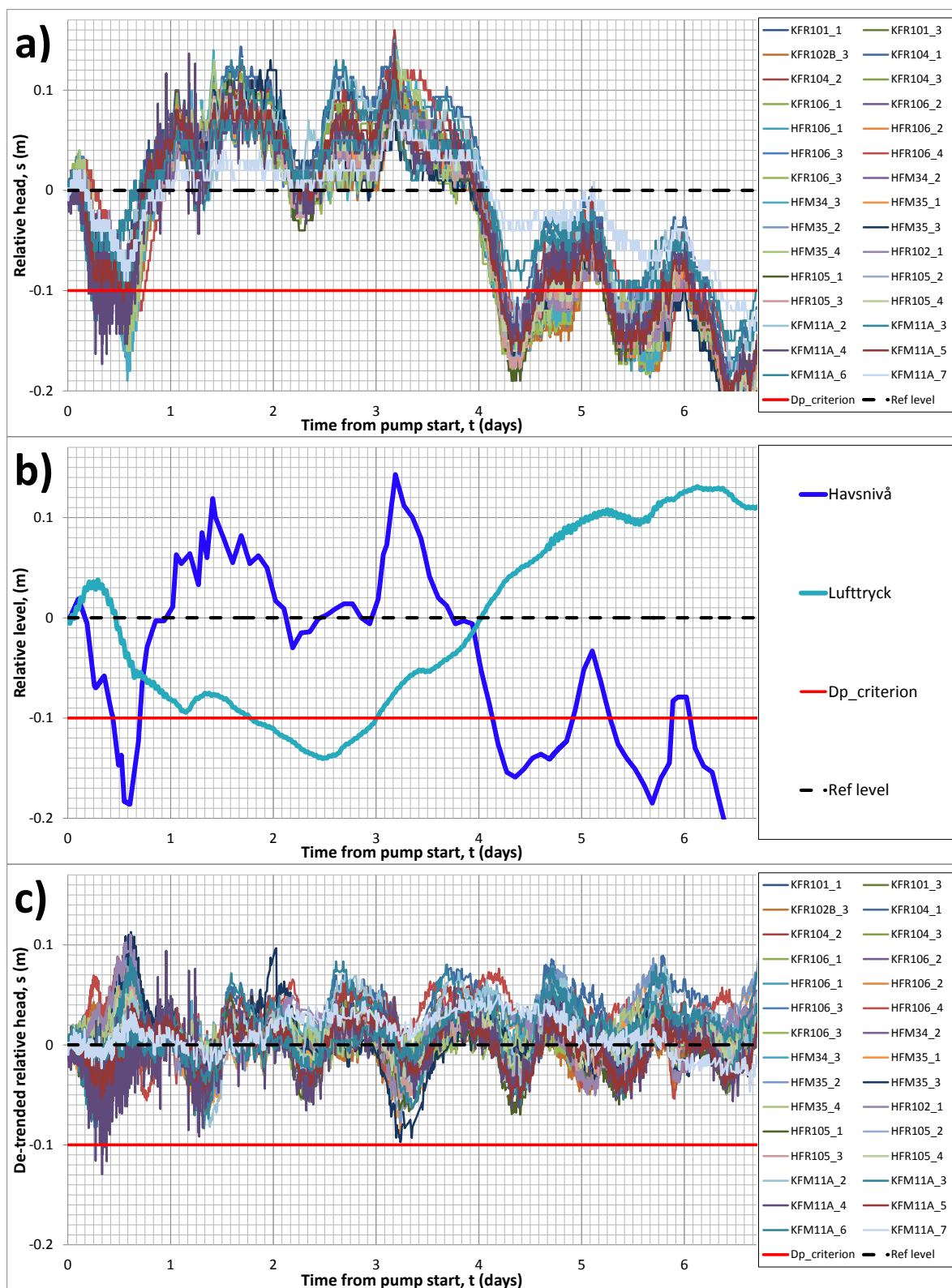TD15 Complementary simulation cases in support of SR-PSU

Figure B-4. *Principle for de-trending variability components in non-responding sections of an interference test (here: test 1 in KFR27); a) monitored head, b) sea-level and air-pressure fluctuations, and c) removing fluctuation noise, using sea-level and air-pressure coefficients from multiple regression.*

Interpretations

In a first step two types of hydraulic responses are identified (see colour marking in Table B-2):

1) high-confidence responses, where both the drawdown and recovery phases are clear, and

2) low-confidence observations, representing various types of anomalies in monitored pressure data. Most of these observations exhibit a disturbance, but lack the corresponding recovery phase; therefore they may reflect ongoing trends that are not necessarily related to the interference test. These observations are classified by appearance, ranging from "No response" to "probable response".

In a second step, a more detailed analysis demonstrates that most of these low-confidence responses can be associated to an unintentional hydraulic interference of de-installing the packer system in KFR27 (see separate section below). High-confidence responses are quantified in terms of two response indicies: *index 1* (m^2/s), which is a proxy for response speed, and *index 2 new*, which is a proxy of distance-normalised drawdown (m). The Aqtesolv software was also used to provide an analytical fit (i.e., Theis type curve) to quantify the responses in SBA structures in terms of transmissivity, T (m^2/s), and storativity, S (-).

Table B-2. Interpreted responses to hydraulic interference tests

Test: SBA1	KFR27 (47 - 57 m)	s_{max}	Index 1	Classification
Section	Interpretation	[m]	[m^2/s]	
KFR101_2	No response, ongoing trend?	0.20	0.29	SBA6, ZFMNW0805A/B
KFR102A_1	No response, ongoing trend?	0.38	1.84	ZFMENE3115
KFR102A_2	No response, ongoing trend?	0.42	1.47	ZFMENE3115
KFR102A_3	Clear	0.86	4.38	ZFMNE3112
KFR102A_4	Clear	1.24	4.60	HRD
KFR102A_5	Clear	1.33	6.96	HRD
KFR102A_6	Clear	1.32	7.14	SBA6
KFR102A_7	Clear	0.38	0.26	ZFMNE3137
KFR102A_8	Clear	0.34	0.19	SBA2
KFR105_1	No response, ongoing trend?	0.32	0.38	ZFMWNW3267
KFR105_2	Clear	0.67	1.37	WNW8042/WNW3267/NE3137
KFR105_3	Clear	0.69	0.82	HRD
KFR105_4	Clear	0.71	0.78	HRD
KFR105_5	No response, ongoing trend?	0.34	0.13	NE3112/ENE3115
KFR102B, KFR103			Non-operative	
Test: SBA6	KFR27 (189.4 - 194.4 m)	s_{max}	Index 1	Classification
Section	Interpretation	[m]	[m^2/s]	
KFR101_1	Clear	1.17	5.90	ZFMNW0805B
KFR101_2	Clear	1.96	13.04	**SBA6**, ZFMNW0805A/B
KFR102A_1	No response, ongoing trend?	0.62	1.32	ZFMENE3115
KFR102A_2	No response, ongoing trend?	0.65	0.76	ZFMENE3115
KFR102A_3	Clear	2.82	7.72	ZFMNE3112
KFR102A_4	Clear	5.08	9.98	HRD
KFR102A_5	Clear	6.05	18.88	HRD
KFR102A_6	Clear	6.28	54.29	**SBA6**
KFR102A_7	Clear	0.34	3.50	ZFMNE3137
KFR102A_8	Possible response, ongoing trend?	0.24	0.50	SBA2

DokumentID
1578373, (1.0)

Sekretess
Öppen

Sida
112(165
)

TD15 Complementary simulation cases in support of SR-PSU

KFR102B_1	Clear	2.32	14.54	**SBA6**, ZFMNE3112
KFR102B_2	Clear	2.08	8.81	HRD
KFR105_5	Clear	0.36	1.65	NE3112/ENE3115
KFR106_1	Possible response, ongoing trend?	0.31	1.47	ZFMNNW1034
KFR103		Non-operative		

Test: SBA2-3	KFR103 (83.5 - 93.5 m)	s_{max}	Index 1	
Section	Interpretation	[m]	[m^2/s]	Classification
HFR106_1	s > 0.1 m, but no recovery.	0.19	0.38	ZFMNNW1034
HFR106_2	s > 0.1 m, but no recovery.	0.18	0.47	ZFMNNW1034
HFR106_3	Likely response, but s < 0.1 m (dt_L based on time point for stabilisation)	0.09	(0.63)	**SBA3**
KFR101_1	s > 0.1 m, but no recovery.	0.21	0.46	ZFMNW0805B
KFR101_2	s > 0.1 m, but no recovery.	0.24	0.20	SBA6, ZFMNW0805A/B
KFR101_3	Probable response	0.10	0.08	ZFMNNW1034
KFR102A_1	s > 0.1 m, but no recovery.	0.29	2.16	ZFMENE3115
KFR102A_2	s > 0.1 m, but no recovery.	0.31	1.42	ZFMENE3115
KFR102A_3	s > 0.1 m, but no recovery.	0.36	1.02	ZFMNE3112
KFR102A_4	s > 0.1 m, but no recovery.	0.31	0.40	HRD
KFR102A_5	s > 0.1 m, but no recovery.	0.29	0.33	HRD
KFR102A_6	s > 0.1 m, but no recovery.	0.28	0.25	SBA6
KFR102A_7	Clear	0.83	0.90	ZFMNE3137
KFR102A_8	Clear	1.53	0.98	**SBA2**
KFR102B_1	s > 0.1 m, but no recovery.	0.23	0.17	SBA6, ZFMNE3112
KFR102B_2	s > 0.1 m, but no recovery.	0.23	0.13	HRD
KFR102B_3	Possible response, but s < 0.1 m	0.07	-1.00	ZFMNE3137
KFR105_2	s > 0.1 m, but no recovery.	0.13	0.33	WNW8042/WNW3267/NE3137
KFR105_3	s > 0.1 m, but no recovery.	0.17	0.30	HRD
KFR105_4	s > 0.1 m, but no recovery.	0.20	0.27	HRD
KFR106_2	s > 0.1 m, but no recovery.	0.19	1.25	SBA5, ZFMNNW1034
KFR106_3	Probable response	0.11	0.73	SBA4, ZFMWNW3262
KFR27_1	s > 0.1 m, but no recovery.	0.28	0.79	SBA6, ZFMWNW0835
KFR27_2	Clear	0.44	1.72	**SBA1-2**, ZFMWNW0835
KFR27_3	Clear	0.25	1.19	HRD

Test: SBA4-5	KFR103 (177 - 187 m)	s_{max}	Index 1	
Section	Interpretation	[m]	[m^2/s]	Classification
HFR106_1	Clear	1.64	7.15	ZFMNNW1034
HFR106_2	Clear	1.59	11.55	ZFMNNW1034
HFR106_3	Response, no recovery	0.14	0.65	SBA3
KFR101_1	s > 0.1 m, but no recovery.			ZFMNW0805B
KFR101_2	s > 0.1 m, but no recovery.			SBA6, ZFMNW0805A/B
KFR102A_1	s > 0.1 m, but no recovery.			ZFMENE3115
KFR102A_2	s > 0.1 m, but no recovery.			ZFMENE3115
KFR102A_3	s > 0.1 m, but no recovery.			ZFMNE3112
KFR102A_4	s > 0.1 m, but no recovery.			HRD
KFR102A_5	s > 0.1 m, but no recovery.			HRD
KFR102A_6	s > 0.1 m, but no recovery.			SBA6

KFR102B_1	s > 0.1 m, but no recovery.			SBA6, ZFMNE3112
KFR102B_2	s > 0.1 m, but no recovery.			HRD
KFR106_1	Unclear, incomplete recovery			ZFMNNW1034
KFR106_2	Clear	1.58	22.90	**SBA5**, ZFMNNW1034
KFR106_3	Clear response, incomplete recovery	0.24	1.84	**SBA4**, ZFMWNW3262
KFR27_1	s > 0.1 m, but no recovery.			SBA6, ZFMWNW0835

Test: Central block KFR105 (120 - 137 m)		s_{max} [m]	Index 1 [m^2/s]	**Classification**
Section	**Interpretation**			
HFR102_1	Clear	0.27	0.19	SBA1
HFR102_2	Unlikely			HRD
KFR102A_3	Unlikely, incomplete recovery			ZFMNE3112
KFR102A_4	Possible, incomplete recovery			HRD
KFR102A_5	Possible, incomplete recovery			HRD
KFR102A_6	Possible, incomplete recovery			SBA6
KFR102A_7	Clear	0.63	0.42	ZFMNE3137
KFR102A_8	Clear	0.50	0.56	SBA2
KFR103_1	Unlikely, incomplete recovery			SBA4-5, ZFMWNW3262
KFR103_2	Clear	0.35	1.16	SBA2-3
KFR27_1	Possible, incomplete recovery			SBA6, ZFMWNW0835
KFR27_2	Clear	1.95	0.92	SBA1-2, ZFMWNW0835
KFR27_3	Clear	0.74	0.58	HRD

Structural inference

The observed responses (Table B-2) were interpreted in context of the deterministically modelled SBA structures (Table B-3; Figure B-5 to Figure B-9). In general, the interference tests confirm the modelled structures, particularly SBA6. Additionally, large-scale, long-term trends are observed in the area can be associated to intercepts with SBA6 (Table B-3; marked black in Figure B-7 and Figure B-8). Closer inspection demonstrates that this is caused by the de-installation of packers in KFR27, prior to the first pumping test, as well as its re-installation, prior to the pump test in KFR103 (see Section B.1). Again, this signifies the hydrogeological role of SBA6, propagating remote drawdown from ZFM871 via the open borehole KFR27. Another important observation is that no responses have been observed at the other end of the Central Block (i.e., in KFR104, HFR105, HFM35, HFM34, or KFM11A).

The outcome of the interference tests suggests a few minor revisions of the deterministically modelled SBA structures. One notion may be combining SBA1, SBA2, and SBA3 to a larger structure SBA1-3, which is updated based on the information from the observed interferences (Table B-3). As an example, the upper intercept in KFR27 (SBA1 at 47 - 57 m) would be discarded and replaced by the lower intercept (SBA2 96 – 101 m). Also the structure could be extended to KFR106_3 and KFR101_3.

Table B-3. Structural inference of observed responses (Table B-2)

Test: SBA1	**KFR27 (47 - 57 m)**
HFR102_1	In contrast to expectations of modelled intercept in SBA1, no response is observed in HFR102_1. Thus, SBA1 should be re-assessed. Possibly, KFR27_2 can be associated to HFR102_1 via SBA2 (as its intercept is also located in KFR27_2).
SBA2	SBA2 can be associated to the connection between KFR27_2, KFR102A_8, KFR105_4, which is also confirmed in both interference tests KFR103 (83.5 - 93.5 m) and KFR105 (120 - 137 m)
KFR102A	Clear responses in several sections of KFR102A (down to KFR102A_3 in the interval z = -230…-379 m). Possibly, hydraulic communication via steeply dipping zones ZFMENE3115 and ZFMWNW0835 and horizontal fractures.
Test: SBA6	**KFR27 (189.4 - 194.4 m)**

Section	Interpretation
KFR101_2 KFR102A_6 KFR102B_1	SBA6 is confirmed by clear responses (s = 2 to 6 m, index 1 > 10 m^2/s)
KFR103	Monitoring non-operative. The potential communication between SBA6 and KFR103 can therefore not be evaluated. Consequently, a reciprocal test is conducted in KFR103.
KFR106_1	SBA6 is expected to terminate against ZFMNNW1034, and hence not intersect KFR106. No PFL-f of SBA type are found in KFR106_1, and therefore the possible response in KFR106_1 is probably an indirect communication via ZFMNNW1034.
KFR104, KFR105	The absence of responses confirms that SBA6 does not extend into the Central Block.

Test: SBA2-3	**KFR103 (83.5 - 93.5 m)**	**s$_{max}$**	**Index 1**
Section	**Interpretation**	**[m]**	**m^2/s**
HFR106_3	Likely response supports SBA3, in spite of low magnitude, s < 0.1 m. Hence, index 1 quantified from the time point of stabilised drawdown. The weak response is probably due to the relatively higher transmissivity in the monitored section (3·10^{-5} m^2/s).		
KFR102A_8	Supports SBA2. Confirms assumed hydraulic connection in Öhman et al. (2012).	1.53	0.98
KFR27_2	Supports SBA2. Confirms assumed hydraulic connection in Öhman et al. (2012).	0.44	1.72
KFR106_3	Supports an extension of SBA2-3 to KFR106 (KFR106 not monitored for evaluation of responses in Öhman et al. (2012)). SBA2 coincides geometrically with PFL_10 in KFR106 (T =9·10^{-7} m^2/s). SBA3 has a potential geometrical match with PFL_4 in KFR106 (T =2·10^{-6} m^2/s)	0.11	0.73
KFR101_3	Probable response, supports an extension of SBA2-3. Geometrical match to PFL_15 (T =5·10^{-7} m^2/s) and PFL_18 (T =5·10^{-7} m^2/s) in KFR101.	0.10	0.08
KFR102B_3	Eventuell respons. Osäker geometrisk koppling till PFL KFR102B_31 (T =10^{-6} m^2/s) och KFR102B_36 (T =3·10^{-7} m^2/s)		
KFR105_4	Potential response. The reciprocal test in KFR105_4 gives responses in KFR103_2, with common responses in KFR27_2-3 and KFR102A_7-8, which could support an extension of SBA2 towards KFR105.		
SBA6	Common pattern observed in all borehole sections classified as instersected by SBA6 (KFR102A_6, KFR101_2, KFR102B_1, KFR27_1): "ongoing drawdown (s>0.1 m) without recovery". Note that KFR103 was not operative during the preceding test in KFR27 (189.4 - 194.4 m), and that therefore, the contact between SBA6 and KFR103 could not be evaluated. The retrospective analysis (Section B.1) suggests that this pattern is caused by the recovery from the re-installation of packers in KFR27.		

Test: SBA4-5	**KFR103 (177 - 187 m)**	**s$_{max}$**	**Index 1**
Section	**Interpretation**	**[m]**	**m^2/s**
KFR106_2	Supports SBA5 (originally interpreted based on an observed response in KFR103 during the drilling of KFR106)	1.58	22.90
KFR106_3	Support for SBA4 (originally interpreted based on an observed response in KFR103 during the drilling of KFR106)	0.24	1.84
HFR106_1-2	Interpreted as an indirect response via SBA5 and ZFMNNW1034 (SBA modelled as terminated against ZFMNNW1034)		
SBA6	Common pattern observed in all borehole sections classified as instersected by SBA6 (KFR102A_6, KFR101_2, KFR102B_1, KFR27_1): "ongoing drawdown (s>0.1 m) without recovery". Note that KFR103 was not operative during the preceding test in KFR27 (189.4 - 194.4 m), and that therefore, the contact between SBA6 and KFR103 could not be evaluated. The retrospective analysis (Section B.1) suggests that this pattern is caused by the recovery from the re-installation of packers in KFR27.		

Table B-4. Compilation of responses to KFR105 disturbances (index 1)

	Drilling	**Interference test**		**Association**
Section	**(133 m BHL)**	**Entire KFR105**	**KFR105 (120 - 137 m)**	
HFR101	0.11	None	None	NE3118/NE0870

HFR102_1	0.45	0.36	0.19	SBA1 (or, continuation of SBA2)
HFR102_2	0.04	None	Uncertain[1]	HRD
KFR27_1	0.47	1.10	Uncertain[1]	SBA6, ZFMWNW0835
KFR27_2	1.26	1.22	0.92	SBA1-2, ZFMWNW0835
KFR27_3	0.92	0.65	0.58	HRD
KFR102A_1	None	1.45	None	ZFMENE3115
KFR102A_2	None	0.99	None	ZFMENE3115
KFR102A_3	0.88	0.86	Uncertain[1]	ZFMNE3112
KFR102A_4	0.31	0.81	Uncertain[1]	HRD
KFR102A_5	0.56	1.23	Uncertain[1]	HRD
KFR102A_6	0.33	1.42	Uncertain[1]	SBA6
KFR102A_7	0.60	0.77	0.42	ZFMNE3137
KFR102A_8	0.84	0.40	0.56	SBA2
KFR103_1	0.24	None	Uncertain[1]	SBA4-5, ZFMWNW3262
KFR103_2	1.19	1.14	1.16	SBA2-3
KFR104_1	0.09	0.12	None	WNW3267/NE3137
KFR104_2	0.06	0.09	None	NE3112/ENE3115
KFR104_3	0.15	None	None	ZFMNE3118

1) Low-confidence responses (see Section B.1)

DokumentID
1578373, (1.0)

Sekretess
Öppen

Sida
116(165
)

TD15 Complementary simulation cases in support of SR-PSU
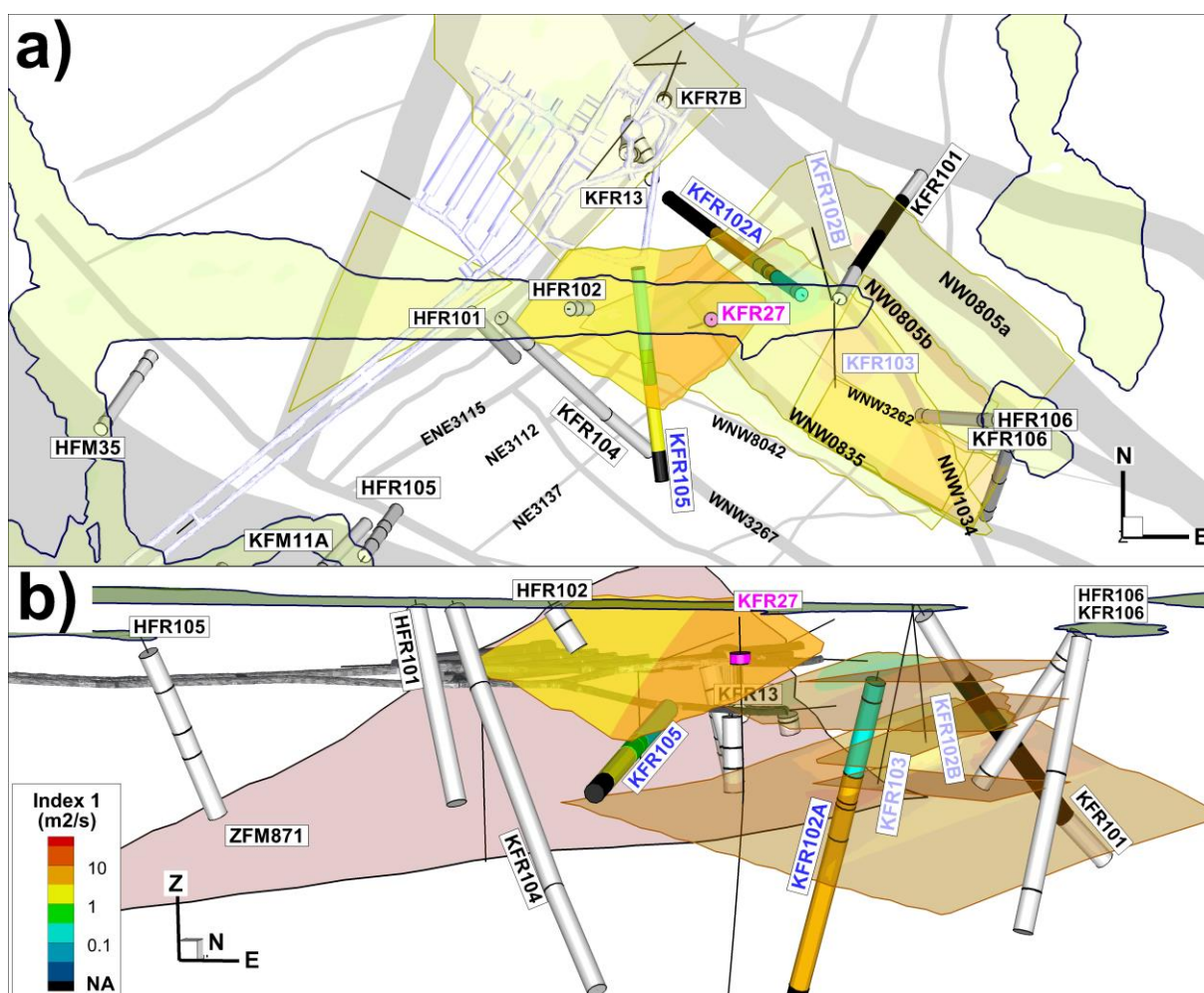
Figure B-5. *Indexed propagation speed for responses in interference test targeting SBA1 (KFR27, 47 - 57 m). Non-responding sections in white and low-confidence responses in black.*
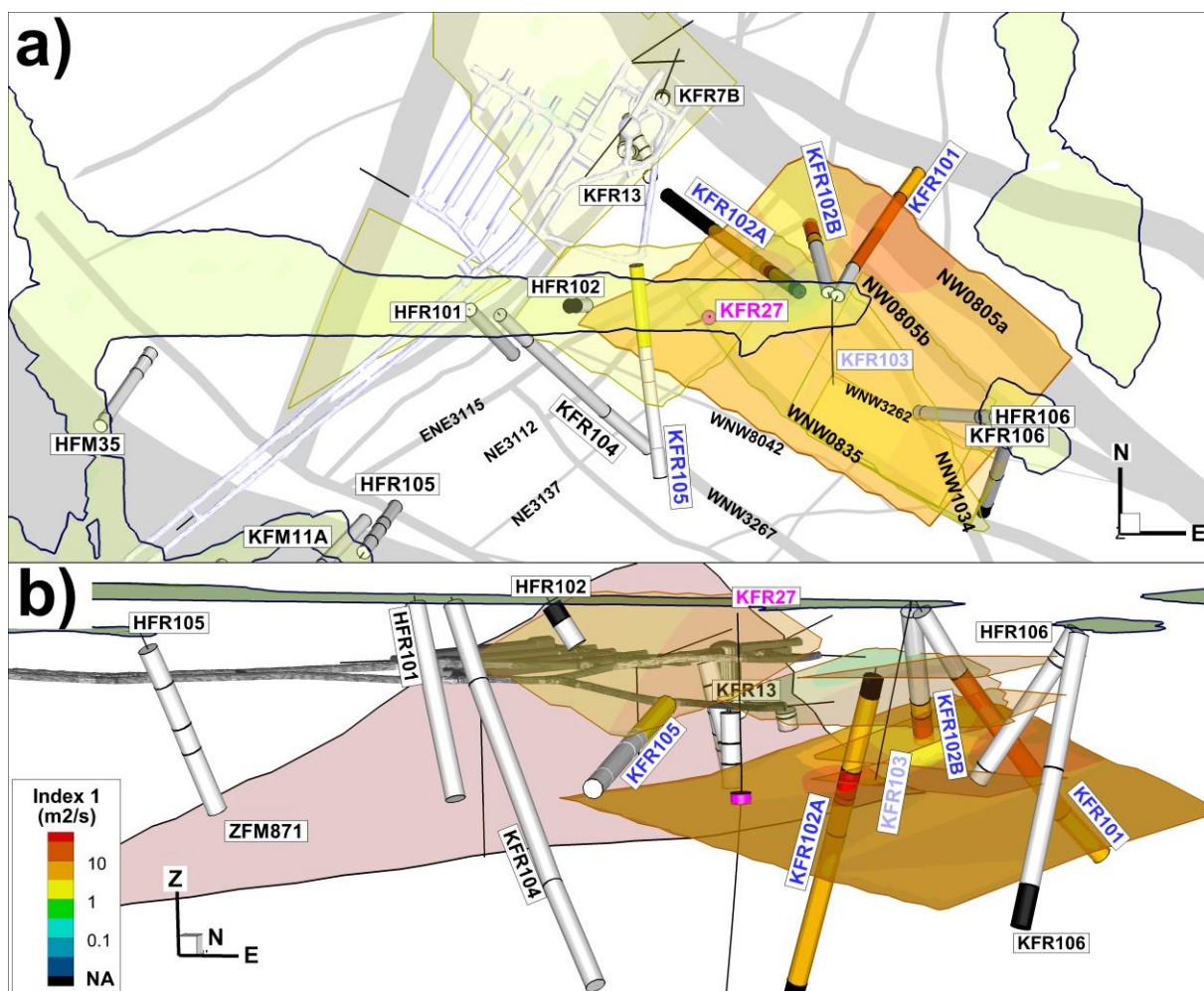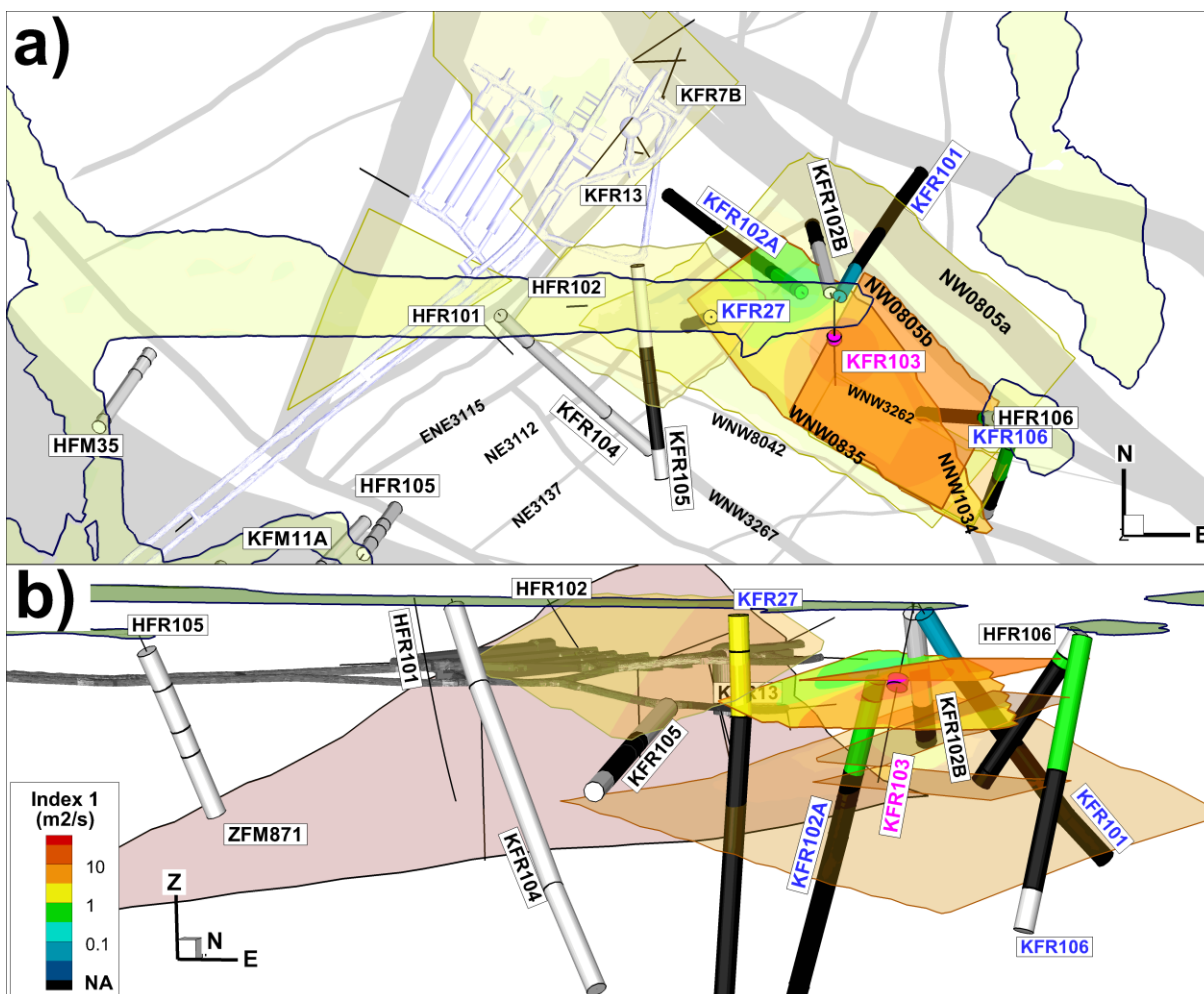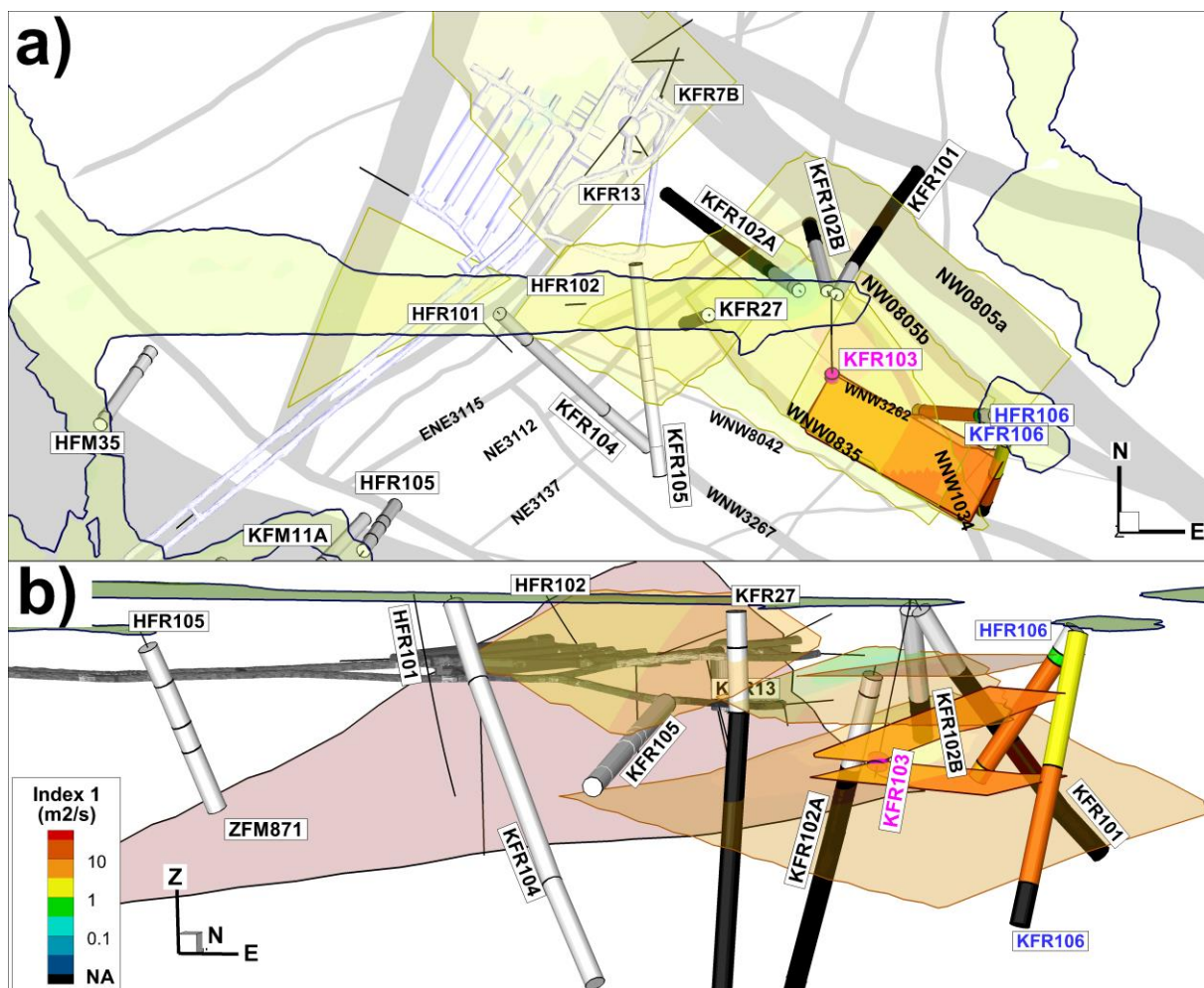

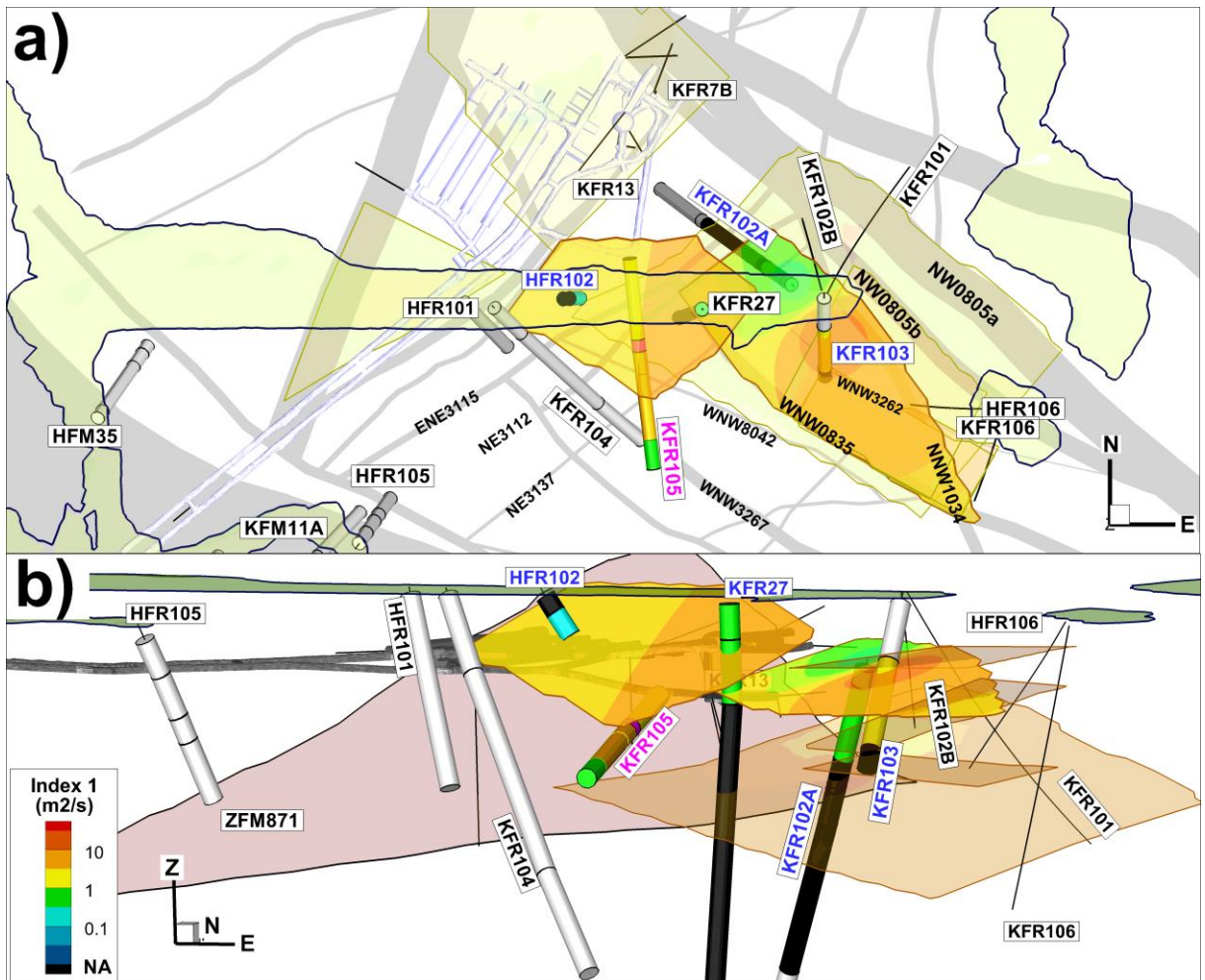**Figure B-6.** *Indexed propagation speed for responses in interference test targeting SBA6 (KFR27, (189.4 - 194.4 m). Non-responding sections in white and low-confidence responses in black.*

Figure B-7. *Indexed propagation speed for responses in interference test targeting SBA2-3 (KFR103, 83.5 - 93.5 m). Non-responding sections in white and low-confidence responses in black.*

Figure B-8. *Indexed propagation speed for responses in interference test targeting SBA4-5 (KFR103, 177 - 187 m). Non-responding sections in white and low-confidence responses in black.*

Figure B-9. *Indexed propagation speed for responses in interference test targeting SBA1 (KFR105, 120 - 137 m). Non-responding sections in white and low-confidence responses in black.*

Table B-5. Evaluated hydraulic parameters for observed responses.

Pumped section (interval)	Observation section	Structure	Distance r (m)	Drawdown s_p (m)	Transmissivity T_o (m^2/s)	Apparent storativity S_o (-)	T_o/S_o (m^2/s)
KFR27	KFR102A:6	SBA6	108.3	6.28	$4.4 \cdot 10^{-6}$	$3.5 \cdot 10^{-6}$	1.25
(189.4 - 194.4 m)	KFR101:2	SBA6	266.6	1.96	$8.8 \cdot 10^{-6}$	$7.9 \cdot 10^{-6}$	1.12
	KFR102B:1	SBA6	197.1	2.32	$8.6 \cdot 10^{-6}$	$9.6 \cdot 10^{-6}$	0.89
	KFR106:1	(SBA6)	475.4	0.31	$1.2 \cdot 10^{-5}$	$4.2 \cdot 10^{-5}$	0.28
KFR103	HFR106:3	SBA3	240.8	0.10	$1.0 \cdot 10^{-4}$	$7.1 \cdot 10^{-5}$	1.42
(83.5 - 93.5 m)	KFR102A:8	SBA2	71.0	1.53	$4.2 \cdot 10^{-6}$	$3.8 \cdot 10^{-5}$	0.11
	KFR27:2	SBA2	174.3	0.44	$9.2 \cdot 10^{-6}$	$2.3 \cdot 10^{-5}$	0.40
	KFR106:3	SBA2-3	290.9	0.11	$8.0 \cdot 10^{-5}$	$4.2 \cdot 10^{-5}$	1.93
	KFR101:3	SBA2-3	83.2	0.10	$2.3 \cdot 10^{-5}$	$3.3 \cdot 10^{-4}$	0.07
KFR103	KFR106:2	SBA4	274.9	1.58	$8.4 \cdot 10^{-6}$	$3.1 \cdot 10^{-6}$	2.71
(177.0 - 187.0 m)	KFR106:3	SBA5	273.0	0.24	$4.0 \cdot 10^{-5}$	$4.9 \cdot 10^{-5}$	0.82
KFR105	KFR102A:8	(SBA2)	254.4	0.50	$4.5 \cdot 10^{-6}$	$4.6 \cdot 10^{-5}$	0.10
(120.0 - 137.0 m)	KFR27:2	(SBA2)	115.8	1.95	$4.6 \cdot 10^{-6}$	$3.4 \cdot 10^{-5}$	0.14

B.1   Large-scale interference from packer de-installation in KFR27

The first interference test in KFR27 (2015-12-09) is preceded by the de-installation of its monitoring system, which causes an unintentional large-scale disturbance (2015-11-23 13:00) that can be observed in monitored sections associated to SBA2 and SBA6. The benefit of this unintentional disturbance is its long

period of undisturbed monitoring, c. 16 days, which provides additional information on the slow responses (i.e., KFR106 is responding, but its response has not even developed fully within the 16 days; Figure B-11). Moreover, the analysis of these long-term responses demonstrates that the subsequent interference tests in KFR103 and KFR105 are performed during ongoing recovery from packer re-installation in KFR27. This implies, in turn, that essentially all "low-confidence" responses (marked blue in Table B-2 and black in Figure B-5 to Figure B-9) can be written off as super-positioned drawdown from SFR that is successively recovering via the deep section KFR27_1 (Figure B-13).

Table B-6. Monitored head in KFR27 prior to interference tests (2015-11-23)

Section	From-To (BHL, m)	Head, H (m)
KFR27_3	11.91[1) - 46	-0.34
KFR27_2	47 - 109	-0.53
KFR27_1	110 - 501.64	-5.51

1) Uppermost section is open. End of casing taken as upper limit of section.

Prior to initiation of interference tests, the deepest section of KFR27 is subject to substantial drawdown (Table B-6), which is associated to the depth interval of ZFM871 (Figure E-28 in Öhman et al. 2012). Thus, the de-installation of the packer system releases the built-up pressure differences between its three installed sections, which causes a large-scale disturbance in structures connected to KFR27 (i.e., SBA2 and SBA6). Based on analysis of responses in surrounding sections (Figure B-11), the head in the de-installed KFR27 is assumed to equilibrate to c. -2.5 m (not measured), which corresponds to the following disturbances (see Figure B-12):

1) a pressure drop in the upper 110 m borehole length (i.e., ΔH ≈ -2 m in KFR27_2-3) and

2) a pressure increase in the bottom 110 to 501.6 m (i.e., ΔH ≈ +3 m in KFR27_1).

The upper 110 m are associated to SBA1-2, while the deeper part of KFR27 is associated to SBA6 (192 m BHL) and a drawdown peak that coincides with a geometrical extrapolation of ZFM871 (i.e., 250 m BHL; Figure E-28 in Öhman et al. 2012). The following can be noted:

1) The monitored sections exhibit similar drawdown from SFR (Figure B-10), depending on if they are associated to SBA2 (typically H ≥ -0.5 m) or SBA6 (H = -5.5 m in KFR27_1 and KFR102A_6, and H = -3.9 m in KFR102B_1 and KFR101_2). Notably, the drawdown in the deep section KFR106_1 is not associated to SBA6.

2) Negative hydraulic responses are found at *shallow* depths (i.e., drawdown in KFR105 and in the two upper sections of KFR102A; Figure B-11), on par with the two upper sections of KFR27, where de-installation causes pressure drop. These responses are consistent with the shallow test in KFR27 (Figure B-5) and the test in KFR105 (Figure B-9). These responses are therefore associated to SBA2.

3) Positive hydraulic responses are found at greater depths (i.e., rising head found in sections associated to SBA6; Figure B-11) that correspond to the pressure drop in the deep section KFR27_1. These responses confirm the findings of the deep test in KFR27 (Figure B-6) and build confidence in the modelled structure SBA6. Notably, the slow response in KFR106_1 (i.e., marked a low-confidence response in the deep KFR27 test; Figure B-6) can be associated to ZFMWNW0835.

4) Having established the impact that shut-in pressures of sections in KFR27 have on the surrounding monitored head (primarily on sections associated to SBA6), the low-confidence responses are re-assessed in context of the re-installation of KFR27 (Figure B-13). Inspection demonstrate that most low-confidence responses in fact are not caused by the controlled interference tests, but rather by the long-term recovery from re-installation of KFR27 (that is: primarily SBA6 intercepts, as the shallow sections of KFR27 recover comparatively fast and/or actively respond to the controlled tests Figure B-13).
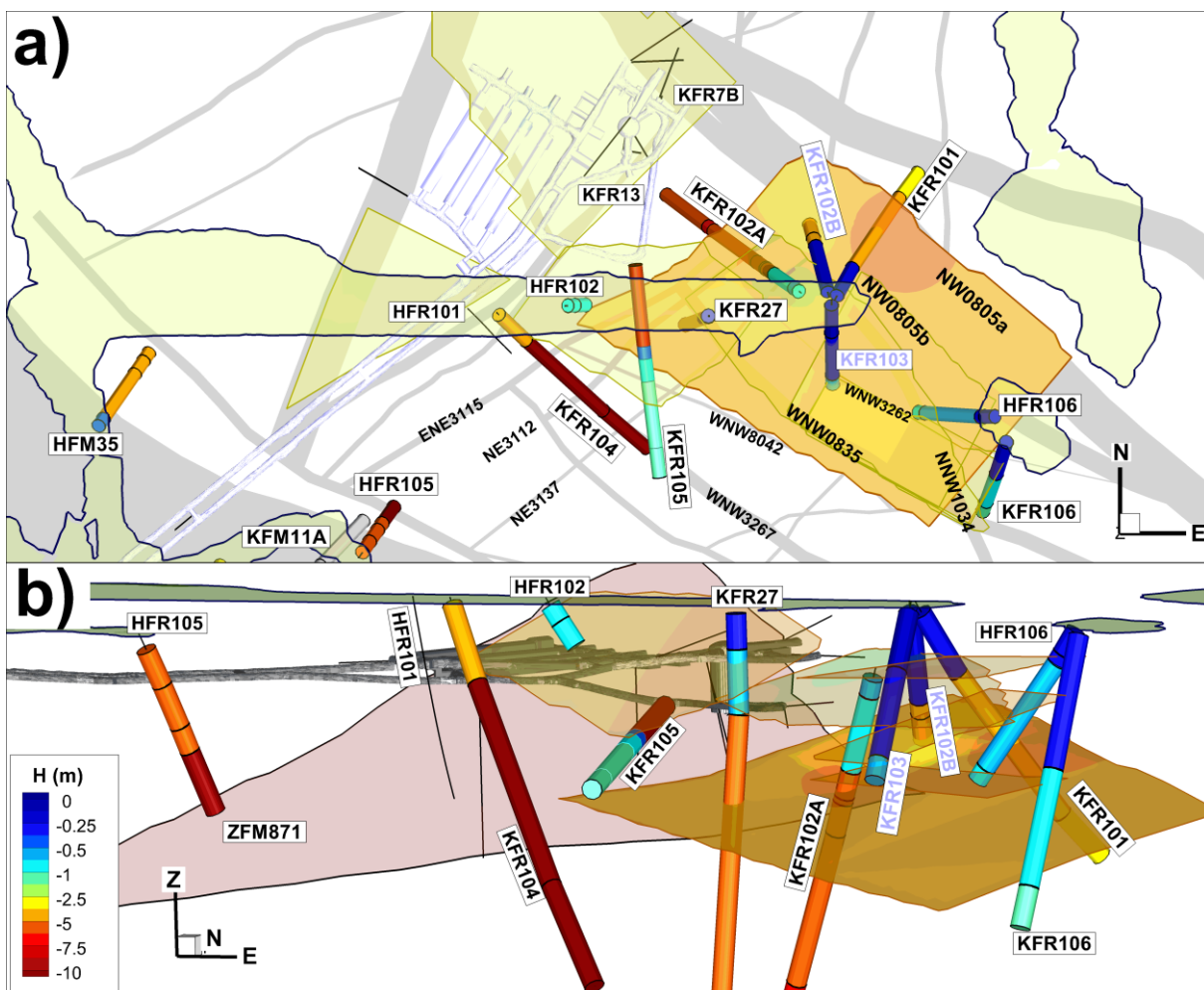
DokumentID
1578373, (1.0)

Sekretess
Öppen

Sida
121(165)

TD15 Complementary simulation cases in support of SR-PSU

Figure B-10. *Monitored pressure prior to de-installation of KFR27 (2015-11-23). Data for KFR103 and KFR102B unavailable, but taken from a representative period in May 2016.*

DokumentID
1578373, (1.0)

Sekretess
Öppen

Sida
122(165
)

TD15 Complementary simulation cases in support of SR-PSU
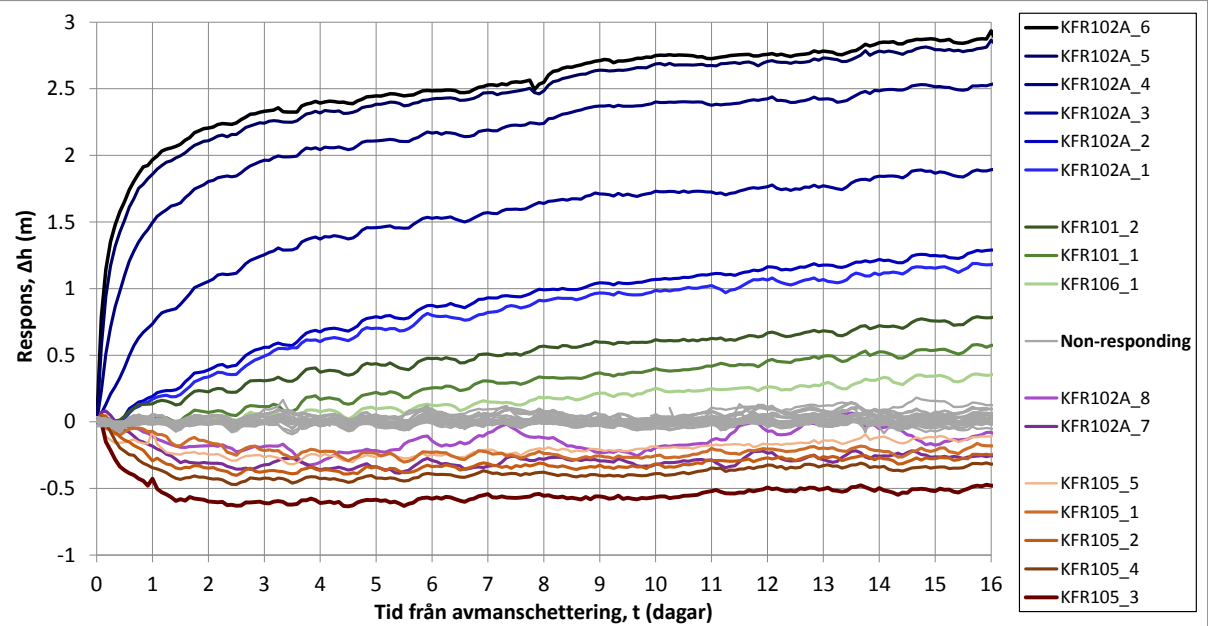
Figure B-11. *Hydraulic responses to de-installation of KFR27 (2015-11-23). No data available for KFR102B and KFR103.*

DokumentID
1578373, (1.0)

Sekretess
Öppen

Sida
123(165
)
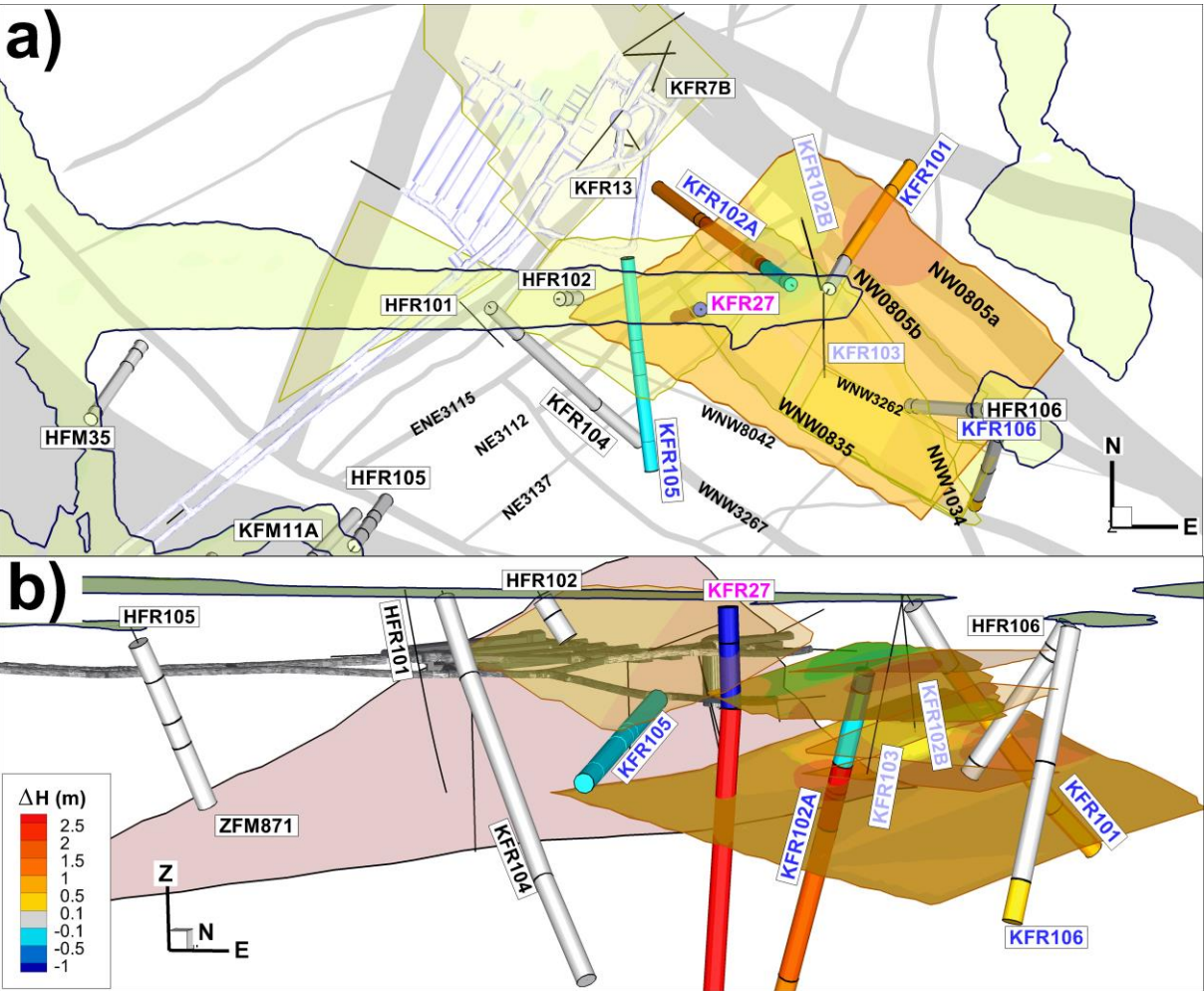
TD15 Complementary simulation cases in support of SR-PSU

Figure B-12. *Hydraulic responses to de-installation of monitored sections in KFR27. No data available for KFR102B and KFR103.*
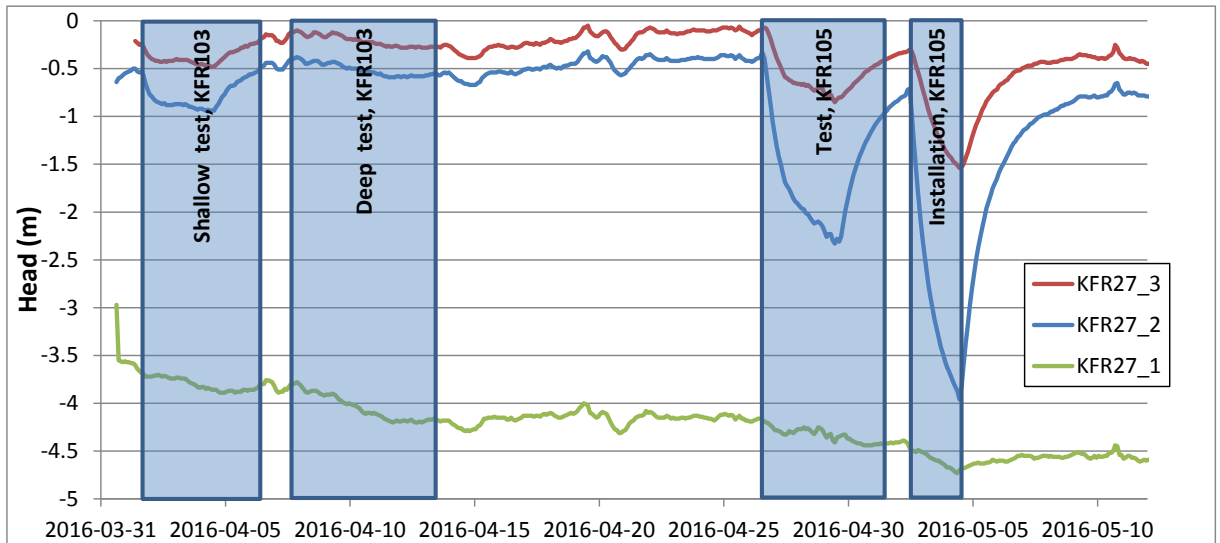
Figure B-13. *Interference testing during non-stationary conditions that arise from recovery in re-installed monitoring sections of KFR27 (2016-03-31) (stationary head in KFR27_1 = -5.5 m; Figure B-10) owing to packer in KFR27.*

Responses in boreholes drilled from SFR

Drilling responses of KFR27 indicated hydraulic connection via ZFM871 in the vicinity around the Silo by responses in borehole sections KFR04, KFR05, KFR13, KFR7B, and KFR55 (see Öhman et al. 2012). The disturbance from the packer de-installation in KFR27 was therefore analysed in these boreholes. Unfortunately, the monitored pressures in these boreholes are severely affected by chemical water sampling during this time period, and hence the hydraulic connection between KFR27 and ZFM871 could not be verified.

SVENSK KÄRNBRÄNSLEHANTERING AB

DokumentID
1578373, (1.0)

Sekretess
Öppen

Sida
124(165
)

TD15 Complementary simulation cases in support of SR-PSU

C.   Appendix

Compartmentalisation of the flowing fracture network

C.1   Comparison between hydraulic test types (PSS and PFL)
Background

The hydrogeological model SDM-PSU primarily is supported by two data sets: 1) the early SFR investigation, 1980-1986, based on short-term double-packer tests, and 2) the recent site investigation, 2008-2009, relying on pseudo-stationary flow logging with the Posiva Flow Logging (PFL) device (Öhman et al. 2012). Both data types have their merits and drawbacks (discussed below), and therefore a comparison between the two investigation methods is useful for constraining conceptual uncertainties, such as *compartmentalisation* of the flowing fracture network (i.e., Figure 4-18 in Follin et al. 2007). However, such an evaluation requires parallel hydraulic data for a given population of borehole sections, i.e., requiring that the very same borehole sections are investigated by both test methods.

SDM-PSU relies heavily on PFL data from the recent site investigation (2008-2009), which lacks complementary packer-test support (i.e., short-term, local, PSS data). The regulating Swedish Radiation Safety Authority, Strålsäkerhetsmyndigheten (SSM), has concluded that the lack of complementary packer-test data causes an uncertainty regarding the presence of *hydraulic chokes* at the site and has therefore requested SKB to clarify how this uncertainty can be delimited[8]. In response to SSM's request, SKB has conducted complementary PSS investigations in KFR27 and in KFR105 during the period autumn 2015 to spring 2016. The execution and evaluation of these tests are documented in detail in (Harrström et al. 2017). The findings and main conclusions are presented in this appendix, in order to summarise relevant information for responding to SSM's request.

SKB employs two principal methods for borehole tests to quantify and characterise the hydraulic properties of fractured rock mass:

1) **PSS**: Short-term double-packer injection tests (20 minutes injection under constant overpressure of 2 bars in a 5 m packed off test interval, followed by 20 minutes of recovery). If the premises are right, the flow histories of both the injection and recovery phases can be evaluated transiently by means of type-curve fitting to a wide selection of analytical models (i.e., provided in the Aqtesolv software). Otherwise, the transmissivity is determined according to Moye, under an assumption of stationary flow conditions. Additionally, skin and transition between flow regimes can be interpreted. PSS-data reflects local properties of the rock mass; however, the spatial testing scale depends on the local transmissivity of the section (i.e., a highly transmissive test has a large radius of influence, while a test below detection limit provides little information outside the borehole).

2) **PFL**: the Posiva Flow Log (PFL) device is used for sequential flow logging with a fixed section test interval (5 m) under pseudo-stationary conditions. Long-term pumping (i.e., after 3-5 days of pumping in surface boreholes, or in the case of underground boreholes, such as KFR105, flowing under atmospheric pressure) is assumed to provide stationary cylindrical flow conditions along the entire borehole. PFL data are therefore, in contrast to PSS data, assumed to reflect persistent, large-scale flow paths. Thus, as PFL data reflect effective hydraulic properties of flow large-scale paths, they may be controlled by so-called *hydraulic chokes* that are not necessarily located in the immediate vicinity of the borehole. The drawback of PFL data is that they do not provide information on skin or flow regime (as opposed to the PSS data), and should therefore be referred to as specific capacity, Q/s (m^2/s).

In SDM-Site Forsmark, the level of compartmentalisation in the flowing fracture network, or existence of so-called *hydraulic bottlenecks*, was discussed based on a comparison between PSS data and sequential

---

[8] Issue no. 3 in "Begäran om komplettering av ansökan om utökad verksamhet vid SFR – hydrogeologi (SSM2015-725-40)"

DokumentID
1578373, (1.0)

Sekretess
Öppen

Sida
125(165
)

TD15 Complementary simulation cases in support of SR-PSU

PFL data (at the 5 m scale; Fig 4-18 in Follin et al. 2007). A corresponding analysis was not possible in SDM-PSU, as overlapping borehole investigations (short-term, local scale versus long-term, large scale) were not available (see Section 6.1 in Öhman et al. 2012). Both data types are available at the PSU site: the PFL-method was employed in the recent site investigation, 2008-2009, while the early SFR investigation, 1980-1986, was based on short-term double-packer tests, i.e., comparable with the PSS system. However, a comparison between the recent and historic data sets is not meaningful, as the two test types do not cover the same boreholes (i.e., subject to uncertainties such as: potential local differences in bedrock properties, or different data quality to support the differentiation into hydrogeological units: HCD, HRD, SBA, Unresolved PDZs).

Expectations

In general, a comparison between short-term, local PSS tests and long-term, large scale PFL tests is expected to demonstrate the presence (or absence) of hydraulic chokes in the flowing fracture system. That is:

1) Consistently higher transmissivity in the short-term tests, as compared to its corresponding PFL data, is an indication of compartmentalisation in the flowing fracture system (i.e., hydraulic chokes at a distance beyond the influence radius of a 20 minute test)

2) Insignificant, non-systematic discrepancies between the two test methods is an indication of a well-connected system (i.e., absence of hydraulic chokes)

In addition to this general expectation, the PFL-logging in KFR105 is suspected to underestimate the hydraulic bedrock properties (i.e., transmissivity or specific capacity). The reason for this is that the underground borehole was logged under atmospheric pressure (free-flowing into the NBT tunnel opening; Nedre ByggTunnel), which may cause the following phenomena:

1) Turbulence in the vicinity of the borehole, which is not representative for fracture flow under present or future re-saturated tunnel conditions. Thus, evaluated parameters do not reflect the prevailing laminar flow, which is assumed to apply in SDM-PSU and SR-PSU. Field tests at Äspö HRL indicate that turbulence may lead to a transmissivity underestimation of up to 2-3.

2) Gas-bubble formation from the de-pressurisation of dissolved gases in the groundwater. Bubbles may become trapped along flow paths or fracture junctions and lead to local, temporary choking of measured flow (i.e., flow that do not represent the natural conditions at the site)

3) Hydro-mechanical fracture closure, induced by the effective stress over fracture apertures, σ_e [Pa] $= \sigma_n - \Delta P$, which increases due to reduction in fluid pressure, P [Pa] (e.g., discussion in Öhman et al. 2013). The PSS test operates with an overpressure of c. 20 m, which on the other hand may induce a minor opening of fracture aperture (i.e., increasing fracture flow). However, the applied overpressure is relatively small compared to the prevailing hydrostatic pressure (c. H = 110 m), and thus, such effects are expected to be small.

4) Underground boreholes near an open tunnel cavity (i.e., SFR) implies the potential presence of drained, or de-pressurised, fractures that are only detectable during injection (not pumping or flowing)

Owing to its central location in the model domain, KFR105 has had a key role for the hydrogeological interpretation in SDM-PSU, where the *Central block* was identified as particularly suitable host rock for the planned extension of SFR. Thus, the drawbacks of hydraulic testing under atmospheric conditions (i.e., four phenomena listed above) imply uncertainties in the conceptual model of SDM-PSU, which potentially can be remediated by the analysis of complementary PSS tests.

Execution

During the autumn 2015 thru spring 2016, SKB conducted PSS investigations in the two boreholes, KFR27 and KFR105, to facilitate a comparison against the existing PFL-logging data (Väisäsvaara 2009, Pekkanen et al. 2008, Hurmerinta and Väisäsvaara 2009). The details of the PSS investigations are

DokumentID
1578373, (1.0)

Sekretess
Öppen

Sida
126(165
)

TD15 Complementary simulation cases in support of SR-PSU

provided in Harrström et al. (2017). A total of 155 sections, with a fixed 5 m test interval, were tested by means of the PSS method (20 min injection with 2 bars of constant overpressure, followed by 20 min recovery) and evaluated according to standard praxis, where the transient flow history is fitted by type-curves to analytical models provided in the software Aqtesolv. The test sections were positioned to match the test sections in the preceding PFL-logging. Most of the test sections, 90%, are positioned within 0.1 m of the reported position for the corresponding PFL measurement (Figure C-1). The accuracy in borehole positioning during PFL-logging is also expected to be on decimetre scale, and hence it is not very meaningful to strive for higher precision. More importantly, the deviation is small relative to the full section length (0.1 m/5 m = 2%), and hence the deviation is expected to be negligible as error term in the comparison between the two data sets.
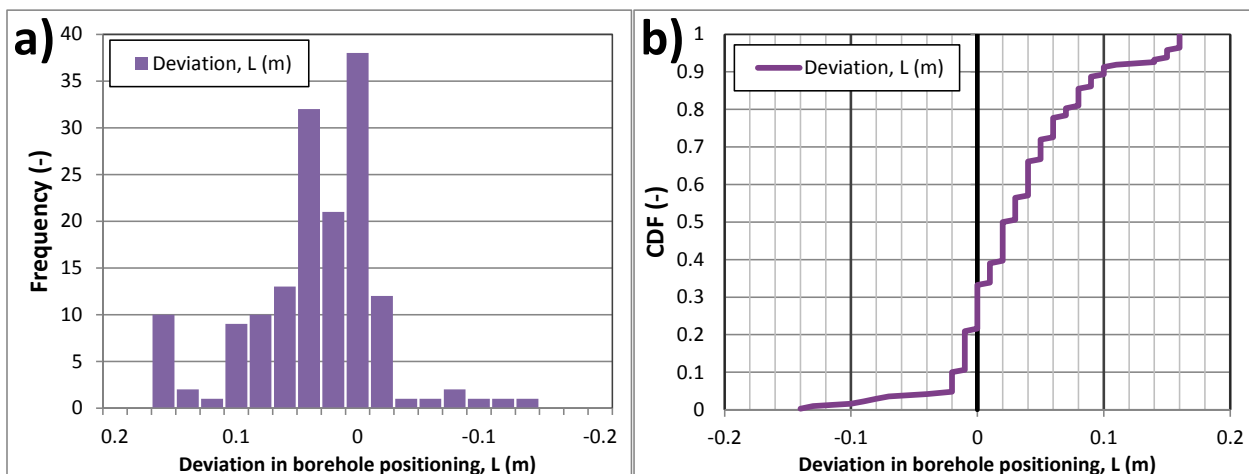
Figure C-1. *Deviation in borehole positioning of tested 5 m section in PSS and PFL investigations.*

The results of the two borehole investigations are compared in cross plots (Figure C-2), where a perfect match would fall onto the unit slope, 1:1 (black line in Figure C-2). The discrepancies related to limitations in measurement precision, test conditions, and evaluation principles manifest as noise around the theoretical line of perfect agreement. The discrepancies are expected to fall below one order of magnitude (as indicated by the enclosing dashed lines in Figure C-2).

The comparison must also account for censoring due to upper and lower measurement limits, which are test- and method-specific for prevailing conditions (as indicated by shaded areas in Figure C-2). Any data falling outside the measurement limits are typically taken as equal to the exceeded limit (indicated by red dots in Figure C-2). In KFR27, the PFL method has two lower practical detection limits: mainly $1.7 \cdot 10^{-9}$ m^2/s, but higher within a confined interval, $1.7 \cdot 10^{-8}$ m^2/s from 150 to 190 m (grey area in Figure C-2). The evaluation for KFR27 is primarily bounded by the lower practical measurement limits in the PFL-logging, while the evaluation for KFR105 data sets is primarily bounded by the lower measurement limit in PSS (red markers Figure C-2).
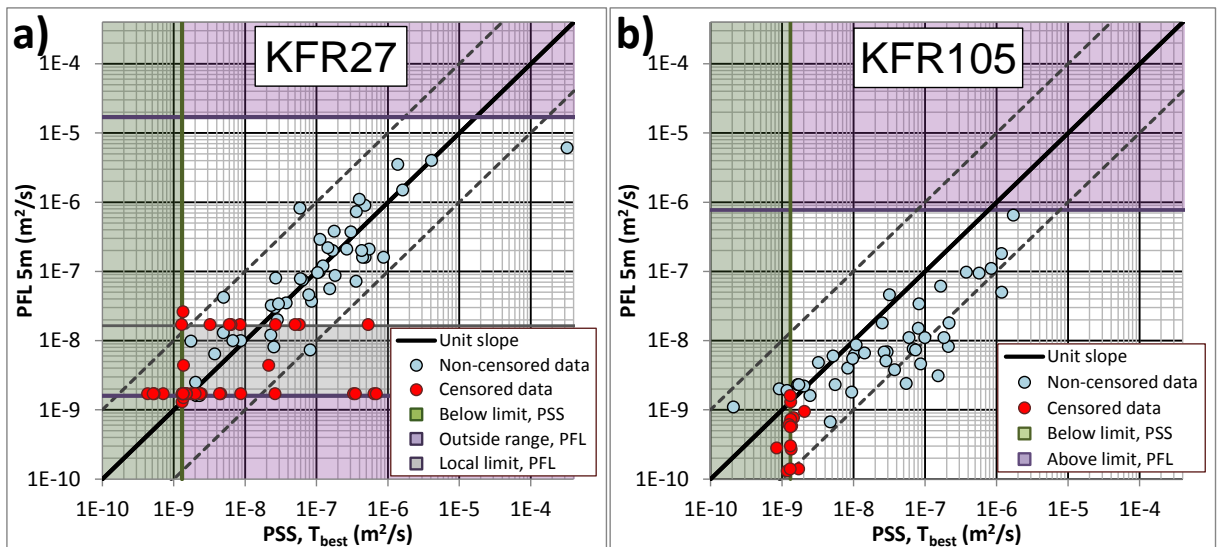
SVENSK KÄRNBRÄNSLEHANTERING AB

DokumentID
1578373, (1.0)

Sekretess
Öppen

Sida
127(165
)

TD15 Complementary simulation cases in support of SR-PSU

Figure C-2. Comparison between PFL and PSS data; a) KFR27 and b) KFR105.

Results

In general, the agreement between the two test methods is in line with expectations (Figure C-3). The two data types are reasonably well-correlated and mainly fall within the bounds of accepted discrepancy. Moreover, two data sets exhibit a slight difference in appearance that is related to the different investigation methods for surface and underground boreholes. The KFR27 data is symmetrically distributed around the unit slope, while the KFR105 data set is clearly asymmetric (see relation between grey and orange lines in Figure C-3).
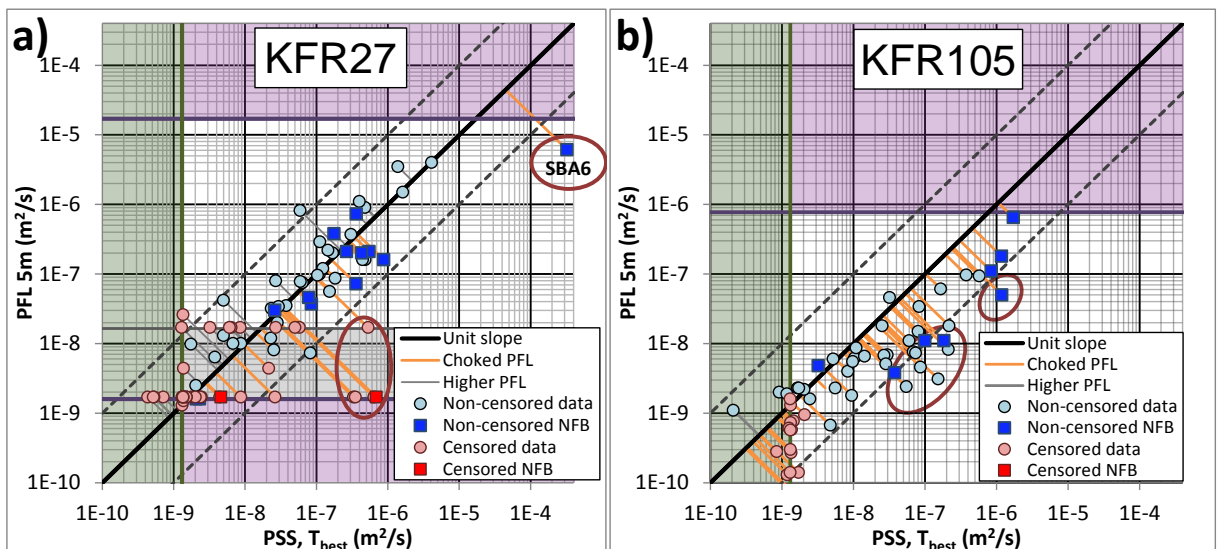
Figure C-3. Comparison between PFL data and the corresponding data from the PSS test, T_{best}; a) KFR27 and b) KFR105. NFB signifies interpreted influence of a Negative Flow Boundary in the transient evaluation. Hydraulic chokes indicated by dark-red ovals.

The asymmetry is clearer when expressed as a ratio, T_{PSS}/T_{PFL} (Figure C-4 and Figure C-5). For KFR27, the median and geometric mean of the transmissivity ratios are close to 1.0, and about 90% of the ratios fall within an order of magnitude (Figure C-4a and Figure C-5a; i.e., irrespectively of how data outside

DokumentID
1578373, (1.0)

Sekretess
Öppen

Sida
128(165
)

TD15 Complementary simulation cases in support of SR-PSU

measurement limits are treated). For KFR105, the ratios have a median of $T_{PSS}/T_{PFL} = 4$, and a geometric mean of $T_{PSS}/T_{PFL} = 3.6$. This quantifies the combined effects of the phenomena associated to flow logging under atmospheric conditions (discussed above), and suggests that the PFL data in KFR105 are underestimated by a factor of 4. Thus, the PSS data indicate that the conceptual model in SDM-PSU, where the *Central Block* has been interpreted as less transmissive and less connected compared to its bounding belts (the Southern and Northern boundary belts), to some extent is exaggerated by the hydraulic test conditions in KFR105.

Overall, the PSS data suggests that the degree of compartmentalisation is less than expected. Hydraulic choking is associated to anomalously high transmissivity ratios, $T_{PSS}/T_{PFL} > 10$ (i.e., ratios exceeding the expected 'noise level'). In KFR27, the fraction of anomalously high transmissivity ratios is $8/96 \approx 8\%$ (dark red ovals in Figure C-3a). The following is noted among these 8 anomalies:

1) Seven of the PFL-logged borehole sections in KFR27 (7/96) were reported to fall below its practical detection limit ($1.7 \cdot 10^{-9}$ m^2/s), but were evaluated as $T \approx 1 \cdot 10^{-7}$ to $7 \cdot 10^{-7}$ m^2/s in the short-term PSS tests. Only two (2/7) indicated a no-flow boundary (NFB in Figure C-3).

2) The most transmissive fracture in KFR27 (associated to SBA6; Figure C-3a) is evaluated as locally highly transmissive $3 \cdot 10^{-4}$ m^2/s, but with a no-flow boundary (NFB in Figure C-3). The no-flow boundary may indicate a limitation in the physical extent of the structure or in its hydraulic properties (Walker and Roberts 2003), which may explain the lower effective transmissivity in long-term tests (see the pump test evaluation in Figure C-6 and Figure C-7).

The most transmissive section in KFR105 (associated to a PFL-f anomaly at 133.63 m borehole length) is probably bounded by the upper measurement limit in PFL-logging (Figure C-3b; see also long-term evaluation in Figure C-6). The identification of hydraulic chokes in KFR105 is complicated by the systematic discrepancy between PFL and PSS, which is suspected to arise from phenomena related to unfavourable test conditions (discussed above). At the lower tail of distributions, the reverse relation can be noted among three test sections, where the PFL exceeds the PSS data by an order of magnitude ($T_{PSS}/T_{PFL} < 0.1$; above dashed line in Figure C-3). Two of these are associated to the detection limit of measurements, while the third is subject to negative skin, modelled as a fictive borehole radius of $r_w = 4.5$ m, which is not accounted for in the PFL logging.
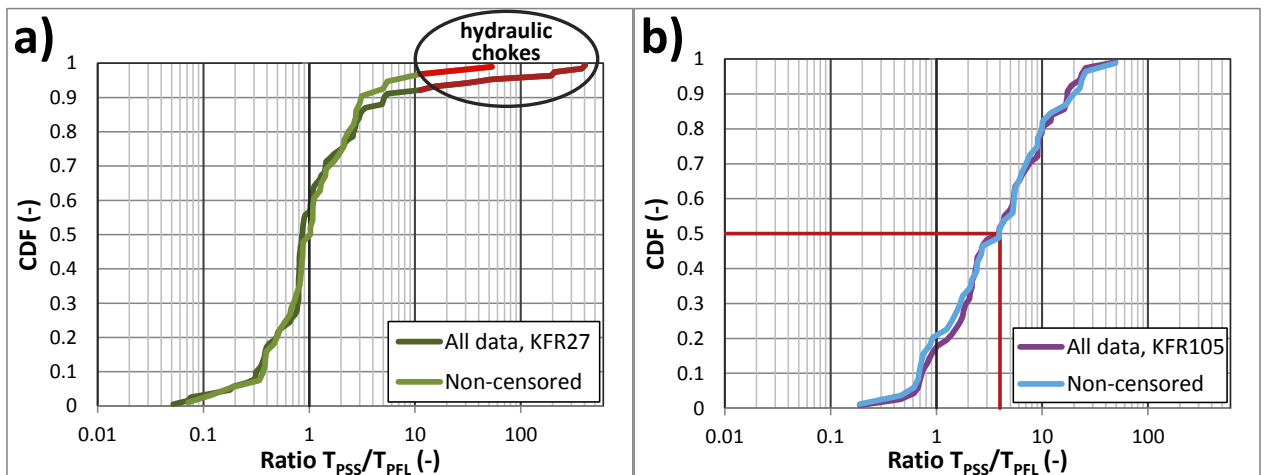

Figure C-4. *Relationship between transmissivity evaluated from short-term tests, T_{PSS}, and pseudo-stationary flow logging, T_{PFL}; a) KFR27 and b) KFR105.*
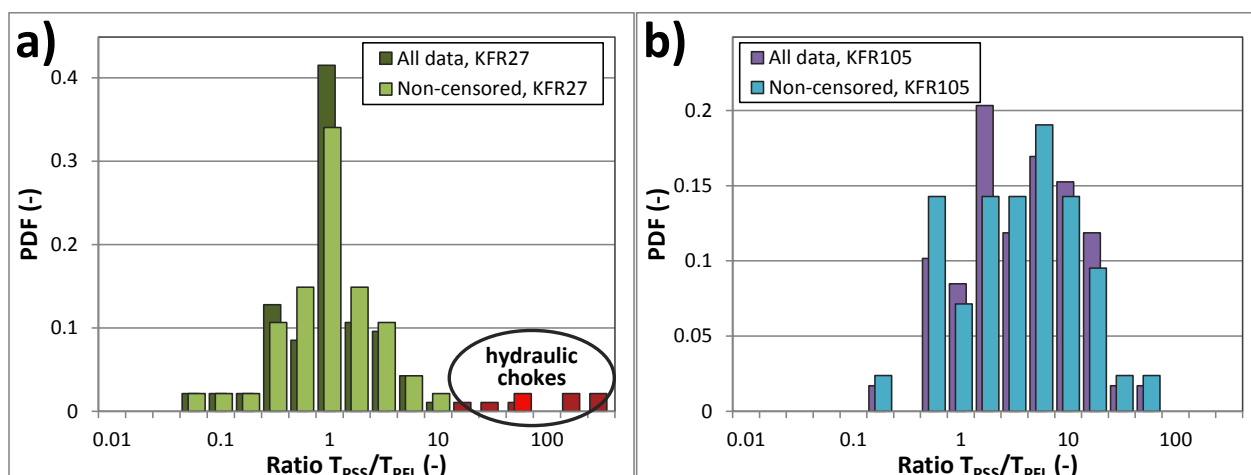
DokumentID
1578373, (1.0)

Sekretess
Öppen

Sida
129(165
)

TD15 Complementary simulation cases in support of SR-PSU

Figure C-5. *Relationship between transmissivity evaluated from short-term tests, T_{PSS}, and pseudo-stationary flow logging, T_{PFL}; a) KFR27 and b) KFR105.*

Long-term pump tests in conductive borehole sections

In connection to the PSS survey, long-term pump tests were conducted in selected borehole sections to assess the so-called SBA structures (see Appendix B). This investigation included the most conductive borehole sections in both KFR27 and KFR105 (note that additionally one section in KFR27 and two sections in KFR103 were also pumped, although not presented here). The pump tests lasted c. 3 days (Table B-1), which is on par with the preparatory pumping for the PFL logging. The underground borehole section KFR105:4 was tested by releasing its built-up pressure to -70 m head (c. atmospheric pressure corresponds to -110 m).

The pump tests in KFR27 and KFR105 were evaluated by type-curve fitting of analytical models to the flow histories (Figure C-7 and Figure C-8). The evaluated transmissivity values fall between the short-term PSS data and the long-term PFL data (Figure C-6). This supports the notion that presence of hydraulic chokes cause scale-dependency in hydraulic properties (i.e., temporal scaling, but also spatial scaling, as the influence radius scales with the square-root of test duration; Cooper and Jacob 1946).

Moreover, the drawdown-curve in KFR27 (189.4-194.4 m) indicates that stationarity has not been reached within the three days of pumping (Figure C-7), which raises the question if the borehole was PFL logged under stationary conditions (the pumping time preceding PFL in KFR27 is reported to be 3 days; Hurmerinta and Väisäsvaara 2009).

DokumentID
1578373, (1.0)

Sekretess
Öppen

Sida
130(165
)

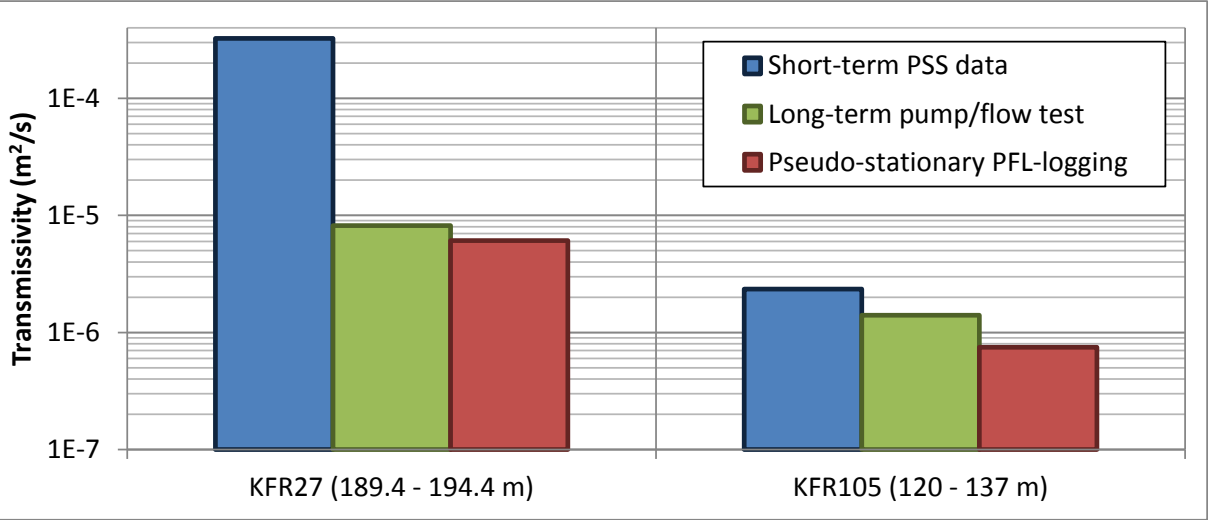TD15 Complementary simulation cases in support of SR-PSU

Figure C-6. *Transmissivity evaluation from three different test methods for the most conductive sections of KFR27 and KFR105 (see Figure C-7 and Figure C-8).*
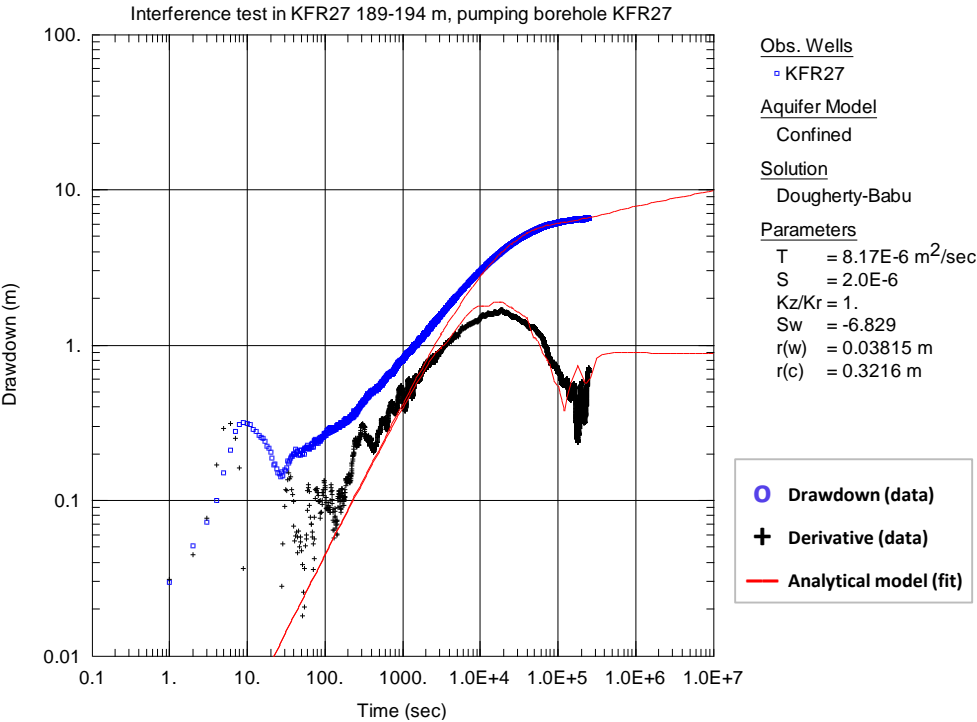
Figure C-7. *Transient evaluation of long-term pump test in the most conductive section of KFR27 (189 – 194 m; associated to SBA6; duration: 2 days and 21 hours).*

SVENSK KÄRNBRÄNSLEHANTERING AB

Interference test in KFR105 sektion 4

Obs. Wells
  ▫ KFR105:4

Aquifer Model
  Leaky

Solution
  Moench (Case 1)

Parameters
T   = 1.384E-6 m^2/sec
S   = 8.22E-7
r/B' = 0.0004696
ß'   = 0.0004866
r/B" = 0.
ß"   = 0.
Sw = -0.7889
r(w) = 0.03815 m
r(c) = 0.004875 m

○ **Drawdown (data)**

+ **Derivative (data)**

— **Analytical model (fit)**
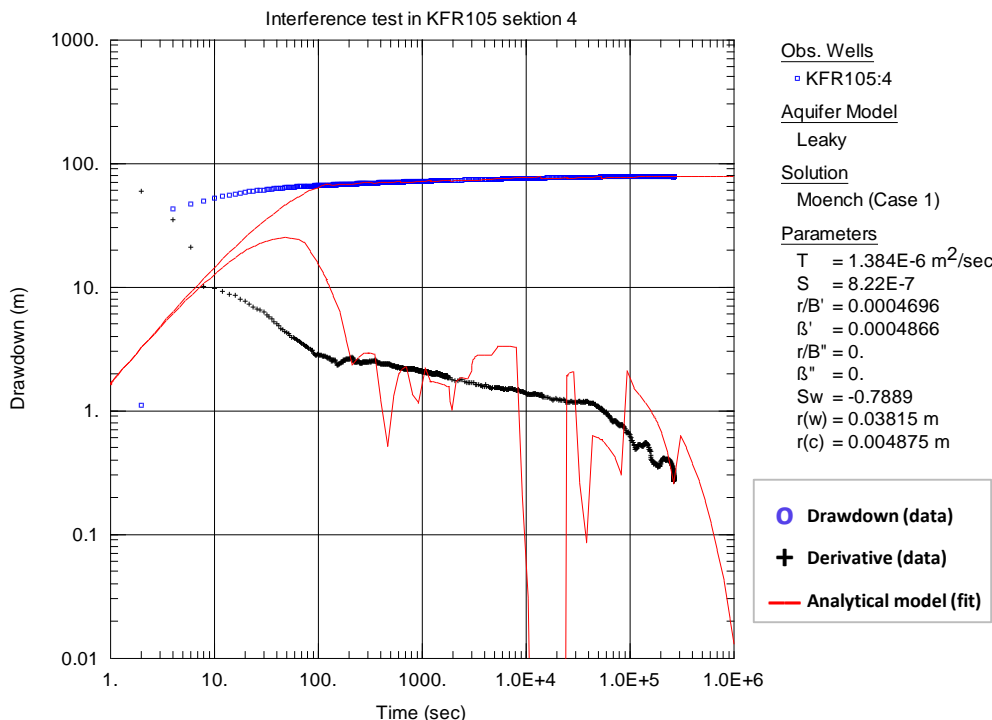
Figure C-8. Transient evaluation of long-term pump test in a 17 m section of KFR105 (120 – 137 m; duration: 3 days and 2 hours). The numerical oscillations in the model derivative are caused by the discretisation of flow history data (which are provided at discrete time steps).

Conclusions

PFL flow logging renders exceptionally detailed information on fracture flow and provides indispensable data for supporting realistic DFN modelling. It can also be argued that the persistent flow paths logged in the PFL method (i.e., continuously flowing fractures) are more representative for large-scale flow modelling in the analysis of long-term safety, SR-PSU, as compared to the short-term, local-scale hydraulic data obtained from PSS tests.

However, the latter are essential for complementing the hydrogeological interpretation in aspects of: 1) compartmentalisation (i.e., studied here), 2) place the historic packer data (1980-1986) in context of the recent PFL data in the area of the planned SFR extension, and 3) to discuss the effect that the construction of the planned facility may have on the large-scale flow (i.e., a facility with hydraulic-cage backfill will have a larger impact on the flow field if the surrounding fracture system is severely compartmentalised).

Hydraulic chokes are indicated by the identification of borehole sections where the two test methods, PSS and PFL, render differing properties (here, the criterion is defined by the ratio $T_{PSS}/T_{PFL} > 10$). The presence of hydraulic chokes can be confirmed in KFR27, although these indications are fewer than expected (8 of 96 tested sections). Two long-term pump tests are compared against PSS data and PFL data, which indicates that the evaluated properties are controlled by test duration (i.e., temporal or spatial scaling effects), rather than test method used. The pump test data indicate that stationary conditions do not necessarily apply after the 3 day pumping which preceded the PFL logging.

In KFR105, the PSS data are systematically higher than the corresponding PFL data (on average, $T_{PSS}/T_{PFL} \approx 4$). This discrepancy may be caused by several phenomena that may be expected for PFL-logging under atmospheric pressure (turbulence, gas-bubble formation, hydro-mechanical fracture closure, and missing drained fractures; see discussion above). This does not automatically imply absence of hydraulic chokes, but it complicates differentiating the degree of compartmentalisation in KFR105 data.

Thus it must be considered that the interpreted lateral transmissivity contrast, between the planned host rock in the *Central block* and its bounding tectonic belts (*Northern* and *Southern boundary belts*; Öhman

SVENSK KÄRNBRÄNSLEHANTERING AB

et al. 2012), may have been exaggerated due to unfavourable test conditions during the PFL logging of KFR105.

D. Appendix

Verification of semi-correlated DFN parameterisation

The transmissivity parameterisation of the semi-correlated approach is compared against the original DFN parameterisation (i.e., the correlated approach) to verify that it is statistically consistent to its original setting, as seen by simulated borehole exploration and truncated below $T_{lim} = 2.5 \cdot 10^{-9}$ m^2/s (Table D-1).

Table D-1. Statistics of sampled fracture transmissivity

Domain	Set	Original parameterisation				Semi-correlated parameterisation			
		No. data[1]	$\sum T_f$	μ_{logT}	σ_{logT}[2]	No. data[1]	$\sum T_f$	μ_{logT}	σ_{logT}[2]
Shallow	EW	243	8.9E-6	-8.06	0.55	242	7.8E-6	-8.08	0.55
	NE	103	7.7E-7	-8.28	0.32	103	8.2E-7	-8.26	0.32
	NW	179	8.5E-6	-8.06	0.56	181	7.7E-6	-8.03	0.56
	HZ	1121	9.3E-4	-7.40	1.01	1041	1.5E-3	-7.33	1.02
	Gd	892	9.6E-5	-7.80	0.73	914	1.1E-4	-7.80	0.72
Repository	EW	107	1.9E-6	-8.01	0.44	104	2.0E-6	-8.07	0.44
	NE	21	4.8E-7	-7.97	0.46	21	4.7E-7	-8.07	0.46
	NW	185	6.2E-6	-7.96	0.56	189	7.7E-6	-7.97	0.56
	HZ	607	4.0E-5	-7.68	0.62	612	3.8E-5	-7.81	0.62
	Gd	674	1.4E-5	-7.98	0.47	621	1.3E-5	-8.03	0.47
Deep	EW	50	2.1E-6	-7.84	0.59	48	6.6E-6	-7.99	0.59
	NE	18	1.2E-7	-8.25	0.25	18	9.9E-8	-8.34	0.25
	NW	31	1.1E-6	-8.01	0.60	31	1.2E-6	-8.00	0.60
	HZ	241	8.0E-6	-7.90	0.54	245	8.4E-6	-7.97	0.54
	Gd	301	1.5E-5	-7.79	0.62	310	1.6E-5	-7.84	0.61

1) Number of sampled fractures in simulated borehole exploration with transmissivity exceeding $T_{lim} = 2.5 \cdot 10^{-9}$ m^2/s.

2) Standard deviation of logarithmic transmissivity of fractures sampled in simulated borehole exploration. Refers to total variability (i.e., both size and stochastic variability components), but differs from Table 2-1, as only transmissivity exceeding $T_{lim} = 2.5 \cdot 10^{-9}$ m^2/s is included.

The semi-correlated parameterisation is also verified in terms of cross plots between fracture transmissivity and size (Figure D-1 to Figure D-3) and as statistical distributions (Figure D-4 to Figure D-6) from simulated-borehole exploration. Finally, the transmissivity distribution of the semi-correlated approach is demonstrated for a full DFN realisation (that is: all the fractures within a c. 6,000,000 fracture realisation, not only the borehole-sampled subset; Figure D-7 and Figure D-8). As expected, the distributions must be weighted by fracture area in order to be consistent with the original fracture-transmissivity parameterisation. This demonstrates once again that the semi-correlated calibration is consistent *as seen by borehole sampling*. (i.e., fracture-area intensity, P_{32}, is a highly efficient estimator of borehole frequency, P_{10}, as it is directly proportional without being limited to a small subset of data).

DokumentID
1578373, (1.0)

Sekretess
Öppen

Sida
134(165
)

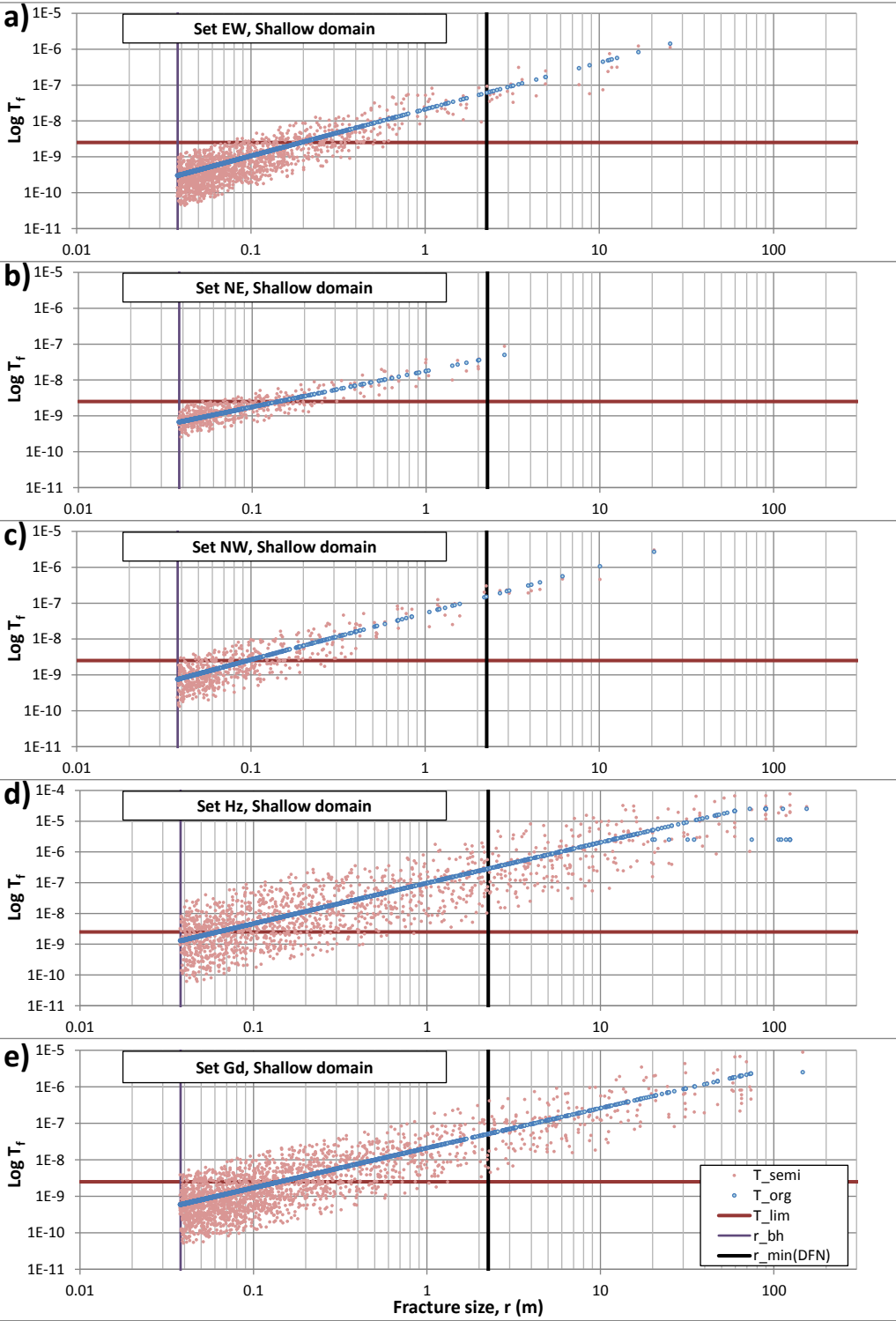TD15 Complementary simulation cases in support of SR-PSU

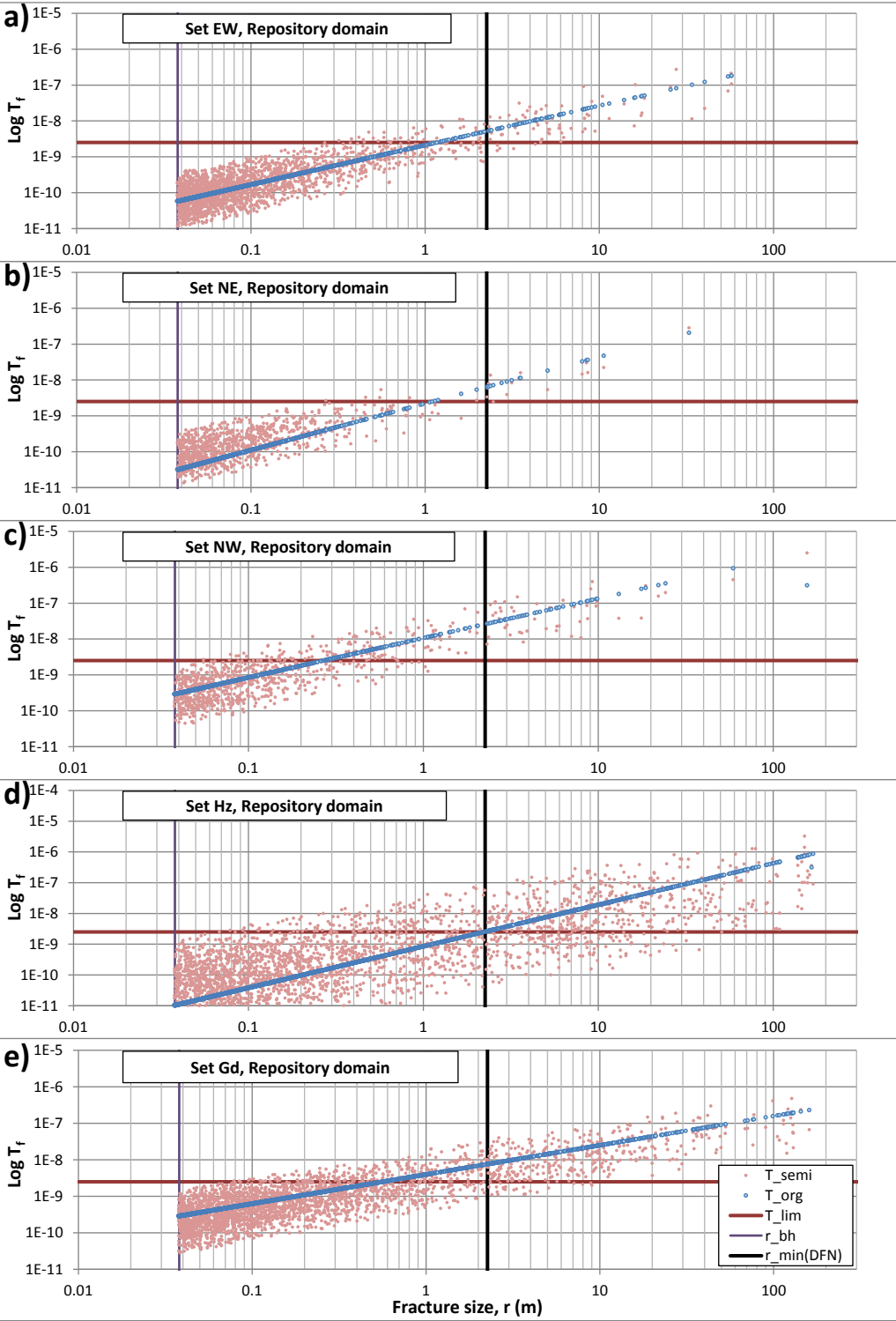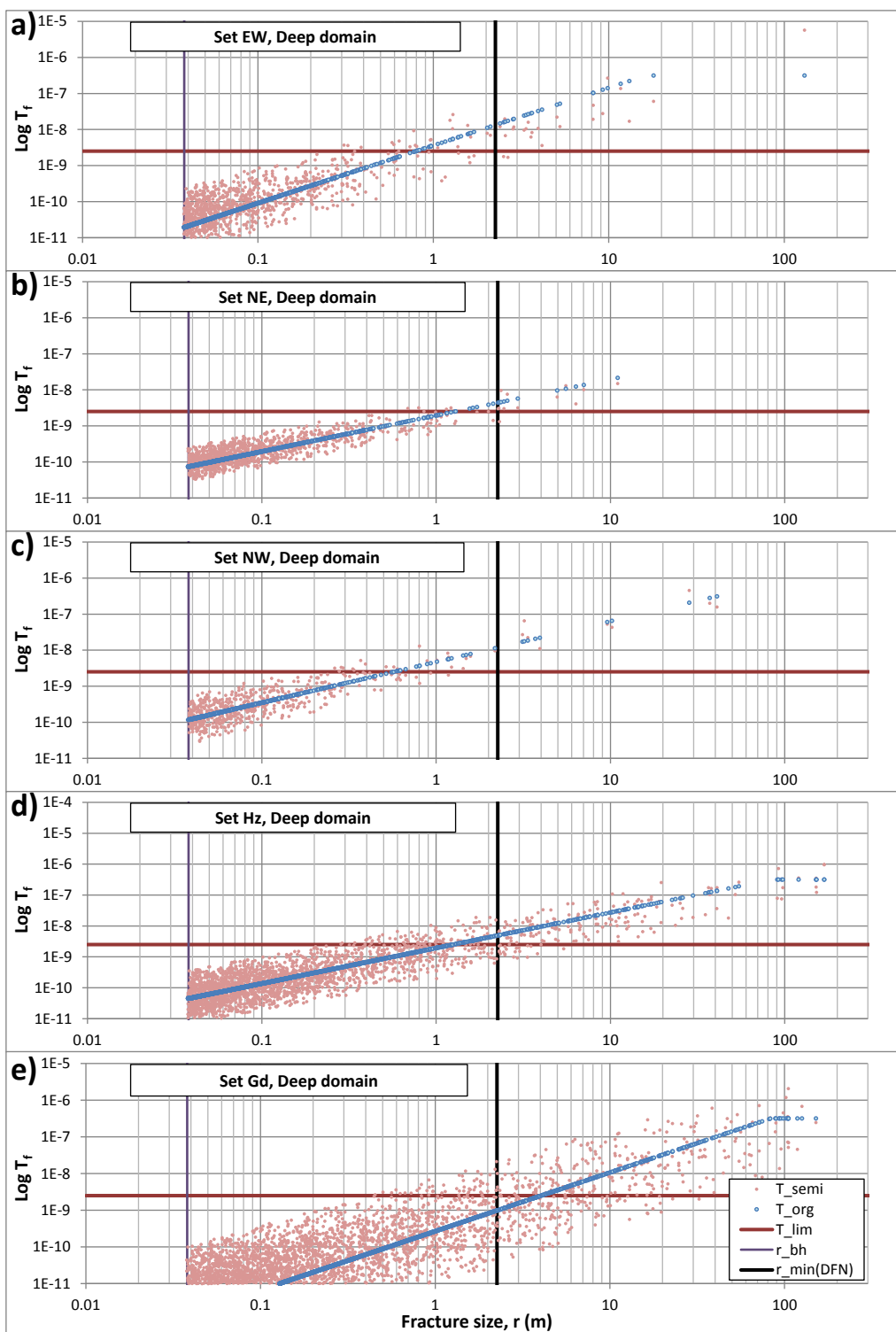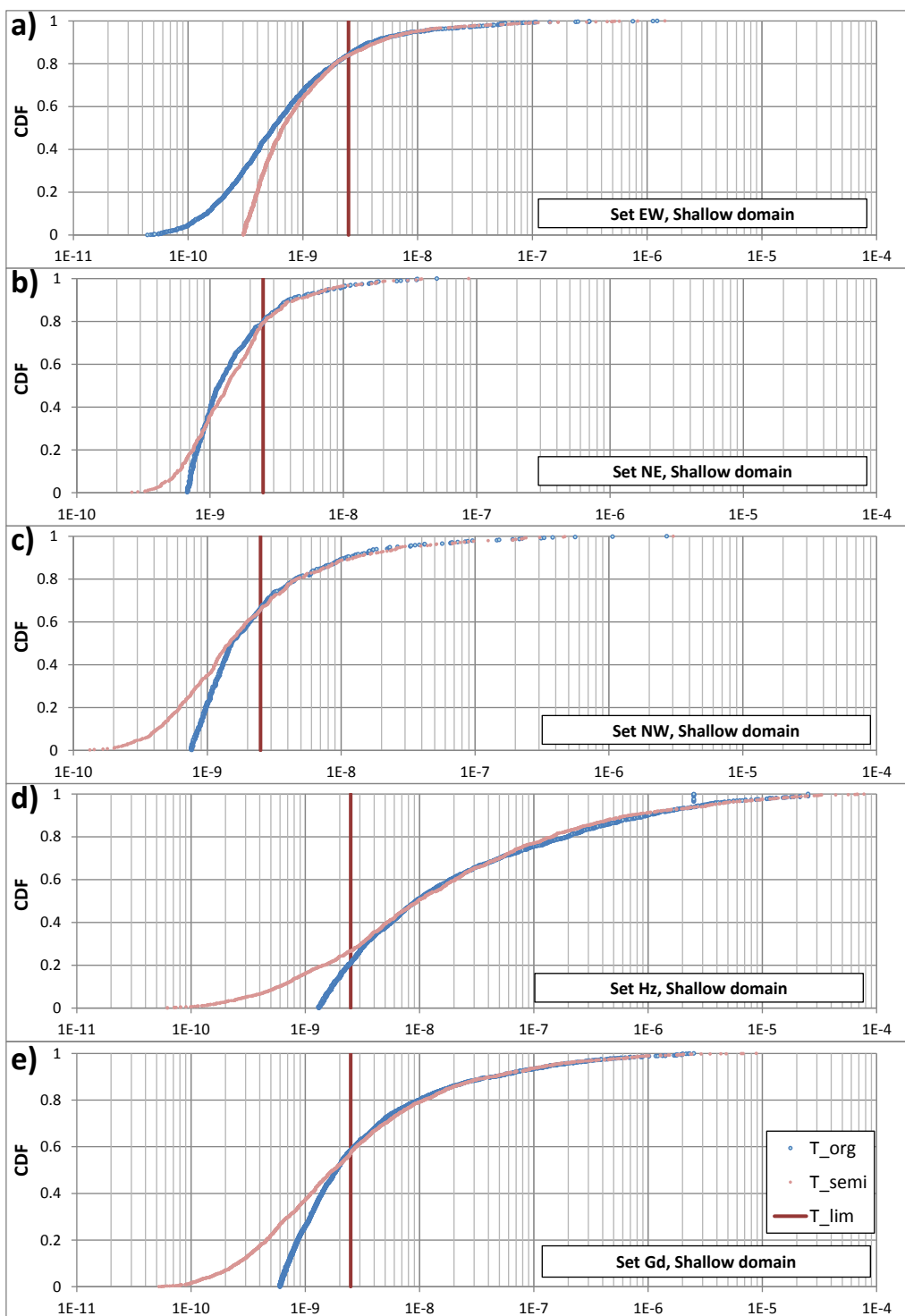***Figure D-1.*** *Fracture transmissivity in simulated borehole exploration; semi-correlated approach compared to original DFN parameterisation (shallow domain).*

DokumentID
1578373, (1.0)

Sekretess
Öppen

Sida
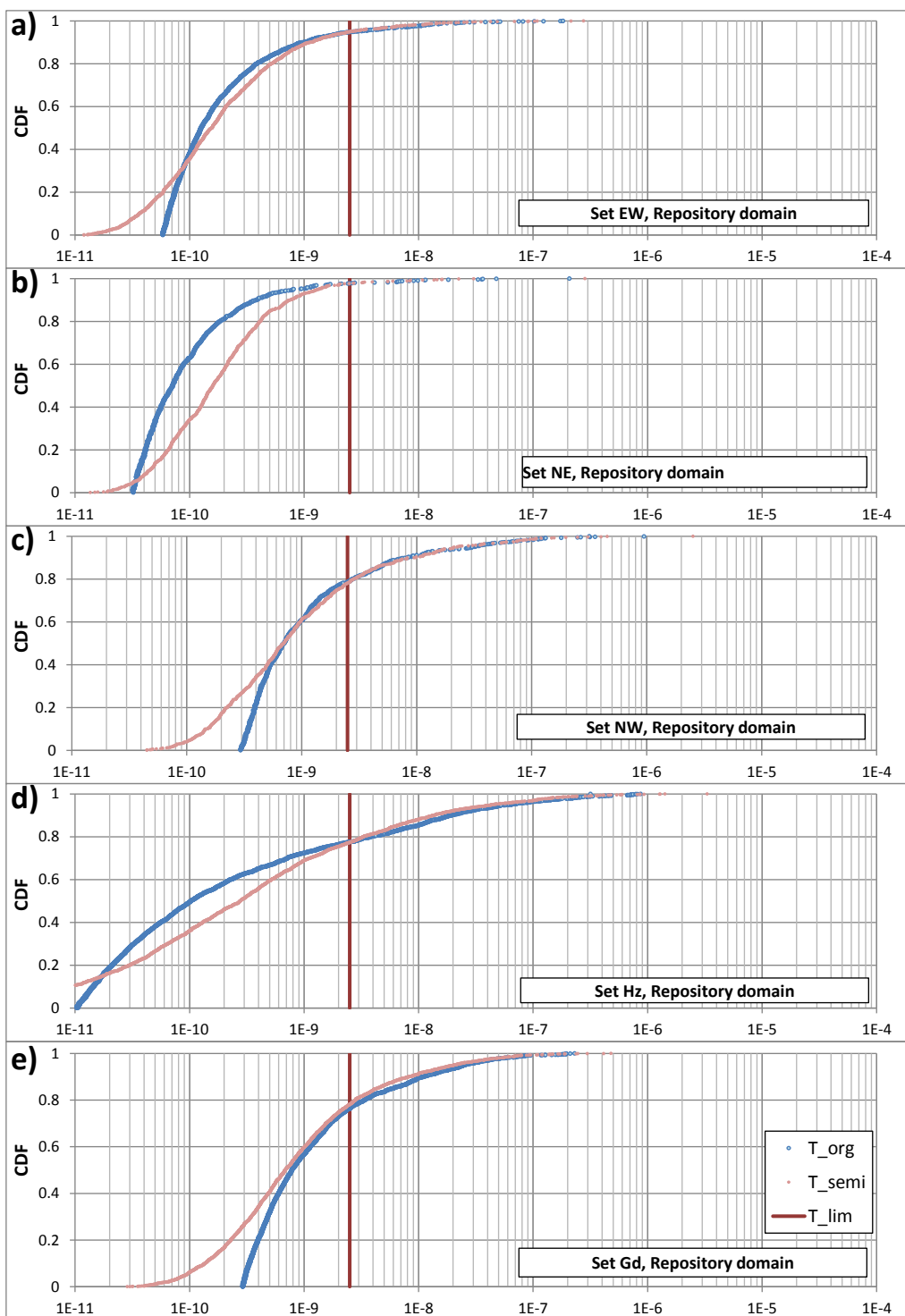135(165
)

TD15 Complementary simulation cases in support of SR-PSU

Figure D-2. Fracture transmissivity in simulated borehole exploration; semi-correlated approach compared to original DFN parameterisation (repository domain).

SVENSK KÄRNBRÄNSLEHANTERING AB

DokumentID
1578373, (1.0)

Sekretess
Öppen

Sida
136(165
)

TD15 Complementary simulation cases in support of SR-PSU

Figure D-3. *Fracture transmissivity in simulated borehole exploration; semi-correlated approach compared to original DFN parameterisation (deep domain).*

SVENSK KÄRNBRÄNSLEHANTERING AB

DokumentID
1578373, (1.0)

Sekretess
Öppen

Sida
137(165
)

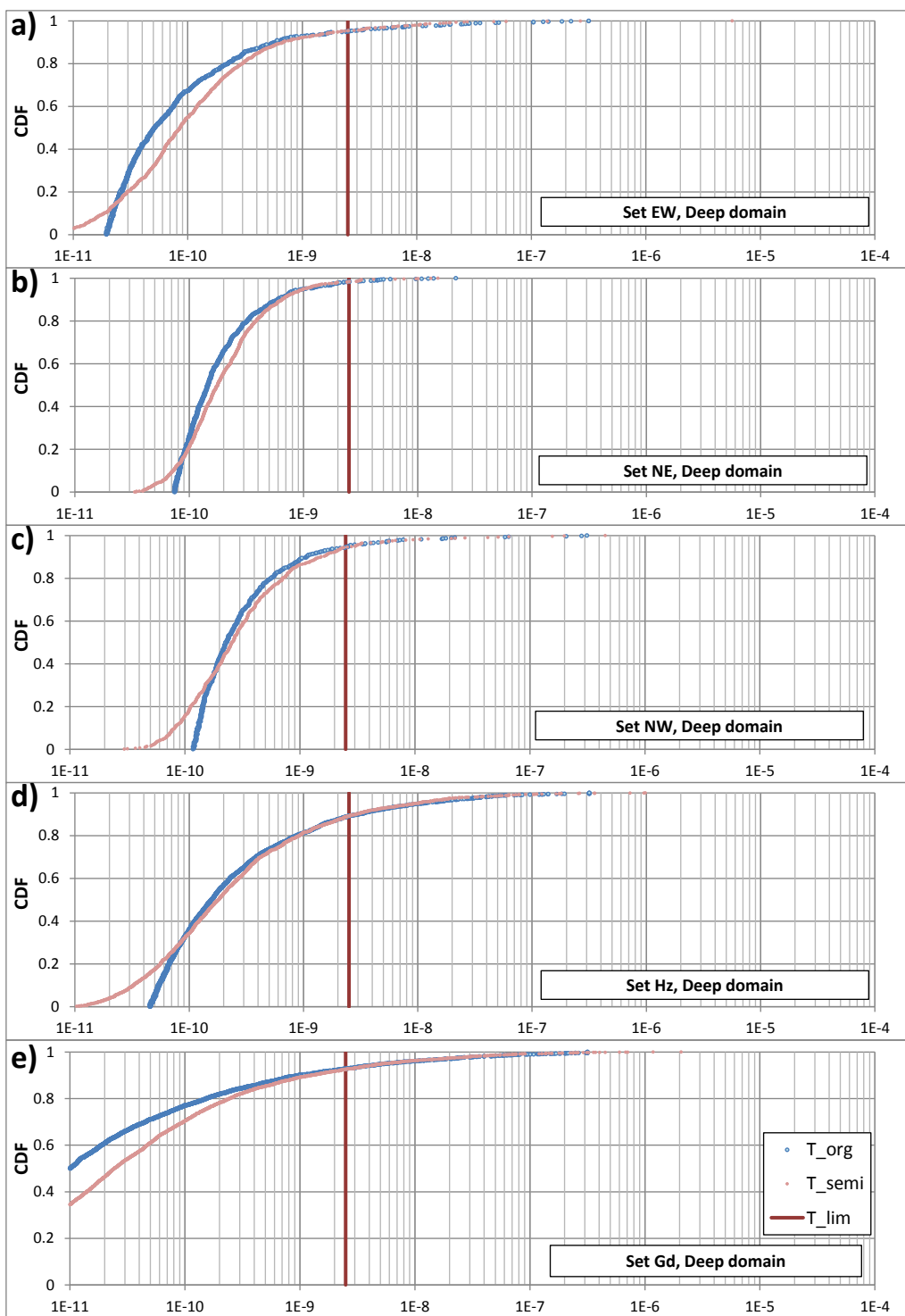TD15 Complementary simulation cases in support of SR-PSU

Figure D-4. *Distribution of fracture transmissivity in simulated borehole exploration; semi-correlated approach compared to original DFN parameterisation (shallow domain).*

DokumentID
1578373, (1.0)

Sekretess
Öppen

Sida
138(165
)

TD15 Complementary simulation cases in support of SR-PSU

Figure D-5. *Distribution of fracture transmissivity in simulated borehole exploration; semi-correlated approach compared to original DFN parameterisation (repository domain).*

DokumentID
1578373, (1.0)

Sekretess
Öppen

Sida
139(165
)

TD15 Complementary simulation cases in support of SR-PSU

Figure D-6. Distribution of fracture transmissivity in simulated borehole exploration; semi-correlated approach compared to original DFN parameterisation (deep domain).

DokumentID
1578373, (1.0)

Sekretess
Öppen

Sida
140(165)

TD15 Complementary simulation cases in support of SR-PSU
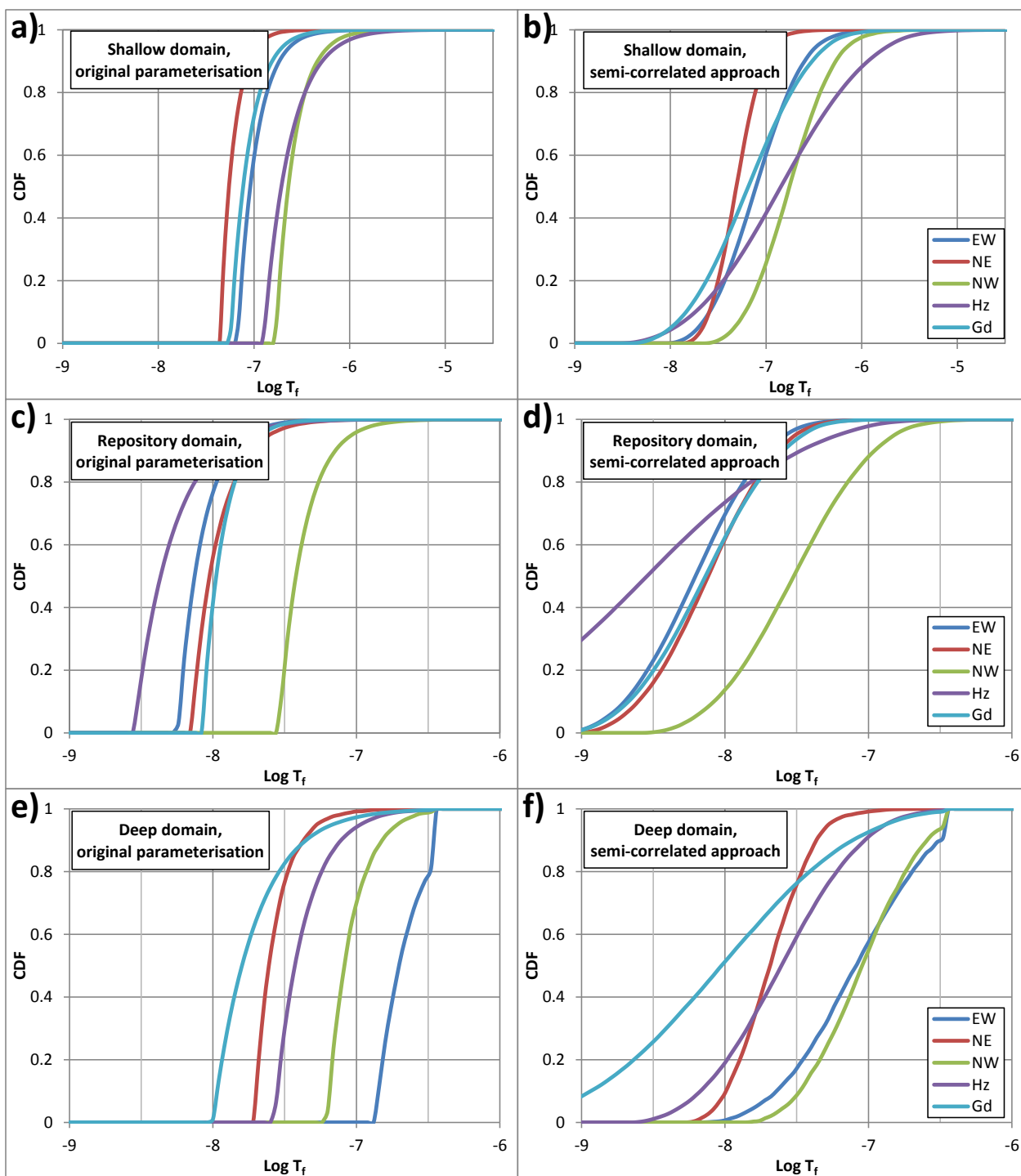
Figure D-7. Distribution of parameterised fracture transmissivity of one connected DFN realisation (R85); semi-correlated approach compared to original DFN parameterisation.

DokumentID
1578373, (1.0)

Sekretess
Öppen

Sida
141(165
)

TD15 Complementary simulation cases in support of SR-PSU
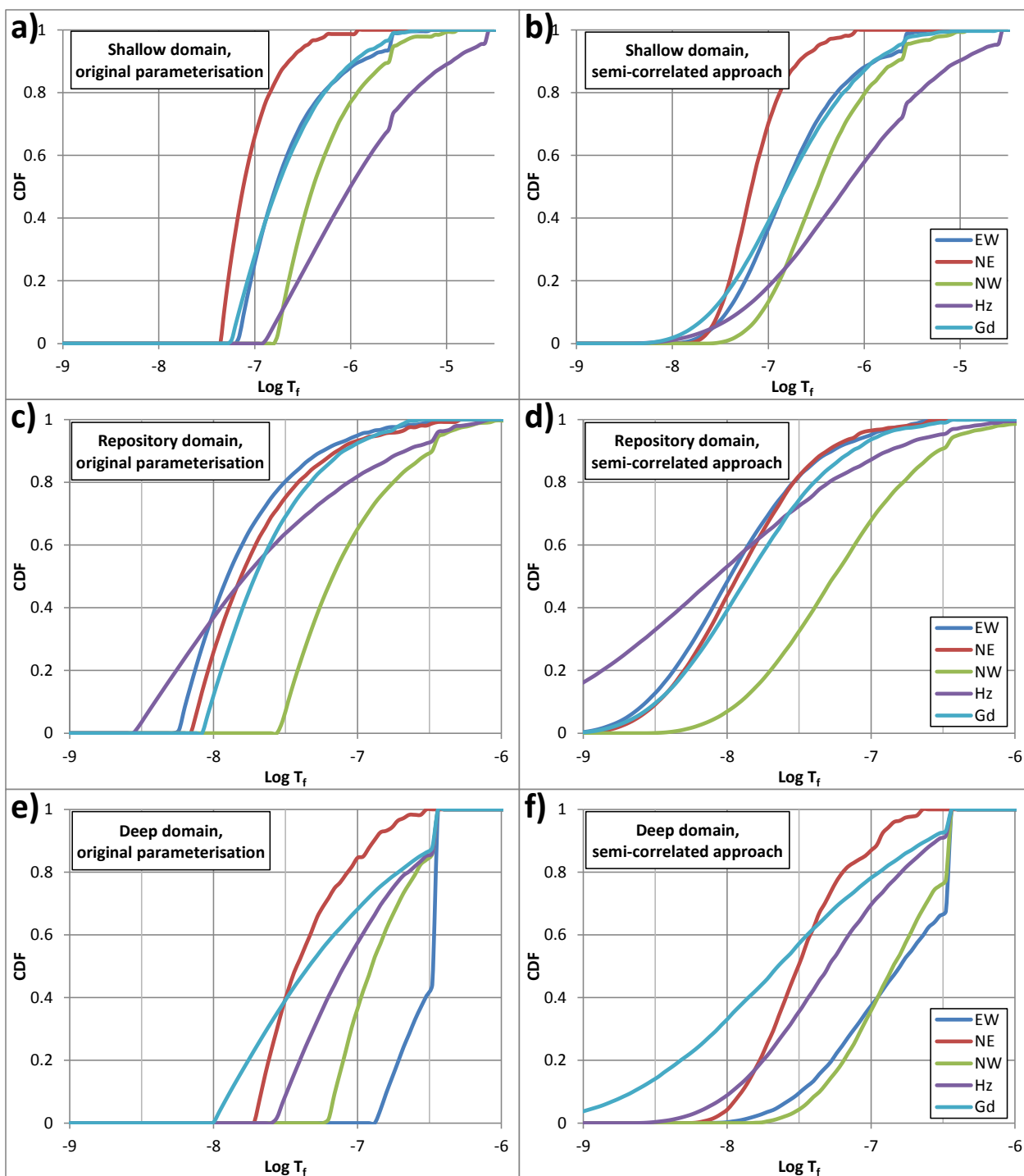
Figure D-8. *Distribution of area-weighted fracture transmissivity of one connected DFN realisation (R85); semi-correlated approach compared to original DFN parameterisation.*

DokumentID
1578373, (1.0)

Sekretess
Öppen

Sida
142(165
)

TD15 Complementary simulation cases in support of SR-PSU

E.   Appendix

Probabilistic analysis of HRD heterogeneity outside SFR Regional domain

Background

The temperate-period analysis of SR-PSU is based on a sensitivity analysis of regional-scale flow simulations (referred to as SR-PSU-TD11). The TD11 sensitivity analysis primarily focussed on evaluating the significance of uncertainty and heterogeneity of the bedrock parameterisation of the SFR Regional model domain. The sensitivity is evaluated in terms of performance measures, for example particle-exit locations to identified biosphere objects (Figure 1-8). Due to practical aspects, a number of model simplifications were employed. One such model simplification is that the uncertainty of the HRD parameterisation in the model area outside the SFR Regional domain was not addressed (i.e., it was represented by a static DFN realisation, which was not varied in the sensitivity analysis).

As part of the proactive modelling to address hydrogeological issues (Section 3.4, main report), the simulated particle exit locations were found to be affected by the HRD heterogeneity outside the SFR Regional domain. More precisely, fractions of particle trajectories are diverted from exiting in the terrestrial biosphere object 157_2, which is the primary recipient of SFR discharge, towards downstream lake objects 157_1, 159, and 116 (Table 3-3 and Figure E-1).

The sensitivity to HRD heterogeneity north-east of the SFR Regional domain varies among the five tested stochastic DFN realisations (Table 3-3). In particular, one (realisation R02) stands out with a drastic impact on particle exits of SFR1, where about half of its exit locations are relocated from biosphere object 157_2 towards the lake objects 157_1 and 116. However, this impact is isolated to realisation R02; the particle-exit from SFR1 is not significantly affected in the other four stochastic DFN realisations. The discharge from SFR3 to is comparatively less sensitive to HRD heterogeneity outside the SFR Regional domain. The tested realisations provide a smaller but more consistent difference versus the static DFN employed in TD11. The average discharge fraction from SFR3 to lake object 116, based on all five stochastic realisations, is c. 10%, as compared to 1% in the static DFN. This difference is assumed to reflect the fact that the connectivity of the static DFN is somewhat underestimated. The static DFN was generated as part of SR-Site to cover the model domain outside the Forsmark lens, and as such it was not specifically accommodated to all details in the deterministic model components of the SFR model (i.e., ZFM and SBA structures), nor its specific stochastic components (DFN realisation R85 and Unresolved PDZs).

Objective

The simulations have demonstrated that performance measures are subject to the HRD heterogeneity located just north-east of the SFR Regional domain (more precisely, in the area between biosphere objects 157_2 and Charlie's lake, 116; Section 3.4, main report). However, the five stochastic realisations (and the static DFN realisation) are insufficient for quantifying this uncertainty component in a probabilistic context for the safety analysis. The objectives of this study are therefore to:
1) identify the particular geometrical/hydraulic traits of DFN realisation R02 that are associated to anomalous discharge from SFR to lake objects 157_1 and 116, and
2) based on these traits, estimate its frequency of occurrence in a larger ensemble of DFN realisations (i.e. the probability/risk of generating similar DFN realisations with comparable impact on simulation results
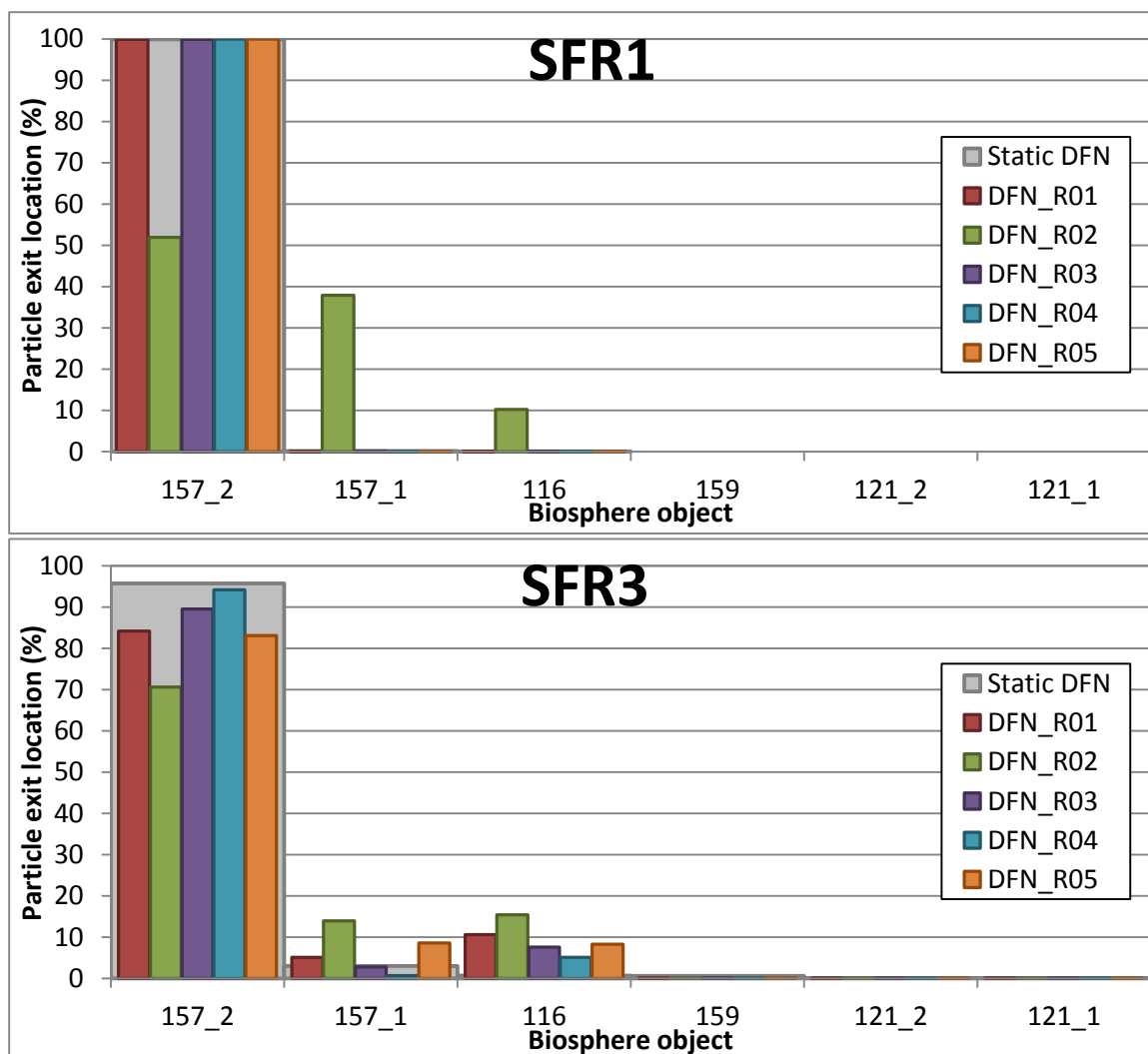
DokumentID
1578373, (1.0)

Sekretess
Öppen

Sida
143(165
)

TD15 Complementary simulation cases in support of SR-PSU

Figure E-1. *Relocation of particle-exit locations from object 157_2 towards the downstream objects 157_1, 116, 159, 121_2 and 121_1.*

Particular hydrogeological traits of DFN R02

In order to understand the particular traits of DFN R02 for particle-tracking output, its role must be analysed in context of the hydrogeological premises for flow paths from SFR. It is notable that the primary discharge of flow paths from SFR occur in biosphere object 157_2 is (Table 3-3) instead of the downstream lake object 116 (basin threshold of 157_2 is c. -12 m RHB70, as compared to the threshold -14.2 m RHB70 for lake 116).

Setting of 157_2

The following particular circumstances can be noted regarding the hydrogeological setting of biosphere object 157_2, which control the flow paths from SFR (see Section 6.3.2 in Öhman et al. 2014):

1) Structural geology: The area occurs just north of a junction of three deformation zones (ZFMNNE0869, ZFMNW0805A/B, and ZFM871), which can be said to –more or less – enclose the discharge from SFR1 and SFR3 (Figure E-2a). From this junction, the particle-exit locations extend north along three zones: ZFMNNW3113, ZFMNNW0999, and ZFMNS3154.

2) Topography: the area is located in a local topographical basin (threshold of $z \approx$ -12 m RHB70), which is upstream from biosphere object 116 (threshold of $z \approx$ -14.2 m RHB70). Discharge is induced by convergent flow from nearby elevated hills (green-brown shaded areas in Figure E-2b).

3) Sediment coverage: the sediment layers are thin inside biosphere object 157_2, but its outlet northwards, is blocked by thick clay sediments (red-contoured areas in Figure E-2).

As the result, the hydrogeological setting tends to drive the flow paths from SFR1 to ground surface within biosphere object 157_2, instead of continuing downstream to lake object 116. The deeper location of SFR3, causes deeper and longer flow paths, which is manifested by a somewhat larger fraction of particles reaching lake 116 (Table 3-3; Figure E-1).

The gently dipping ZFM871 convey most of the discharge from both SFR1 and SFR3. Its terminations against deformation zones ZFMNNE0869, ZFMNW0805A/B tends to re-direct the particle trajectories towards the ground surface in biosphere object 157_2. Thus, it is important to note that the discharging flow reaching object 157_2 is typically upward-directed down to an elevation of c. -100 m. It can therefore be expected that the discharge to lake object 116 is controlled by the presence of stochastic fractures below object 157_2, down to c. 100 m depth.
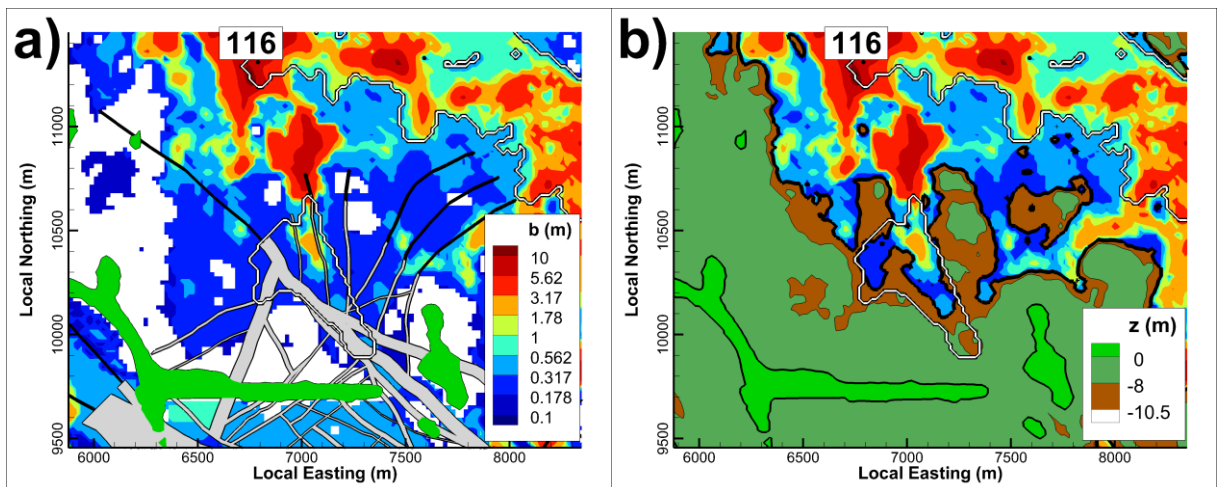

Figure E-2. Low-permeable clay thickness, b (m), in the vicinity of biosphere object 157_2 (5000 AD), in context of a) deformation-zone traces, and b) elevated topography.

Analysis of the 5 DFN realisations

Next, the five stochastic DFN realisations are analysed in order to identify the characteristics that are unique to realisation R02. All of the five realisations (including the static DFN from TD11) do form connected fracture networks that allow particle trajectories to reach lake 116 (Figure E-3); however, in all cases but one, the fraction of particles from SFR1 reaching lake 116 is negligible (Figure E-1). However, the anomalous DFN R02 stands out with a large sub-horizontal fracture that forms a highly transmissive, single-handed connection between objects 157_2 and 116.

A reality check is made to evaluate the credibility in such features in context of the hydrogeological understanding of the site. Firstly, all features exceeding 300 m in side length are expected to have been covered by deterministic modelling. Inspection demonstrates that the intrusion of the stochastic feature in DFN R02 into the SFR Regional domain is smaller than 300 x 300 m^2 (see red reference line in Figure 3-33). Secondly, stochastic sub-horizontal features outside the SFR domain are not expected to extend across the deformation zones ZFMNNE0869 and ZFMNW0805A/B. Inspection demonstrates that the stochastic feature of DFN R02 is located outside these zones, and hence in an unchartered area of the SFR site investigation.

Close inspection demonstrates that the discharging flow from SFR that occurs in the overlapping area between this fracture and biosphere object 157_2 is being re-directed downstream to lake 116 (white arrow; Figure 3-33). The intrusion of this fracture occurs at an elevation of c. -40 m RHB70, which is

within the depth interval where flow paths are typically upward-directed (i.e., -100 to -10 m). Moreover, the same fracture extends into lake object 116 within a depth interval ranging from c. -100 to -20 m, from where a number of steeply dipping fractures provide several connections to ground surface (Figure 3-34).

This suggests that the following criteria control exit locations in lake 116:
1) Presence of one, or more, highly transmissive stochastic fracture(s) that provides large-scale connectivity between objects 157_2 and 116.
2) In order to re-direct particle flow, the fracture(s) must extend into objects 157_2 and 116 within relevant depth interval (c. -20 to -100 m elevation)

At the other end, close inspection of the other realisations provides a handful of examples of fracture-network configurations that do not cause discharge in lake object 116. For example the exit locations to lake 116 are few in DFN R05, in spite of having both: 1) a similarly large, transmissive fracture extending into object 157_2 (Figure E-6), as well as, 2) a network of inter-connected highly transmissive fractures that adjoin objects 157_2 and 116. However, in this case the single large fracture extends too deep below lake object 116 (well below 100 m depth: see grey-shading in Figure E-6) and the effective hydraulic connection of inter-linked fractures is considerably weaker than the connectivity of a single-fracture connection.

Geometrical analysis of large ensemble of DFN realisations

It has been demonsrated that even the hydrogeological bedrock properties outside the SFR Regional domain, as stochastically modelled by DFN realisations, can affect the simulated flow paths from SFR. The analysis of the hydrogeological conditions for discharge from SFR (Figure E-2) and the simulated DFN realisations (Section 3.4, main report), suggests that two basic criteria are *required*, in order to substantially affect the balance between discharge to objects 157_2 and 116 (Table E-1). Moreover, it is assumed that the effect that a given single-fracture connection has on the discharge balance between the two biosphere objects is correlated to a set of four *key properties* (Table E-1).

Based on these defined criteria and the geometrical/hydraulic indicators, it is assumed that the risk of "anomalous discharge to lake object 116" can be estimated based on a geometrical analysis of a larger DFN ensemble (1000 realisations). More precisely, the risk of atypical flow paths from SFR, silimar to that found for DFN R02, or worse, is estimated as the frequency of occurrence for a single-fracture connection between the two biosphere objects, which is at least as strong as that in DFN R02. A separate code is used in this geometrical analysis [Scan_DFN_OUTSIDE_SFR_Reg_dom.f] (Appendix G). To build confidence in this geometrical approach and the assumed representative estimators, a few representative realisations are selected and examined by means of flow simulations (see below).

Table E-1. Criteria and properties in probabilistic analysis of exit-location control

Basic criteria for biosphere-object connection (157_2 and 116)

1	Both biosphere objects must be directly connected[1] by large fracture
2	Biosphere connection must occur above -100 m elevation[2].

Key properties affecting exit locations

1	High fracture transmissivity, $T > 10^{-6}$ to 10^{-5} m^2/s[3]
2	Intersectional length, L (m), with object 157_2[4]
3	Intersectional length, L (m), with object lake object 116[4]
4	Horizontal exposure area, A (m^2)[5]

1) Inter-connected fractures are assumed to form less transmissive flow paths, owing to the hydraulic bottle necks that typically occur at fracture intersections (Figure E-6)
2) Connection must also occur below bedrock surface (which is on the order -20 m elevation). The contact is determined by means of sampling objects, which have the approximate geometry of objects 157_2 and 116 (Figure E-7).
3) Typically applies automatically, as transmissivity is assumed to be correlated to size

TD15 Complementary simulation cases in support of SR-PSU

4) Geometrical intersectional length, L (m), between the connecting fracture and the biosphere object (only intersection within relevant elevation interval, z_{rock} to -100 m considered)

5) Of the fracture connecting the two biosphere objetcs within the relevant depth interval (only within relevant elevation interval, z_{rock} to -100 m considered)
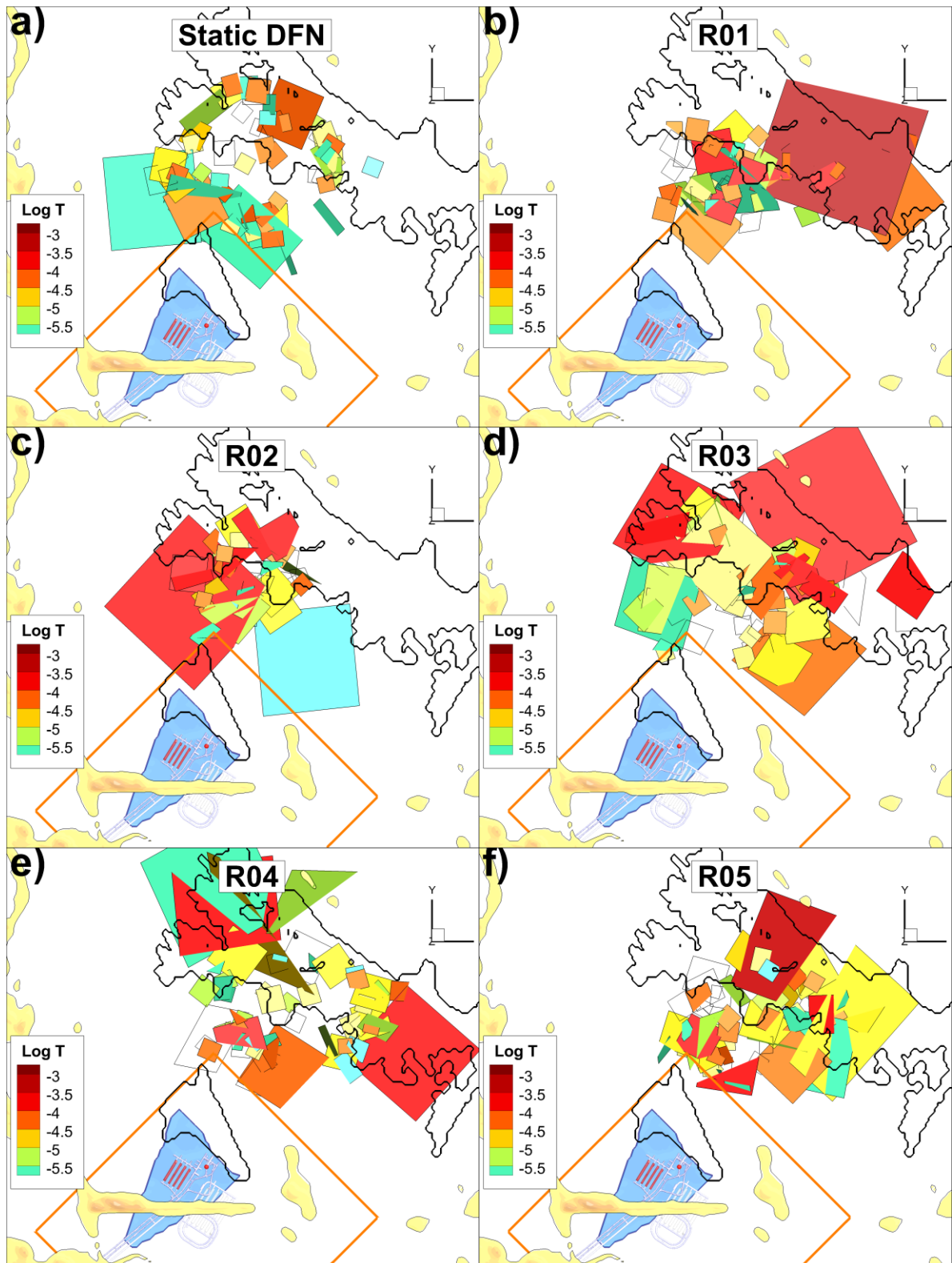

Figure E-3. *Fractures involved in particle trajectories outside SFR Regional domain for 5 stochastic DFN realisations.*

DokumentID
1578373, (1.0)

Sekretess
Öppen

Sida
147(165
)

TD15 Complementary simulation cases in support of SR-PSU
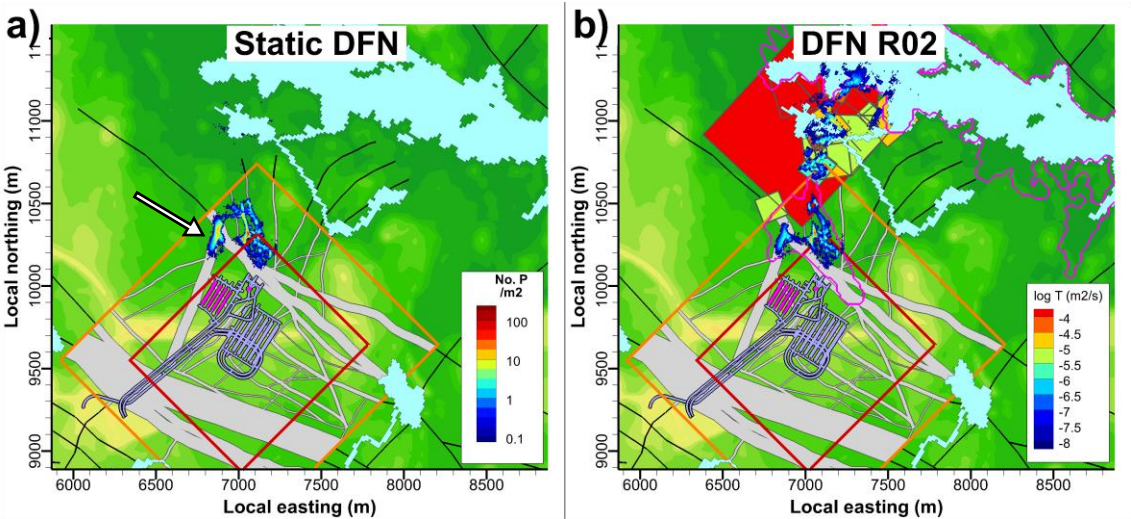

Figure E-4. *Detailed analysis of sensitivity to DFN outside SFR Regional domain; a) the discharging flow paths from SFR1 to ZFMNNE0869 (white arrow) can be re-directed by b) large sub-horizontal fractures (red plane). A 300 m respect distance (red line) to the SFR Regional domain (orange line) provided for spatial reference.*
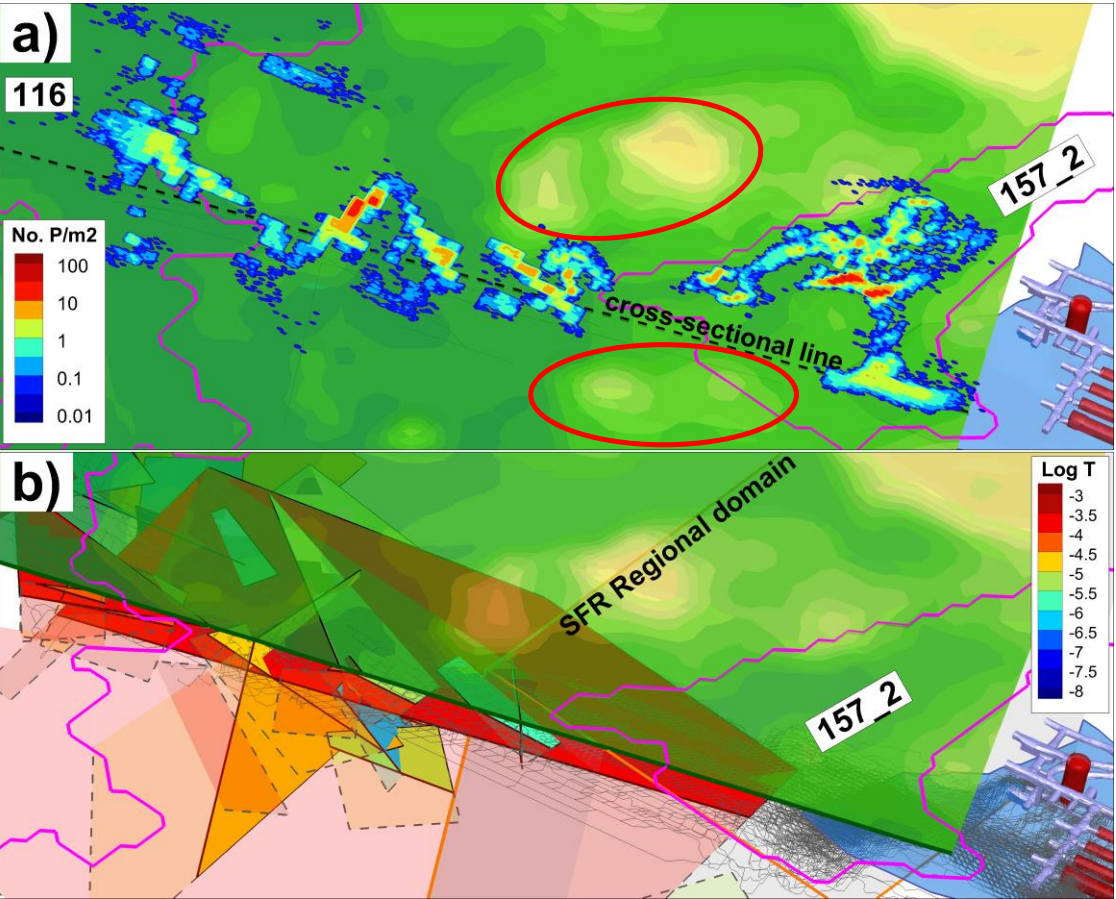

Figure E-5. *Three-dimensional visualisation of the structure re-directing flow paths in DFN R02.*

SVENSK KÄRNBRÄNSLEHANTERING AB

DokumentID
1578373, (1.0)

Sekretess
Öppen

Sida
148(165
)

TD15 Complementary simulation cases in support of SR-PSU
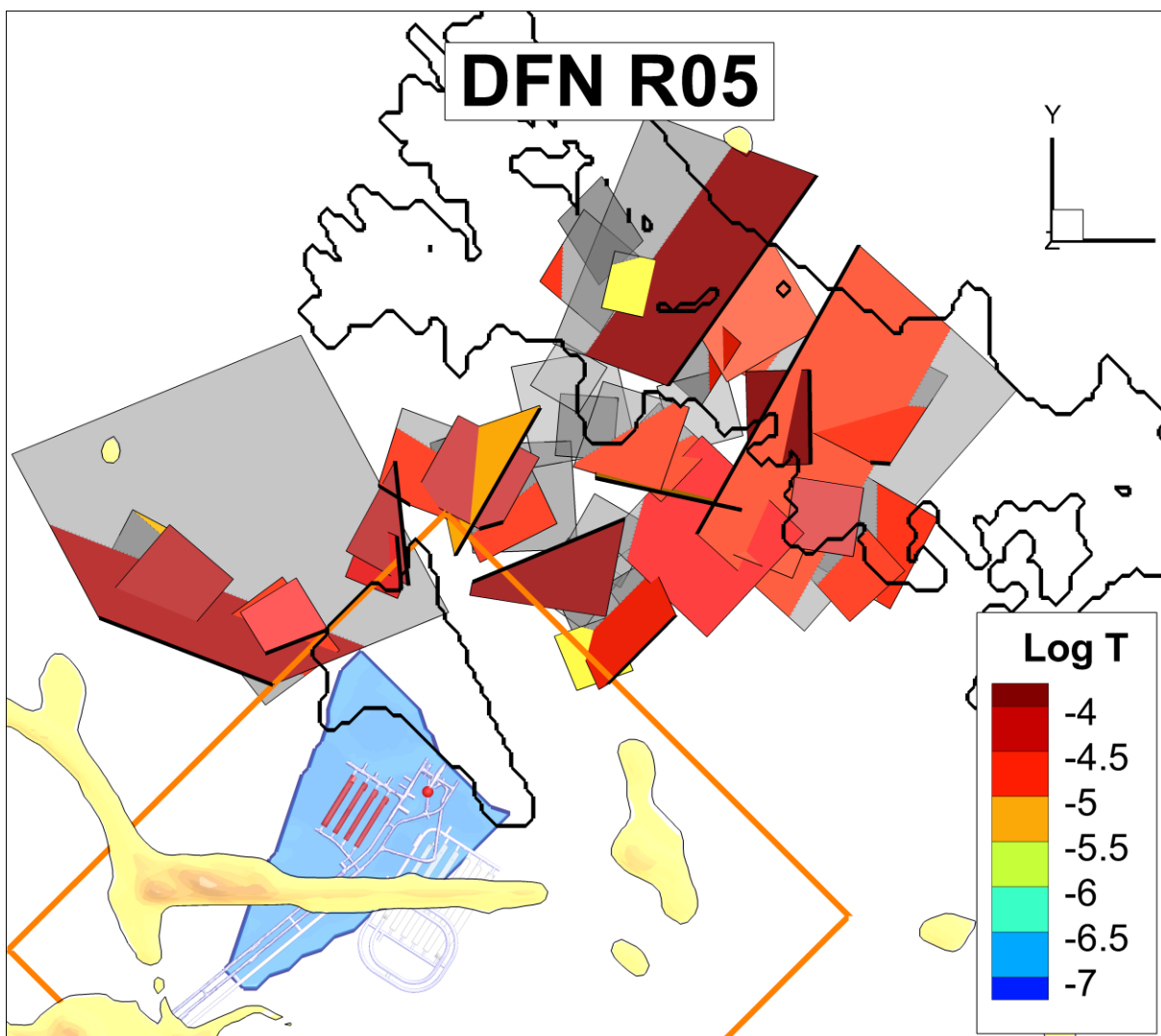

Figure E-6. *Geometrically connected network of highly transmissive fractures in DFN R05. Fractures terminated at ground surface (traces in black) and grey-shaded below a depth of -100 m.*
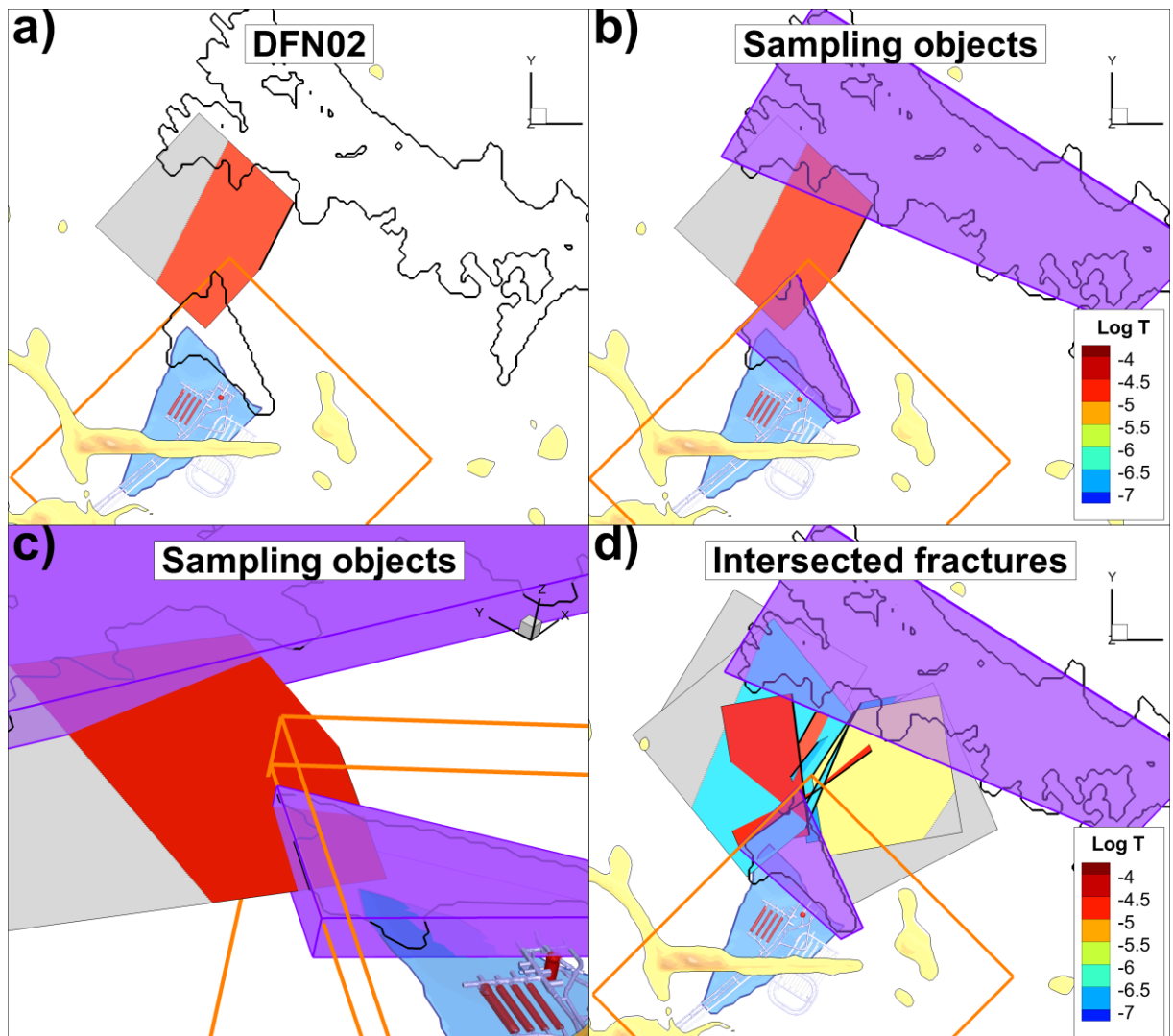
Figure E-7. Definition of geometrical sampling geometries; a) based on the single-fracture connection in DFN R02, b) approximated geometries based on biosphere object 157_2 and 116 (purple), c) sampling geometries extruded down to -100 m elevation, and d) example of single-fracture connection identified in DFN ensemble (here 8 of 100). Fractures terminated at ground surface (traces in black) and grey-shaded below a depth of -100 m.

Results

In the ensemble of 1,000 realisations, only 88 realisations have at least one direct fracture connection between objects 157_2 and 116. These 88 realisations are ranked in terms of the suggested geometrical/hydraulic indicators and compared against "the anomalous realisation" DFN R02 (Figure E-8). One realisation had two fractures connecting the two biosphere objects (R574); in this case the evaluated properties of both fractures (i.e., in terms of geometrical/hydraulic indicators) were in combined to determine the total rank of the realisation.

The analysis indicates that the probability/risk of a DFN realisation, with similar impact of flow paths as observed for R02, or worse, ranges from 1% to 5% (Figure E-8). A joined estimation, where the ranks of all 4 indicators are summed, suggests a risk of 1.4%. This approach relies heavily on the assumptions that
1) the anomalous hydrogeological characteristics of DFN R02 can be delineated by a set of criteria/indicators, and
2) these criteria/indicators can be used in a geometrical analysis of multiple realisations to identify realisations with similar effect on discharge from SFR (i.e., similar to that found for DFN R02)

TD15 Complementary simulation cases in support of SR-PSU

3) the criteria/indicators can be used to quantify the risk, or frequency of occurrence, of a situation where the discharge locations from SFR appear very different from that observed in Öhman et al. 2014; i.e., the "static DFN realisation").

To strengthen the reliability in the geometrical sampling approach, the following realisations were selected for evaluation in flow simulations (Table E-2):

1) 4 demonstrative realisations. These are selected to demonstrate the representativity of the four indicators (Figure E-9). In particular, R838 is expected to demonstrate anomalous particle exit in lake object 116.

2) 5 arbitrary realisations (i.e., R006…R010). These are **not** expected to render anomalous particle exit in lake object 116. The purpose of these is to reduce uncertainty by expanding the sample size of simulated cases, from one static and 5 stochastic realisations to one static and 10 stochastic realisations. Thus, regardless of confidence in the geometrical approach, the frequency of simulation output of type DFN R02 may reduce from 1/6 to 1/11.
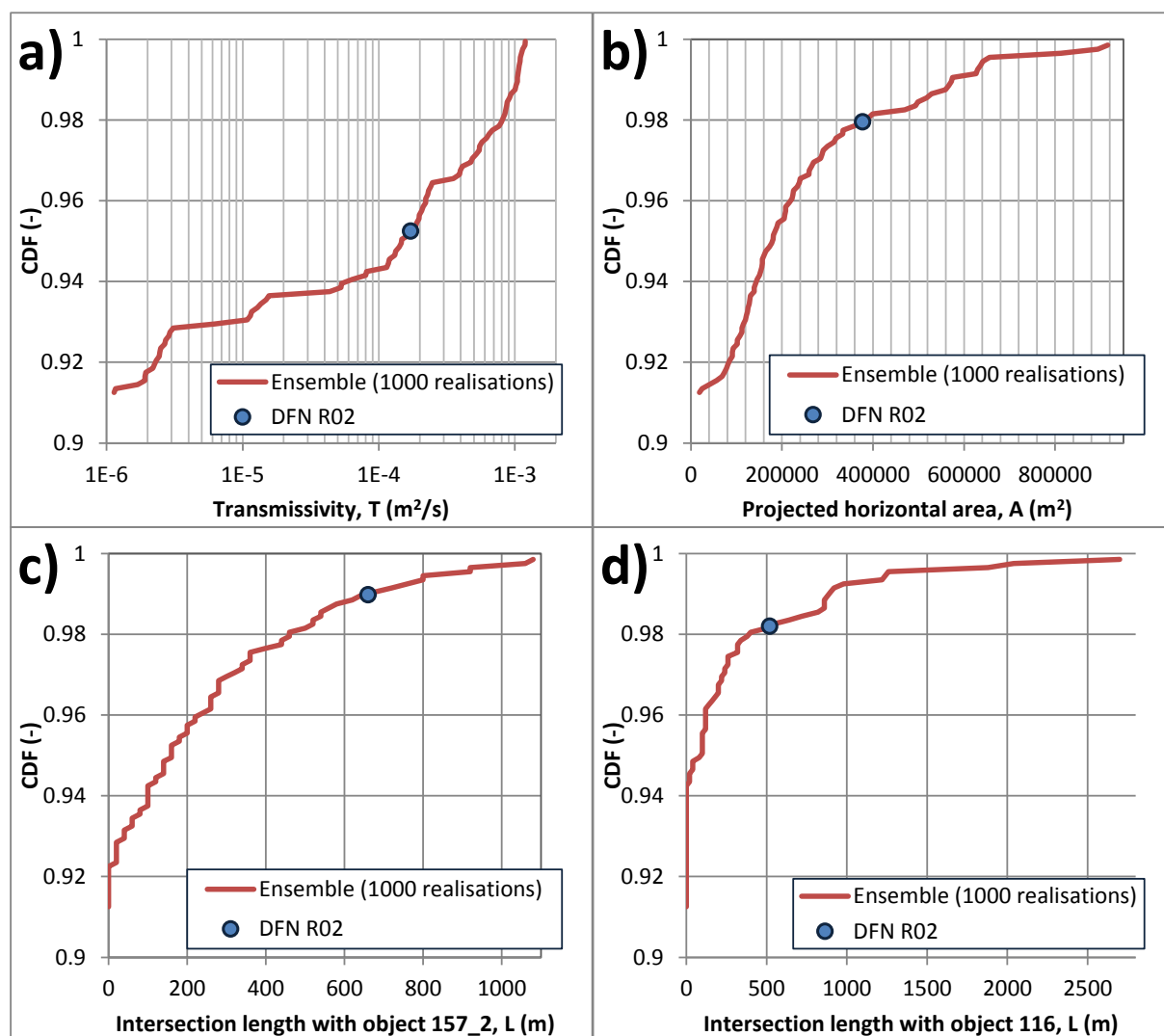

Figure E-8. Ranking the single-fracture connection in DFN R02 in context of a larger ensemble (1,000 realisations), based on geometrical/hydraulic properties used as indicators in DFN sampling (x-axis). The cumulative ensemble rank (CDF on the y-axis) starts at 0.912, as only 88 of its 1,000 realisations have a direct fracture connection between objects 157_2 and 116.

Of the four demonstrative realisations, R838 is ranked as the most likely to cause a high fraction of SFR discharge to lake object 116. The other three demonstrative realisations are examples of potential discharge to lake 116 that is limited in some aspect: R005 does not intersect the shoreline of lake 116

(although it connects to the sampling object; c.f. Figure E-7 and Figure E-9); R093 is poorly connected to object 157_2, and R907 has a limited horizontal area within the depth interval of relevance.
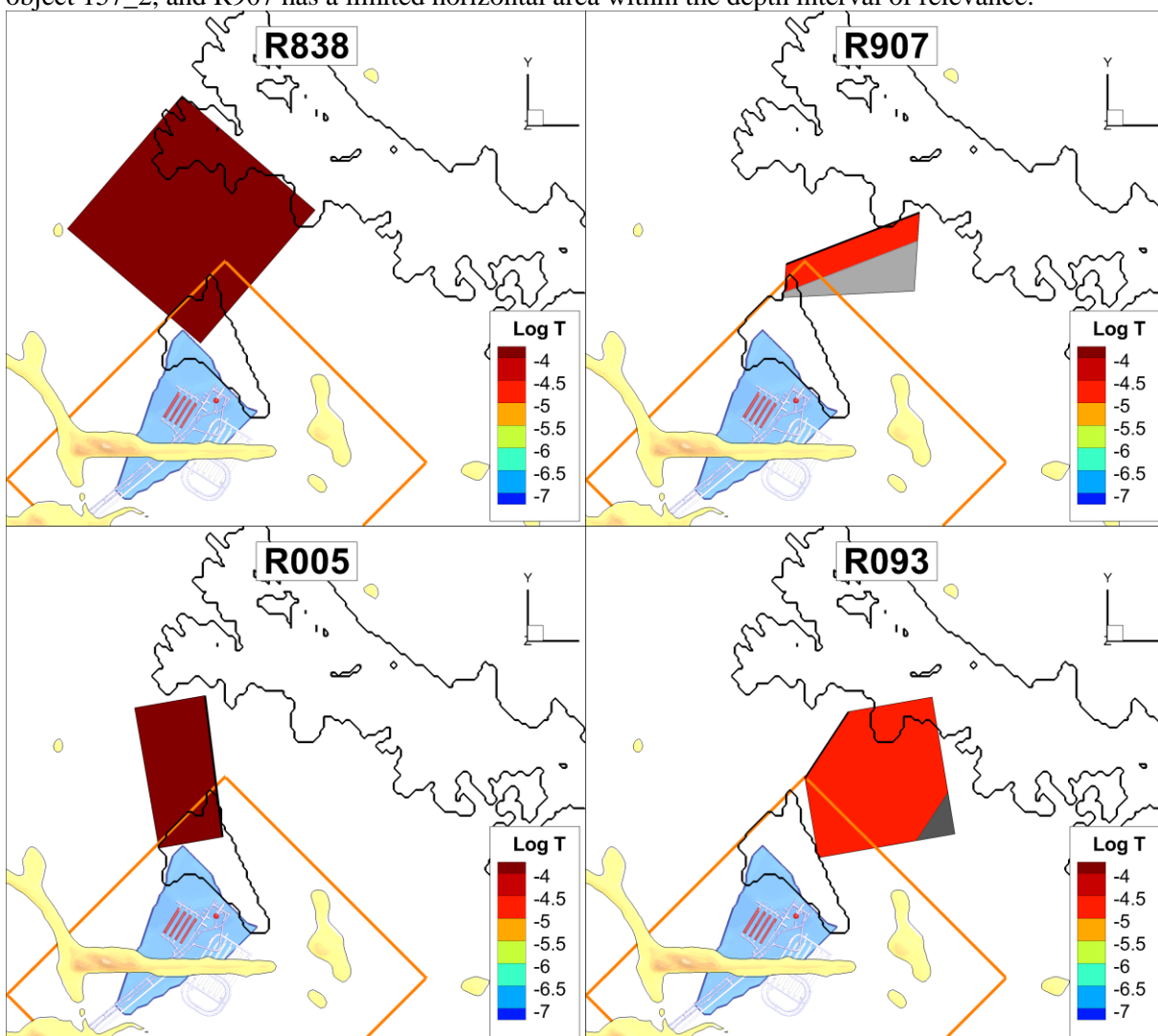

Figure E-9. *Selected realisations of the DFN ensemble to verify the geometrical/hydraulic indicators used in ranking. The single-fracture connection is terminated above ground surface and grey-shaded below a depth of 100 m.*

Table E-2. Selected cases to verify geometrical/hydraulic indicators (Table E-1)[1)]

Realisation Demonstrative case	Percentile	log T (m²/s)	Area (m²)	Intersection L (m) 157_2	116	Motivation for selection
R838	0.9995	-2.9 (3)	915600 (1)	800 (6)	2700 (1)	Ranked most likely to cause exit locations in object 116
R005[2)]	0.9715	-3.1 (22)	285200 (29)	800 (6)	**0** (87)	Poorly connected to object 116
R093	0.9655	-4.8 (65)	498800 (15)	**20** (76)	820 (14)	Poorly connected to object 157_2
R907	0.9425	-4.8 (65)	**108000** (73)	200 (44)	100 (49)	Low-ranked, limited horizontal exposure within depth interval

1) Ranked by the four estimators (Table E-1). Both numerical value and rank of estimators are provided. Rank provided within brackets (out of the 88 identified single-fracture connections). The percentile of realisations represents the overall rank in the ensemble, and is calculated based on the summed ranks of the four estimators. For example: R838 has the

rank sum 3+1+6+1 = 11, which is the lowest rank sum of the 1,000 realisations, and therefore it is given the highest percentile in the ensemble CDF: $1 - (\frac{1}{2}/n) = 0.9995$

2) Note that R005 is different from realisation R05.

The simulation results are in line with expectations, which confirms the reliability in the suggested geometrical/hydraulic indicators (Table E-3). R838 stands out with exceptionally high discharge, from both SFR1 and SFR3, reaching lakes 157_1 and 116 (i.e., even exceeding R02; Table E-3). R005 is similar to R838 in several aspects (Table E-2), but as it does not fully reach lake 116, its anomalous discharge primarily occurs in lake 157_1 (i.e., particularly discharge from SFR1). Realisations R093 and R907 do not stand out markedly from the average statistics, which demonstrates that both connectivity to object 157_2 and horizontal exposure within the relevant depth interval are critical aspects for controlling the SFR discharge location (i.e., the 11% discharge from SFR3 to object 116 is not considered to stand out significantly from the average of 6.5%).

In general the arbitrary realisations without single-fracture contact to lake 116 (R006…R010) falls in line with the earlier results (i.e., presented as average in Table E-3). The 11% discharge from SFR3 to objects 157_1 and 116 in R008 is not considered to stand out significantly from the average, 4.0% and 6.5%, respectively).

Table E-3. Confirmatory simulated discharge to biosphere objects (Figure 1-8).

	Fraction of particle exit per biosphere object (%)					
	157_2	157_1	116	159	121_2	121_1
SFR1						
Average[1]	**99.94**	**0.053**	**0.008**			
R02	*51.9*	*37.9*	*10.2*			
R838	*6.8*	*31.9*	*61.2*			
R005	*28.6*	*71.4*	0.05	0.003		
R093	99.9	0.05	0.01	0.0001		
R907	99.9	0.10	0.04			
R006	100.0	0.03	0.01			
R007	99.9	0.10	0.02			
R008	99.8	0.15	0.05			
R009	100.0	0.004	0.002			
R010	100.0	0.001	0.003			
SFR3						
Average[1]	**89.3**	**4.0**	**6.5**	**0.13**	**0.0099**	**0.0012**
R02	*70.6*	*13.9*	*15.4*	*0.0035*	*0.0089*	*0.0012*
R838	*38.9*	*11.1*	*50.0*	0.00	0.007	0.001
R005	*62.1*	*23.3*	*11.2*	3.3	0.010	0.001
R093	86.6	2.5	*10.8*	0.08	0.008	0.002
R907	87.3	2.0	*10.6*	0.002	0.009	0.001
R006	96.9	1.4	1.7	0.01	0.008	0.006
R007	86.7	8.2	5.1	0.003	0.007	0.001
R008	76.7	*11.9*	*11.3*	0.03	0.004	0.0004
R009	96.6	0.4	3.0	0.005	0.009	0.002
R010	95.6	0.3	4.1	0.003	0.004	0.006

1) Average excluding R02, i.e., based on: static DFN, R01, R03, R04, and R05. Note that R05 and R005 refer to different realisations.

DokumentID
1578373, (1.0)

Sekretess
Öppen

Sida
153(165
)

TD15 Complementary simulation cases in support of SR-PSU

Summary

The particular hydrogeological setting of biosphere objects 157_2, relative to downstream lake objects 157_1 and 116, makes the discharge from SFR dependent on the HRD heterogeneity/connectivity outside the SFR Regional domain, at least for the DFN-modelling concepts employed in SR-PSU with formulation of model domains and presence of highly transmissive sub-horizontal fractures. The risk of anomalously high discharge to lake objects 157_1 and 116 (i.e., as compared to results from the static DFN, which covered the area outside the SFR Regional domain in the SR-PSU sensitivity analysis, TD11) is estimated to be c. 1.4%.
The results also suggest that the static DFN outside the SFR Regional domain somewhat underestimates the discharge from SFR3 to objects 157_1 and 116 (c. 5% to each object, as compared to 3% and 0.7% estimated in the static DFN).

DokumentID
1578373, (1.0)

Sekretess
Öppen

Sida
154(165
)

TD15 Complementary simulation cases in support of SR-PSU

F. Appendix

Role of HSD parameterisation in bedrock flow

This appendix demonstrates a detailed analysis of the role of HSD parameterisation cases on the hydraulic gradients and flow rates in the underlying bedrock. The objectives of this analysis are to demonstrate the role of HSD in the hydrogeological setting at SFR and to provide a conceptual interpretation of the results found in section 3.1 (main report). As such, it was considered practical to employ a highly simplified model setup.

F.1 Demonstration of the role of HSD in simplified 2D-simulations

This modelling task, referred to as SR-PSU TD15, has demonstrated a sensitivity analysis of the model parameterisation of the Hydraulic Soil Domain (HSD; Sections 1.3 and 3.1). The simulation results have demonstrated somewhat counter-intuitive relationship between HSD parameterisation and simulated tunnel flow, namely that the flow is inversely proportional to hydraulic conductivity, K_{HSD} (Section 3.1). A conceptual interpretation has been suggested (Section 3.1), which may apply for specific hydrogeological settings (topography and thickness of regolith deposits) and the relationship between HSD and the underlying bedrock. This appendix demonstrates a detailed analysis of HSD-parameterisation cases at two stages of shoreline retreat (Table F-1) that are simulated in a two-dimensional cross section (Figure F-1).

Table F-1. HSD parameterisation variants in simplified 2D-simulations

HSD case		Hydraulic conductivity, K_{HSD} (m/s)	Time slice
1	Low-conductive	Base case / 10	2500 AD
			5000 AD
2	Reference case[1]	Base case (i.e., Table 4-5 in Öhman et al. 2014)	2500 AD
			5000 AD
3	High-conductive	Base case × 10	2500 AD
			5000 AD

1) The bedrock is parameterised as homogeneous, $K_{Rock} = 6.5 \cdot 10^{-8}$ m/s, based on Holmén and Stigsson (2001), which is intended to reflect both deformation zones and the rock mass outside deformation zones.
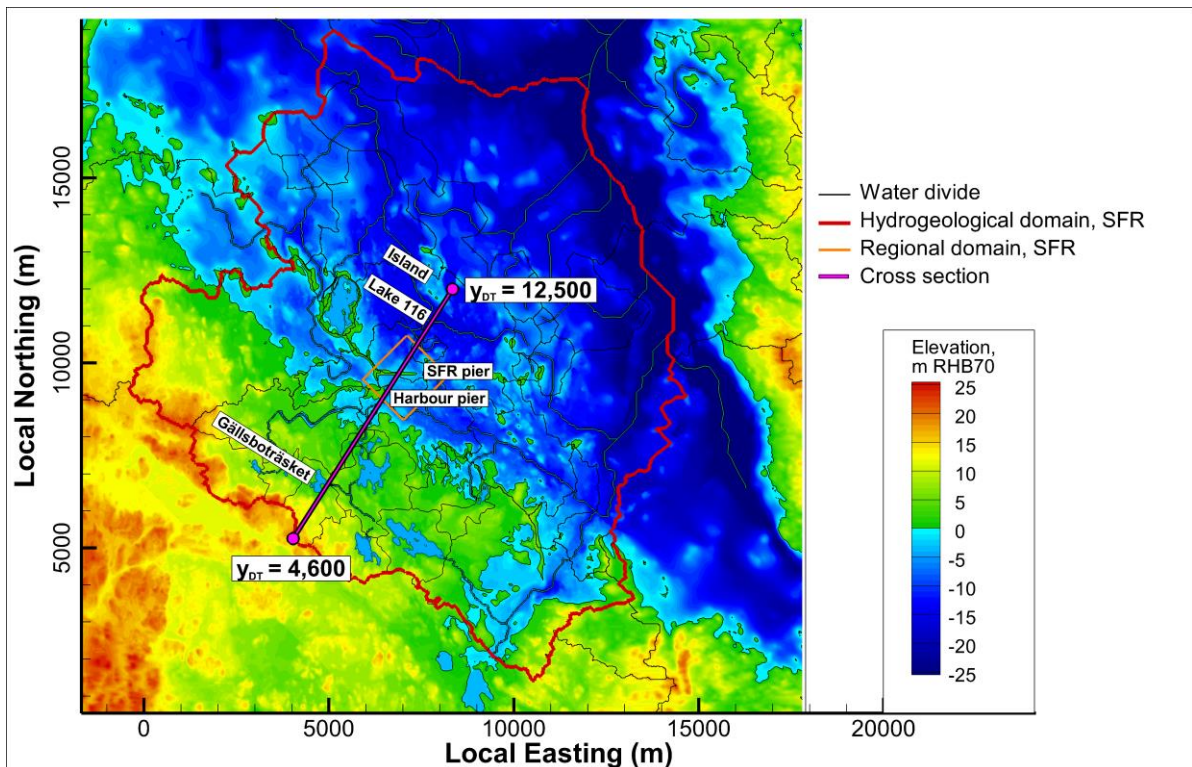
DokumentID
1578373, (1.0)

Sekretess
Öppen

Sida
155(165
)

TD15 Complementary simulation cases in support of SR-PSU

Figure F-1. *Trajectory of cross section in 2D simulations (pink line). Land marks included for reference. Trajectory defined in the rotated local coordinate system, y_{DT}, ranging from 4,600 to 12,500 m.*

Model setup

The modelled cross section is geometrically defined based intersection with the centre of the Silo (Figure F-1). The cross section has unit width (1.0 m) and extends vertically from +15 m to -480 m. The longitudinal range extends from the elevated water divide of the Hydrogeological domain (red line in Figure F-1) to a small island north of Lake object 116. A high grid discretisation is employed with cell sizes ranging from 1.0 m to 0.25 m. As stated earlier, a highly simplified model setup is employed for detailed analysis and conceptual interpretation, and therefore the simulated output is limited to conceptual interpretation.

The orientation of the cross section follows the established grid alignment parallel to the regional-scale flow field (i.e., the grid orientation that has been used in earlier flow simulations of SDM-PSU and SR-PSU, rotation angle = 32.58816946°). Thus, the cross section is orthogonal to shoreline and parallel to the extension of disposal rooms. In the rotated model coordinate system (notated x_{DT}, y_{DT}; Öhman et al. 2014), the cross section covers the range $y_{DT} = 4,600$ m to 12,500 m (Figure F-1). It should be noted that by 5000AD, the shoreline has actually withdrawn beyond $y_{DT} = 12,500$ m (i.e., hence Lake 116 comprises the outflow boundary).

Parameterisation

A homogeneous bedrock parameterisation is employed, $K_{Rock} = 6.5 \cdot 10^{-8}$ m/s. The reason for employing a homogeneous bedrock parameterisation is to make the results more general (i.e., avoiding effects of local deformation zones, or fractures of a particular DFN realisation). The value is taken from a case study in Holmén and Stigsson (2001). The authors applied this value to reflect an effective value combined from: 1) the rock mass outside deformation zones ($K_{HRD} = 6.5 \cdot 10^{-9}$ m/s), and 2) to account for non-resolved deformation zones, the value was increased by an order of magnitude. This value, $K_{Rock} = 6.5 \cdot 10^{-8}$ m/s, is

DokumentID
1578373, (1.0)

Sekretess
Öppen

Sida
156(165
)

TD15 Complementary simulation cases in support of SR-PSU

understood to belong to the upper end, and hence useful for examining the conditions where even the low K_{HSD} case exceeds the hydraulic conductivity of the underlying bedrock.

Three cases of HSD parameterisation are compared (Table F-1), which are based on the HSD sensitivity analysis in the main report (Section 1.3). The base case is used as a reference case (i.e., Öhman et al. 2014). A low K_{HSD} case is defined by reducing the base-case hydraulic conductivity by an order of magnitude and high K_{HSD} case is defined by increasing the base-case hydraulic conductivity by an order of magnitude.

Analysis

The following can be noted (Figure F-2 and Figure F-3):

1) The regolith thickness is c. 5 m, which comprises a comparably large fraction of the land elevation that controls the regional-scale hydraulic gradient (i.e., for the present-day situation: the elevated land above sea is composed of 5 m Quaternary deposits on top of 10 m bedrock)

2) The modelled bedrock surface has variable topography (peaks and depressions), which forms local "basins of regolith deposits"

3) In terms of soil-layer thickness, the HSD is dominated by till (the deepest layer). In all three cases the hydraulic conductivity of till exceeds that of the underlying bedrock.

4) Low-topography areas (near or below the shoreline) tend to be confined by overlying low-permeable clay layers (i.e., marine/lacustrine accumulated post glacial deposits or glacial clay). The hydraulic conductivity of these layers is on par with, or below, that of the underlying bedrock.

5) Minor differences in HSD thickness between the 2500AD and 5000AD are identified as accumulation or peat growth (particularly in the swamp Gällsboträsket and in the future Lake object 116)

6) The simulated head at bedrock surface, which less-strictly speaking can be envisaged as the groundwater table (black line in Figure F-2 and Figure F-3), is clearly affected by the HSD parameterisation; from closely following the topography in the low K_{HSD} case to a more smoothened appearance in the high K_{HSD} case. The simulated head has a realistic appearance, including artesian levels in the discharge areas (Gällsboträsket and Lake 116).
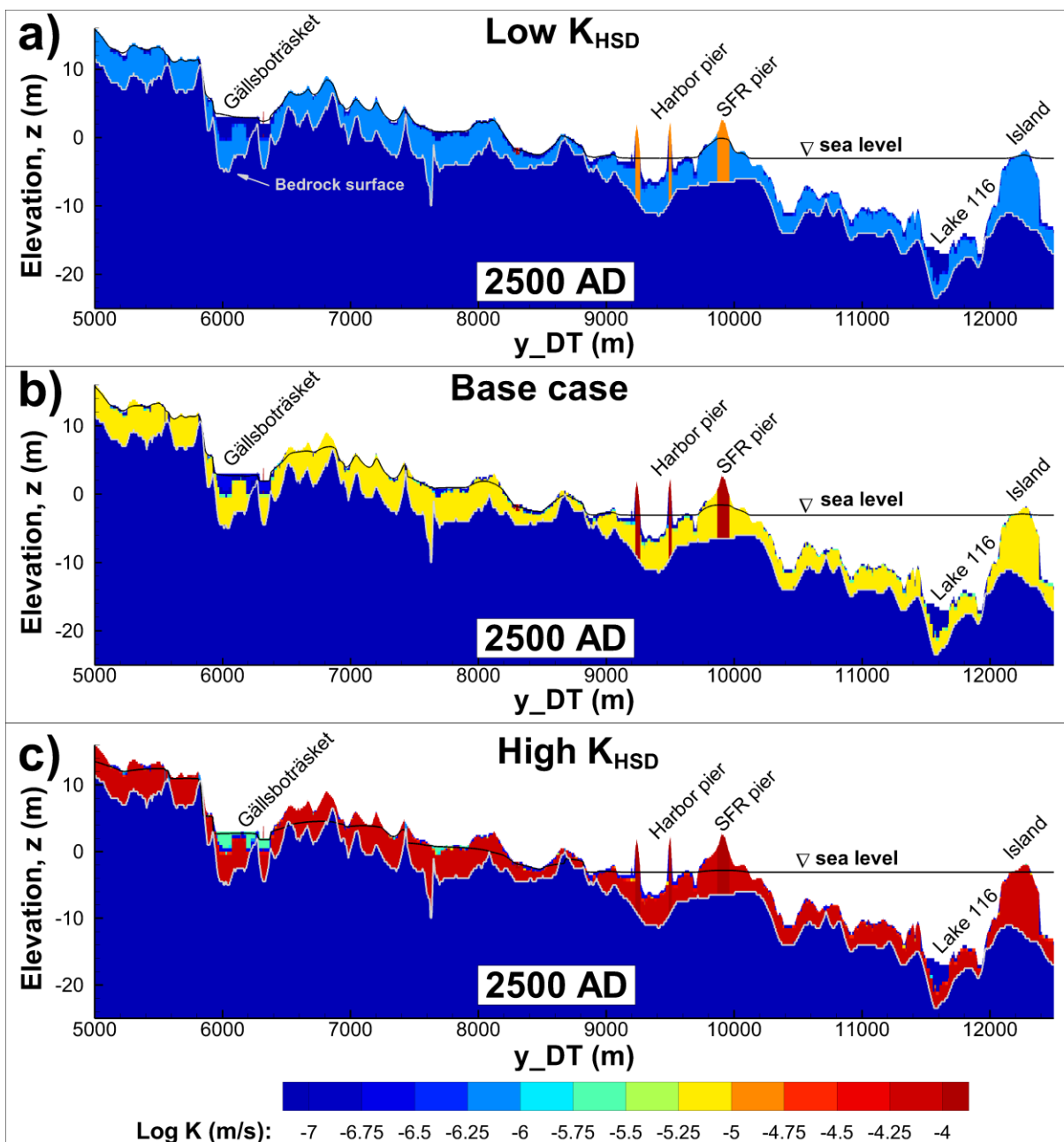
Figure F-2. *HSD parameterisation variants at 2500 AD (z_{sea} = -3.08 m); a) low K_{HSD} (K_{HSD} reduced by an order of magnitude), b) base case, and c) high K_{HSD} (K_{HSD} increased by an order of magnitude). Simulated head at bedrock surface as black line and bedrock surface as grey line. Landmarks included for reference.*
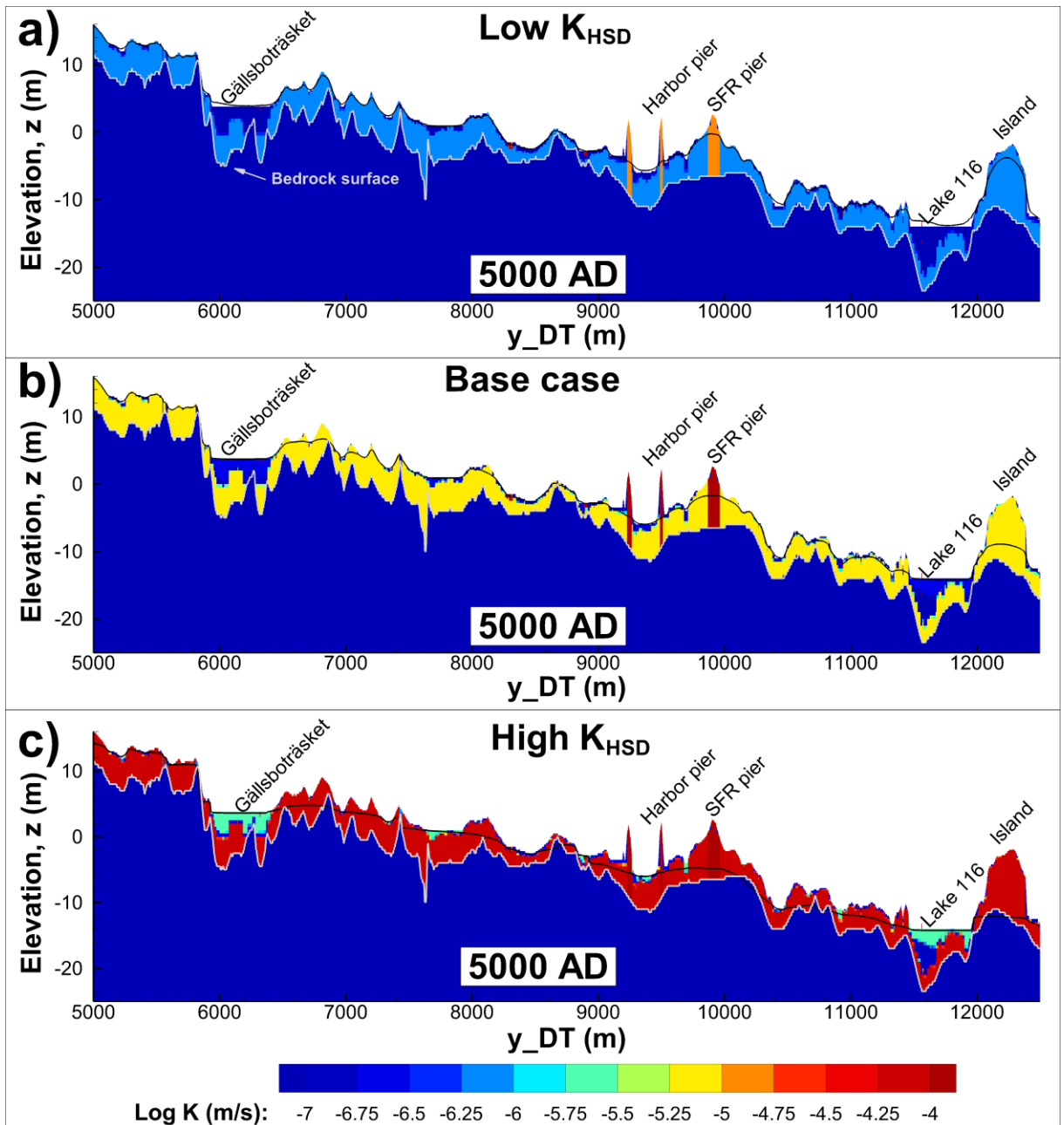
DokumentID
1578373, (1.0)

Sekretess
Öppen

Sida
158(165
)

TD15 Complementary simulation cases in support of SR-PSU

Figure F-3. *HSD parameterisation variants at 5000 AD (z_{sea} = -16.60 m); a) low K_{HSD} (K_{HSD} reduced by an order of magnitude), b) base case, and c) high K_{HSD} (K_{HSD} increased by an order of magnitude). Simulated head at bedrock surface as black line and bedrock surface as grey line. Landmarks included for reference.*

Analysis of simulated head above bedrock surface (i.e., piezometric head) is considered to be useful for understanding the role of HSD in SR-PSU flow simulations, as the scope of DarcyTools simulations (i.e., performance measures) is limited to bedrock flow (i.e., near-surface processes are handled by separate Mike-SHE modelling). It is also useful for controlling if potential errors in the simulated mixed boundary condition (imposed at ground surface) have propagated down to the bedrock surface. However, the simulated piezometric head at the bedrock surface appears realistic; it typically falls within the HSD layer (i.e., where the level depends on K_{HSD}). In the low K_{HSD} case, the piezometric head at bedrock is artesic in discharge areas (i.e., exceeds ground topography, indicating upward gradient). In the high K_{HSD} case, the

DokumentID
1578373, (1.0)

Sekretess
Öppen

Sida
159(165
)

TD15 Complementary simulation cases in support of SR-PSU

piezometric head may fall below the bedrock surface at peaks, where the bedrock surface forms a threshold for HSD flow.
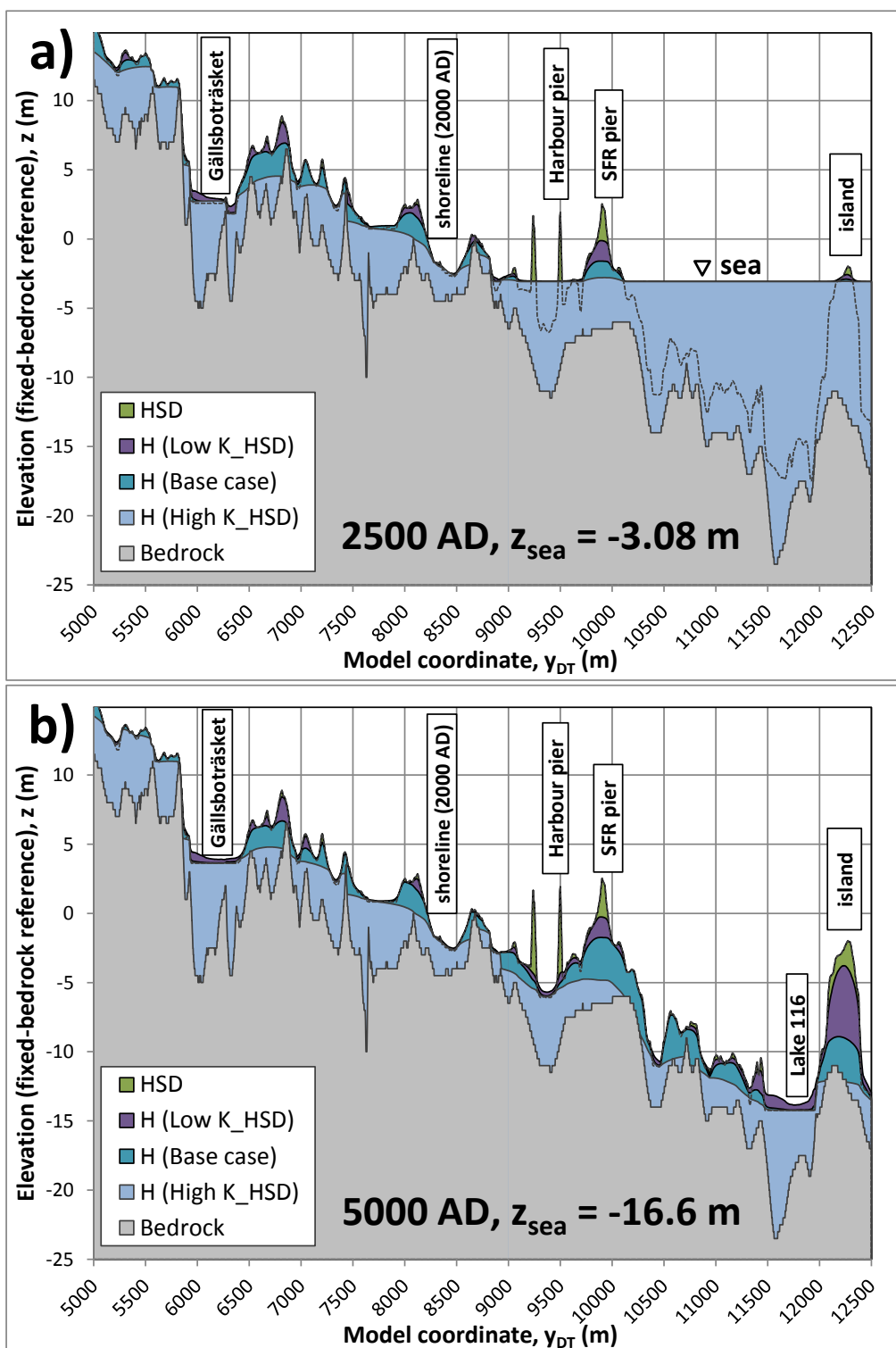

Figure F-4. *Simulated head at bedrock surface for three HSD parameterisation variants; a) at 2500 AD (z_{sea} = -3.08 m), b) at 5000 AD (z_{sea} = -16.60 m). Landmarks included for reference. Seafloor dashed line.*

DokumentID
1578373, (1.0)

Sekretess
Öppen

Sida
160(165
)

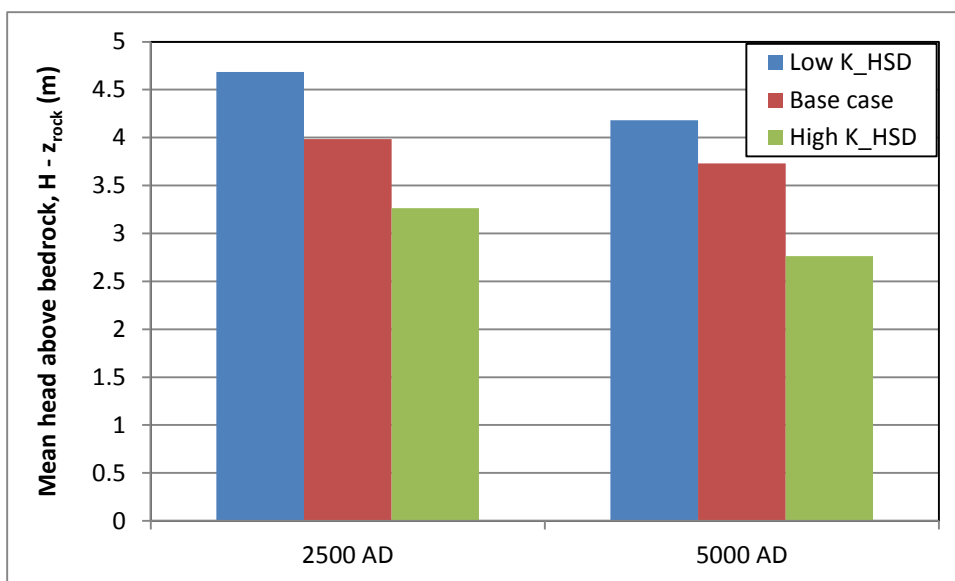TD15 Complementary simulation cases in support of SR-PSU

Figure F-5. *Average piezometric head at bedrock surface simulated for three HSD parameterisation variants under two stages of shoreline retreat.*

The regional-scale hydraulic gradient can be envisaged as being composed of two components:
1) elevation head of the sloping bedrock surface (i.e., a static component), and
2) piezometric head above bedrock (i.e., a component is controlled by HSD parameterisation).

Thus, for the present-day situation, the influence of HSD parameterisation of regional-scale gradient can be ballpark-estimated as "up to ⅓", as the maximum groundwater level range is confined to 5 m deposits on top of 10 m bedrock (Figure F-4). However, simulations suggest that the range in simulated piezometric head at bedrock surface is limited to c. ±1m (Figure F-5), such that one order of magnitude in hydraulic conductivity corresponds, inversely, to an average piezometric head of one meter. Note here that the calculation of average piezometric head includes does not include areas that are submerged below sea level.

As may be expected, a correlation between mean piezometric bedrock head and tunnel cross flow is confirmed (Figure F-6 and Figure F-7). However, it has been demonstrated in earlier flow simulations in SR-PSU that, from the shoreline retreat at 2500 AD and onwards, the disposal-room cross flow in the shallow SFR facility is not dominated by regional-scale flow, but by the local topographical gradients imposed by the emerging seafloor. A local hydraulic potential is therefore calculated as the difference between the mean piezometric head at the bedrock surface below the SFR pier ($y_{DT} = 9700$ to 10120 m; or more precisely, the natural ridge below the SFR pier) and the prevailing sea level. This allows putting the sensitivity to HSD parameterisation in context with changing flow regime due to the retreating shoreline (Figure F-8). The significance of the simulated groundwater level in the natural ridge below the SFR pier on disposal-room cross flow is demonstrated by the proportionality in Figure F-8 (i.e., observations falling more or less onto the same line, irrespectively of if the hydraulic potential is caused by HSD parameterisation variant or shoreline retreat).

DokumentID
1578373, (1.0)

Sekretess
Öppen

Sida
161(165
)

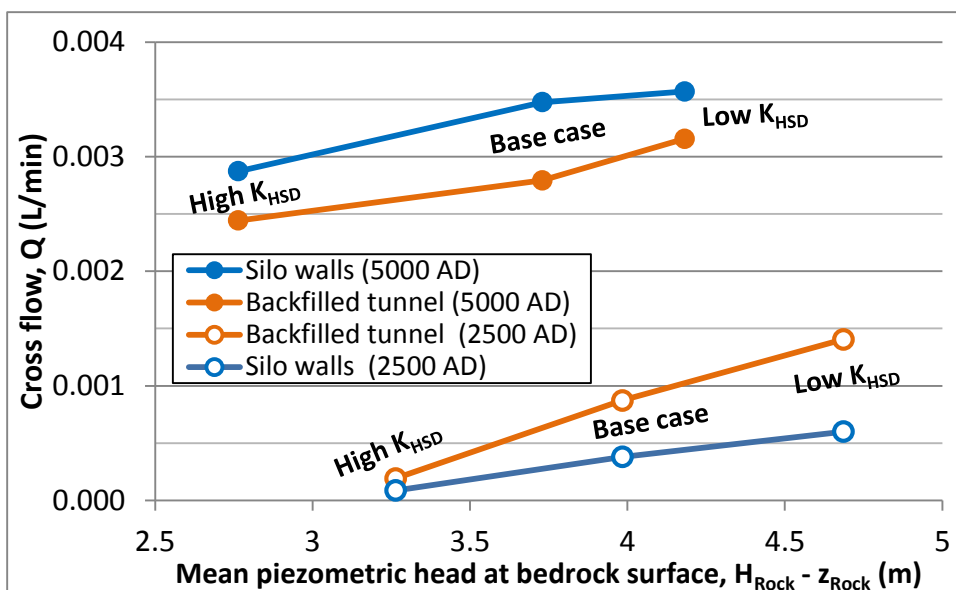TD15 Complementary simulation cases in support of SR-PSU

Figure F-6. *Simulated cross flow versus mean piezometric head at bedrock surface, depending on HSD parameterisation and stage of shoreline retreat.*
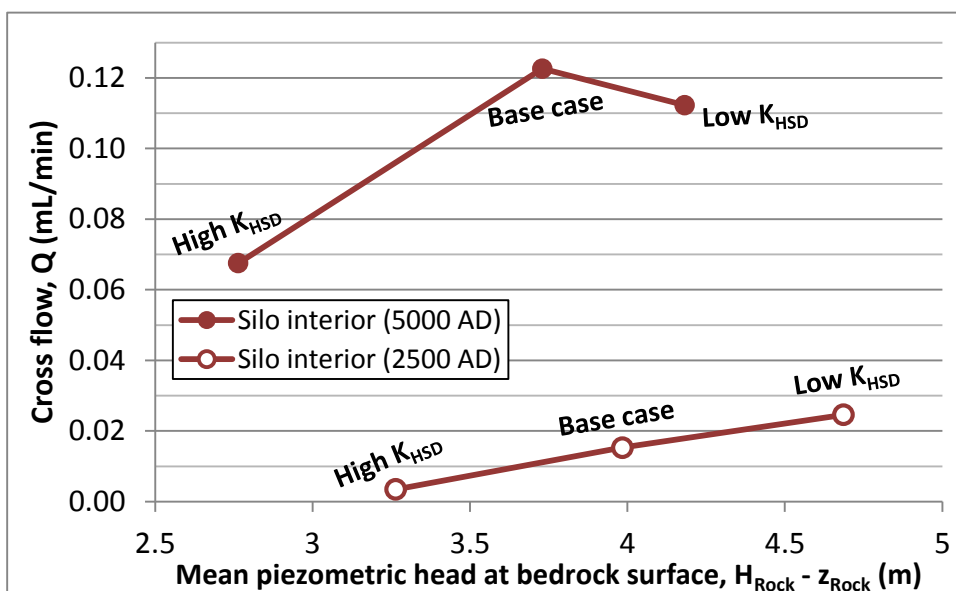

Figure F-7. *Simulated cross flow through Silo versus mean piezometric head at bedrock surface, depending on HSD parameterisation and stage of shoreline retreat.*
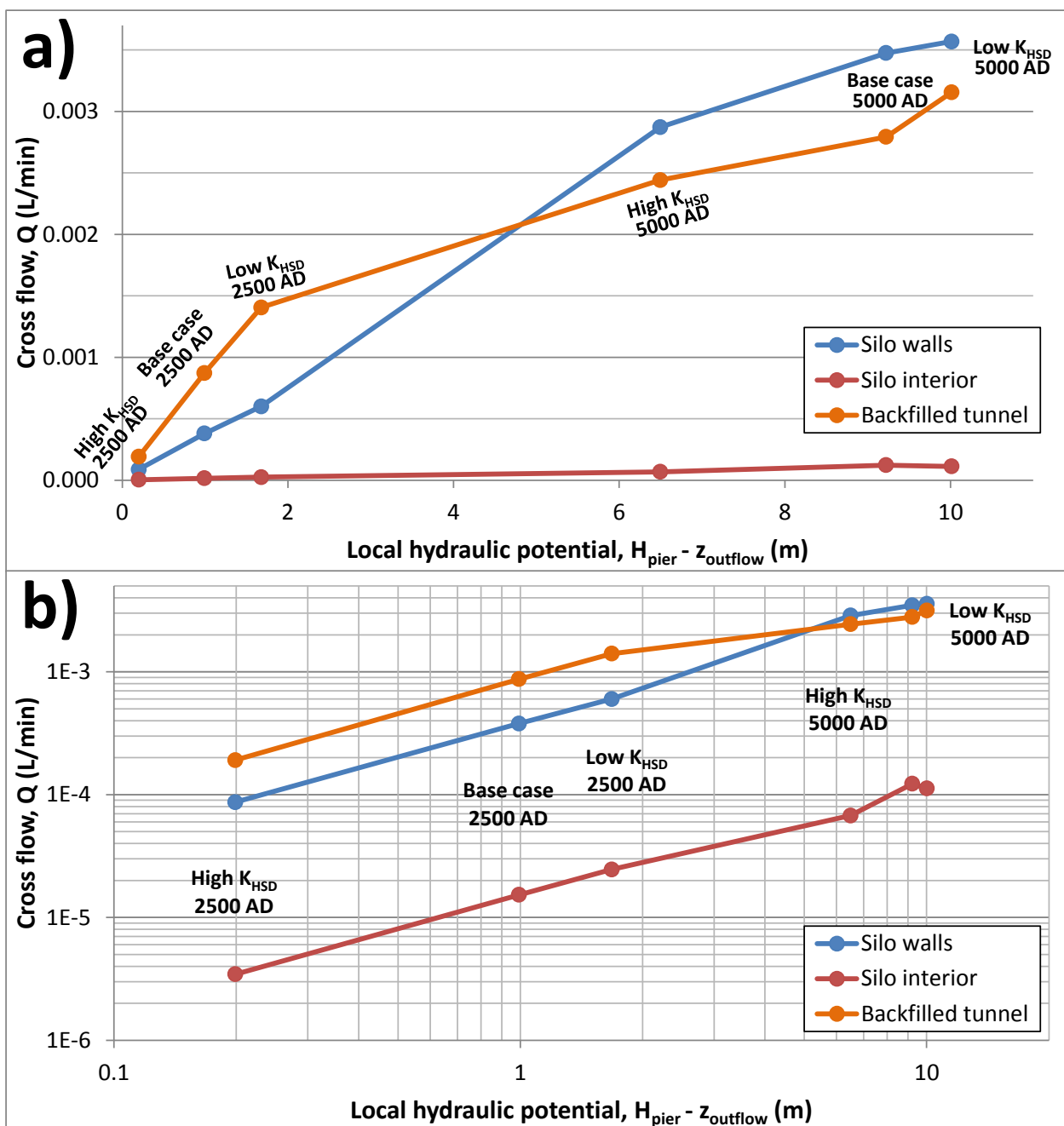
TD15 Complementary simulation cases in support of SR-PSU

Figure F-8. *Simulated tunnel cross flow versus the local hydraulic potential; a) linear scaling and b) logarithmic scaling. The hydraulic potential is estimated as the difference in mean head at bedrock surface, ΔH_{Rock} (m), between the SFR pier and the main outflow boundary (sea level, $z_{outflow} = -3.08$ m, at 2500 AD, and basin threshold of object 157_2, $z_{outflow} = -11.5$ m, at 5000 AD).*

Conclusion

This appendix has demonstrated the role of HSD parameterisation on flow rates in the underlying bedrock by a simplistic model setup of flow in a vertical cross section. The DarcyTools flow modelling does not address groundwater flow in HSD *per se*; however the HSD serves an important role in providing a realistic top boundary condition for the simulation of flow in the underlying bedrock.

Conceptually, two roles of HSD can be considered in regional-scale flow:
1) If the HSD is less permeable than the underlying bedrock, the HSD will re-direct much of the net precipitation as runoff, which will constrain the bedrock infiltration (Figure F-9a). This situation

TD15 Complementary simulation cases in support of SR-PSU

would suggest a *direct* proportionality between HSD conductivity and flow rates in the bedrock, where in the most extreme case – a fully impermeable HSD cover – would imply zero infiltration and no flow in the underlying bedrock.

2) If, on the other hand, HSD is more permeable than the underlying bedrock, and the regolith thickness is on par with the range of topographical gradients, a substantial groundwater flow will occur in the HSD, leading to a redistribution of groundwater levels within the regolith deposits (Figure F-9b). Thus, K_{HSD} may come to determine the degree of coupling between the ground-surface topography and the hydraulic gradient in the underlying bedrock. In other words, groundwater levels may be drained in highly permeable regolith deposits, which may – depending on the hydrogeological setting – imply low hydraulic gradients and flow rates in the underlying bedrock (Figure F-9b). This situation would suggest an *inverse* proportionality between HSD conductivity and flow rates in the bedrock.

Within the investigated range of K_{HSD}, the hydraulic conductivity of the domain soil layer (till) exceeds the conductivity of the bedrock, which would suggest that the situation in Figure F-9b prevails at SFR.
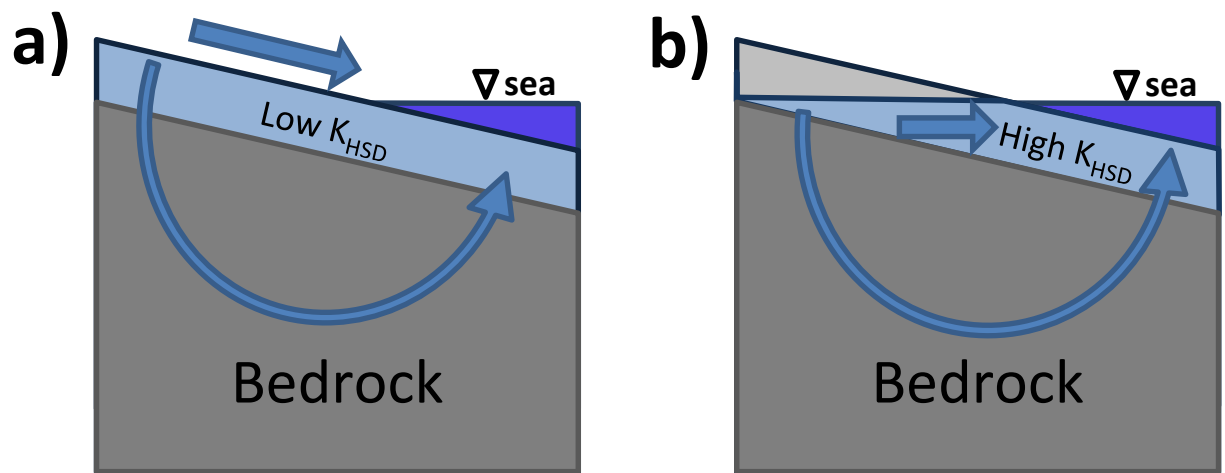

Figure F-9. Conceptual endpoints of the role of HSD on regional-scale flow; a) low K_{HSD} upholds the hydraulic gradient in the underlying bedrock, but constrains the bedrock infiltration (flow), and b) high K_{HSD} drains the groundwater levels, which reduces the hydraulic gradient in the underlying bedrock.

SVENSK KÄRNBRÄNSLEHANTERING AB

DokumentID
1578373, (1.0)

Sekretess
Öppen

Sida
164(165
)

TD15 Complementary simulation cases in support of SR-PSU

G.   Appendix

Codes used in analyses

This appendix lists the key codes used in this study, which can be divided into:

1) stand-alone codes (Table G-1), which are used outside the DarcyTools environment. The codes are primarily for simulated borehole/tunnel exploration, with the purpose to analyse, calibrate, or modify DFN realisations.
2) Algorithms that are developed specifically for the DarcyTools environment (Table G-2). The purpose of these is to: a) finalise the model setup, b) control the flow simulations during execution, and c) analysing the simulation output.

The geometrical sampling codes are based on established algorithms that have been implemented in FORTRAN, by courtesy of Martin Stigsson at SKB, and tested against other computational software (FracMan and DarcyTools).

Table G-1. Stand-alone codes for simulated exploration of fractures (FORTRAN)

File name	Purpose
[Semi-corr_DFN.F90]	Simulates borehole exploration in 10 stochastic DFN realisations for the SFR Regional domain (true borehole geometry of all cored boreholes and spatial resolution of PFL). Variant of the code used in DFN calibration in Appendix G of Öhman et al. (2012).
[APPLY_Semi-corr_parameterisation_knwnf.f]	Applies log-normal distributed random component to fracture transmissivity, on a trial and error basis, until calibration criteria are met (Section 2.4). The verification of the semi-correlated model is presented in Appendix D.
[Visualise_tunnel_intersections_2.F90]	Simulated trace mapping of the disposal rooms in the alternative localisation of SFR 3 (Section 2.8, main report) with the purpose to select representative DFN realisations of the Forsmark lense. The code is verified by means of visual inspection in TecPlot (e.g., Figure 2-13, Figure 2-14, Figure 2-15).
[Read_Serco_fracts_IN_FFM-HOLE.F90]	Used to form a combined DFN realisation, merged three sources: 1) The SFR base-case realisation, DFN R85, *inside* the SFR 2) Regional domain *inside* the SR-Site Forsmark FFMs 3) The static DFN, referred to as SR-Site extended heterogeneity case, to cover the remaining domain: *outside* the SFR Regional domain and *outside* the SDM-Site Forsmark FFMs
[Sample_DFN_OUTSIDE_SFR_Reg_dom.f]	Used to execute the generation of the DFN ensemble (1,000 realisations) outside SFR Regional domain (Appendix E) to identify the frequency of potentially critical fractures for discharge from SFR. These fractures form a direct connection between the biosphere objects 157_2 and 116 (i.e., fractures fulfilling the criteria in Table E-1). The code is verified for test samples, as well as by means of visual inspection in TecPlot (e.g., Figure E-6 and Figure E-7).
[Scan_DFN_OUTSIDE_SFR_Reg_dom.f]	Evaluates hydraulic connection of the identified directly-connecting fractures in terms of the four defined hydraulic/geometrical estimators (Table E-1). The code is verified for test samples, as well as by means of visual inspection in TecPlot (e.g., Figure E-9).

Table G-2. Algorithms used within the DarcyTools environment (FORTRAN)

File name	Purpose
[prpgen_TD15_ALTER_HSD.f]	Set up the model parameterisation, by merging upscaled K_{ECPM} from the DarcyTools module FracGen with hard-coded parameterisation alternatives (such as e.g., HSD variants). Visual verification in TecPlot (e.g., Figure 2-2, Figure 2-3, Figure 2-4, Figure 2-5, Figure F-2, Figure F-3).
[fif-RECHARGE_TD11_NEW_Pier.f]	Mixed-boundary condition in the DarcyTools simulations. The top-

	boundary condition (prescribed flux or prescribed head) is determined locally depending on the prevailing hydrological setting. Developed and presented in SR-PSU-TD11 (Öhman et al. 2014). Visual verification in TecPlot (e.g., Figure 3-5 to Figure 3-8 and Figure F-2 to Figure F-4).
[fif_TD11_Steady_state_NEW_Pier.f]	Implements the groundwater level determined in the preceeding recharge phase (or more precisely head in the uppermost active cell layer). Developed and presented in SR-PSU-TD11 (Öhman et al. 2014).
[Get_flows_SFR3_in_LENSE.f]	A somewhat adapted version of the vector-based method [Get_flows_and_grad_TD10.f], which was developed to avoid numerical artefacts that otherwise arise when calculating sub-parallel flow along saturated tunnels that are not aligned with the computational grid (Section 2.8, main report). The algorithm is referred to as "method 3" and has been extensively demonstrated in a PM to SR-PSU-TD10 (Öhman 2013).
[TD15_Particle_tracking.f]	Determine performance measures of flow paths to or from SFR disposal rooms, and particle exit to biosphere objects. Verified by detailed confirmatory calculations on sample trajectories. Verified by comparison to DarcyTools (Patrik Vidstrand, SKB). Visual verification in TecPlot (e.g., Figure 3-8,Figure 3-9, Figure 3-15, Figure 3-27 to Figure 3-34, Figure 3-36, Figure 3-50).